TUM School of Natural Sciences
Technische Universität München

Novel Strategies to Guide Sample Preparation for Compound-Specific Isotope Analysis

Christopher Claus Wabnitz

Vollständiger Abdruck der von der TUM School of Natural Sciences der Technischen Universität München zur Erlangung des akademischen Grades eines

Doktors der Naturwissenschaften (Dr. rer. nat.)

genehmigten Dissertation.

Vorsitz:
Prof. Dr. Nicole Strittmatter

Prüfer der Dissertation:
1. Prof. Dr. Martin Elsner
2. Prof. Dr. Michael Schuster

Die Dissertation wurde am 26.02.2024 bei der Technischen Universität München eingereicht und durch die TUM School of Natural Sciences am 12.07.2024 angenommen.

Acknowledgment

I want to thank everyone who advised, helped, and supported me during my last year's PhD journey. First, I would like to express my deepest gratitude to my PhD supervisor, Prof. Dr. Martin Elsner. Dear Martin, I got to know to you as a student when you made me curious about the field of analytical chemistry and I am very grateful that I had the opportunity to persue my interest with you during my PhD and that you became from a teacher to a supervisor and mentor. Thank you for your friendly and empathetic support during this time and for all of your insights and expertise, which have shaped this work in profound ways.

I am also thankful to Dr. Rani Bakkour, whose role as my direct supervisor has been instrumental in navigating the complexities of research. Dear Rani, thank you for guiding me from my starts during my research internship till the end of my PhD. Thank you for always taking the time for me, for your support during difficult times, and for all of your insightful feedback that has been indispensable in shaping the direction and the details of this thesis. I will never forget all the fun and memorable moments we shared during this period!

I sincerely thank Prof. Dr. Michael Schuster. I appreciate the time and efforts you dedicated to reviewing the dissertation. Further, I would like to thank Dr. Mathias Reisbeck. Thanks for the smooth and successful collaboration on producing the microfluidic spray-dryer.

A big thanks go to my current and former colleagues from the groups of *Targeted Environmental Analytics* and *Isotopes and Environmental Chemistry*, who made every day at work enjoyable and memorable: Aoife, Andrea, Armela, Chen, David, Felix, Fengchao, Gabriel, Habib, Leo, and Lihong. Thanks to all your advice, chats, help, friendship in and out of work, and all your support in the good and the bad times. David, thank you so much for being such a great colleague and advisor for nearly six years. You taught me countless things, but most importantly, you were always a great friend! Felix, your support in the lab was irreplicable. You were always there to fix instrumental- and non-instrumental-related problems or just have fun! Aoife, thanks for helping me kicking off my project on the QCM with your excellent work during your master's thesis. Armela, thanks for all the laughter and discussions on our shared office table. Thanks to both of you for being the best colleagues I could have wished for, for your support, and the countless and valuable scientific and non-scientific chats. Chen, thanks for your outstanding work during your internship and thesis and the great time we had together. A big thank you to my research internship students, David, Carmen, and Malte, who contributed significantly to my research projects with their excellent work.

I want to express my thanks to all current and former colleagues at the Chair of Analytical Chemistry and Water Chemistry for the always friendly working atmosphere and the numerous professional and personal exchanges during cake breaks, lunches, excursions, or festivities. I especially want to thank Oleksii for his Raman measurements and Max for the interesting microplastic project. Thanks to Christine Benning, who kindly supported me with SEM and EDX measurements. Many thanks to Christine Beese, Cornelia Popp, and Sonja Rottler for all the organizational help and to Roland Hoppe and Sebastian Wiesemann for the great and always quick help in the workshop.

Lastly, I would like to thank my friends and family from the bottom of my heart for all the support and joy you have brought me during this time. I would especially like to thank my parents, who always supported me unconditionally in every area throughout my entire time in school and university. Last but not least, I want to thank you from all my heart, Tanya. Thanks for all your love, patience, and (programming) support.

Abstract

Numerous research fields, from forensic to environmental sciences, benefit from information about the variation of stable isotope abundances (e.g., by measuring $\delta^{13}C$ as the ratio of ^{13}C and ^{12}C) in (bio)chemical substances. In compound-specific isotope analysis (CSIA), the isotopic signature of a compound can be measured with high precision using an isotope ratio mass spectrometer (IRMS) hyphenated to gas- or liquid chromatography (GC- and LC-IRMS). During the isotope measurement using the IRMS, the compound of interest is combusted into a universal analyte, in the case of carbon measurements to CO_2. The structural information gets lost during this process, which makes CSIA prone to matrix interferences in case the separation power provided by GC/LC is insufficient. For many real-world applications, large amounts of matrix compounds are co-enriched during the extraction of the sample and, thus, must be removed using further purification steps to guarantee accurate CSIA. While there are many purification techniques available, like molecularly imprinted solid phase extraction (MISPE) or the most commonly used one, reversed-phase high-performance liquid chromatography (RP HPLC), optimizing matrix removal during the respective purification is still one of the greatest challenges of CSIA sample preparation. For optimal and efficient purification using RP HPLC, for example, simultaneous online monitoring and quantification of both the target analyte and the matrix is highly valuable. Still, no commercially available detector can quantify the entirety of the matrix online during an RP HPLC purification. Hence, the overarching goal of this dissertation was to expand the applicability of CSIA by investigating the effectiveness of strategies to optimize the matrix removal during the purification of sample extracts prior to GC-IRMS isotope analysis, with a specific focus on developing a novel detection technique for the online quantification of the sample matrix during RP HPLC purification.

The first part of the thesis investigated the influence of the anionic character of the environmental matrix natural organic matter (NOM) on non-specific sorption of NOM during MISPE to increase the understanding of processes governing non-specific binding of the sample matrix. To this end, acidic functional groups of NOM were methylated to significantly reduce the charge density of NOM and, thus, the electrostatic repulsion of dissolved and sorbed NOM compounds. The study successfully shows the reduction of the charge density of NOM by a factor of 3.4 using a trimethylsilyl diazomethane (TMSD) based selective methylation of NOM carboxy groups. Breakthrough curves revealed that 30% more methylated NOM compared to untreated NOM remained on the MIP after a washing procedure using dichloromethane (DCM). This implies stronger MIP-methylated NOM interactions, which are most likely caused by the smaller charge density of the methylated

NOM and the consequently smaller electrostatic repulsion between NOM molecules. The presented findings prove the importance of NOM's anionic character for the sorption on MIPs and provide a knowledge base for future research on non-specific binding of the sample matrix NOM during MISPE.

The second and major part of the thesis addressed the challenge of developing a detection technique that can quantify matrix components online during RP HPLC. For this purpose, this thesis investigated the suitability of quartz crystal microbalance (QCM) using two different strategies: (i) QCM liquid sensing and (ii) QCM dry mass sensing. First, a suitable coating must be found to quantify matrix components in the liquid phase using QCM liquid sensing. The second chapter thus investigated for the first time a grafting approach for a hypercrosslinked divinylbenzene (DVB)-based copolymer using ethylene glycol dimethacrylate (EGDMA) as a hydrophilic modifier on a QCM sensor, characterized the sensor coating, and evaluated the interaction of the coating with humic acids. The study demonstrates the successful grafting of a DVB-EGDMA co-polymer onto the QCM sensor using radical polymerization. A laterally heterogeneous polymer layer with a thickness of 200-300 nm inside the dynamic range of QCM measurements was further achieved. While humic acids did sorb onto the grafted copolymer during sorption experiments, leading to a high frequency decrease of 18-20 Hz in comparison to other studies, this number is still too low for matrix online monitoring. Future research can build upon this study's grafting and characterization procedure to optimize and explore other co-polymers further.

The third chapter explored the feasibility of coupling a commercial HPLC with a microfluidic spray-dryer and a QCM using a flow splitter for online monitoring of organic matrix components during RP HPLC gradient purification. To this end, a measuring, calibration, and data processing strategy was developed, and the system was characterized in terms of lower and upper quantification limits and accuracy. Validation of NOM in an environmental sample against offline total organic carbon analysis confirmed the approach's feasibility with an absolute recovery of 103±10%. A correlation ($R^2 \geq 95$) between the amount of matrix quantified by QCM dry mass sensing during an HPLC clean-up of a brown rice extract and matrix effects measured during the subsequent GC-MS analysis of the investigated pesticides was found. This suggests that QCM dry mass sensing can be a valuable tool to the analyst where HPLC clean-up is routinely performed and can thus benefit many analytical fields.

The fourth chapter investigated the limitations and enhancement of HPLC purification on C_{18} and C_8 phases for single- and multiple-targets using QCM dry mass sensing. Further, the benefit of such an optimized HPLC purification for isotope analysis of polar micropollutants typically present in environmental samples was examined. Strong isotopic shifts of up to 3.3‰ towards the isotopic signature of NOM were observed for samples with a NOM-to-analyte ratio ≥ 10. Thanks to QCM sensing, optimization of matrix removal of up to 97 for early and 99.8% for late-eluting compounds was possible. The efficiency of HPLC purification deteriorated when aiming for simultaneous purification of two or three compounds, leading to up to 2.5% less NOM removal. Our results suggest that one optimized HPLC purification can be achieved through systematic

screening of 3 to 5 different gradients, thereby shifting the boundaries of accurate carbon-CSIA by up to two orders of magnitude toward lower micropollutant concentrations.

Overall, the results of this work emphasize the importance (i) of suitable detection techniques for the specific requirements of analytical tasks and (ii) of optimized, highly selective, and automated purification techniques for sample clean-up to use the full potential of CSIA. Specifically, QCM dry mass sensing proved to be successful in online quantifying of the entirety of the extracted sample matrix during RP HPLC purification, thus tremendously increasing the percentage of NOM that can be removed in one clean-up step. QCM dry mass sensing paves the way to efficiently develop optimized purification strategies for various purification problems using a large range of liquid chromatographic solid phase materials and modes. Using optimized chromatographic purification in combination with selective extraction procedures that were recently developed will, in the future, help to expand the applicability of CSIA to compounds present in real-world samples in the low to middle ng/L range, enabling thus insights into environmental and biological processes and forensic cases that are presently not accessible. Furthermore, the possibility of online detection of both the target and the matrix during RP HPLC is a big step towards a fully automated method development and optimization of CSIA sample preparation.

Zusammenfassung

Zahlreiche Forschungsbereiche, von der Forensik bis zu den Umweltwissenschaften, profitieren von Informationen über die Variation stabiler Isotopenhäufigkeiten (z.B. durch Messung von δ^{13}C als Verhältnis von ^{13}C und ^{12}C) in (bio)chemischen Stoffen. Bei der substanzspezifischen Isotopenanalyse (engl. *compound-specific isotope analysis*, CSIA) kann die Isotopensignatur einer Verbindung mithilfe eines Isotopenverhältnis-Massenspektrometers (engl. *isotope ratio mass spectrometry*, IRMS) verbunden mit Gas- oder Flüssigkeitschromatographie (engl. *gas- or liquid chromatography*, GC- und LC-IRMS) mit hoher Präzision gemessen werden. Bei der Isotopenmessung mit dem IRMS wird die Zielverbindung zu einem universellen Analyten verbrannt, bei Kohlenstoffmessungen zu CO_2. Die Strukturinformation geht bei diesem Prozess verloren, was CSIA anfällig für Matrixinterferenzen macht, falls die Trennleistung der GC/LC nicht ausreicht. Bei vielen Realanwendungen werden bei der Extraktion der Probe große Mengen an Matrixverbindungen angereichert und müssen daher durch weitere Aufreinigungsschritte entfernt werden, um eine genaue CSIA zu gewährleisten. Auch wenn viele Aufreinigungstechniken zur Verfügung stehen, wie beispielsweise die molekular geprägte Festphasenextraktion (engl. *molecularly imprinted solid phase extraction*, MISPE) oder die am häufigsten verwendete Methode, die Umkehrphasen-Hochleistungsflüssigkeitschromatographie (engl. *reversed-phase high-performance liquid chromatography*, RP HPLC), ist die Optimierung der Matrixentfernung während der jeweiligen Aufreinigung immer noch eine der größten Herausforderungen der CSIA-Probenvorbereitung. Für eine optimale und effiziente Aufreinigung beispielsweise mittels RP-HPLC ist die gleichzeitige Online-Überwachung und Quantifizierung sowohl des Zielanalyten als auch der Probenmatrix von großem Wert. Dennoch kann kein kommerziell erhältlicher Detektor die gesamte Matrix während einer RP-HPLC-Reinigung online quantifizieren. Daher bestand das übergeordnete Ziel dieser Dissertation darin, den Anwendungsbereich von CSIA zu erweitern, indem die Wirksamkeit von Strategien zur Optimierung der Matrixentfernung während der Aufreinigung von Probenextrakten vor GC-IRMS-Isotopenmessungen untersucht wurde. Ein besonderer Schwerpunkt lag dabei auf der Entwicklung einer neuartigen Messtechnik zur Online-Quantifizierung der Probenmatrix während RP-HPLC Probenaufreinigung.

Der erste Teil der Arbeit untersuchte den Einfluss des anionischen Charakters der natürlichen organischen Materie (engl. *natural organic matter*, NOM) auf die unspezifische Sorption von NOM während MISPE, um das Verständnis der Prozesse zu verbessern, die die unspezifische Bindung der Probenmatrix steuern. Zu diesem Zweck wurden saure funktionelle Gruppen von NOM methyliert, um die Ladungsdichte von NOM und

damit die elektrostatische Abstoßung gelöster und sorbierter NOM-Verbindungen deutlich zu reduzieren. Die Studie zeigt erfolgreich die Reduzierung der Ladungsdichte von NOM um den Faktor 3,4 mithilfe einer auf Trimethylsilyldiazomethan (engl. *trimethylsilyl diazomethane*, TMSD) basierenden selektiven Methylierung von NOM-Carboxygruppen. Durchbruchskurven zeigten, dass nach einem Waschvorgang mit Dichlormethan (DCM) 30% mehr methyliertes NOM im Vergleich zu unbehandeltem NOM auf dem MIP verblieben. Dies lässt auf stärkere Wechselwirkungen zwischen MIP und methyliertem NOM schließen, welche höchstwahrscheinlich durch die geringere Ladungsdichte des methylierten NOM verursacht werden und der daraus resultierenden geringeren elektrostatischen Abstoßung zwischen NOM-Molekülen. Die präsentierten Ergebnisse belegen die Bedeutung des anionischen Charakters von NOM für die Sorption an MIPs und bieten eine Wissensbasis für zukünftige Forschungen zur unspezifischen Bindung der Probenmatrix NOM während MISPE.

Der Hauptteil der Arbeit befasste sich mit der Herausforderung, eine Detektionstechnik zu entwickeln, mit der Matrixkomponenten online während RP-HPLC quantifiziert werden können. Zu diesem Zweck untersuchte diese Arbeit die Eignung der Quarzkristall-Mikrowaage (engl. *quartz crystal microbalance*, QCM) mit zwei verschiedenen Strategien: (i) QCM Messungen in Flüssigkeiten (engl. *QCM liquid sensing*, Flüssigkeiten-QCM) und (ii) QCM Messung von Trockenmassen (engl. *QCM dry mass sensing*, Trockenmassen-QCM). Zunächst muss eine geeignete Beschichtung gefunden werden, um Matrixkomponenten in der flüssigen Phase mithilfe der Flüssigkeiten-QCM zu quantifizieren. Das zweite Kapitel untersuchte daher erstmals eine Methode, ein hypervernetztes Divinylbenzol (engl. *divinylbenzene*, DVB)-basiertes Copolymer unter Verwendung von Ethylenglykoldimethacrylat (engl. *ethylene glycol dimethacrylate*, EGDMA) als hydrophilem Modifikator auf einem QCM-Sensor zu synthetisieren, die Sensorbeschichtung zu charakterisieren und die Wechselwirkung der Beschichtung mit Huminsäuren zu quantifizieren. Die Studie demonstriert das erfolgreiche Synthetisieren eines DVB-EGDMA-Copolymers auf den QCM-Sensor mittels radikalischer Polymerisation. Die Polymerschicht war lateral heterogen mit einer Dicke von 200-300 nm, womit sie innerhalb des dynamischen Bereichs von QCM-Messungen liegt. Auch wenn Huminsäuren während der Sorptionsexperimente an das Copolymer sorbierten, was im Vergleich zu anderen Studien zu einer starken Frequenzabnahme von 18–20 Hz führte, ist diese Zahl für Online-Quantifizierung von Matrix Substanzen immer noch zu niedrig. Zukünftige Forschung kann auf dem in dieser Studie präsentierten Synthese- und Charakterisierungsverfahren aufbauen, um andere Copolymere zu synthetisieren, weiter zu optimieren und zu erforschen.

Das dritte Kapitel untersuchte die Machbarkeit der Kopplung einer kommerziellen HPLC mit einem mikrofluidischen Sprühtrockner und einer QCM unter Verwendung eines Flusssplitters zur Online-Überwachung organischer Matrixkomponenten während RP-HPLC-Gradientenaufreinigung. Zu diesem Zweck wurde eine Mess-, Kalibrierungs- und Datenverarbeitungsstrategie entwickelt und das System hinsichtlich unterer und oberer Quantifizierungsgrenzen und Genauigkeit charakterisiert. Die Validierung von NOM in einer Umweltprobe gegen eine Offline-Analyse des gesamten organischen Kohlenstoffs bestätigte die Machbarkeit des Ansatzes mit

einer absoluten Rückgewinnung von 103 ±10%. Eine Korrelation ($R^2 \geq 95$) zwischen der Matrixmenge, die durch Trockenmassen-QCM während einer HPLC-Reinigung eines Braunreisextrakts quantifiziert wurde, und Matrixeffekten, die während der anschließenden GC-MS-Analyse von Pestiziden im Extrakt gemessen wurden, wurde identifiziert. Dies deutet darauf hin, dass Trockenmassen-QCM ein wertvolles Werkzeug für den Analytiker sein kann überall wo eine HPLC-Aufreinigung routinemäßig durchgeführt wird, und daher vielen analytischen Bereichen zugutekommen kann.

Das vierte Kapitel untersuchte die Limitierungen und Möglichkeiten der HPLC-Aufreinigung mit Hilfe von C_{18}- und C_8-Phasen für Einzel- und Mehrfachanalytprobleme mithilfe Trockenmassen-QCM. Darüber hinaus wurde der Nutzen einer solchen optimierten HPLC-Aufreinigung für die Isotopenanalyse polarer Mikroschadstoffe untersucht, die typischerweise in Umweltproben vorkommen. Für Proben mit einem NOM-zu-Analyt-Verhältnis von ≥ 10 wurden starke Isotopenverschiebungen von bis zu 3.3 ‰ in Richtung der Isotopensignatur von NOM beobachtet. Dank QCM war eine Optimierung der Matrixentfernung auf bis zu 97% für früh und 99,8% für spät eluierende Verbindungen möglich. Die Effizienz der HPLC-Aufreinigung verschlechterte sich, wenn zwei oder drei Verbindungen gleichzeitig aufgereinigt werden sollten, was zu einer um bis zu 2,5% geringeren Entfernung von NOM führte. Unsere Ergebnisse legen nahe, dass eine optimierte HPLC-Aufreinigung durch systematisches Screening von 3 bis 5 verschiedenen Gradienten erreicht werden kann, wodurch die Grenzen einer genauen Kohlenstoff-CSIA um bis zu zwei Größenordnungen hin zu niedrigeren Mikroschadstoffkonzentrationen verschoben werden kann.

Insgesamt unterstreichen die Ergebnisse dieser Arbeit die Bedeutung (i) geeigneter Nachweistechniken für die spezifischen Anforderungen analytischer Aufgaben und (ii) optimierter, hochselektiver und automatisierter Aufreinigungstechniken für die Probenaufreinigung, um das volle Potenzial von CSIA auszuschöpfen. Insbesondere erwies sich Trockenmassen-QCM als erfolgreich bei der Online-Quantifizierung der gesamten extrahierten Probenmatrix während der RP-HPLC-Aufreinigung und erhöhte so enorm den Prozentsatz an NOM, der in einem Reinigungsschritt entfernt werden kann. Trockenmassen-QCM ebnet den Weg zur effizienten Entwicklung optimierter Aufreinigungsstrategien für verschiedene Aufreinigungsprobleme unter Verwendung einer Vielzahl von Festphasenmaterialien und -modi für die Flüssigchromatographie. Die Verwendung einer optimierten chromatographischen Aufreinigung in Kombination mit kürzlich entwickelten selektiven Extraktionsverfahren wird in Zukunft dazu beitragen, das Anwendungsspektrum von CSIA auf Verbindungen zu erweitern, die in realen Proben im niedrigen bis mittleren ng/L-Bereich vorhanden sind, und so Einblicke in Umwelt- und biologische Prozesse und forensische Fälle zu ermöglichen, die noch nicht zugänglich waren. Darüber hinaus ist die Möglichkeit der Online-Quantifizierung sowohl des Zielanalyts als auch der Probenmatrix während RP-HPLC ein großer Schritt hin zu einer vollautomatischen Methodenentwicklung und -optimierung zur Vorbereitung von CSIA.

List of Publications

Parts of this doctoral thesis have been published or submitted to peer-reviewed scientific journals:

1. **Christopher Wabnitz**, Aoife Canavan, Wei Chen, Mathias Reisbeck, and Rani Bakkour. Quartz Crystal Microbalance as Holistic Detector for Quantifying Complex Organic Matrices During Liquid Chromatography: 1. Coupling, Characterization, and Validation. *Analytical Chemistry* **2024**, *96*, 7429–7435.

2. **Christopher Wabnitz**, Wei Chen, Martin Elsner, and Rani Bakkour. Quartz Crystal Microbalance as Holistic Detector for Quantifying Complex Organic Matrices During Liquid Chromatography: 2. Compound Specific Isotope Analysis. *Analytical Chemistry* **2024**, *96*, 7436–7443.

3. Rani Bakkour and **Christopher Wabnitz**, and David Glöckler. Lack of selectivity in sample preparation – An achilles heel of compound-specific isotope analysis for environmental micropollutants. *Trends in Analytical Chemistry* **2024**, *180*, 117908.

Co-author contributions beyond the scope of this doctoral thesis:

1. David Glöckler, **Christopher Wabnitz**, Martin Elsner, Rani Bakkour. Avoiding Interferences in Advance: Cyclodextrin Polymers to Enhance Selectivity in Extraction of Organic Micropollutants for Carbon Isotope Analysis. *Analytical Chemistry* **2023**, *95* (20), 7839-7848. DOI: 10.1021/acs.analchem.2c05465

2. Gabriel Sigmund, Stephanie Castan, **Christopher Wabnitz**, Rani Bakkour, Thorsten Hüffer, Thilo Hofmann and Martin Elsner. NO_2 and natural organic matter affect both soot aggregation behavior and sorption of *S*-metolachlor. *Environmental science. Processes & impacts* **2019**, *21*, 1729-1735. DOI: 10.1039/c9em00354

Student Research Supervised During This Work

The following student reports contain data contributing to the research presented in this dissertation. I have supervised all internships and theses.
Research internships:

1. David Kostadinov (2020), Towards the Synthesis of Molecularly Imprinted Polymers with a Grafting Approach for Sample Preparation in Automated Solid Phase Extraction.

2. Wei Chen (2021), Improvement of Molecularly Imprinted Polymer Solid Phase Extraction for Environmental Organic Pollutants by Derivatizing Natural Organic Matter.

3. Malte Kubisz (2022), Matrix Effect of Pesticides on Gas Chromatography – Mass Spectrometry caused by Natural Rice and Natural Organic Matter Matrices.

4. Carmen Pedri (2022), Possibilities and Limitations of GC and HPLC Sample Purification for GC/C/IRMS Measurements.

Master's thesis:

1. Aoife Canavan (2021), Quartz Crystal Microbalance as a Tool for Online Monitoring of Natural Organic Matter during Clean-Up of Organic Extracts.

2. Wei Chen (2022), The Application of Online Matrix Monitoring during HPLC Purification Using Dry Mass Sensing on a Quartz Crystal Microbalance.

Contents

1 General Introduction

Parts of the introduction were published in a modified form in a peer-reviewed journal.

Reprinted with permission from:

Rani Bakkour and **Christopher Wabnitz**, and David Glöckler. Lack of selectivity in sample preparation – An achilles heel of compound-specific isotope analysis for environmental micropollutants. *Trends in Analytical Chemistry* **2024**, *180*, 117908.

1.1 Compound-Specific Isotope Analysis

Numerous research fields, from forensic to environmental sciences, benefit from information about the variation of stable isotope abundances (e.g. by measuring $\delta^{13}C$ as the ratio of ^{13}C and ^{12}C) in (bio)chemical substances.[1–10] These isotopic variations can have different origins: (i) Different processes or raw materials in the synthesis of the compounds or (ii) transformation processes that act on these chemicals, including chemical reactions, biological processes, or phase transfer. (i) In case of a different synthesis, the relative abundance of isotopes can provide information like a fingerprint that can distinguish a different provenance of otherwise identical chemicals.[11–15] (ii) In contrast, isotope ratios change during transformation processes. These changes over time are like a footprint left by reaction-specific kinetic isotope effects that give insight into the path by which the compounds are transformed.[16–20] Measuring the isotopic signature of a compound with high precision requires Isotope Ratio Mass Spectrometry (IRMS).[21–24] The ability to distinguish different sources of the same compound makes IRMS unique; the information gained is challenging to acquire from concentration measurements or other techniques.

To achieve high trueness with IRMS, isotopic values must be measured relative to a reference standard. Further, it is necessary to combust the compound of interest into a universal analyte, in the case of carbon measurements to CO_2.[6,21–23] The downside is, however, that the structural information gets lost during this process, and thus, only bulk measurements are possible. Coupling gas chromatography (GC) with IRMS revolutionized the field in the late 70s/ early 80s by providing the separation power to move from bulk isotope analysis to compound-specific isotope analysis (CSIA).[21–23] Later, other chromatographic techniques were hyphenated with IRMS, such as liquid chromatography (LC) in 1991.[25] The ability to separate compounds and measure compound-specific isotope ratios opened various applications with different timescales that would not have been accessible otherwise. Paleo-/ geochemists use CSIA to reconstruct paleoclimate profiles by measuring variations in $\delta^{13}C$ of biomarkers, like plant waxes preserved in fossils.[8,26,27] In doping analysis, GC-IRMS is used as a confirmation procedure to prove exogenous administration of endogenous anabolic androgenic steroids by utilizing depleted $\delta^{13}C$ values in synthesized steroids.[28,29] In environmental sciences, CSIA helps to identify the source and the fate of micropollutants, their degradation products, and pathways by measuring isotope fractionation.[3,30–33] In food analysis, CSIA can be used for authentication purposes.[9,34–36]

1.2 Analytical Challenges of Real-World Applications of CSIA

Despite these enormous advances, the separation power provided by GC is insufficient for many real-world applications to separate the target analyte and other components present in the sample, known as the sample matrix. An incomplete separation can lead, however, to biased isotope values since (i) the IRMS is not able to distinguish between CO_2 from the analyte and from the sample matrix with the same retention time and

(ii) since the isotope ratio varies over the chromatographic peak due to vapor pressure isotope effects.[2,21,37–41] Consequently, correction techniques used in conventional mass spectrometry to account for adverse effects of matrix compounds using, for example, curve fitting to restore overlapped peaks,[41] internal standards,[42–45] analyte protectants,[46,47] or matrix-matched calibration,[42,45,48] can not be used in CSIA. To guarantee accurate CSIA, there is thus no substitute for complete baseline separation during GC. Bakkour et al.[49] and Glöckler et al.[50] observed for a typical water sample containing environmental micropollutants isotopic shifts in carbon CSIA due to incomplete baseline separation during GC. These isotope shifts occurred as soon as there was ten times more carbon from matrix substances than from the target analyte in the sample extract that was injected into GC-IRMS. Consequently, samples containing higher amounts of matrix often necessitate further purification measures.

On the one hand, such measures can involve increasing chromatographic resolution using longer columns[51] or hyphenated multi-dimensional chromatography instead of one-dimensional chromatography.[34,52–55] On the other hand, suitable sample preparation is often crucial to get rid of matrix components before injecting the sample into the GC-IRMS.[2,3,5,50,56] In contrast to its importance, however, sample preparation in CSIA is pursued on a case-by-case basis rather than systematically and is still underdeveloped. Consequently, the applicability of CSIA is limited by matrix interferences in real-world samples and the lack of suitable sample preparation strategies to remove them.

1.2.1 Case Study 1: Limited Field-Applicability of CSIA for Non-Volatile Compounds

In few applications, limitations by matrix interferences are as prominent as in extracts from soil and water samples. Here, CSIA in environmental contaminant chemistry, therefore, serves to show how these limitations affect the real-world applicability of CSIA and which analytical challenges need to be overcome. For this purpose, more than 600 publications from isotope analysis in environmental chemistry (see Table A.1) have been evaluated by grouping them into classes of compounds and plotting them according to their air-water partitioning, using Henry‘s law constant, and octanol-water partitioning as a proxy for their distribution in different environmental compartments (see Figure 1.1). The publications in every group are classified as work on new methods to measure a given compound with isotope analysis (method, grey circles), as a study on the lab scale (lab, green circles), or as a field study using real-world samples (field, black circles).

It becomes apparent from Figure 1 that most of the work on CSIA in environmental contaminant chemistry was published on volatile organic compounds present in the air-water or air-water-soil compartment such as BTEX (e.g., benzene) or volatile chlorinated aliphatics (e.g., trichloroethene). There is, however, not just a difference in the total number of papers published on volatile compounds (i.e., volatile chlorinated aliphatics: 266) and non-volatile compounds present in the water or soil compartment (i.e., pesticides: 57), but also a difference in the ratio of studies on method development (grey) and laboratory studies (green) in comparison

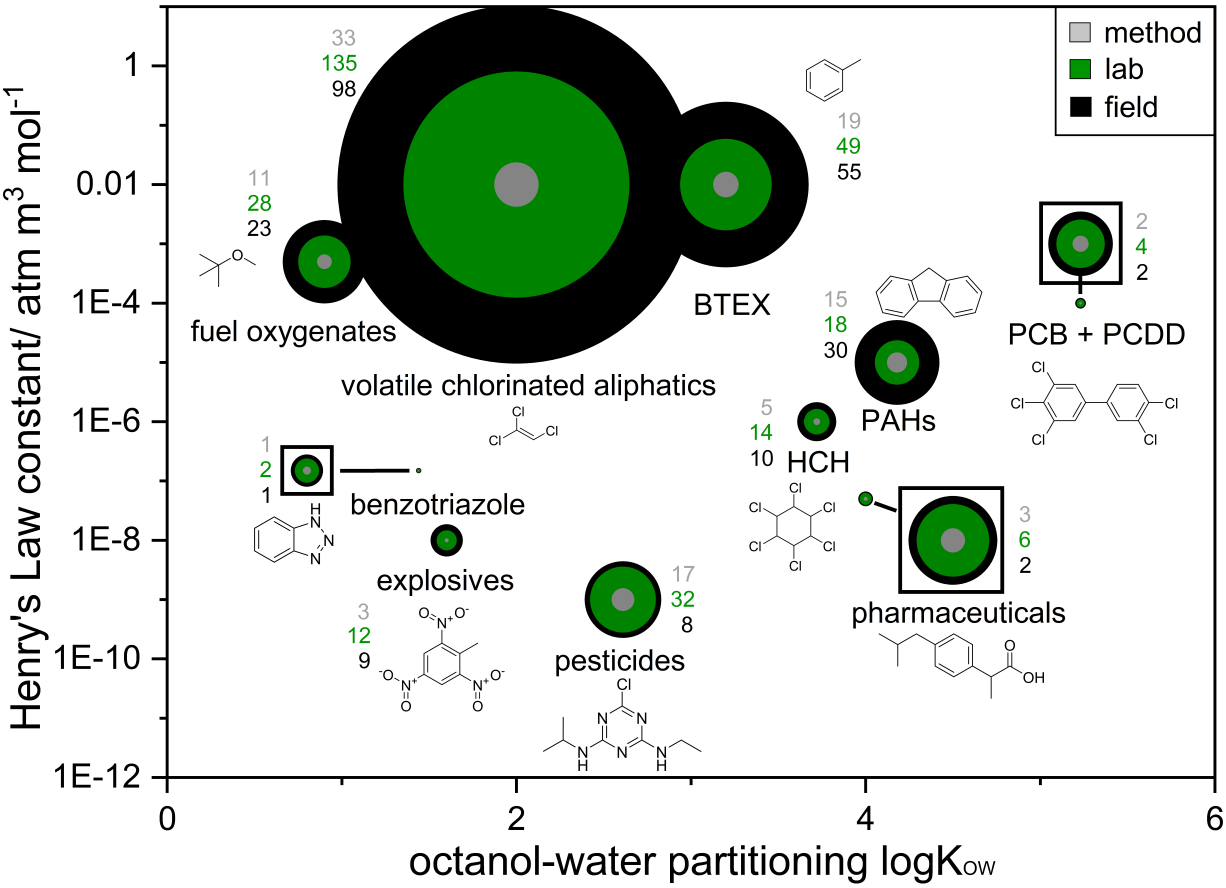

Figure 1.1 Number of published papers of different compound classes in the environmental sciences subdivided into publications on method development (grey), laboratory studies (green), and field studies (black). The size of each bubble correlates to the amount of papers published. Compound classes with fewer than 15 publications are enlarged by factor 6 for better visibility (bubbles in frames). BTEX: aromatic hydrocarbons benzene, toluene, ethylbenzene, and xylene, PCB: polychlorinated biphenyl, PCDD: polychlorinated dibenzodioxins, PAH: polycyclic aromatic hydrocarbon, HCH: hexachlorocyclohexane. Source: Kuntze et al.[57] and Web of Science. Publications were considered till 04.10.2023. All publications together with their classification are listed in Table A.1.

to field studies (black). While there is nearly an equal number of publications on method development and laboratory studies in comparison to field studies available for volatile compounds (ratio (lab+method)/field: fuel oxygenates: 1.7, volatile chlorinated aliphatics: 1.7, BTEX: 1.2), field studies are scarce for non-volatile compounds (ratio: pesticides: 6.1, pharmaceuticals: 4.5). There are two main reasons for this predominance of field studies on volatile compounds: (i) The contaminant concentration in the field relative to the matrix concentration and (ii) available sample preparation strategies to separate the contaminant from the sample matrix.

(i) Many of these volatile compounds were ubiquitously used as solvents in the past and, therefore, correspond to priority pollutants at contaminated sites, where they occur at concentrations ranging from mg/L to even g/L.[58–61] The sample matrix, namely natural organic matter (NOM), is present in environmental water samples in the low mg/L range and thus in lower or equal concentrations than the volatile contaminants. In contrast, pesticides and pharmaceuticals usually occur at a ng/L to µg/L range and thus at 10^3 to 10^6 lower concentrations than NOM.[62] (ii) Separating volatile compounds from other matrix components is straightforward using the Purge and Trap (P&T) technique. In P&T, volatile compounds are purged from the sample by a gas stream and then concentrated in a trap, while matrix interferences are left behind.[2,63,64] To measure non-volatile compounds using GC-IRMS, they are extracted from the environmental sample using, for example, solid-phase extraction (SPE).[50,65,66] Their low natural abundance, in combination with the method detection limits (MQL) of carbon CSIA on GC-IRMS ($\geq$ 0.8 nmol C on column), make the extraction of several liters of water necessary.[2,37,62,67,68] High amounts of NOM are potentially co-extracted and must be removed using further purification steps.[50,69]

1.2.2 Case Study 2: Tediousness of Sample Preparation for Non-Volatile Compounds

In the recent two decades, sample preparation strategies were developed to purify extracts containing high amounts of matrix in several fields of CSIA. Various purification techniques are utilized in these strategies, ranging from liquid-liquid extraction (LLE)[26,28,70,71] to several types of chromatography, including size-exclusion,[72] silica gel,[73,74] ion-exchange chromatography,[70] or the most commonly used reversed-phase (RP) high-performance liquid chromatography (HPLC).[28,66,68,75–79] Frequently, the high amount of matrix co-extracted during the sample extraction (see Figure 1.2, light blue) in combination with the heterogeneity of the sample matrix — NOM consists, for example, of thousands of different organic compounds[80] — renders the separation of the target analyte and matrix interferences challenging using only one purification step (see purification steps in brown colors in Figure 1.2). In doping analysis, eight steps, including two HPLC clean-up steps, are used to extract steroids from urine, to purify the extract, derivatize the steroids, and accurately measure them using GC-IRMS.[28] The required time to process one sample for the final isotope measurement using this eight-step procedure can be up to two days, which shows how time- and labor-intensive the sample preparation

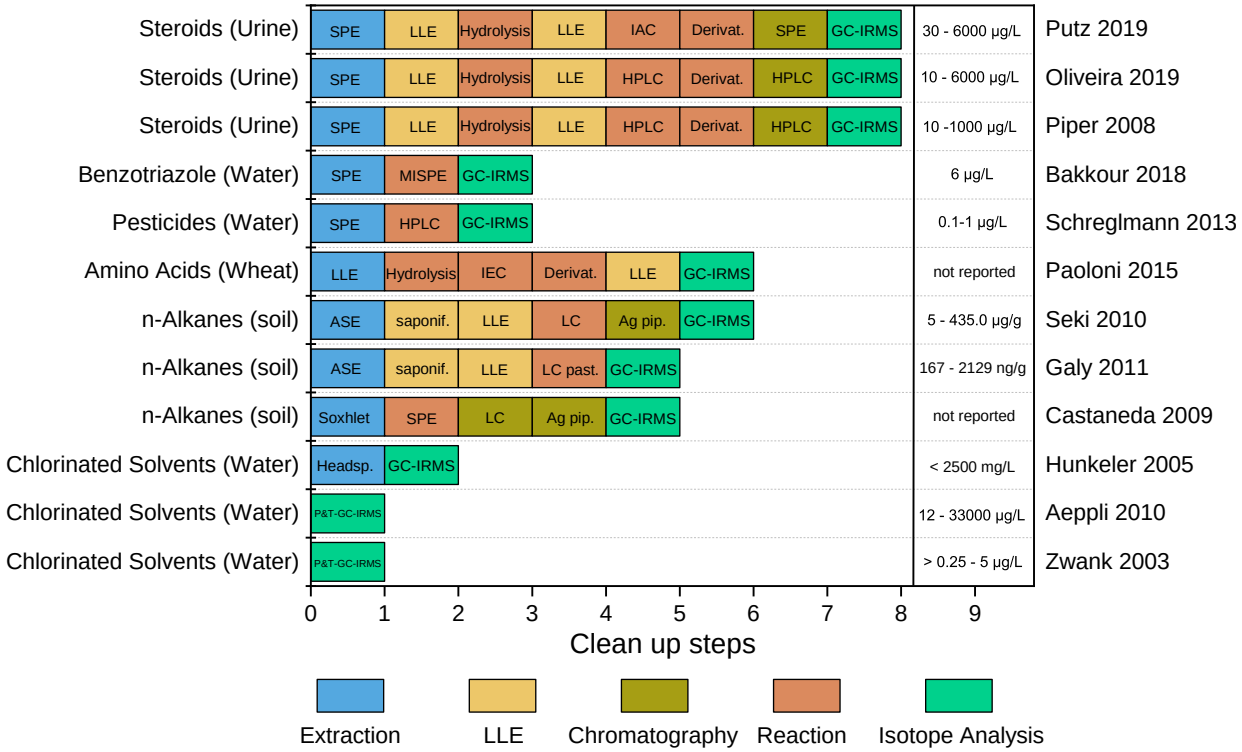

Figure 1.2 Comparison of the number and the type of sample preparation steps used in established sample preparation techniques in the environmental sciences (pesticides, 1H-benzotriazole, chlorinated solvents), food science (amino acids), geosciences (*n*-alkanes), and doping analysis (steroids). Sampling steps are not included. The concentration of the target analyte in the sample is reported on the right side of the diagram. Abbreviations: SPE: solid phase extraction, LLE: liquid-liquid extraction, IAC: immunoaffinity chromatography, Derivat.: Derivatization reaction, HPLC: preparative HPLC, MISPE: molecularly imprinted solid phase extraction, IEC: ion-exchange chromatography, ult. extr.: ultrasonic extraction, urea reac.: urea reaction, ASE: accelerated solvent extraction, saponif.: saponification, LC: liquid chromatography, Ag pip.: Ag^+ impregnated silica pipette, LC past.: LC on a pasteur pipette, Soxhlet: Soxhlet extraction, Headspace: headspace extraction, P&T-GC-IRMS: Purge and Trap coupled to GC-IRMS.

of non-volatile compounds for CSIA can be.[28,81] On the contrary, the sample purification of volatile compounds using P&T hyphenated to GC-IRMS is a fast, wholly automated one-step process (see Figure 1.2, chlorinated solvents (water)).[2,60,63,64] Furthermore, it is not only the sample preparation that is time-consuming but also the development of a tailor-made multi-step solution as used in doping analysis.

To reduce the time of both sample preparation and method development and enable field measurements of non-volatile compounds present in the sample matrix in low concentrations, optimized, highly selective purification steps are warranted to reduce the overall number of purification steps. In recent years, efforts have been put into optimizing the selectivity of each sample preparation step. For instance, Glöckler et al.[50] optimized the initial extraction of aquatic micropollutants. Using cyclodextrin polymers as selective SPE sorbent instead of commercially available sorbents (i.e., Oasis HLB), it was possible to reduce the amount of co-extracted NOM by a factor of 7.5, which reduced GC-IRMS backgrounds significantly.[50,82,83] Other works investigated new selective materials to enhance the selectivity of purification steps of the sample extract, using, for example, molecularly imprinted polymers (MIPs)[49,56] or immunoaffinity sorbents.[81] Using these optimized procedures, it was possible to extend the applicability of CSIA to micropollutants in the environment present in the high ng/L to low µg/L range. To enable CSIA of real-world samples for compounds present at even lower concentrations (low to mid ng/L range) or present in samples containing higher amounts of the matrix (i.e., wastewater, food, biological samples), additional optimization approaches of sample purification for target analytes are warranted. To fill this gap, novel strategies to optimize the selectivity of sample purification for CSIA are outlined in the following chapters.

1.3 Strategies to Optimize Matrix Removal During CSIA Sample Preparation

1.3.1 Influence of Charge on Non-Specific Sorption of Matrix During MISPE

One strategy to optimize the selectivity of CSIA sample preparation and thus reduce the number of steps needed to purify the sample for accurate isotope measurements is to use a highly selective sorbent like MIPs. MIPs possess specific recognition sites that can extract target molecules in a very selective way.[84–90] These recognition sites are tailored to the analyte of choice during the synthesis, where a three-dimensional polymer network is created around them or a similar molecule. In this way, a cavity that has complementary shape, size, and chemical binding sites to the analyte is produced.[88–92] While MIPs are frequently used in, for example, chromatographic separation,[93–95] as (bio)sensors,[96–98] or in drug delivery,[99–101] only recently they have been utilized in CSIA sample preparation for the first time.[49,56] Bakkour et al.[49,56] developed successful sample preparation strategies for CSIA for three classes of compounds involving MIPs, namely benzotriazoles, triazines, and glyphosate, demonstrated their purification power with significantly reduced backgrounds in GC-IRMS chromatograms and matrix to analyte ratios before and after the purification, and outlined strategies to

assess and circumvent challenges of MIPs for CSIA regarding potential isotope fractionation or the inherent low capacity of MIPs.

Even though MIPs are a powerful purification tool, they potentially co-extract matrix components due to non-specific binding of matrix components on the MIP polymer.[102,103] Assessing and reducing this non-specific binding is crucial to maximize matrix removal during MIP purification steps for CSIA. While there is much literature available on reducing non-specific binding by optimizing the MIP synthesis, including functional monomers, reaction conditions, and treatments to block the accessibility of functional groups on the MIP surface or optimizing molecularly imprinted solid phase extraction (MISPE) procedures, to date the underlaying processes that govern the non-specific sorption of the matrix are not studied systematically but rather on a case by case basis.[90,91,104–107] Despite its importance for the sorption of matrices,[80,108,109] little is known, for example, about the role of charge on non-specific binding of the sample matrix during molecularly imprinted solid phase extraction (MISPE). However, improving our understanding of these underlying mechanisms has the potential to help reduce non-specific binding in the future and thus significantly increase matrix removal during MISPE before CSIA.

1.3.2 Improving Chromatographic Purification by Monitoring both the Target and the Matrix

While MIPs are a promising novel strategy to remove matrix components selectively during CSIA sample preparation, the most often used strategy for this purpose is RP HPLC.[28,66,68,75–79] RP HPLC is a versatile and powerful purification technique suitable for a wide range of analytes.[110–113] While the RP HPLC purification is fully automated, the method development of the purification of analytes present in organic extracts is often tedious and challenging. This is the case since there is no straightforward way to monitor and quantify the sample matrix online during RP HPLC. Monitoring both the target analytes and the sample matrix online is, however, necessary to optimize their respective separation during the HPLC purification optimally and efficiently and to thus use the full potential of the purification power of RP HPLC for CSIA sample preparation. For the online monitoring of organic target analytes, detectors commonly hyphenated with HPLC, like UV-Visible spectrometry (UV/Vis), fluorescence spectrometry, or MS, can be used. In contrast, these detectors can not be used for the online quantification of the sample matrix. UV/Vis, fluorescence, or MS can only measure certain fractions of the matrix that are either chromophoric, fluorescent, or ionizable.[114,115] Other detectors that are considered to be semi-universal, like (i) the total organic carbon (TOC) analyzer, (ii) the charged aerosol detector (CAD), or (iii) the evaporative light-scattering detector (ELSD), have other shortcomings: (i) The TOC analyzer can only measure the carbon content of compounds that are soluble in water.[114,115] (ii) + (iii) The ELSD and the CAD detector can measure all non-volatile compounds but show inter-compound response differences (ELSD: deviations higher than 50%, CAD: up to 11%), thus prohibiting the quantification of the

sample matrix during RP HPLC.[116–118] There is thus a need for a novel detection technique that can be coupled to RP HPLC and can quantify the entirety of the sample matrix online during chromatographic purification in a robust way. Such a detector would enable the optimization of the separation of the target analyte and the sample matrix during the HPLC purification and, thus, improve the selectivity of the respective purification step.

1.3.3 Strategies for Quantifying Complex Organic Matrices During Liquid Chromatography using Quartz Crystal Microbalance

Quartz Crystal Microbalance: Theoretical Background

The most straightforward way to measure the mass of the matrix online during a chromatographic run is by using a detector that can measure mass directly and does not rely on other principles such as absorption or ionization, which can vary from compound to compound. Since the mass measurement should be at the same time as sensitive as possible, the quartz crystal microbalance (QCM) holds potential as a promising detector with its sub-nanogram resolution.[119,120] The QCM is a resonator consisting of a quartz crystal, which can be excited electrically to resonate acoustically due to its piezoelectric nature.[119,120] For QCM measurements, AT-cut crystals that vibrate in the thickness-shear mode are used.[119,120] When the acoustic wave produced by the excited crystal is in resonance, the deformation is a standing wave with the crystal surface at the antinodes.[119,120] This standing wave can be described using Eq. 1.1.

$$f_\mathrm{r} = \frac{c_\mathrm{q}}{\lambda} = \frac{c_\mathrm{q}}{2d} \tag{1.1}$$

Here, f_r is the resonance frequency of the vibrating crystal, c_q is the speed of sound in quartz, and λ the wavelength of the sound.[120] Since λ is two times the crystal thickness d, f_n is inversely proportional to the crystal thickness. If mass is deposited on the sensor crystal in the form of a rigid film — a very thin film where the acoustic wave propagates through without energy loss —, the acoustic thickness increases and can now be described by Eq. 1.2, where d_q is the original thickness of the quartz crystal and d_f the film thickness.[120]

$$f_\mathrm{r} = \frac{c_\mathrm{q}}{2d} = \frac{c_\mathrm{q}}{2(d_\mathrm{q} + d_\mathrm{f})} \tag{1.2}$$

From this equation, one can derive the Sauerbrey equation (see Eq. 1.3, see Johannsmann et al.[120] for the exact mathematical steps), which can be used to calculate the deposited mass on the sensor crystal.[121]

$$\Delta m = -\frac{A\sqrt{\rho_\mathrm{q}\mu_\mathrm{q}}}{2{f_0}^2}\frac{\Delta f}{n} \tag{1.3}$$

Here, the mass change Δm is calculated using the active area of the sensor crystal (A), the density (ρ_q), the fundamental frequency (f_0, e.g., 5 MHz) and the shear modulus (μ_q) of the quartz crystal, Δf, which is the

resonance frequency change, and the overtone order (odd) of the standing wave n. All constants (ρ_q, f_0, μ_q) can be summarized using the mass sensitivity coefficient C (see Eq. 1.4), which is 17.7 ng/(cm^{2}Hz) for 5 MHz quartz crystals and 4.42 ng/(cm^{2}Hz) for 10 MHz quartz crystals.[120]

$$\frac{\Delta m}{A} = -C\frac{\Delta f}{n} \tag{1.4}$$

Since shear waves decay rapidly in gas and liquid media and since, for the Sauerbrey equation, the deposited mass layer must be rigid, and the deposited mass small in comparison to the mass of the sensor, next to the frequency, the overall energy loss is usually measured.[119,120] Information about the energy loss can be gained from measuring the dissipation (D), which is the sum of all energy losses, or the bandwidth of the resonance (Γ), which is proportional to the dissipation (see Eq. 1.5).[120]

$$\Delta\Gamma = \frac{f_0}{2}\Delta D \tag{1.5}$$

The Sauerbrey equation can only be used to measure mass changes if the shift in the bandwidth is much smaller than the frequency change (see Eq. 1.6).[119,120]

$$|\Delta\Gamma| << |\Delta f| \tag{1.6}$$

If Eq. 1.6 is not valid, viscoelastic modelling can be used, which necessitates the measurement of several overtones.[119,120,122]

Quartz Crystal Microbalance: Different Interfaces for Different Measurements

Depending on the exact interface used, different parameters for the energy loss are measured, and information is gained to interpret the QCM measurement. There are three different ways to perform QCM measurements to get a resonance frequency and an output parameter for the energy loss, namely using (i) an oscillator circuit, (ii) impedance analysis, or (iii) the ring-down method. In this thesis, a QCM with resistance measurement (QCM-R) based on (i) and a QCM with dissipation monitoring (QCM-D) based on (iii) are used. One requirement for all measurement approaches is that the quartz crystal is coated with electrodes made frequently of gold. (i) A simplified model (Butterworth-van Dyke electrical model) of the oscillator circuit can be seen in Figure 1.3a, where R_m is a resistor, C_m a capacitor, L_m an inductor, C_0 the parasitic capacitance, AMP an amplifier, and R_L a load resistor. For a more detailed illustration of the oscillator circuit, see Arnau et al.[123] For sensing applications, a frequency counter must be added to the oscillator circuit. While this technique is the cheapest of the three, it has several disadvantages: The bandwidth can only be measured indirectly using the motional resistance, which prevents an absolute quantification of energy losses and allows only the acquisition of relative data. Further, it is not well suited for liquid sensing since only one harmonic is measured, and thus, data interpretation is severely

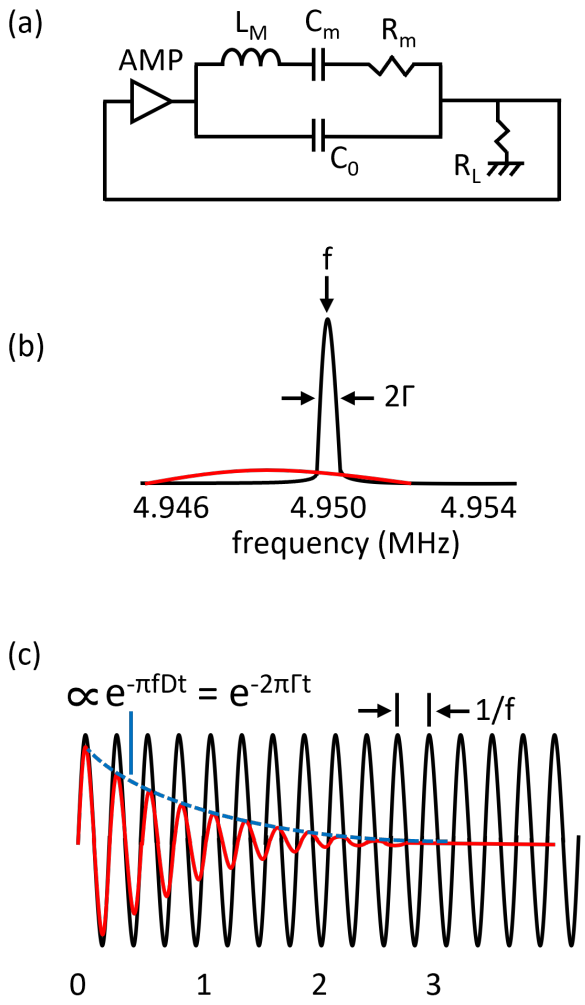

Figure 1.3 (a) QCM-R: Simplified oscillator circuit model, where R_m is a resistor, C_m a capacitor, L_m an inductor, C_0 the parasitic capacitance, AMP an amplifier, and R_L a load resistor. In this thesis, a QCM-R is used for dry-mass sensing. (b) QCM-I: Frequency and bandwidth are determined using the resonator‘s electrical impedance, which is acquired by measuring different frequencies near resonance. (c) QCM-D: Ring-down method, where the frequency and the dissipation are determined by intermittently switching the driving voltage on and off using the decay of the oscillation and the generated voltage during the decay. In this thesis, a QCM-D is used for liquid sensing. The scheme is adapted from Ref.[119,120]

limited. In contrast, due to its superior measurement stability, the oscillating circuit approach is the method of choice for gravimetric sensing in air on one overtone.[120,124] (ii) In the impedance analysis, the frequency and the bandwidth are determined using the resonator‘s electrical impedance, which is acquired by measuring different frequencies near resonance (see Figure 1.3b).[123] Impedance analysis is especially suited for complex experimental setups since measurement interferences can be identified using the impedance curve.[120] (iii) In the ring-down method, the frequency and the bandwidth are determined by intermittently switching the driving voltage on and off. The oscillation of the quartz crystal decays while the driving voltage is off (see Figure 1.3c), and another voltage is generated due to the piezoelectric nature of the quartz crystal, which can be measured and transferred into the frequency and the dissipation, which is equivalent to the bandwidth.[119,125] In this way, several overtones can be measured quickly, enabling viscoelastic modeling and thus the measurement and interpretation of complex samples in vacuum, air and liquid media.[120,125]

Using these different measurement techniques, the QCM has been used in the last decades for various applications, including the sensing of small molecules, proteins, bacteria, or lipids in both gas and liquid phases, the investigation of the formation or deposition of membranes, polymer films, and other composites like MOFs, and the behavior of films under different conditions.[122,126–130] Two different strategies could enable the QCM to monitor matrix compounds online during the RP HPLC purification of an organic extract prior to GC-IRMS. Firstly, a part of the HPLC eluate could be passed over the QCM sensor coated with a polymer, on which the matrix can sorb to. Secondly, a rigid film could be produced by spraying a part of the HPLC eluate onto the QCM sensor and immediately evaporating the solvents using a gas stream to enable dry-mass sensing in the gas phase. Both strategies could enable the quantification of matrix substances in the HPLC eluate at each time point of the measurement. They, including potential challenges, research gaps, and ways to overcome them, are discussed in detail in the following sections of this chapter.

Strategy 1: Liquid Sensing Using a Polymer Coated QCM Sensor

The first strategy is based on QCM liquid sensing, which is one of the most frequently used techniques to study interactions between compounds in a liquid phase and materials coated on the QCM sensor.[122,126–130] Here, the QCM crystal is fully immersed in a liquid media, which is passed over it. The sorption of different types of analytes onto the QCM crystal, or most of the time onto a crystal coating, can be measured using the frequency change during the sorption process. Thus, the concentration of analyte in a solution can be determined. Different QCM sensor coatings are produced and studied for each analyte to observe the interactions during the sorption procedure. For NOM, a variety of model coatings were already investigated, including silica,[131] polystyrene,[131] aluminum oxide,[131–135] iron oxide,[131] hydroxyapatite,[131] poly(vinylidene) fluoride,[136] positively charged polyelectrolyte layer,[137–142] and self-assembled monolayers.[143,144] Even if many insights were gained using these model sorbents regarding the sorption behavior of NOM, they can not be used

for the quantification of the entirety of NOM during liquid chromatography, since (i) only certain fractions of NOM sorb onto these coatings (i.e., charged fractions)[131–135] and since (ii) the capacity of the different coatings is minimal.[131,134,136,143] To use liquid sensing for real-time quantification of matrices like NOM during an HPLC purification of a formerly extracted sample, a new sensor coating that can extract all NOM compounds present in the sample extract and has a higher capacity than available coatings must be developed. For this purpose, it is ideal to coat the sorbent used during the original extraction of the water sample on the QCM crystal. For the extraction of environmental water samples, frequently polystyrene-divinylbenzene (PS-DVB)-based polymers modified with a hydrophilic monomer are used.[69,145–148] Since these types of polymers are often hyper crosslinked and possess, therefore, a high capacity,[149] it seems ideal to coat a QCM sensor with a PS-DVB-based polymer modified with a hydrophilic monomer. Such a coated sensor could be used to quantify NOM in the liquid phase.

Strategy 2: QCM Dry Mass Sensing

The second strategy is based on QCM dry mass sensing, where the analyte-containing solution is sprayed onto the QCM sensor. During this process, the solvent evaporates, and the non-volatile matrix substances remain on the sensor. Their dry weight can be determined using the frequency change measured with the QCM.[150–153] While liquid sensing used in strategy 1 is frequently used in the field of QCM for many different studies, QCM dry mass sensing was introduced by Schulz and King in the 70s[150] but, however, only recently developed further and applied. In the last decade, microfluidic sprays were optimized to make dry mass sensing possible by Müller et al.[151] and Kartanas et al..[152] This development, together with technical advancement on the QCM,[120] made the first application of dry mass sensing possible. Kartanas et al.[153] coupled a QCM with the help of a microfluidic spray-dryer with aquatic size-exclusion LC for the separation and detection of proteins. While this system seems to be ideal for online monitoring of matrix compounds during HPLC purification prior to CSIA, several development steps need to be taken, and challenges need to be overcome: First, till now, QCM dry mass sensing has been used only for aquatic LC. For the purification of micropollutants for CSIA, RP gradient HPLC is necessary. Therefore, investigations must be conducted on how organic solvent gradients affect the spraying and measuring process. Secondly, while the system could successfully quantify proteins, it was never used for a mixture as complex as an environmental extract. Hence, the suitability of this measurement approach for such samples needs to be fully validated. Thirdly, a strategy for calibrating, processing, and evaluating the data needs to be developed.

1.4 Objectives and Approach

The overall goal of this work was to develop novel strategies to optimize the selectivity of sample purification for CSIA. This thesis specifically focused on MISPE, a promising purification strategy only recently applied to CSIA, and RP HPLC, the most frequently used purification strategy for CSIA.

Chapter 2, entitled *Influence of the Anionic Character of Natural Organic Matter on Sorption on Molecularly Imprinted Polymers*, investigates the influence of the anionic character of NOM on non-specific sorption of NOM during MISPE. To this end, (i) acidic NOM groups were methylated using trimethylsilyl diazomethane (TMSD), (ii) the change in the charge density of NOM was assessed, and (iii) the different behavior of NOM and methylated NOM determined during MISPE by constructing MIP breakthrough curves.

Chapters 3-5 systematically explore the feasibility of QCM liquid sensing and QCM dry mass sensing for online matrix quantification during RP HPLC, with the ultimate goal of using such a detector to optimize the separation of the target analyte and the sample matrix during the respective purification to improve the selectivity of the RP HPLC purification prior to CSIA. Chapter 3, entitled *Application and Preparation of Hydrophilic-Lipophilic Balance-Type Polymers Grafted on Quartz Crystal Microbalance Sensors*, focuses on developing a procedure to coat a QCM sensor with a hypercrosslinked DVB-based copolymer using ethylene glycol dimethacrylate (EGDMA) as a hydrophilic modifier to enable QCM liquid sensing of NOM. The chemical composition, thickness, and surface coverage of the coating were characterized using Fourier-transform infrared (FTIR), Raman spectroscopy, scanning electron microscopy imaging (SEM), and energy dispersive X-ray mapping (EDX). The interaction of NOM with the novel QCM coating was investigated using flow-based sorption experiments.

Chapters 4 and 5 explore the feasibility of coupling QCM dry mass sensing with RP HPLC for online quantification of organic matrix components during the respective chromatographic gradient purification. To this end, chapter 4, entitled *Quartz Crystal Microbalance as Holistic Detector for Quantifying Complex Organic Matrices During Liquid Chromatography: 1. Coupling, Characterization, and Validation*, lays the technical and fundamental groundwork for the matrix online monitoring using QCM dry mass sensing during RP HPLC. It systematically studies the connection, characterization, calibration, and validation of QCM dry mass sensing with RP HPLC. Moreover, the lower and upper limits of quantification were determined, and the applicability of HPLC purification of pesticides in brown rice for subsequent GC-MS residue analysis was evaluated.

Chapter 5, entitled *Quartz Crystal Microbalance as Holistic Detector for Quantifying Complex Organic Matrices During Liquid Chromatography: 2. Compound Specific Isotope Analysis*, applies QCM dry mass sensing coupled with RP HPLC to CSIA. Here, the limitations and enhancement of HPLC purification using QCM dry mass sensing on C_{18} and C_8 phases for single- and multiple-targets were investigated, and the impact on accurate $^{13}C/^{12}C$ analysis of polar micropollutants present in environmental water samples explored.

In the concluding chapter 6, the essential discoveries of this study are highlighted to form a comprehensive conclusion. Further, unresolved aspects that beckon further exploration in future research are identified.

2 Influence of the Anionic Character of Natural Organic Matter on Sorption on Molecularly Imprinted Polymers

2.1 Introduction

Organic and inorganic compounds present in real-world samples (i.e., environmental, biological) can prevent the accurate identification and quantification of organic target analytes in trace analysis and have a negative effect on the sensitivity of the detection.[3,88,112,154,155] The removal of these organic and inorganic compounds, known as sample matrix, during sample preparation is often considered to be the bottleneck of the analytical process.[88,154,156,157] To this end, molecularly imprinted polymers (MIPs) are frequently used as tailor-made sorbent materials to selectively extract or purify organic target analytes from the sample matrix. MIPs are customized, synthetically produced materials that show a high recognition of a target analyte due to their antibody mimicking structures.[84–90] In molecular imprinting, a three-dimensional polymer network is polymerized around a template molecule (i.e., the target analyte) using functional monomers and a cross-linker in the presence of a porogen. After the polymerization, the template is removed, leaving behind a cavity with complementary size, shape, and chemical binding sites to the template molecule, which acts with high selectivity as antibody mimicking recognition site.[88–92] In non-covalent imprinting, the recognition is driven by molecular interactions like van-der-Waals interactions, pi-pi stacking, ionic interactions, or hydrogen bridges.[84,90,91] The exact molecular interactions that are determinant for the recognition of a specific MIP impact the whole MIP solid phase extraction (MISPE) procedure: After the sample loading during MISPE, non-specifically bound matrix substances are washed off using a solvent mixture that at the same time cannot disrupt the specific analyte binding.[84,89,90] Increasing the selectivity of the MIP by, for example, reducing the non-specific binding of matrix compounds on the MIP and increasing their removal during the washing step is one of the current research focuses in the field of molecular imprinting.[90,91,104–107]

So far, the emphasis on enhancing selectivity by decreasing non-specific binding has been on optimizing the MIP synthesis (i.e., polymerization conditions, the choice of functional monomers, blocking agents) or optimizing MISPE procedure (i.e., washing solvent).[90,91,104–107] Designing a tailor-made MIP for a specific

target analyte and optimizing its selectivity by screening these different parameters is, however, a time- and labor-intensive procedure.[89,90,104] Therefore, gaining as much knowledge as possible on the factors governing the sorption of the matrix onto the MIP and desorption processes during the washing step using organic solvents is essential. While there is a lot of information available regarding the optimization of the MIP, the role of the matrix is usually not studied systematically but rather on a case-by-case basis.[90,91,104–107] Such a systematic study would, however, be beneficial for the understanding of sorption processes of matrices that occur in many different applications, like the environmental matrix natural organic matter (NOM).[49,56,108,158–160] NOM can be found in natural water or soil, consisting of thousands of different organic compounds with acidic functionalities like humic, fulvic, or hydrophilic acids.[80,161] The abundance of acids in NOM — especially in the form of carboxylic functional groups — leads to an anionic character due to their dissociation that is responsible for many characteristics of NOM, such as solubility, binding sites, electrostatic attraction/repulsion, and represents a significant factor in its sorption behavior.[80,108,109,162] Despite its importance for sorption processes, no literature is available on the role of its anionic character on the non-specific sorption on MIPs.

The overall goal of this work is to investigate the influence of the anionic character of NOM — and particularly the role of carboxylic acids — on non-specific sorption of NOM during MISPE. To study this influence, a masking approach using selective methylation of carboxy groups can give unique insights due to the possibility of directly comparing the sorption of NOM and masked NOM with a different charge.[163,164] To this end, we (i) methylated acidic NOM groups using trimethylsilyl diazomethane (TMSD), (ii) assessed the change in the charge density of NOM, and (iii) determined the different behavior of NOM and methylated NOM during MISPE by constructing breakthrough curves using DCM as washing solvent.

2.2 Experimental

2.2.1 Chemicals and Materials

A list of purchased chemicals, materials, and solvents used in this study is provided in the supporting information section B.1.

2.2.2 Extraction of NOM from River Water

River water samples (Wiesäckerbach, Garching, Germany, latitude 48.269009, longitude 11.667976) were passed through glass microfiber filter membranes (1.2 µm particle retention, 47 mm diameter, Whatman, UK). The filtrate was acidified to pH 3.0 using HCl (32%). NOM was subsequently extracted from the acidified sample under conventional SPE conditions at 5 mL/min using Oasis HLB SPE cartridges (Waters, 500 mg, 12 cc) and an automated SPE system (Smart Prep Extractor, Horizon Technology, USA). The Oasis HLB cartridges were dried overnight under vacuum and eluted using 5 mL of DCM containing 3% methanol. The eluates were

combined, the solvents evaporated, and NOM was reconstituted in methanol. The dissolved NOM was filtrated using a glass microfiber syringe filter (1.2 µm particle retention, 13 mm diameter, Whatman, UK) and stored at -18 °C.

2.2.3 Molecular Masking of NOM - Methylation Procedure

To methylate NOM carboxy groups, 5 mL methanol were added to 1 mg extracted NOM in a Teflon beaker. 100 µL of a 2 M TMSD solution in hexane were added to the solution, which was then stirred at room temperature for 1 h. Afterward, TMSD-hexane solution was added in increments of 100 µL every 30 min until a total volume of 600 µL was reached. See Figure B.1 for mechanistic details of the methylation reaction. Methanol and hexane were evaporated using a gentle stream of nitrogen at 50 °C, followed by 30 min evaporation at 105 °C to remove potential by-products.

2.2.4 Determination of Methylation Efficiency and Charge Density Change Using Acid-Base Titration

The carboxyl and phenolic content were estimated for the extracted NOM before and after the methylating procedure using acid-base titration according to a procedure used for samples of the International Humic Substances Society.[165,166] After organic solvents were removed from (methylated) NOM (3 mgC), 15 mL 0.1 M NaCl solution as background electrolyte was added in a Teflon beaker with 1-2 mL 0.1 M NaOH to reach pH 10. Afterward, the pH was adjusted to 3-3.3 using 0.1 M HCl. The titration was performed at 25 °C, which was maintained using a water bath under a nitrogen gas atmosphere. The titrant (0.1 M NaOH) was added in increments of 15 µL using a Multipipette (E3x, Eppendorf, Germany). The pH (stable for 7s with drift of no more than 0.01 pH units) was recorded after each titrant addition using a pH meter (Lab850, SI Analytics, Germany). The sample was titrated from the initial pH of 3-3.3 to a final pH of 10.5. At each titration point, the ionic strength (I) was calculated using Equation 2.1.

$$I = \frac{1}{2}([Na^+] + [Cl^-] + [OH^-] + [H^+] + \sum_i [Org_i^-]) \tag{2.1}$$

Here, the contribution of ionized functional groups of NOM to the ionic strength, $[Org_i^-]$, was approximated using the assumption that NOM consists of monoprotic acids. $[Org_i^-]$ during the titration can be thus calculated using the electroneutrality Equation 2.2.

$$\sum_i [Org_i^-] = [Na^+] - [Cl^-] - [OH^-] + [H^+] \tag{2.2}$$

I is, therefore, given by Equation 2.3.

$$I = [Na^+] + [H^+] \tag{2.3}$$

[Na^+] is the dilution-corrected concentration of the initial NaCl and the added NaOH. [H^+] was derived from the pH. To this end, the activity for the hydrogen ion (α_{H^+}) was calculated using the Davies Equation[167] with A=0.5, B=0.30 to obtain the activity coefficient for hydrogen ion, γ_H (see Equations 2.4, 2.5, and 2.6).

$$log\gamma_{H^+} = -0.5(\frac{\sqrt{I}}{1+\sqrt{I}} + 0.3I) \tag{2.4}$$

$$pH = -log_{10}\alpha_{H^+} \tag{2.5}$$

$$\alpha_{H^+} = \gamma_{H^+}[H^+] \tag{2.6}$$

These calculations were iteratively repeated till [H^+] change was smaller than 1%. The charge density (Q_{tot}/ meq g/C) can then be calculated using the concentration (c_a) and volume (v_a) of strong acid HCl added, the concentration (c_b) and volume (v_b) of strong base NaOH added, the total volume (V_{tot}), and the mass of carbon originating from NOM (m_{NOM}) in the titration cell (see Equation 2.7).

$$Q_{tot} = \frac{c_b V_b - c_a V_a + ([H^+] - [OH^-])V_{tot}}{m_{NOM}} \tag{2.7}$$

The carboxyl content can be estimated as the Q_{tot} value at pH 8 and the phenolic value as two times the change of Q_{tot} between pH 8 and pH 10.[80,166,168]

2.2.5 Impact of Methylation on NOM Retention during MISPE

Cartridges filled with 1 g triazine MIPs (Affinisep) were soaked with methanol from the bottom to guarantee a complete wetting of the MIP surface. The cartridges were sequentially conditioned with two times 5 mL methanol, two times 5 mL methanol/ formic acid (9/1 v/v), and three times 5 mL DCM. To quantify material bleed during MISPE, the cartridges were further washed using three times 5 mL DCM (bleed samples 1-3), one time 10 mL MeOH (bleed sample 4), one time 5 mL methanol/ formic acid (9/1 v/v), 3 times 5 mL DCM, 3 times 5 mL DCM (bleed samples 5-7), one time 10 mL MeOH (bleed sample 8), one time 5 mL methanol/ formic acid (9/1 v/v), and 3 times 5 mL DCM. The 5 mL sample consisting of either (i) 0.5 mgC NOM, (ii) 0.5 mgC NOM that was methylated using the previously described procedure, or (iii) a control, which included no NOM but was subjected to the same reaction conditions used for the NOM methylation, was passed over the MIP (sample 1). The MIP was then washed using 16 times 5 mL DCM (samples 2-17) and one time 10 mL methanol (sample 18). Afterward, the bleed sample eluates and the sample eluates were evaporated to dryness under a gentle stream of N_2 at 30 °C and reconstituted in 16 mL water using an ultrasonic lab homogenizer (UP200St, Hielscher, Germany; 5 min, power = 190 W, puls = 100%, amplitude = 100%). The organic carbon

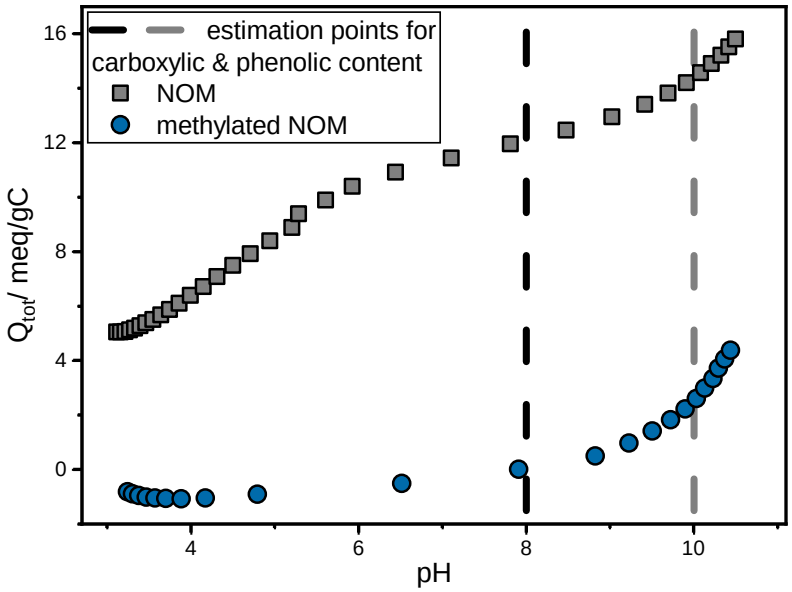

Figure 2.1 Titration data for NOM (gray) and methylated NOM (blue). The charge density is shown on the y-axis. All carboxyl groups are titrated at pH 8 (black dashed line), and all phenolic groups between pH 8 and 10 (difference between gray and black dashed line).

content was then determined in the reconstituted sample using a TOC analyzer (TOC-L, Shimadzu, Japan) equipped with a combustion catalytic oxidation reactor (680 °C) and a non-dispersive infrared detector.

2.3 Results and Discussion

2.3.1 Methylation Efficiency and Change in Charge Density

We assessed the change in charge density as a result of the methylation of NOM acidic groups and the overall efficiency and selectivity of the methylation of NOM carboxy groups using an acid-base titration. To this end, we assumed that the only two classes of proton-binding sites are phenolic and carboxylic hydroxy groups.[80,166,168] We titrated extracted NOM (gray) and, after the extraction methylated NOM (blue) from an initial pH of 3-3.3 to a final pH of 10.5 using 0.1 M NaOH, measured the pH after each 15 µL increment, and plotted the pH against the calculated charge density Q_{tot} (see Figure 2.1). All carboxyl groups are titrated at pH 8 (black dashed line), and all phenolic groups between pH 8 and 10 (gray and black dashed line).

We determined a carboxyl content in the extracted NOM (gray) of 12.1 meq/gC and a phenolic content of 4.7 meq/gC. These values are in the range of values found by the international humic substance society for other organic matter samples.[165,166] We observed a significant shift of the NOM titration curve to lower Q_{tot} values for the methylated NOM curve (blue). While the carboxyl content dropped from 12.1 meq/gC for NOM to 0 meq/gC for methylated NOM, the phenolic content (NOM: 4.7 meq/gC, methylated NOM: 5 meq/gC) stayed constant within our results' uncertainty of 0.4% according to triplicate measurements (see Figure B.2). This shows that the overall lower Q_{tot} values originate exclusively from changes in the carboxyl content. These results prove the

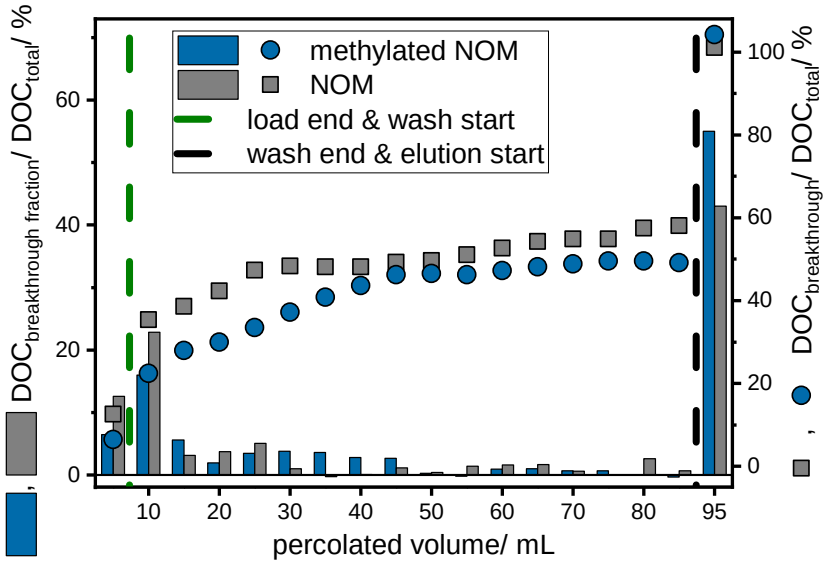

Figure 2.2 Breakthrough curves of NOM (gray) and methylated NOM (blue) on MISPE. After sample loading (green dashed line), the MIP is washed with 80 mL DCM in 5 mL increments, followed by a 10 mL methanol elution step (black dashed line). The percentage of DOC in each breakthrough fraction (bars, left y-axis) and the total breakthrough (dots, right y-axis) are shown.

success of the charge density reduction by methylating all carboxy groups present in the sample. They further confirm the selectivity of the used methylation procedure: Diazomethane methylates only carboxylic and acidic phenolic hydroxy groups; it does not react with weakly acidic phenolic or alcoholic groups.[163,169–171] The presented methylating procedure can thus significantly change the acidity and charge of NOM in a controlled manner.

2.3.2 Impact of Methylation on NOM Retention during MISPE

After the NOM carboxy groups were successfully methylated and the charge density significantly reduced, we investigated how NOM (gray) and methylated NOM (blue) retention behavior differs during MISPE. MISPE breakthrough curves (see Figure 2.2) were determined by washing the MIP after sample loading (green dashed line) with 80 mL DCM in 5 mL increments followed by a 10 mL methanol elution step (black dashed line); organic carbon present in the breakthrough was quantified using TOC analysis. In the case of the methylated NOM breakthrough curve, the control was used to subtract contaminations present in the sample originating from the methylating procedure (see Figure B.4). A complete mass balance was determined for both breakthrough curves (NOM: 101±4%, methylated NOM 104±4%), confirming the suitability of the approach to quantify organic carbon in the breakthrough.

Methylated NOM (blue) shows a stronger retention to the MIP, resulting in 55% methylated NOM remaining after the DCM washing procedure in comparison to only 43% remaining in the case of the untreated NOM (see Figure 2.2 gray square and blue dots before black dashed line). To explain the different sorption behaviors of methylated NOM and NOM, the (i) MIP-NOM interactions and (ii) DCM-NOM interactions play an essential

role. (i) The initial sorption of NOM to the MIP is caused by a variety of intermolecular interactions like hydrogen bridges, van der Waals forces, and ionic interactions.[49,56,80,108,109,158–160,162,172] While the MIP has strong hydrogen acceptor and hydrogen donor functions originating from both building blocks methacrylic acid (MAA) and ethylene glycol dimethacrylate (EGDMA) and the possibility to accommodate negative charge with the hydrogen donor function of MAA,[89,173–175] for NOM the hydrogen accepting functions in the form of ether and carbonyl groups dominate.[80,109,176,177] Since the hydrogen accepting function of NOM is not impacted by the methylation, the role of hydrogen bridges for the different behaviour of NOM and methylated NOM should thus be negligible. On the other hand, the more NOM sorbs onto the MIP, the higher the charge density will get on the surface of the MIP and thus the electrostatic repulsion that prevents more NOM to sorb.[80,177–180] In contrast, this effect is nearly wholly taken out of the picture by methylating NOM carboxy groups and reducing thus the charge density of NOM by a factor of 3.4, which leads to more methylated NOM sorbing onto the MIP as observed during the breakthrough curves.

(ii) The lower charge density did, however, impact not only the sorption of NOM onto the MIP but also the total desorption and the volume of DCM necessary to wash off all elutable fractions of NOM. During the first 10 mL percolated through the MIP, 1.6 times more NOM breaks through than methylated NOM (compare to Figure 2.2 gray and blue bars). Furthermore, while the elutable fraction of NOM broke through in the first 25 mL, it took nearly double the volume of DCM (45 mL) until the elutable fraction of methylated NOM broke through. This observation can again be explained using the reduced charge density: The higher the charge density, the more readily NOM will desorb and vice versa due to electrostatic repulsion.[80,177–180] DCM, with its weak hydrogen donor ability, can still interact with NOM‘s strong hydrogen acceptor functions, but it takes a higher volume to wash off all elutable fractions, and less total methylated NOM can be washed off.[181] These results show that methylation of NOM leads to higher non-specific binding of NOM during MISPE due to the change in charge density.

2.4 Conclusion

The current work investigates the influence of NOM’s anionic character on NOM’s non-specific sorption during MISPE by comparing breakthrough curves of NOM and methylated NOM. We demonstrate that the charge density of NOM can be significantly reduced by a factor of 3.4 by methylating NOM carboxy groups using TMSD. Breakthrough curves revealed that less methylated NOM, compared to untreated NOM, could be washed off the MIP using DCM during a MISPE procedure. This implies stronger MIP-methylated NOM interactions, which are most likely caused by the smaller charge density of the methylated NOM and the consequently smaller electrostatic repulsion between NOM molecules.[80,177–180] These results prove the importance of NOM’s anionic character for the sorption on MIPs and emphasize the influence of the charge of the sample matrix on non-specific sorption. Manipulating electrostatic repulsion between the MIP and the sample matrix, or compounds

sorbed onto the MIP and the remaining sample matrix, could help in the future to reduce non-specific binding and thus significantly increase matrix removal during MISPE.

3 Application and Preparation of Hydrophilic-Lipophilic Balance-Type Polymers Grafted on Quartz Crystal Microbalance Sensors

3.1 Introduction

Natural organic matter (NOM), which is produced from the decomposition of animal and plant biomass, is a key environmental aquatic component, which represents a very complex mixture of organic compounds like humic acids, fulvic acids, or hydrophilic acids.[80,161] The adsorption of NOM to surfaces and the sorption of compounds to NOM influence the properties of (i) NOM and the respective (ii) surface or (iii) compound. (i) The adsorption of NOM on surfaces prevents NOM degradation and alters the composition of NOM in solution due to preferential adsorption.[182–185] (ii) NOM sorption on particle surfaces affects the particle's deposition and coagulation behavior, while the sorption on membranes causes membrane fouling.[186–190] (iii) Compounds sorbing onto NOM often show altered properties regarding their degradation or transport behavior.[191–195] Since (i-iii) can have a significant impact on, among others, water quality, water treatment efficiency, or carbon cycling, it is essential to get a comprehensive understanding of NOM sorption processes.[131,143,185,196,197]

These NOM sorption processes, together with the corresponding adlayer properties and the influence of external factors (i.e., pH, oxidants, ionic strength), are studied using different analytical techniques, including spectroscopic methods, chromatographic methods, batch sorption experiments, titrations, or in situ surface techniques.[114,144,198–202] Especially the quartz crystal microbalance with dissipation monitoring (QCM-D) as an in situ surface technique led in the recent decade to essential insights into NOM sorption processes.[131–144] This information can be acquired using the QCM-Ds ability to measure small mass changes on its sensor surface as resonance frequency changes of its oscillating piezoelectric quartz crystal with a sub-nanogram resolution in combination with information on layer viscoelasticity and thickness gained from the dissipation monitoring.[119,121] For the NOM sorption studies, different model sensor surfaces were used that are either commercially available (i.e., silica, polystyrene, aluminium oxide, iron oxide, hydroxyapatite),[131–135] can be produced using spin coating (i.e., poly(vinylidene fluoride)),[136] or can be made in the lab using established procedures (positively charged polyelectrolyte layer, self-assembled monolayers).[137–144] While it is possible to answer many

important questions regarding NOM sorption behavior using these few sensor coatings, many research questions regarding interactions of NOM and sorbent materials, polymers, or membranes used, for example, during water treatment cannot yet be investigated because of the lack of suitable novel sensor coatings.[69,147,148,203,204] Such novel sensor coatings could open up new possibilities to study the interaction of NOM with polymers used as sorbent or membrane materials using the QCM-D.

Thin polymer layers with different compositions, surface properties, and structures can be coated on the QCM using various polymerization techniques.[205] Polymer grafting from the QCM substrate is, for example, a controllable, versatile approach that enables the coating of a thin and dense polymer brush layer with high stability.[205,206] Grafting different polymer chains (i.e., polyvinyl, -acryl, -styrene-based) from the QCM sensor has been achieved in the past using photo, reversible addition-fragmentation chain-transfer (RAFT) or radical polymerization.[205,207–209] One of the most frequently used polymers as sorbents for environmental applications are polystyrene-divinylbenzene (PS-DVB)-based polymers (commercial products: i.e., Chromabond HR-P, Isolute ENV+, or Lichrolut EN) or (PS-DVB)-based polymers modified with a hydrophilic monomer to get a co-polymer with hydrophilic moieties (commercial products: i.e., Oasis HLB with N-vinylpyrrolidone (NVP) as modifier).[69,145–148] Establishing a grafting procedure for hypercrosslinked (PS-DVB)-based polar-modified co-polymers would enable the study of interfacial dynamics between NOM and one of the most important sorbent classes and could be used as a model approach for the grafting of other relevant co-polymers on a QCM sensor.

In this work, we report for the first time a grafting approach for a hypercrosslinked DVB-based copolymer using ethylene glycol dimethacrylate (EGDMA) as a hydrophilic modifier on a QCM sensor. (i) We characterized the sensor coating regarding chemical composition using Fourier-transform infrared (FTIR) and Raman spectroscopy. (ii) Further, we assessed the polymer distribution, the thickness, and the chemical composition of the grafted polymer layer using scanning electron microscopy imaging (SEM) and energy dispersive X-ray mapping (EDX). (iii) Lastly, we performed flow-based sorption experiments to evaluate the interaction between humic acids as a proxy for NOM and the polymer coating.

3.2 Experimental

3.2.1 Chemicals and Materials

A list of purchased chemicals and materials and a description of the standard solutions and ultrapure water is provided in the supporting information section C.1.

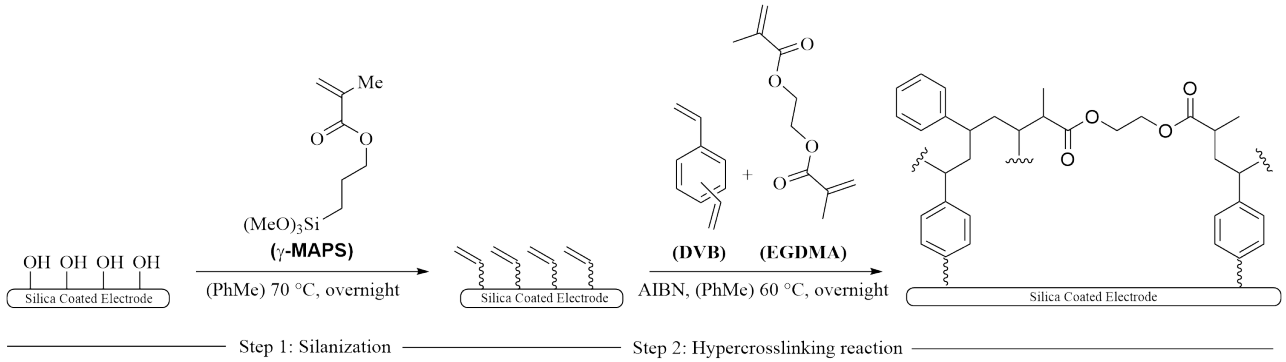

Figure 3.1 Schematic representation of the modification procedure used to graft a DVB-based copolymer in a two-step process onto a QCM sensor. Step 1: Silanization of the silica coated electrode using γ-MAPS. Step 2: Hypercrosslinking polymerization reaction using DVB, EGDMA, and AIBN as initiator.

3.2.2 Surface Modification of Quartz Crystal Microbalance Sensor

10 MHz QCM sensor crystals (Au coated with SiO_2, Novaetech S.r.l., Italy) were coated with a DVB-based copolymer in a two-step process (see Figure 3.1). The sensor crystals were immersed in the first step, the silanization, in toluene (100 mL) using a tailor-made sensor holder (see Figure C.1). γ-Methacryloxypropyltrimethoxysilane (γ-MAPS) (5.00 mL, 20.9 mmol) were added, and the solution stirred at 70 °C overnight. Afterward, the sensor crystal was cleaned using acetone (5 mL) and water (5 mL) and then dried at 60 °C. In the second step, the hypercrosslinking of a co-polymer, the silanized crystal in its holder is immersed in toluene (40 mL). DVB (276 mL, 1.94 mmol, 1.0 eq.) and EGDMA (91.3 mL, 0.484 mmol, 0.25 eq.) were added. The polymerization was initiated using 2,2'-Azobis(2-methylpropionitrile) (AIBN) (8.70 mg, 53.0 mmol). The mixture was stirred at 60 °C overnight under an argon atmosphere. The sensor crystal was then again cleaned using acetone (5 mL) and water (5 mL) and dried at 60 °C.

3.2.3 Surface Characterization of Quartz Crystal Microbalance Sensor

The chemical composition of the grafted co-polymer was studied using FTIR spectroscopy (FTIR spectrophotometer, Elmer Perkin Frontier, Germany) and Raman spectroscopy (alpha300R Confocal Raman Microscope, WITec GmbH, Germany). The IR spectra were recorded with a resolution of 1 cm^{-1} in the spectral range of 4000-650 cm^{-1}. The Raman spectra were recorded using 10 mW laser power, an integration time of 1 s, and 50 accumulations. The surface morphology and elemental composition of the coated QCM sensor were investigated using SEM (ZEISS SIGMA VP Field Emission Scanning Electron Microscope, Carl Zeiss Microscopy GmbH, Germany) equipped with an EDX detector (EDS Quantax XFlash 6l60 Detector, Bruker Nano GmbH, Germany).

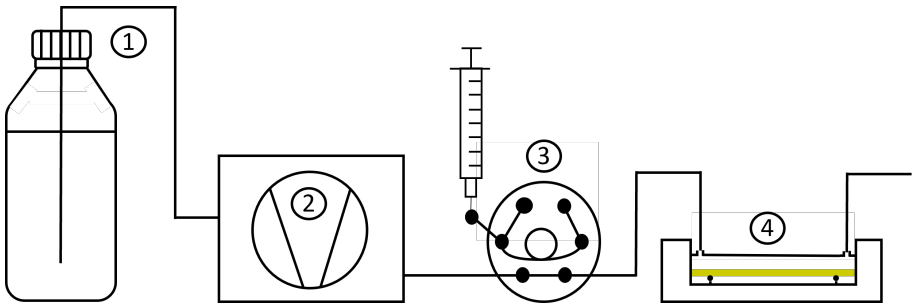

Figure 3.2 Schematic overview of the setup used for sorption experiments. 1: Water bottle, 2: Peristaltic Pump, 3: Sample injector, 4: QCM

Table 3.1 Measurement parameters of sorption experiments 1 and 2.

Parameter	Unit	Exp. 1	Exp. 2
humic acid concentration	mgC/L	4	5
injection volume	µL	19	200
number of injections		15	6
mass per injection	ngC	77	1000
mass injected in total	ngC	1152	6000
flow rate	µL/min	30	30

3.2.4 Preparation of Humic Acid Solutions

A humic acid stock solution was prepared by dissolving 50 mg in water (50 mL). The solution was filtered through glass microfiber filter membranes (1.2 µm particle retention, 47 mm diameter, Whatman, UK) and stored at -4 °C. Organic carbon concentrations were determined using a total organic carbon (TOC) analyzer (TOC-L, Shimadzu, Japan) equipped with a combustion catalytic oxidation reactor (680 °C) and a non-dispersive infrared detector. Humic acid samples were prepared by diluting aliquots of the stock solution.

3.2.5 Sorption Experiments

Figure 3.2 shows a schematic overview of the setup used for sorption experiments. In this setup, degassed water (1) is constantly passed over a QCM (openQCM Q^{-1}, openQCM by Novaetech S.r.l., Italy) (4) using a peristaltic pump (IPC 24, Ismatec, Germany) (2) with a flow rate of 30 µL/min. The instruments were connected using inert tubes (Tygon MHSL 2001, inner diameter: 1.52 mm, wall thickness: 0.85 mm, Ismatec, Germany). Samples were injected using an injection valve (Model 7725i, Rheodyne, USA) (3). The measurement parameters, including injection volume, injected mass of humic acids, and times of injections for experiment 1 and experiment 2, are shown in Table 3.1. The experiments were conducted at room temperature with temperature fluctuations below 1 °C.

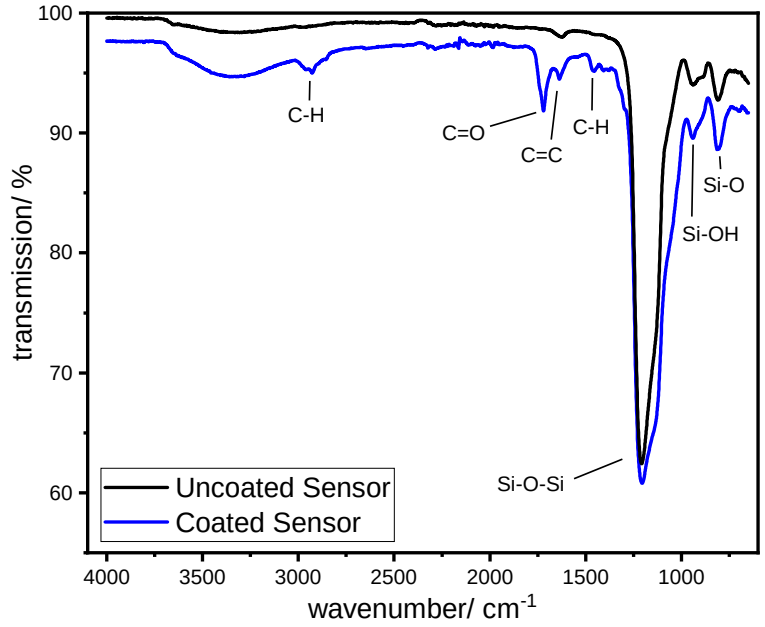

Figure 3.3 IR spectrum of a silica QCM sensor (uncoated sensor, black) and a silica QCM sensor coated with a DVB-EGDMA polymer (coated sensor, blue).

3.2.6 Data Evaluation

We defined the resonance frequency shift measured during the sorption experiments as the difference between the average of 250 measured data points before and after the injection of the sample. The resonance frequency shift was corrected using the baseline drift observed before the injection of the sample. The baseline drift was determined using a linear regression of the weighted average of 701 data points within the moving window (adjacent-averaging method). The code used for the data processing is shown in section C.3.

$$\Delta\Gamma = \frac{f_0}{2}\Delta D \tag{3.1}$$

The half-bandwidth at half height of a resonance ($\Delta\Gamma$) is calculated using Eq. 3.1 by dividing the fundamental resonance frequency of the oscillating quartz (f_0 = 10 MHz) by 2 and multiplying it with the measured dissipation change (ΔD).[119,120]

3.3 Results and Discussion

3.3.1 Chemical Composition of the Grafted DVB-EGDMA Co-Polymer

To evaluate the success of the grafting of a DVB-based copolymer using EGDMA as a hydrophilic modifier on a QCM sensor (Au coated with SiO_2), we analyzed the chemical composition of the coated and the uncoated sensor crystal using FTIR spectroscopy and Raman spectroscopy. The IR spectrum is shown in Figure 3.3 (blue data: coated sensor, black data: uncoated sensor), the Raman spectrum in Figure A.4.1, and the peak

Table 3.2 IR and Raman peak assignment for grafted DVB-EGDMA copolymer.

IR Peak cm^{-1}	Raman Peak cm^{-1}	Peak Assignment[210–214]	Monomer Assignment
-	3106	ν(C-$H_{aromatic}$)	DVB
2918	2928	ν(C-$H_{aliphatic}$)	DVB, EGDMA
2851	-	ν(C-$H_{aliphatic}$)	DVB, EGDMA
1721	1714	ν_s(C=O)	EGDMA
1637	1639	ν(C=$C_{aliphatic}$)	DVB, EGDMA
-	1609	Ring skeletal stretch	DVB
1454	1454	δ_a(C-H) of α(C-H_3)	EGDMA
1408	1406	δ(C-H_{vinyl}), γ(C-H_2)	DVB, EGDMA
-	1201	ν_a(C-O-C)	EGDMA
-	1013	Ring breathing mode	DVB

assignment in Table 3.2. Even if the main part of the fingerprint region in the IR spectrum is overlayed by intense peaks from the silica coating (below 1250 cm^{-1}),[215] there are several additional signals visible in the IR spectrum of the coated sensor crystal (see Figure 3.3 blue data and Table 3.2) originating from the two polymer building blocks DVB and EGDMA. The peaks around 2900 cm^{-1} can be assigned to the aliphatic C-H vibration of DVB and EGDMA, while the pronounced peak at 1721 cm^{-1} likely originates from the C=O stretching vibration of EGDMA. The stretch vibration of the methacrylate C=C double bond can be observed at 1637 cm^{-1}, the deformation vibration of the methyl group of EGDMA at 1454 cm^{-1}, and the deformation of the CH2=CH bond at 1408 cm^{-1}.[210,211,213] Raman (see Table 3.2), on the other hand, reveals additionally the aromatic C-H vibration at 3106 cm^{-1}, the ring skeletal stretch at 1609 cm^{-1}, the C-O-C stretch at 1201 cm^{-1}, and the ring breathing mode at 1013 cm^{-1}.[212,214] These additional signals on the spectrum of the coated sensor measured with IR and Raman, two complementary techniques, prove the successful grafting of a DVB/ EGDMA copolymer onto the sensor crystal.

3.3.2 Thickness and Surface Morphology of the Grafted DVB-EGDMA Co-Polymer

We assessed the surface morphology, polymer distribution, layer thickness, and chemical composition of the grafted DVB-EGDMA polymer layer using SEM and EDX. SEM images of the top and the side view of the sensor crystal before and after the grafting and EDX imaging of the side view are shown in Figure 3.4. SEM pictures of the top (Figure 3.4, a: uncoated, b: coated) and the side view (Figure 3.4, c: uncoated, d: coated) confirm the successful grafting of a polymer on the sensor crystal. SEM picture of the top view (Figure 3.4b) shows that the grafted polymer film is laterally heterogeneous, consisting of areas with a homogeneously grafted polymer film and regions without any coating. This heterogeneous coverage can potentially lead to energy dissipation during the QCM measurement.[119] The side view (Figure 3.4d) also shows that the polymer layer's thickness varies with a maximal thickness of up to 300 nm. This film thickness lies in the optimal range since a few hundred nanometres is the upper limit of the dynamic range in liquid applications where polymer swelling

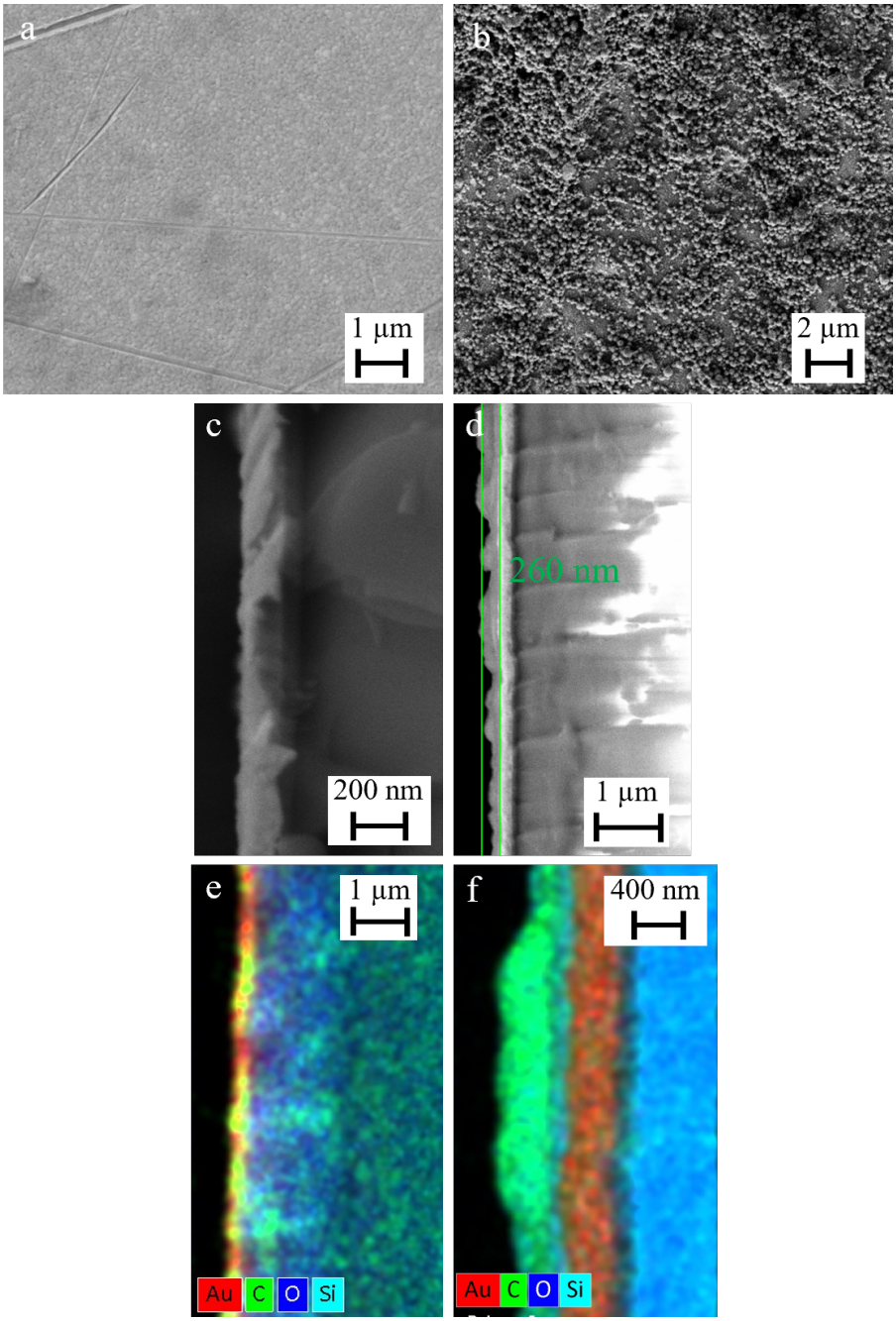

Figure 3.4 SEM and EDX images of the QCM sensor coated and uncoated with the DVB-EGDMA polymer. The QCM sensor consists of a quartz crystal coated with a 200 nm thick gold coating and a 50 nm thick silicon dioxide layer. SEM images: (a) Top view of QCM sensor, (b) top view of coated QCM sensor, (c) side view of QCM sensor, (d) side view of coated QCM sensor. EDX images for the elements gold (Au, red), carbon (C, green), oxygen (O, dark blue), and silicon (Si, light blue): (e) Side view of QCM sensor, (f) side view of coated QCM sensor.

Table 3.3 Determined values for the frequency change (Δf), the dissipation change (ΔD), and the bandwidth change ΔΓ during sorption experiment 1 and 2.

Experiment	Δf	ΔD	ΔΓ
1	18±2	1.9±0.2	10±1
2	20±2	6.1±0.1	31±1

can occur.[120,216] A lower thickness is, however, not beneficial since the capacity of the coating is dependent on the thickness. The EDX images visualize the different layers of the sensor crystal and give information about the elemental composition of the grafted film (see Figure 3.4). The quartz crystal (dark and light blue for oxygen and silicon) is coated with a 200 nm thick gold coating (red) and a 50 nm thick silicon dioxide layer. The crystal with the grafted polymer (Figure 3.4f) has an additional layer (approximately 200 nm) that mainly consists of carbon (green) with some oxygen incorporated (dark blue), supporting the findings of FTIR and Raman spectroscopy and confirming the incorporation of both DVB (only green signals for carbon) and EGDMA (green and blue signals for carbon and oxygen) in the grafted polymer.

3.3.3 Interactions Between DVB-EGDMA Co-Polymer and Humic Acids during Flow-Based Sorption Experiments Revealed by QCM-D

After characterizing the successfully grafted DVB-EGDMA co-polymer, we further assessed the interaction between the grafted co-polymer and humic acids. To this end, we carried out two continuous flow experiments: In the first one, we injected 1152 ngC humic acids dissolved in MilliQ distributed over 15 injections, and in the second one, 6000 ngC dissolved humic acids distributed over 6 injections. The resonance frequency shift during these experiments is shown in (Figure 3.5). The measurement results are summarized in Table 3.3. Passing humic acids over the coated QCM sensor led to a significant frequency decrease (experiment 1: 18±2 Hz, experiment 2: 20±2 Hz). Injecting water on a coated sensor and humic acids on an uncoated silica sensor led to no significant frequency shift (see Figure A.4.2), thus demonstrating that the changes in the resonance frequency in experiment 1 and 2 are a result of the interaction between humic acids and the sensor coating. There is no sorption on the uncoated silica sensor since the negatively charged humic acids at neutral pH are electrostatically repulsed from the negatively charged silica surface.[217] The extent of the frequency decrease due to humic acid sorption on the coated sensor is comparable to numbers reported in the literature for the sorption of humic acids or NOM to different model surfaces (silica: 0 Hz,[131] PS: 0.1-2.4 Hz,[131] aluminium oxide: 3-15 Hz,[131,134] poly(vinylidene fluoride) blended with SiO2 nanoparticles: 20-35 Hz,[136] alkylthiol self-assembled monolayer: 4-14 Hz[143]). It has to be noted that we can compare frequency changes and cannot quantify the absolute sorbed mass since the Sauerbrey equation cannot be used for this application. This is the case since one requirement for the Sauerbrey equation is the small load approximation, which is only valid if ΔΓ is much smaller than the frequency change.[119,120] This approximation does not apply to our measurements since ΔΓ is only by a factor of 2 smaller than the frequency change in experiment 1 and even bigger than the frequency

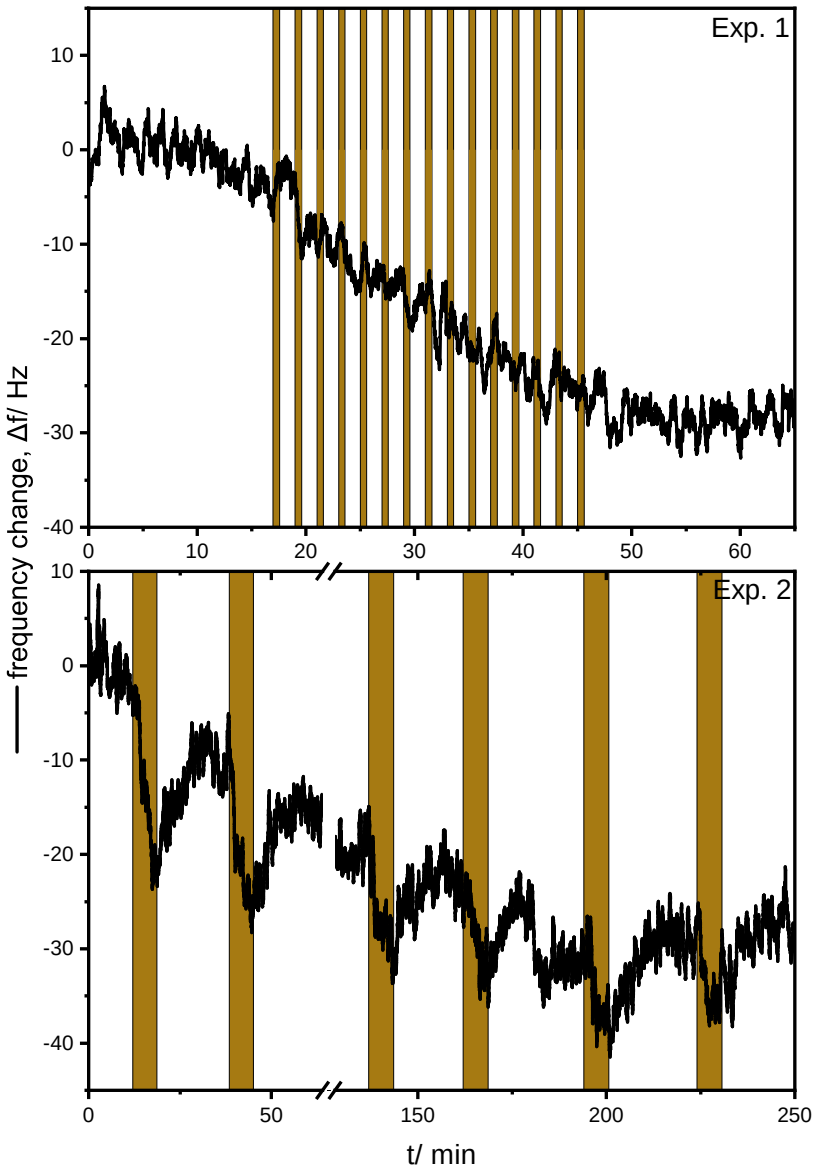

Figure 3.5 Frequency change (black) during humic acid sorption experiments 1 and 2 on a QCM sensor coated with the DVB-EGDMA copolymer. Water was passed constantly over the sensor with a flow rate of 30 µL/min. Using an injection valve, humic acid solutions were injected during the flow experiments. The brown bars visualize the time when the humic acid solution is passed over the sensor.

change in experiment 2. The reason for this is that — as the SEM images showed — the surface coating is not homogeneous and not rigid, prohibiting humic acids from being sorbed and distributed evenly across the sensor. Instead of the Sauerbrey equation, which would significantly underestimate the sorbed mass, viscoelastic modeling has to be used. This is, however, not possible using openQCM Q^{-1} since only one overtone can be measured per experimental run, while for viscoelastic modeling, at least two are necessary.[119–121]

The extent of sorption is not constant among the different injections for both experiments. There is a decline of the frequency decrease visible that leads, in the case of experiment 2, to no significant frequency change after the 4th injection. Together with the observation that the overall frequency decrease in both experiments 1 and 2 are similar — even if in experiment 2 nearly 6 times more humic acids were passed over the sensor — we conclude that the non-linear sorption behavior is a result of reaching the capacity limits for the coated polymer.[218] Experiment 2 shows further that after the initial sorption, parts of the adsorbed humic acids desorb until an equilibrium, the capacity limit, is reached. This sorption behavior is comparable to the observations of Eita et al.[134] for the sorption of humic acids on aluminium oxide. However, rinsing the surface with excess water did not lead to any further removal of sorbed humic acids. In a consecutive sorption experiment, we further rinsed the sensor after humic acid sorption equilibrium was reached with three different organic solvents (acetonitrile, isopropyl alcohol, methanol). Again, no significant frequency change could be detected (acetonitrile: +2±2 Hz, isopropyl alcohol: -2±1 Hz, methanol: +2±1 Hz). These results suggest that the fraction of humic acids sorbing to the grafted DVB-EGDMA co-polymer forms a very stable adlayer.[131]

3.4 Conclusion

The current work presents the grafting of a DVB-EGDMA co-polymer onto a QCM sensor using radical polymerization. FTIR and Raman spectroscopy confirmed the successful incorporation of DVB and EGDMA into the polymer. SEM and EDX measurements showed that the polymer is coated laterally heterogeneous on the sensor chip. These techniques further revealed that the polymer layer is 200-300 nm thick and thus inside the dynamic range of QCM measurements.[120,216] The demonstrated polymerization and characterization strategy can be used as a model to graft other (DVB-based) co-polymers onto QCM sensors. We observed humic acid sorption during two flow experiments, leading to a significant frequency decrease of 18-20 Hz. This decrease is on the higher end compared to frequency changes measured during the sorption of humic acids to other model surfaces — especially considering the lateral heterogeneity of the coating. The stability of the adlayer formation further proves the strong interactions between the DVB-EGDMA co-polymer coating and humic acids — and prohibits, at the same time, regeneration of the sensor with common organic solvents. Future research can build upon our findings and optimize the presented polymerization strategy to enable the coating of a more homogeneous polymer layer to study NOM sorption processes using the QCM.

4 Quartz Crystal Microbalance as Holistic Detector for Quantifying Complex Organic Matrices During Liquid Chromatography: 1. Coupling, Characterization, and Validation

Abstract

Matrix in highly complex samples can cause adverse effects on trace analysis of targeted organic compounds. A suitable separation of target analyte(s) and matrix before the instrumental analysis is often a vital step for which chromatographic clean-up methods remain one of the most frequently used strategies, particularly high-performance liquid chromatography (HPLC). The lack of a simple real-time detection technique that can quantify the entirety of the matrix during this step renders optimization of the clean-up challenging. This paper, along with a companion one, explore the possibilities and limitations of quartz crystal microbalance (QCM) dry mass sensing for quantifying complex organic matrices during gradient HPLC. To this end, this work coupled a QCM and a microfluidic spray-dryer with a commercial HPLC system using a flow splitter and developed a calibration and data processing strategy. The system was characterized in terms of quantification limits, accuracy, and applicability for subsequent pesticide residue analysis in food using gas chromatography-mass spectrometry (GC-MS). Validation of natural organic matter in an environmental sample against offline total organic carbon analysis confirmed the approach's feasibility with an absolute recovery of 103±10%. We found a correlation ($R^2 \geq 95$) between the amount of matrix quantified by QCM dry mass sensing during an HPLC clean-up of a brown rice extract and matrix effects measured during the subsequent GC-MS analysis of the investigated pesticides. This suggests that QCM dry mass sensing can be a valuable tool to the analyst where HPLC clean-up is routinely performed and can thus benefit many analytical fields.

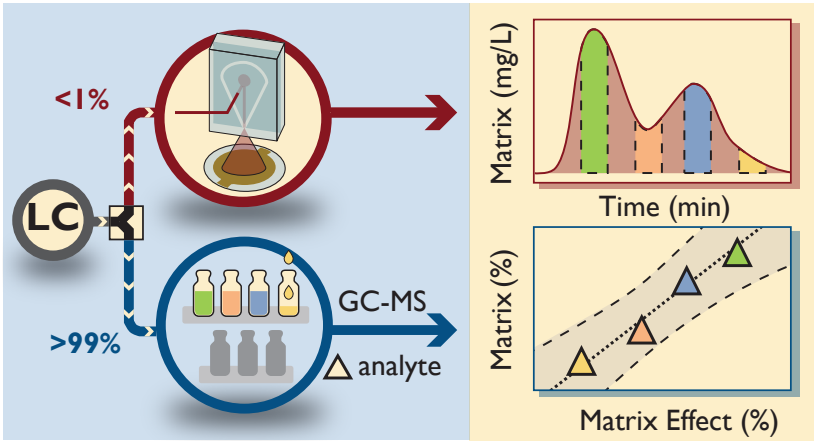

The results of this chapter were published in a modified form in a peer-reviewed journal.

Reprinted with permission from:

Christopher Wabnitz, Aoife Canavan, Wei Chen, Mathias Reisbeck, and Rani Bakkour. Quartz Crystal Microbalance as Holistic Detector for Quantifying Complex Organic Matrices During Liquid Chromatography: 1. Coupling, Characterization, and Validation. *Analytical Chemistry* **2024**, *96*, 7429–7435.

4.1 Introduction

A challenge in trace analysis of targeted organic compounds are highly complex samples, such as environmental,[3,112] biological,[219,220] or food samples.[154,157,221] This is the case because abundant organic and inorganic constituents of the complex sample, other than the target analyte(s) and also known as matrix, can have a variety of adverse effects on the analytical mode of detection. These adverse effects include increased detection noise, higher detection limits, obscured peaks, false positive signals/ results, signal suppression (negative matrix effect), or signal enhancement (positive matrix effect).[154,155] Despite many instrumental developments that improved the overall detection or the separation of the sample matrix and target analytes, e.g., high-resolution mass spectrometry or multi-dimensional hyphenated chromatography, there are still limitations in trace analysis of targeted organic compounds due to the sample matrix.[154,157,222] A suitable sample preparation before the instrumental analysis is often a vital key to the reduction of matrix-related adverse effects.[154,156,157]

An efficient separation of the matrix constituents from the target analyte(s) is usually the focus of such sample preparation procedures for which chromatographic clean-up methods remain one of the most often used strategies, particularly high-performance liquid chromatography (HPLC). As a stand-alone purification system or directly coupled to a detector, HPLC cleanup finds many applications mainly due to the wide variety of available column materials and modes (e.g., reversed phase (RP)),[110,111] as well as the possibility to optimize purification using an unlimited combination of solvents.[110–112] In addition to the easy automation of the sample clean-up, which increases reliability and accuracy,[223–225] the possibility to pack columns with highly selective materials[226,227] makes the sample preparation tunable to any target analyte of interest. Yet, the HPLC method development becomes tedious and challenging when the matrix is a complex mixture that cannot be quantified with straightforward measures. In fact, an optimal and efficient optimization of the HPLC clean-up warrants a simultaneous online quantification of both the target analyte(s) and the interfering matrix.

While there are numerous detectors for organic target analytes (UV-Visible spectrometry (UV/Vis), mass spectrometry (MS)), they cannot be directly used for the online quantification of organic matrices. This is because the matrix composition is often very heterogeneous and complex. Natural organic matter (NOM) consists, for example, of thousands of different compounds with a wide variety of physicochemical properties, while food matrices are a complex mixture of different fatty acids, proteins, carbohydrates, vitamins, and many more compounds.[80,228] Also, most instruments typically used to quantify analytes can only monitor certain matrix fractions (e.g., chromophoric or ionizable).[114,115] Semi-universal sensors like the total organic carbon (TOC) analyzer, the charged aerosol detector (CAD), or the evaporative light-scattering detector (ELSD) are limited by their inter-compound response differences (TOC: solubility in H_2O, only carbon content is measured; CAD: up to 11% relative standard deviation for different compounds, ELSD: relative standard deviations higher than 50% are reported),[115–118] which play an important role if not just one compound but the sample matrix should be quantified. A robust, simple, and inexpensive detection technique capable of quantifying the entirety

of the matrix online during a gradient HPLC purification would help improve the selectivity of the respective separation process in a straightforward approach.

One promising detector that could be used for this purpose is the quartz crystal microbalance (QCM). The QCM measures small mass changes with a sub-nanogram resolution on the surface of its oscillating piezoelectric quartz crystal by measuring changes in the oscillating resonance frequency as a function of deposited mass on its surface.[119,121] Several studies showed how the QCM can be used to measure the sorption of the matrix NOM directly in a solution or the adsorption of dissolved compounds onto NOM and get thus insights into adsorption, adlayer formation, and interfacial dynamics of this matrix.[131–144] NOM real-time quantification directly in liquid phase is, however, challenging to achieve due to (i) the limited capacity of available sensor surface coatings,[131] (ii) the dependency of the sorption behavior on the type or fraction of NOM,[132,143] the pH,[132,134] and the continuous desorption,[134] (iii) the often slow deposition rate,[131] (iv) and other known challenges of liquid-based QCM measurements (e.g., viscous damping).[119,151] The challenges of liquid-based QCM measurements can, however, be overcome using QCM dry mass sensing introduced in the 70s by Schulz et al.[150] Technical advancement on the QCM and substantial optimization measures in the last decade make dry mass sensing seem to be an ideal solution for a robust and inexpensive strategy to monitor and quantify the entire matrix.[120,151–153] In QCM dry mass sensing, a small fraction of the HPLC column effluent is diverted and nebulized into micron-sized droplets using a microfluidic spray nozzle and sprayed onto the QCM sensor. The nebulized solvent evaporates, while non-volatile components are deposited evenly on the QCM sensor, which can be quantified using the direct correlation between frequency change and mass.[151–153] Kartanas et al.[153] showed how this QCM dry-mass sensing could be used in combination with aquatic size-exclusion LC to separate and detect different proteins. It has, however, never been explored for a mixture as complex as an environmental extract or a food matrix. Moreover, the transition from aquatic to RP gradient elution is expected to cause variations in QCM response as a result of changing fluid dynamics and evaporation rates. To this end, comprehensive characterization and validation of such a system is warranted to deal with organic solvents along with the development of a suitable calibration strategy.

The work presented in this and the companion paper[229] has the overall goal of exploring the feasibility of coupling a commercial HPLC with a microfluidic spray-dryer and a QCM for online monitoring of organic matrix components during RP HPLC gradient purification for different mass spectrometry-based applications in environmental and food sciences. Both studies focus on organic matrices in already extracted samples where most inorganic salts are excluded through a first solid-phase extraction step. The specific objectives of this paper were to (i) connect, characterize, and calibrate a microfluidic spray-dryer with RP HPLC using an adjustable post-column flow splitter, (ii) define the lower and upper limits of quantification for QCM dry mass sensing, and (iii) validate the online approach against offline TOC fraction analysis of NOM. Lastly, we (iv) illustrate its applicability and analytical implications for the analysis of pesticides in brown rice through

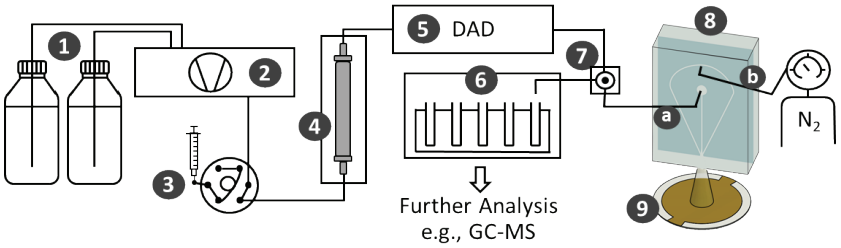

Figure 4.1 Schematic overview of the coupled HPLC-QCM system. 1: HPLC grade solvents, 2: Binary HPLC pump, 3: Sample injector/autosampler, 4: Chromatographic column; 5: DAD detector, 6: Fraction collector, 7: Post-column adjustable flow splitter, 8: Microfluidic spray-dryer, a: connection to liquid channel, b: connection to gas channel, 9: QCM sensor.

qualitative assessment during separation of matrix compared with UV/Vis, and quantification of matrix effects in subsequent gas chromatography (GC)-MS analysis, respectively.

4.2 Experimental Section

4.2.1 Chemicals and Materials

A description of purchased chemicals, materials, as well as standard solutions used in this study are provided in the supporting information (section D.1).

4.2.2 Instrumental Setup of QCM Dry Mass Sensing

Coupling of QCM Dry Mass Sensing with RP HPLC using a Flow Splitter

An HPLC system, Figure 4.1 (**parts 1-6**), was coupled through an adjustable flow splitter, Figure 4.1 (**7**), to QCM dry mass sensing, Figure 4.1 (**8-9**). Chromatography was performed on a Nexera XR HPLC system (Shimadzu, Japan) equipped with a solvent delivery module (LC-20AD, Shimadzu, Japan) (**2**), an RP column (**4**) (XTerra RP18 Column, length: 150 mm, diameter: 3.0 mm, particle size: 3.5 µm, Waters, USA), a diode array detector (DAD) (**5**) (SPD-M20A, Shimadzu, Japan), and a fraction collector (**6**) (FRC-10A, Shimadzu, Japan). A flow rate of 0.5 mL/min, a sample injection volume of 200 µL (**3**), and a column oven temperature of 40 °C were used for all HPLC measurements. Binary phase gradients with H_2O (A) and 90% CH_3OH 10% H_2O (B) were used as eluents (**1**).

The column effluent is split after the DAD using an analytical post-column adjustable flow splitter (**7**) (ASI 610-PO10-01, Analytical Scientific Instruments, USA, 50:1 to 1000:1 Split Ratio). Vernier scale settings were set to 65 unless otherwise stated. The high-flow port was connected with the fraction collector and the low flow port with a microfluidic spray-dryer (**8**) using polytetrafluorethylene (PTFE) tubing. The low-flow port was connected with the liquid channel of the spray-dryer via PTFE tubes (**a**) (tube 1: outer diameter 1/16 inch, inner diameter 0.010 inch; tube 2: outer diameter 1/32 inch, inner diameter 1/75 inch) that were connected through an

adapter (1/16 inch to 1/32 inch, PEEK, IDEX Health and Science) to meet the requirements of both the splitter and the spray-dryer.

We fabricated the microfluidic spray-dryer (**8**) in-house using an optimized protocol (details in section D.1) of a previously published standard polydimethylsiloxane (PDMS) soft-lithography approach.[152] The microfluidic spray-dryer had two inlets, one connected to a nitrogen supply (**b**) set to 3 bar and another to the low-flow port of the flow splitter (**a**). The liquid channel had a length of 8.1 mm and a cross-section of 25 times 20 µm^2, the gas channels had a length of 8.4 mm and a cross-section of 100 times 70 µm^2. The mobile phase was sprayed onto the frequency counter QCM200 from Stanford Research Systems (USA) equipped with a 5 MHz QCM crystal (**9**) (Stanford Research Systems 100RX1, Cr/Au, USA); a gate time of 0.1 s was used. To this end, the spray-dryer was centered 3.5 cm above the QCM.

Determination of Split Ratios

Split ratios (R_{split}) were determined for different Vernier scale settings (56, 66, 73, 79, 94, 112) for three different CH_3OH/H_2O mobile phase compositions (85/15, 50/50, and 15/85 (v/v)) by spraying the mobile phase containing 500 mg/L NaCl for 30 min into a vial. The dried salt was reconstituted in 8 mL H_2O. The salt concentration in solution was determined by measuring the salinity using a salinometer (MultiLine F/SET-3, WTW, Germany).

$$\kappa_{corrected} = \kappa_{sample} - \kappa_{control} \tag{4.1}$$

$$c_{sample} = \frac{\kappa_{corrected}}{\Lambda_m^{NaCl}} \tag{4.2}$$

Dividing the corrected salinity ($\kappa_{corrected}$) by the molar conductivity of NaCl (Λ_m^{NaCl}) results in the concentration of the sample in the vial (c_{sample}) (see Eq 4.1 and 4.2).

$$Q_{spray} = \frac{m_{sample}}{c_{NaCl} \cdot t} \tag{4.3}$$

The flow to the spray-dryer (Q_{spray}) was calculated using Eq 4.3 by dividing the sprayed mass (m_{sample}), calculated using c_{sample}, by the sprayed time (t) and by the concentration of salt (C_{NaCl}) in the mobile phase.

$$R_{split} = \frac{Q_{input} - Q_{spray}}{Q_{spray}} \tag{4.4}$$

The split ratio (R_{split}) was calculated using Eq 4.4. Here, the high flow, which is the difference of the input flow (Q_{input}) and the low flow (Q_{spray}), is divided by the low flow.

Measurement, Calibration and Data Processing

Prior to each sample, a blank was run on the system described in Figure 4.1 under identical conditions where 200 µL of 25/75 CH_3OH/H_2O (v/v) were injected instead of the sample. After the sample measurement, a one-point calibration was performed through constant mass spraying on the sensor achieved under the same chromatographic conditions but with the eluents containing NaCl (c_{cal} = 300 mg/L). The obtained frequencies given in Hz for each time point were translated into mass concentrations given in mg/L using Eq. 4.5, as well as detailed in a Matlab script (see section D.8).

$$c_{sample} = c_{cal} \cdot \frac{\partial \Delta f_{sample}}{\partial t} / \frac{\partial \Delta f_{cal}}{\partial t} \tag{4.5}$$

In this procedure, the blank (f_{blank}) is subtracted from both the sample (f_{sample}) and the calibration measurement (f_{cal}) to obtain corrected frequencies Δf_{sample} and Δf_{cal}, respectively. Then, the 1st derivative ($\partial \Delta f_{sample}/\partial t$ and $\partial \Delta f_{cal}/\partial t$) is produced and smoothed using a Savitzky-Golay filter (polynomial order 3, 301 points). The derivatives ratio multiplied by the salt concentration for calibration (c_{cal}) yields mass concentrations in the sample (c_{sample}).

Determination of Lower and Upper Limits of Detection and Quantification

The limits of detection (LOD) and limits of quantification (LOQ) of the system were determined for three different CH_3OH/H_2O mobile phase compositions (85/15, 50/50, and 15/85 (v/v)) according to the calibration method (DIN 32645).[230] To this end, we sprayed the mobile phase containing NaCl in different concentrations (0, 30, 60, 90, 120, 150, and 180 mg/L) for 10 minutes onto the QCM. The average slope of quadruplicates of the frequency decrease was used for the signal intensity.

For the determination of the upper limit of the system for the three different mobile phase compositions, the mobile phase containing 500 mg/L NaCl was sprayed onto the QCM in triplicates. The upper limit was then estimated by calculating the amount of salt being sprayed till the resistance was by a factor of three higher than the starting resistance (12-17 ohm). This value was then converted into a maximal concentration for a 10 minute measurement.

Validation of QCM Dry Mass Sensing Approach

We compared dry-mass sensing with TOC analysis to validate our measurement approach. The elution of 1.65 mg NOM during a typical HPLC gradient (see Table A.4.2) was monitored and quantified online using QCM dry mass sensing and offline using TOC analysis. To this end, fractions of the HPLC eluate were taken every 30 s using a fraction collector (**6**). The fractionated eluate was evaporated to dryness under a gentle stream of N_2 at 30 °C and then reconstituted in 16 mL of H_2O. Organic carbon concentrations in each reconstituted sample were

determined using a TOC analyzer (TOC-L, Shimadzu, Japan) equipped with a combustion catalytic oxidation reactor (680 °C) and a non-dispersive infrared detector to analyze the generated CO_2.

4.2.3 Extraction Procedures to Isolate Environmental and Food Matrices

Extraction of Rice Matrix

Brown rice was treated using a modified version of the QuEChERS method.[46,231] Frozen brown rice (500 g) was homogenized using cryogenic milling. Ten grams of the homogenized sample were weighed in a 50 mL centrifuge tube and soaked in 10 mL Milli-Q H_2O for 1 h. Afterwards, 10 mL of acetonitrile were added together with a buffer salt mixture of 4 g of magnesium sulfate anhydrous grit, 1 g of sodium chloride, 0.5 g of disodium hydrogen citrate sesquihydrate, and 1 g of trisodium citrate dihydrate. The mixture was shaken vigorously by hand for 1 minute and then centrifuged at 3500×g for 5 minutes. The acetonitrile phase was collected and stored at -18 °C for further experiments.

Extraction of Riverine NOM

Samples were taken from creek Wiesäckerbach (Garching, Germany, latitude 48.269009, longitude 11.667976) and filtered through glass microfiber filter membranes (1.2 µm particle retention, 47 mm diameter, Whatman, UK). The filtered samples were passed over OASIS HLB cartridges under conventional solid-phase extraction conditions (Waters, 200 mg, 6 cc) using an automated SPE system (Smart Prep Extractor, Horizon Technology, USA) at 5 mL/min. The cartridges were subsequently dried under vacuum overnight and eluted in 5 mL of CH_3OH. The volume of combined eluates was reduced under a gentle stream of N_2 at 30 °C and then stored at -18 °C.

4.2.4 Experiments

Quantification of Brown Rice Matrix During Reversed-Phase Liquid Chromatography

Brown rice matrix collected from the acetonitrile phase was evaporated to dryness at 50 °C under a gentle stream of N_2. The dry residues (2.6 mg) were then reconstituted in 250 µL H_2O/isopropanol 1/1 (v/v) and introduced using a manual injection valve into the HPLC-QCM dry mass sensing system with a Vernier scale setting of 65. The HPLC gradient parameters are listed in Table A.4.3. Matrix quantification data from the QCM dry mass sensing (Figure 4.1, **8**&**9**, low-flow port) were collected and processed after calibration with a blank measurement constituting a QuEChERS extract in absence of rice matrix for baseline correction. Data from the DAD detector (Figure 4.1, **5**) was collected using the software LabSolutions and chromatograms were extracted at wavelengths of 220, 254, and 310 nm. Comparison of data from QCM dry mass sensing and DAD

detector are plotted as intensity (mV) and mass concentration (mg/L), respectively, as a function of elution time after correction for the dead time (2.5 min) between the DAD detector and the QCM sensor.

Quantification of Matrix Effects in Residue Analysis of Pesticides Using GC-MS

Extracted brown rice matrix was fractionated into 5 portions after HPLC. Each fraction was evaporated to dryness under a gentle stream of N_2 at 50 °C, reconstituted in CH_3OH, and spiked with five different model analytes, namely 2,6-dichlorobenzamide (BAM), atrazine (ATZ), boscalid (BOSC), desethylatrazine (DEA), and propargite (Prop) to reach a volume of 1 mL and a pesticide concentration of 5 mg/L. The rice matrix fractions were measured using a GC-MS consisting of an Agilent 7890A GC system (Column: RestekTM RxiTM-5ms, 30 m, 250 µm i.d., 0.25 µm thickness, Restek Corporation, Bellefonte, USA) equipped with a 5975C Triple-Axis Detector MS from Agilent Technologies (Santa Clara, USA) and a High-Efficiency Source (HES). Liquid samples were injected (1 µL injection volume) using a CTC Pal combi-xt autosampler (CTC Analytics AG, Zwingen, Switzerland) with split injection mode (split-ratio 1:10) at an injection temperature of 250 °C with an injection liner pressure of 14.86 psi. The analyte separation was accomplished at a helium flow of 1.4 mL/min using the following temperature program of the GC oven: Starting temperature was 90 °C (0.5 min hold time), followed by a temperature ramp of 7.5 °C/min to 224 °C, a ramp of 25 °C/min to 290 °C and a ramp of 10 °C/min to 300 °C (4 min hold time). The electron ionization energy was 70 eV. For the MS detection single ion mode was used, retention times and masses are shown in Table A.4.4. Every sample was measured in triplicates and bracketed by triplicates of a standard containing the five pesticides in pure CH_3OH at the same concentration.

$$ME\% = \left(\frac{SignalArea_{\text{Sample}}}{SignalArea_{\text{Standard}}} - 1\right) \times 100 \tag{4.6}$$

The absolute matrix effect in percent (ME%) was calculated according to Eq. 4.6, in which the area of each pesticide in the sample (Signal $Area_{Sample}$) is divided by the mean of the area of the six bracketing standards (Signal $Area_{Standard}$).[232,233]

4.3 Results and Discussion

4.3.1 Coupling, Flow Control, and Calibration

We coupled an HPLC system (**1-6** in Figure 4.1, flow range = 0.1-1 mL/min) with a microfluidic spray-dryer and QCM sensor (**8**&**9**, respectively; flow range = 1-4 µL/min) through an adjustable flow splitter (**7**). The narrow flow dynamic range of components **8**&**9** warrants accurate control of the split ratio under chromatographic conditions. Therefore, we evaluated split ratios for three different solvent compositions (CH_3OH/H_2O 15/85, 50/50, and 85/15 v/v) and six different Vernier scale settings in the range between 56 and 112 (see Figure 4.2a).

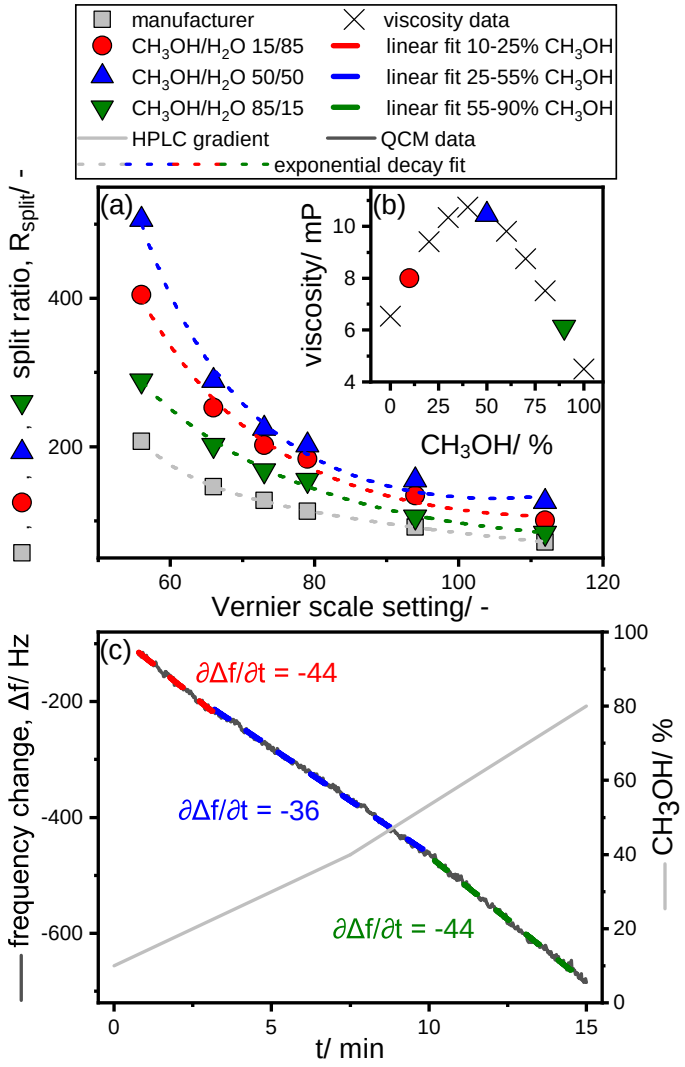

Figure 4.2 (a) Comparison of split ratios measured for the HPLC-QCM system at different Vernier scale settings for three different CH_3OH/H_2O compositions at 40 °C. The values were fitted with an exponential decay function. The values provided by the manufacturer at 25 °C for pure H_2O are shown in gray. (b) Viscosity values of CH_3OH/H_2O mixtures at 40 °C from Mikhail et al.[234] in millipoise (mP). (c) Correlation of frequency slope and measured split ratios during a calibration (black). The eluent composition during the gradient run is shown in gray in vol. % of CH_3OH (containing constantly 300 mg/L NaCl).

The split ratios increase up to 2.4 times for the HPLC-QCM dry mass sensing system using CH_3OH/H_2O solvent compositions (Figure 4.2a blue, red, and green data) in comparison with the data provided by the manufacturer (Figure 4.2a, gray data), using only H_2O as a solvent with no restrictions after the flow splitter. Moreover, variations by a factor of 1.1 - 1.8 were observed for different solvent compositions in the order CH_3OH/H_2O 50/50 (**blue**) > 15/85 (**red**) > 85/15 (**green**). These variations are significant enough to induce shifts towards lower flow rates to the spray-dryer that may lead to operation outside its dynamic range (split ratios between 125 and 500), thus affirming the need to quantify split ratios for the system. The overall split ratio shift for the HPLC-QCM dry mass sensing system is caused by backpressure originating from the small inner diameter of the liquid channel of the spray-dryer (25×20 μm^2), which is the only additional constriction in the system compared to manufacturer's data.[235–237] In addition, the pressure in the system leads to a deformation of the liquid channel made of PDMS and thus to an increase of its hydraulic diameter (D_{hyd}) as reported by Kartanas et al.[153] This deformation strongly influences the hydraulic resistance ($R_{res} \propto 1/(D_{hyd})^4$) and thus the generated backpressure. Since D_{hyd} is dependent on the liquid dynamic viscosity, the trend of the split ratios must follow the trend of the dynamic viscosities of the respective solvent compositions. Indeed, this is the case as shown in Figure 4.2b where the highest viscosity is for CH_3OH/H_2O 50/50 (10.5 mP, **blue**) > 10/90 (8.0 mP, **red**) > 90/10 (6.1 mP, **green**).

These results imply that while the split ratio, and thus the flow to the microfluidic spray-dryer, will stay constant during an isocratic HPLC run, flows will constantly change in a gradient HPLC mode. If the split ratio shifts are within the dynamic range (split ratios between 125 and 500), QCM dry mass sensing response is still expected to vary. Indeed, spraying a fixed concentration of solute (300 mg/L NaCl) returns a non-linear frequency response (Figure 4.2c) during CH_3OH/H_2O gradient run (Figure 4.2c, **gray**). The slope of the frequency change as a function of CH_3OH content follows in fact the observed shifts in split ratio earlier determined in the order CH_3OH 25-55% ($\partial\Delta f/\partial t$: -36, **blue**) < 10-25% & 55-90% ($\partial\Delta f/\partial t$: -44, **red**&**green**). Based on these results, we developed a calibration and data processing strategy, where we prepare calibration solvents (e.g., H_2O, CH_3OH) with an NaCl concentration of 300 mg/L for binary solvent systems and record the QCM response as a function of time during the same gradient run of the sample. This calibration is used to quantify the amount of solutes in the sample by dividing the frequency change of the sample with the one of the calibration. This strategy is not only valid for solute concentrations of 300 mg/L but also for large range of concentrations as the sprayed mass gives linear response of the frequency change in this range (30 to 500 mg/L, see supporting information Figure A.4.1).

4.3.2 Evaluation of Lower and Upper Quantification Limits

The concentration range in which accurate quantification of masses is achievable using the presented QCM dry mass sensing approach was investigated next by spraying different concentrations of NaCl (from 0 to 180 mg/L)

Table 4.1 LODs, LOQs and upper limit determined for dry-mass sensing for three solvent compositions over 10 minute duration.

CH_3OH/H_2O (v/v)	LOD mg/L	LOQ mg/L	upper limit mg/L
15/85	15	52	336±7
50/50	4.3	16	408±2
85/15	12	42	475±4

in a binary mobile phase system (i.e., CH_3OH/H_2O) for three different compositions (CH_3OH/H_2O 15/85, 50/50, and 85/15 (v/v)). The LOD and LOQ were determined according to the calibration method by using the slope of the frequency change per minute for each measurement as signal intensity term (y); the results are shown in Table 4.1.

The LOD for the different mobile phase compositions ranged from 4.3 mg/L to 15 mg/L, whereas the LOQ was found to be from 16 mg/L to 52 mg/L. The presented system's detection limits are at least 6 times lower than that estimated by Kartanas et al.[153] for aquatic conditions (LOQ: 100 mg/L). Although we observed lower noise levels in this study (5-15 Hz) compared with Kartanas et al.[153] (aquatic: 30 Hz), this cannot alone explain these results. In our study, the lowest detection limits were determined for CH_3OH/H_2O 50/50 composition (LOD = 4.3 mg/L, noise = 10 Hz), whereas the observed noise was found to be smallest for CH_3OH/H_2O 85/15 composition (LOD = 12 mg/L, noise = 5 Hz). Flow rates cannot fully explain the observed trends of the detection limits either, as they do not follow the same order we observed earlier. This indicates that the exact limits are not merely dependent on the noise and the flow rate, but also on other interconnected factors that are influenced by both the solvent composition and the flow rate including the spray cone dimensions, uniformity of the generated spray, droplet size, and evaporation rate of solvent(s).[238–240]

There exists, however, not only a lower limit of the QCM quantification but also an upper limit, above which both trueness and precision of QCM dry mass sensing is compromised. Indeed, spraying a salt solution with high concentration (500 mg/L) on the QCM led over time to an increase in noise, to a shift of the slope of the frequency change, and to increased resistance values measured on the QCM (see Figure 4.3). Since higher resistance values indicate a change in oscillation behavior of the quartz crystal, and hence a change of the frequency-mass correlation,[241] we defined an operational upper limit when the measured resistance is by a factor of three higher than the starting resistance. This corresponds to a change of the noise over time ≤ 5 Hz/min and a difference of the frequency change ≤ 7 Hz/min among triplicates. For a 10 minute measurement, the upper limit was found to be above 330 mg/L for all solvent compositions (see Table 4.1), which corresponds to 2 measurements at c_{sample} = 5000 mg/L (injection volume = 200 µL) and $R_{split} = 200 - 290$. This suggests that cleaning the QCM sensor after each measurement may be necessary to guarantee reproducible and accurate results. Such a step was accomplished in this study by 2-3 gentle swipes of the QCM sensor surface using a wet microfiber cloth that proved to be effective with no significant deviation of frequency change over time even after

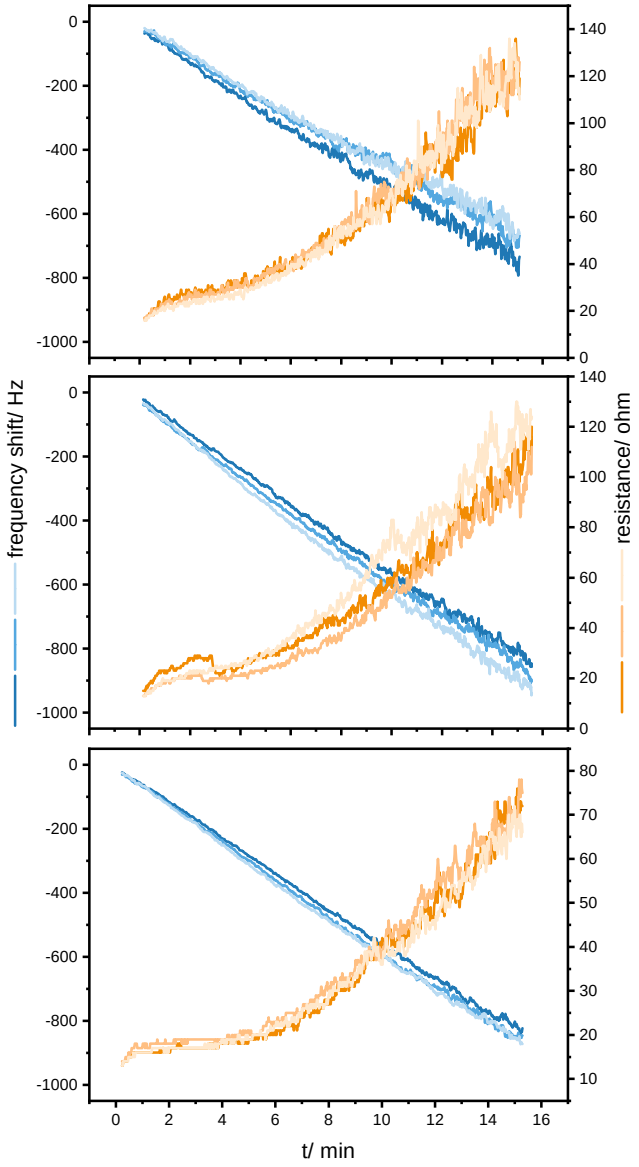

Figure 4.3 Frequency (blue) and resistance (orange) raw data of triplicate measurements of three different CH_3OH/H_2O compositions ((a): 15/85, (b): 50/50, (c): 85/15 (v/v)) containing 500 mg/L NaCl.

100 deposition and cleaning cycles (deviation from new sensor: $\partial \Delta f / \partial t$ = 0.4±2.4 Hz/min). Alternatively, depositing a droplet of CH_3OH/H_2O on the surface and blowing it away using pressurized air was equally effective — a step that can be easily automated.

4.3.3 Validation of Online QCM Dry Mass Sensing Against Offline TOC Fraction Analysis for Organic Matrix

We validated the accuracy of QCM dry-mass sensing coupled to HPLC by real-time monitoring of an NOM extract during HPLC separation using our system and compared it with the results of offline TOC analysis of collected HPLC fractions during the same run as a reference strategy. This was possible since the extracted NOM could be reconstituted in H_2O without significant losses (NOM recovery ≥ 98%) while inorganic salts

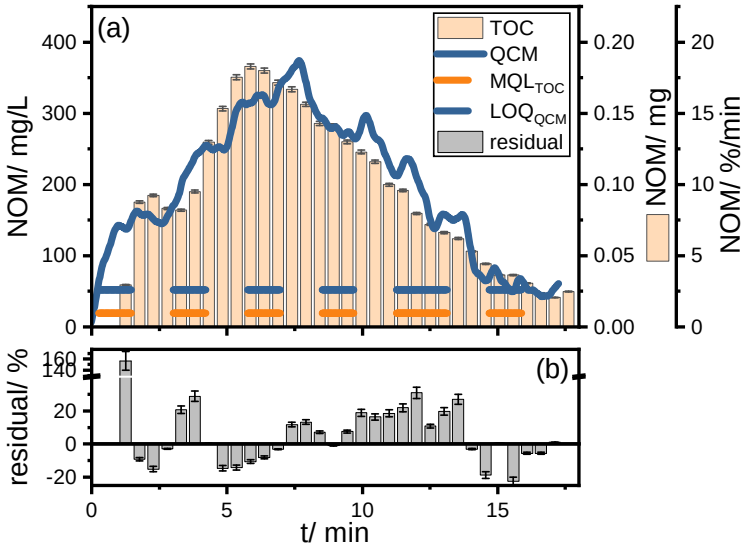

Figure 4.4 (a) Comparison of the NOM matrix monitoring results obtained by dry-mass sensing (blue line) with the results of offline TOC analysis of LC fractions (orange bar chart) during isocratic HPLC separation (CH_3OH/H_2O 30/70 v/v; 0.5 mL/min) of NOM (injected mass = 1 mg) on column (XTerra RP18, 150 × 3.0 mm, 3.5 µm). Orange dashed line: MQL of TOC analysis (13.2 mg/L). Blue dashed line: LOQ of QCM (40 mg/L). (b) Gray bar chart: Variance of QCM and TOC measurement per fraction shown as residual in %.

were already removed during the pre-extraction step. NOM quantification using QCM dry-mass sensing (see Figure 4.4a, **blue line**, see Figure A.4.3 for QCM raw data) is in good agreement with fraction analysis using TOC (Figure 4.4a, **orange bars**). Both detection techniques show that NOM elutes as an unresolved hump with maxima between 4 and 9 min, which is a typical behavior of NOM during RP HPLC using C18 separation columns of similar dimensions.[242,243] Moreover, absolute recoveries obtained by real-time QCM dry mass sensing (= 103±10%) agree well with that of offline TOC fraction analysis (= 98±1%). These results confirm the suitability of QCM dry mass sensing for real-time monitoring of complex matrices during a typical HPLC separation. The lower precision achieved by QCM dry mass sensing (= ±10%) compared to TOC analysis (= ±1%) is conceivably the result of the variations associated with the continuous spraying/evaporation processes (typical precision of QCM measurements without spray-drying: 0.1 Hz).[120]

Analysis of variance shows a tendency of QCM to overestimate NOM (see Figure 4.4b). This overestimation sums up to a total of 5±11% until the retention time where limit of quantification for QCM is reached (t = 17.2 min, LOQ_{QCM} = 52 mg/L, Figure 4.4a **blue dashed line**), which is still within the measured QCM precision. Note that LOQ of dry mass sensing is 2.7 times higher than the method quantification limit of offline TOC analysis (MQL = 19.2 mg/L, Figure 4.4a **orange dashed line**, for calculation from LOD to MQL see Figure A.4.2). This narrow sensitivity gap could easily be closed by further fine-tuning the performance of the spray-dryer such as spraying a higher fraction of the mass in the mobile phase on the QCM.

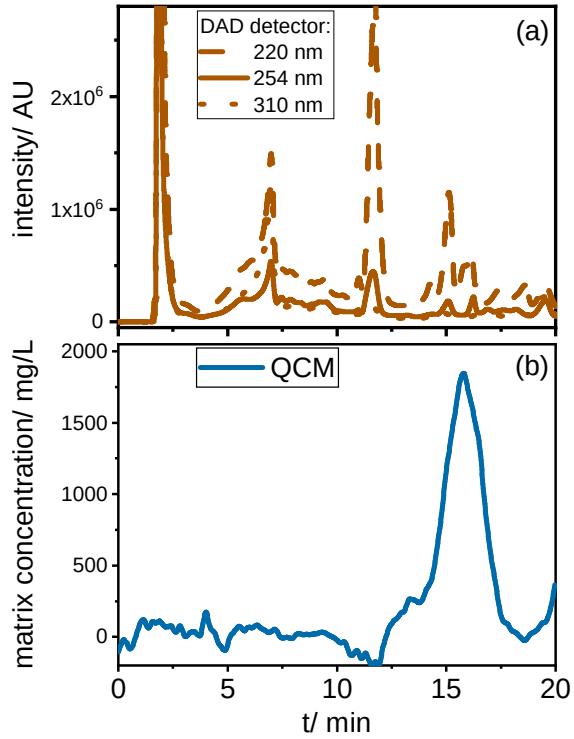

Figure 4.5 (a) UV/Vis chromatogram of RP HPLC purification of rice matrix (injected mass = 2.6 mg) at three different wavelengths (brown; 220 nm, 254 nm, 310 nm). (b) Monitoring of rice matrix during the same RP HPLC purification using dry-mass sensing (blue).

4.3.4 Applicability and Analytical Implication of QCM Dry Mass Sensing for the Analysis of Pesticides in Food

After a successful coupling, characterization, and validation of QCM dry mass sensing, it is important to (i) assess its applicability, as a holistic detector of complex matrices, to a real-world analytical task, and (ii) examine the implications of the data collected by QCM dry mass sensing for sample preparation. To this end, we chose a typical example of pesticide analysis (DEA, BAM, ATZ, BOSC, and Prop) in brown rice as food matrix using GC-MS after QuEChERS extraction followed by a typical HPLC cleanup step.

Qualitative Assessment – Reversed-Phase Separation of Brown Rice Matrix and Monitoring Using UV/Vis Detection and QCM Dry Mass Sensing

We applied QCM dry-mass sensing during RP HPLC of brown rice matrix and compared the response of the DAD detector and the QCM. Figure 4.5a shows the HPLC chromatogram measured with the DAD detector at three different wavelengths (brown: 220 nm (dashed line), 254 nm (solid line), 310 nm (dotted)) while Figure 4.5b represents the results of the QCM dry-mass sensing (blue). Data were acquired over a range of 190 nm – 800 nm but no significant changes in intensity ratios were observed across the chromatogram within the visible range and hence not discussed.

There is a vast discrepancy between the validated data acquired by the QCM compared with the DAD detector where most matrix elutes in the time window 13.5-17.5 min whereas UV absorption shows only some scattered peaks. This demonstrates the unsuitability of using UV/Vis for food matrix monitoring and quantification purposes. This further confirms other studies that compared UV/Vis and TOC analysis during HPLC purification of NOM.[243,244] It comes as no surprise that UV/Vis detection can not quantify matrix compounds since the response depends on the specific chemical compound/class and its molar absorptivity,[245] as well as absorption wavelength (e.g., 220 nm: aromatic and carboxylic chromophores, 254 nm: aromatic groups with varying degrees of activation).[114,246] Sugitate et al.[228] identified monoacylglycerols as the most abundant chemical class found in GC-MS analysis of the QuEChERS extract of brown rice. The lack of UV/Vis absorption of most fatty acids can conceivably explain the discrepancy between QCM and UV/Vis data between minute 13.5 and 17.5.[247,248] We identified, in fact, oleic acid as one of the main substances eluting in this range with GC-MS analysis using the NIST database (see Figure A.4.4). These results illustrate that mere reliance on UV detection during HPLC clean-up does not necessarily reveal information about the matrix's behavior and is thus inadequate to assess this analytical step's efficiency. Yet, combining the information gained from the DAD detector (i.e., insights into the compound structure and analyte retention times) with the complementary information obtained by QCM dry mass sensing (i.e., quantification of entire matrix) provides the analyst with a complete picture of the separation process.

Quantitative Implication – Matrix Effect Correlations in GC-MS Residue Analysis With QCM Dry Mass Sensing Data

We further examined the interpretability of acquired data using QCM dry mass sensing during a typical HPLC clean-up on a subsequent analysis using GC-MS as an example. To this end, five fractions that were quantified using QCM dry mass sensing (see retention windows in Table A.4.5) were collected during an HPLC clean-up of brown rice matrix, spiked with an analyte mixture (DEA, BAM, ATZ, BOSC, and Prop), and matrix effects associated with each analyte in each fraction were measured using GC-MS (see Figure 4.6 and Table A.4.5).

The relative amount of matrix in each fraction ($matrix_{frac}/matrix_{total}$) determined by QCM dry mass sensing correlates with the observed matrix effects (blue symbols in Figure 4.6). These correlations were found for all investigated compounds with signal enhancement for DEA (R^2 = 0.99), BAM (0.99), ATZ (0.99), and BOSC (0.99), and with signal suppression, observed for Prop (0.95). In contrast, such a correlation couldn't be observed when UV/Vis data were used to estimate the percentage of the total matrix in the respective fraction (brown symbols in Figure 4.6). Our findings, which primarily demonstrate signal enhancement, are consistent with the literature since this effect is the most common type (> 90%) observed in GC-MS residue analysis.[155,228,249] While we can not explain the correlation for signal suppression since no mechanism has been proposed and accepted in literature for this phenomenon,[155,228,249] the signal enhancement correlations

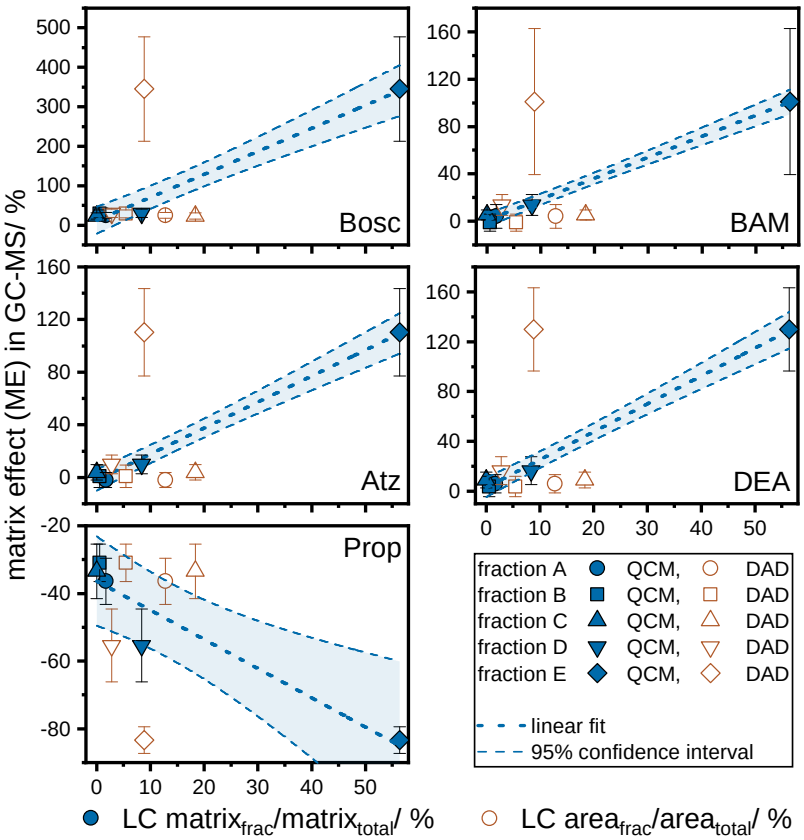

Figure 4.6 Observed matrix effects (ME) for DEA, BAM, ATZ, BOSC, and Prop during GC-MS analysis in 5 different fractions (A-E) of brown rice matrix after HPLC clean-up plotted against the percentage of total matrix contained in the respective fraction ($matrix_{frac}/matrix_{total}$) according to QCM dry mass sensing (blue symbols). GC-MS conditions were V_{inj} = 1 µL, split ratio = 1/10, detection mode = SIM, column = Restek™RxiTM-5ms, 30 m×0.25 mm, 0.25 µm. Each HPLC fraction corresponds to a retention window of 1.5 min (see Table A.4.5). The respective DAD results at 220 nm are shown for comparison (brown symbols).

can be explained using the established mechanism of matrix-induced chromatographic response enhancement in GC. Signal enhancement is caused by matrix components competing with the analyte for the adsorption on active sites present in the injection liner and chromatographic column, which are mainly free silanol groups. In this way, analyte losses are reduced due to irreversible adsorption or catalytic decomposition.[155] Literature shows that the extent of such signal enhancement is dependent on (i) the mass of the matrix in the sample,[228,250] which the found correlations corroborate.

The extent of the signal enhancement further depends on (ii) the strength of interaction between the active sites and the components in the matrix, as well as (iii) the analyte properties.[47,228,250] Although the limited number of investigated compounds in this study doesn't allow a comprehensive disentanglement of (ii) and (iii), the results still show that different compounds have different sensitivities to matrix effects as a function of the matrix mass (i.e. $\partial ME/\partial m_{matrix}$) following the order BAM (1.8±0.1) ≈ ATZ (2.0±0.1) ≈ DEA (2.2±0.1) < BOSC (5.8±0.4). This suggests that the late-eluting compound on GC BOSC (22.9 min) is the most susceptible to signal enhancement compared with the early-eluting DEA, BAM, and ATZ (12-13.9 min). This agrees with Anastassiades et al.,[250] who illustrated that monoacylglycerols, the most abundant matrix component in brown rice,[228] elutes in the late window of chromatography giving rise to the highest matrix effects for late-eluting pesticides. These results demonstrate that the data acquired by QCM dry mass sensing during a typical HPLC clean-up of a complex sample provide, in fact, meaningful information on the efficiency of this clean-up step. The analyst can use the acquired data to minimize matrix co-elution reducing thereby adverse matrix effects in the subsequent analysis.

4.4 Conclusion

The current work presents the successful coupling of a commercial HPLC system with a QCM using a microfluidic spray-dryer. We demonstrate that QCM dry mass sensing is suitable as a holistic detector for quantifying complex organic matrices during HPLC clean-up, in contrast to other detectors such as UV/Vis. Validation against offline TOC analysis confirmed the successful coupling, calibration and data processing strategy and its suitability within a precision of 10%. The demonstrated results of NOM and brown rice matrix, in conjunction with the system's current LOQ (16-52 mg/L), prove that the employed technique is relevant for a large range of real samples in environmental and food chemistry. This can possibly be further extended to other fields (e.g., archaeology, forensics) with similar loads of matrix, whereas further reduction of the systems LOQ may be necessary for more matrix-susceptible samples. The direct correlation found between the amount of brown rice matrix, quantified by QCM dry mass sensing, and matrix effects measured in GC-MS agrees with the established understanding of matrix-induced chromatographic response enhancement. This implies that the developed system can be a useful tool to minimize matrix co-elution reducing thereby adverse matrix effects in

a subsequent analysis, which is the ultimate goal of a clean-up. The exact potential gain of such an optimized clean-up is further evaluated in the companion paper.[229]

5 Quartz Crystal Microbalance as Holistic Detector for Quantifying Complex Organic Matrices During Liquid Chromatography: 2. Compound Specific Isotope Analysis

Abstract

In carbon-compound-specific isotope analysis (carbon-CSIA) of environmental micropollutants, purification of samples is often required to guarantee accurate measurements of a target compound. A companion paper has brought forward an innovative approach to couple quartz crystal microbalance (QCM) with high-performance liquid chromatography (HPLC) for online quantification of matrices during a gradient HPLC purification. This paper investigates the benefit for isotope analysis of polar micropollutants typically present in environmental samples. Here, we studied the impact of natural organic matter (NOM) on the isotopic integrity of model analytes and the suitability of the NOM-to-analyte ratio as a proxy for sample purity. We further investigated limitations and enhancement of HPLC purification using QCM on C_{18} and C_8 phases for single- and multiple-targets. Strong isotopic shifts of up to 3.3‰ towards the isotopic signature of NOM were observed for samples with a NOM-to-analyte ratio $\geq$ 10. Thanks to QCM, optimization of matrix removal of up to 99.8% of NOM was possible for late-eluting compounds. The efficiency of HPLC purification deteriorated when aiming for simultaneous purification of two or three compounds, leading to up to 2.5% less NOM removal. Our results suggest that one optimized HPLC purification can be achieved through systematic screening of 3 to 5 different gradients thereby leading to a shift of the boundaries of accurate carbon-CSIA by up to two orders of magnitude toward lower micropollutant concentrations.

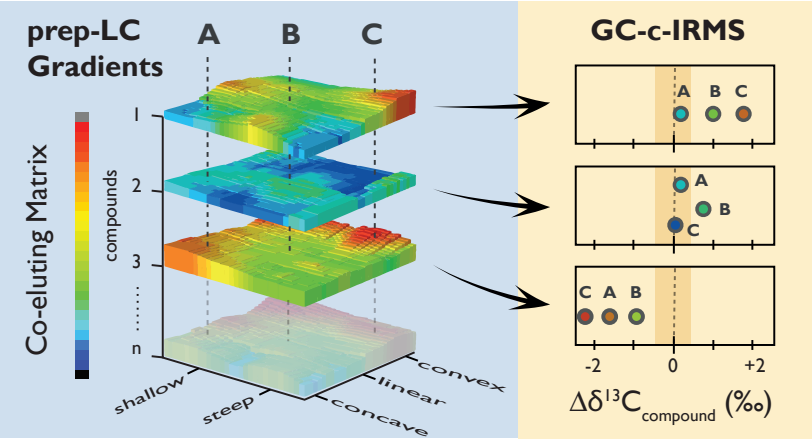

The results of this chapter were published in a modified form in a peer-reviewed journal.

Reprinted with permission from:

Christopher Wabnitz, Wei Chen, Martin Elsner, and Rani Bakkour. Quartz Crystal Microbalance as Holistic Detector for Quantifying Complex Organic Matrices During Liquid Chromatography: 2. Compound Specific Isotope Analysis. *Analytical Chemistry* **2024**, *96*, 7436–7443.

5.1 Introduction

Compound-specific isotope analysis (CSIA) has proven to be a powerful tool for identifying environmental contamination sources and delineating their natural and engineered degradation pathways by measuring isotopic ratios (i.e., $^{13}C/^{12}C$, $^{15}N/^{14}N$) of the contaminant/target analyte at natural abundance.[2,3,17–19,30,31,33,251–253] To this end, gas chromatography combustion isotope ratio mass spectrometry (GC-c-IRMS) is typically used, where the contaminant is separated from other components in the sample using a GC, then converted in a combustion oven to a universal gas (i.e., CO_2, N_2), and measured using a sector field MS.[6,21–23] The structural information of the compound gets, however, lost during this process, which makes accurate CSIA susceptible to interferences by concurrent carbon-/ nitrogen-containing constituents in the same sample.[3–5] This represents a challenge for carbon CSIA of polar environmental contaminants that occur in low concentrations, such as pesticides and pharmaceuticals, for the following reasons. (i) The concentrations of such contaminants occur in the ng/L to µg/L range, whereas the potential interferences, namely natural organic matter (NOM), occur at 10^3 to 10^6 higher concentrations in the mg/L range.[62] (ii) The heterogeneity of NOM, which consists of thousands of different organic compounds found in environmental samples like river water, renders an efficient separation of the target analyte and interferences challenging in one extraction step.[50,80] While classical mass spectrometry can correct for adverse effects caused by such interferences using, for example, internal standards,[42–45] analyte protectants,[46,47] or matrix-matched calibration,[42,45,48] such corrections are not possible in GC-c-IRMS. Therefore, CSIA critically depends on highly purified samples.

Several purification strategies are at the analyst's disposal to separate target analytes from sample interferences, also referred to as matrix, in carbon-CSIA sample preparation. These strategies range from offline chromatographic techniques using conventional solid-phase extraction (SPE) materials,[65,66] molecularly imprinted polymers (MIPs),[56] cyclodextrin polymers,[50] immunoaffinity chromatography,[81] silica gel chromatography,[73,74] or ion-exchange chromatography,[70] to different types of online chromatographic purification techniques including size-exclusion chromatography,[72] or the most widely used reversed-phase (RP) high-performance liquid chromatography (HPLC).[28,66,68,75–79] While the target analytes are monitored in most of these works, this is not necessarily the case for all interferences. For example, consider $^{13}C/^{12}C$ measurement of atrazine in a groundwater extract containing interfering NOM, where chromatographic clean-up is warranted prior to GC-c-IRMS. To screen for the optimal clean-up conditions, fractions have to be collected, organic solvents removed, the sample reconstituted in water, and each fraction measured using a total organic carbon (TOC) analyzer. On the other hand, quantification of matrix interferences during online purification procedures like HPLC is often hindered by a lack of suitable detectors.[254] Detectors usually combined with HPLC are only able to monitor specific fractions of common matrices like NOM (i.e., chromophoric, fluorescent, or ionizable)[114,115] or show inter-compound response differences, as discussed in detail in the companion paper.[115–118,254] Alternatively, monitoring and quantifying potential interferences during the purification would, in fact, give insights into the

success of the clean-up and its exact gain. We have brought forward in the companion study an innovative approach using quartz crystal microbalance (QCM) dry mass sensing that was coupled to RP HPLC and used to monitor and gravimetrically quantify different types of matrices (NOM, brown rice) during a gradient HPLC purification.[254]

In the current and the companion study,[254] we spray a small part (<1%) of the column effluent on a QCM using a microfluidic spray-dryer, adopting elements of other works by Schulz et al.,[150] Müller et al.,[151] and Kartanas et al.[153] In this process, the column effluent is nebulized into micron-sized droplets, which leads to the immediate evaporation of the solvent and deposits the non-volatile components on the QCM. Their absolute mass is measured due to the QCM's ability to measure mass changes on the oscillating piezoelectric quartz crystal with sub-nanogram resolution.[119,121] Using this approach, it was possible to quantify matrix interferences in real-time during RP HPLC. Remarkably, these matrix interferences correlated with the extent of matrix effects on observable instrument response (signal enhancement/ suppression) observed during subsequent GC-MS analysis ($R^2 \geq 95$).[254] This approach, hence, circumvented challenges for QCM dry mass sensing before application to RP HPLC clean-up through (i) enabling the use of organic solvents including gradients by using a microfluidic spray-dryer, (ii) characterizing variations of the QCM response caused by gradients, and (iii) alleviating the impact of the latter through a suitable calibration strategy.[254] It seems ideal to apply this approach for environmental extracts intended for carbon-CSIA measurements after RP HPLC. Yet, a quantitative assessment of the gain of optimizing RP HPLC purification using real-time matrix monitoring has never been conducted — and its impact on accurate carbon-CSIA never been explored.

The work presented in this and the companion paper[254] has the overall goal of exploring the feasibility of coupling a commercial HPLC with a microfluidic spray-dryer and a QCM for online monitoring of organic matrix components during RP HPLC gradient purification for different mass spectrometry-based applications in environmental and food sciences. Both studies focus on organic matrices in already extracted samples where most inorganic salts are excluded through a first SPE step. While the technical and fundamental groundwork for matrix online monitoring using QCM dry mass sensing during RP HPLC was laid out in the companion study,[254] this paper systematically investigates the purification potential of RP HPLC before $^{13}C/^{12}C$ analysis of polar micropollutants present in environmental water samples using GC-c-IRMS. To this end, we (i) studied the impact of NOM on the isotopic integrity of model analytes and whether the NOM-to-analyte ratio ($C_{NOM}/C_{analyte}$, nmol C/nmol C) can be used as a proxy for the sample purity and (ii) investigated limitations and enhancement of HPLC purification using QCM dry mass sensing on C_{18} and C_8 phases for single- and multiple-targets.

5.2 Experimental Section

5.2.1 Chemicals, Materials, and Samples

A list of purchased chemicals and materials, a description of standard solutions, and working solutions used in this study are provided in the supporting information (section E.1). NOM was extracted from surface water samples as detailed in the companion paper[254] and summarized in section E.2. Samples for isotope analysis with different NOM/analyte ratios (10, 20, 50, 100), $C_{NOM}/C_{analyte}$ in mol C/mol C, were prepared in methanol by mixing the stock solution of extracted NOM with stock solution of corresponding analyte to reach an analyte concentration of 1667 nmol C/mL, corresponding to 5 nmol C per injection on GC-c-IRMS. Extracts for HPLC purification were prepared in methanol/water (25/75 v/v) and contained 3 mg/L of eight different model analytes, namely 2,6-dichlorobenzamide (BAM), atrazine (ATZ), azoxystrobin (AZOX), boscalid (BOSC), caffeine (CAF), desethylatrazine (DEA), desisopropylatrazine (DIA), and simazine (SIM), and 9000 mg/L of the extracted river water NOM. These extracts correspond to original water samples with 3.6 mg/L NOM and 120 ng/L analyte.

5.2.2 Chemical Analysis

Compound Specific Isotope Analysis

Carbon isotope measurements were performed on a GC-c-IRMS system consisting of a GC (TRACE GC Ultra multi-channel gas chromatograph, Thermo Fisher Scientific, Germany; Column: J&W DB-5MS UI column, L = 30 m × ID = 0.25 × film thickness = 1.0 µm, Agilent, Germany), a combustion interface (Finnigan GC Combustion III interface, Thermo Fisher Scientific, Germany), and an IRMS (Finnigan MAT 253 IRMS, Thermo Fisher Scientific, Germany). The combustion interface consisted of an oxidation reactor (1050 °C) with an alumina tube (L = 320 mm, ID = 0.5 mm, OD = 1.5 mm, Friatec, Germany) containing one platinum wire (D = 0.1 mm, 99.99% purity, Goodfellow, GB) and two nickel wires (D = 0.1 mm, 99.99% purity, Alfa Aesar, Germany). An identical alumina tube enclosing three copper wires (0.1 mm diameter, 99.99% purity, Alfa Aeser, Germany) was used for the reduction reactor (650 °C). Extracts in methanol were injected (3 µL injection volume) using an autosampler (GC PAL, CTC, Switzerland) with splitless injection mode (liner: ID = 5 mm × L = 105 mm, Thermo Fisher Scientific, Germany) at 250 at a surge pressure of 250 kPa. Analytes were separated at a helium flow of 1.4 mL/min using the following temperature program. The starting temperature was 120 °C (1 min hold time), followed by a temperature ramp of 22 °C/min to 250 °C, and a ramp of 40 °C/min to 325 °C (9 min hold time). The peaks were automatically detected and baseline-corrected (individual background algorithm) using the Isodat software of Thermo Fisher Scientific, Germany. Isotope ratios were calculated in relation to a CO_2 reference gas (Carbo, Germany) and are reported as arithmetic means of at least triplicate measurements as $\delta^{13}C$ values (in ‰) with the respective 95% Confidence Interval (CI) relative

to the international reference material Vienna PeeDee Belemnite (VPDB).[255] In addition, standard bracketing procedures were used to ensure identical treatment of standard and sample[256] and method quantification limits were determined according to the moving mean procedure (see Figure A.4.1 and Table A.4.5).[64]

High-Performance Liquid Chromatography

A Nexera XR HPLC system (Shimadzu, Japan) was used for chromatographic separation. It consists of a solvent delivery module (LC-20AD, Shimadzu, Japan), a diode array detector (DAD) (SPD-M20A, Shimadzu, Japan), and a fraction collector (FRC-10A, Shimadzu, Japan). As the stationary phase, two different columns were used: XTerra RP18 column (particle size = 3.5 µm, L×D = 150 × 3.0 mm, pore size = 125 Å, Waters, USA) and Orbit 100 C8 column (particle size = 3.5 µm, L×D = 150 × 3.0 mm, pore size = 100 Å, MZ Analysentechnik, Germany). As the mobile phase, binary gradients consisting of water (A) and methanol/water (90/10 v/v) (B) were used. A column oven temperature of 40 , a flow rate of 0.5 mL/min, and a sample injection volume of 200 µL were used for all measurements. Using the DAD detector, the retention time and peak width of each analyte were determined at the corresponding maximum absorption wavelength and used to constrain the fraction in which the analyte was completely recovered. For HPLC optimization, the RP gradient conditions were systematically varied by changing the percentage of CH_3OH in the mobile phase at minute 7.5 (30, 40, 50, 60, 70, 80, or 90%) and minute 15 (60, 70, 80, or 90%) covering thereby linear, concave, and convex gradients. Twenty-two and 7 different gradients were studied for XTerra RP18 column and Orbit 100 C8 column, respectively (see Table A.4.7 and A.4.8).

QCM Dry Mass Sensing Coupled to HPLC

The QCM dry mass sensing system was coupled to the HPLC, characterized, and validated as described in detail in the companion paper.[254] In short, the HPLC effluent was split after the DAD detector and prior to the fraction collector using a post-column adjustable flow splitter. The high-flow port was connected to the fraction collector, whereas the low-flow port to a microfluidic spray-dryer. The latter was fabricated in-house using a standard polydimethylsiloxane (PDMS) soft lithography approach.[254] Using the spray-dryer, the HPLC effluent was sprayed onto a 5 MHz QCM crystal (100RX1, Cr/Au, Stanford Research Systems, USA) placed in a frequency counter (QCM200, gate time: 0.1 s, Stanford Research Systems, USA). Each measurement consisted of a blank run (methanol/water 25/75 v/v), the sample (NOM-containing extract), and a one-point calibration (c(NaCl) = 300 mg/L in mobile phase), which were used to derive the concentration of matrix in mg/L in the sample during chromatography.

5.2.3 Data Evaluation

QCM Dry Mass Sensing

The QCM dry mass sensing data was evaluated using a Matlab script as reported in the companion paper.[254] In short, after correcting the frequency measurement of the sample and that of the calibration using the one of the blank, the 1st derivative was derived from the corrected frequencies. Then, 1st derivatives were smoothed using a Savitzky-Golay filter. To get the mass concentration of the sample in mg/L, the smoothed 1st derivative of the sample measurement was divided by the smoothed 1st derivative of the calibration measurement and multiplied by the concentration of the calibration solution (see Eq. 1 in companion paper[254]).

$C_{NOM}/C_{analyte}$ Ratio and Gain Factor

The $C_{NOM}/C_{analyte}$ ratio in mol C/mol C before HPLC purification ($[C_{NOM}/C_{analyte}]_{no\,LC}$) was calculated by dividing the molar concentration of NOM by the molar concentration of the respective analyte in the extract. To calculate the $C_{NOM}/C_{analyte}$ ratio after the HPLC purification ($[C_{NOM}/C_{analyte}]_{LC}$), the integral of the NOM data measured using QCM dry mass sensing during the HPLC purification was taken over the corresponding time window of the analyte peak ($area_{fraction}$). The latter was divided by the integral of the NOM data over the whole chromatogram ($area_{total}$), where complete recovery of NOM was validated, to get the percentage of NOM co-eluting during the analyte fraction (see Eq. 5.1).

$$NOM_{co\text{-}elution} = \frac{area_{fraction}}{area_{total}} \cdot 100 \tag{5.1}$$

$[C_{NOM}/C_{analyte}]_{no\,LC}$ was multiplied by the percentage of NOM co-eluting in the respective fraction to get $[C_{NOM}/C_{analyte}]_{LC}$ (see Eq. 5.2).

$$[C_{NOM}/C_{analyte}]_{LC} = \frac{NOM_{co\text{-}elution} \cdot [C_{NOM}/C_{analyte}]_{no\,LC}}{100} \tag{5.2}$$

The gain factor, which is the factor by which the $C_{NOM}/C_{analyte}$ was improved, was calculated by dividing $[C_{NOM}/C_{analyte}]_{no\,LC}$ by $[C_{NOM}/C_{analyte}]_{LC}$ (see Eq 5.3).

$$\text{gain factor} = \frac{[C_{NOM}/C_{analyte}]_{no\,LC}}{[C_{NOM}/C_{analyte}]_{LC}} \tag{5.3}$$

Matrix Removal for Individual and Multiple Compounds

The matrix removal in % for individual compounds was calculated by subtracting the percentage of co-eluting NOM from 100 (see Eq. 5.4).

$$\text{matrix removal}_{individual} = 100 - NOM_{co\text{-}elution} \tag{5.4}$$

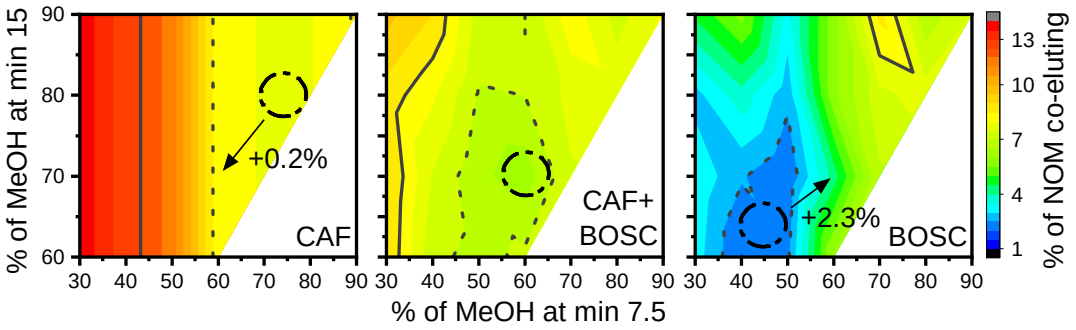

Figure 5.1 Gradient screening for the individual compounds CAF and BOSC and their NOM co-elution average for HPLC purification on XTerra RP18 of both compounds at the same time (CAF+BOSC). The optimal gradient with the lowest NOM co-elution is encircled both for the individual compound purification (CAF, BOSC, $gradient_i$) and multiple compound purification (CAF+BOSC, $gradient_m$). The arrows show the difference between the optimal $gradient_i$ and the optimal $gradient_m$, the number next to the arrows the difference of NOM co-elution in % between $gradient_i$ and $gradient_m$.

To determine the maximal matrix removal during multiple compound purification, we added for each investigated HPLC gradient the respective matrix removal of the individual compounds and divided the value by the number of compounds n to get the average matrix removal for n-compounds ($\text{matrix removal}_{\text{n-compounds}}$) (see Eq. 5.5; see examples in Figure 5.1 and A.4.15).

$$\text{matrix removal}_{\text{n-compounds}} = \frac{\sum_{k=1}^{n} \text{matrix removal (k)}}{n} \tag{5.5}$$

This calculation was made for each HPLC gradient separately. The gradient with the highest $\text{matrix removal}_{\text{n-compounds}}$ ($gradient_m$) was selected as the optimal gradient for the respective combination of compounds. The exact matrix removal of each of the compounds for $gradient_m$ was used as the maximal matrix removal for this exact purification problem. The difference between the optimal gradient determined for the individual compound ($gradient_i$) and $gradient_m$ is reported as loss in matrix removal. Repeating this procedure for several combinations of two or three early, middle, and late eluting compounds (see Table A.4.17 and A.4.18) made it possible to determine an average matrix removal and to plot the different determined numbers in a box plot (see Figure 5.5).

5.3 Results and Discussion

5.3.1 Natural Organic Matter-to-Analyte Ratio as Proxy for Sample Purity and its Impact on Isotopic Integrity

We assessed the NOM/analyte ratio, $C_{NOM}/C_{analyte}$ in mol C/mol C, as representative indicator of sample purity and its impact on accurate isotope analysis. Figure 5.2a shows measured $\delta^{13}C$ values on GC-c-IRMS of four different model analytes, namely DIA ($\delta^{13}C$ = -36.8±0.5‰), ATZ (-29.6±0.5‰), DEA (-29.4±0.5‰), and CAF ($\delta^{13}C$ = -1.2±0.5‰), in extracts containing different $C_{NOM}/C_{analyte}$ ratios (10, 20, 50, 100 mol C/mol C) and compared to standard measurements in the absence of NOM. Analyte concentrations were kept constant for all

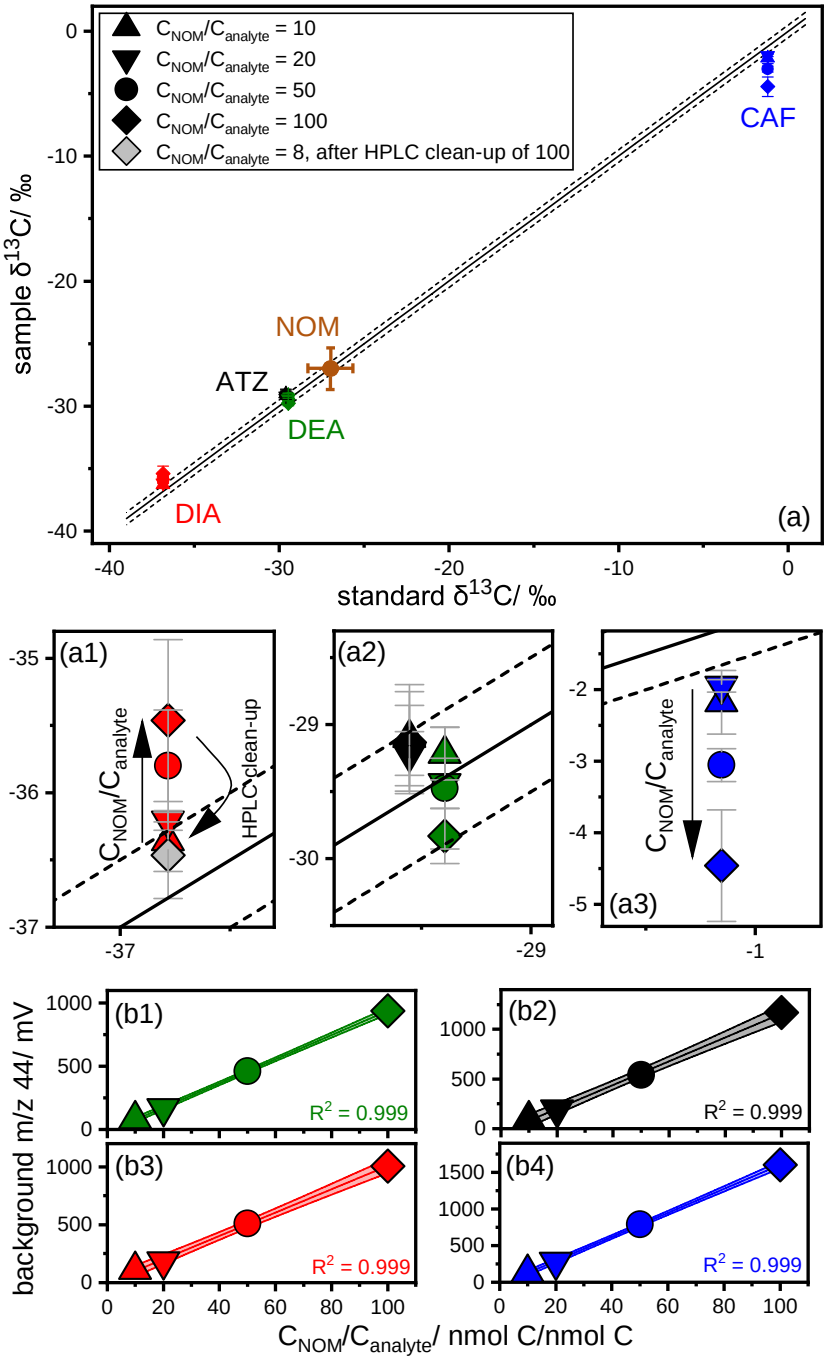

Figure 5.2 (a) The isotope value of standard measurements of four different analytes (DEA: green, ATZ: black, DIA: red, CAF: blue) is plotted against the isotope value measured in extracts containing NOM in different $C_{NOM}/C_{analyte}$ ratios (10: triangle up, 20: triangle down, 50: circle, 100: diamond). The range of typical NOM isotope values ($\delta^{13}C$ = 27±1‰) is highlighted (brown circle). (a1-a3) show the enlarged areas of the four analytes. (a1) gray: Extract with concentration of NOM equal to ratio 100 was subjected to HPLC clean-up using XTerra RP18 (see HPLC gradient in Table A.4.4). The respective fraction of DIA was collected, the solvents evaporated, NOM reconstituted and spiked with DIA to reach an analyte concentration of 1667 nmol C/mL and a total volume equal to the original NOM extract (200 µL). (b1-b4) Correlation of the background intensity (m/z 44/ mV) at the respective analyte retention time in the GC-c-IRMS chromatogram and the amount of NOM injected.

samples at 5 nmol C injected in each measurement, corresponding to concentrations of 57.9 mg/L (DIA), 44.9 mg/L (ATZ), 52.1 mg/L (DEA), and 40.5 mg/L (CAF) in the extract. The corresponding background intensities at m/z 44 are depicted in Figure 5.2b at the respective analyte retention time in the GC-c-IRMS chromatogram as a function of $C_{NOM}/C_{analyte}$.

We observed significant $\delta^{13}C$ shifts in the presence of NOM for DIA (Figure 5.2a1, red data, positive shift) and CAF (Figure 5.2a3, blue data, negative shift), while no significant shifts are visible for ATZ and DEA (Figure 5.2a2, black and green data). The absence of isotopic shifts for ATZ and DEA confirms the observation of Glöckler et al.[50] that compounds with an isotopic signature close to the one of NOM do not suffer from isotopic shifts induced by the sample matrix. Indeed, $\delta^{13}C$ of ATZ (-29.6±0.5‰) and DEA (-29.4±0.5‰) are both in the proximity of that of NOM (-27±1‰)[257] on the carbon isotopic scale. This implies that the obtained $\delta^{13}C$ values of the analytes are not only attributable to the compound but, strictly speaking, a bulk measurement of analyte and matrix. In contrast, the effect of NOM on $\delta^{13}C$ integrity of DIA (-36.8±0.5‰) and CAF (-1.2±0.5‰) is evident and becomes most pronounced the greater the distance of their isotopic signatures to that of NOM is. This is corroborated by the direction of the isotopic shift, which consistently goes in the direction of the isotopic signature of NOM (postive for DIA, negative for CAF), and the magnitude of the shift, which is greater for CAF ($\delta^{13}C_{sample}$ - $\delta^{13}C_{standard}$ for $C_{NOM}/C_{analyte}$ ratio 100: -3.3±0.8‰) compared to DIA (+1.3±0.6‰) reflecting the greater difference to the one of NOM on the isotopic scale (CAF-NOM = +25.8±1.1, DIA-NOM = -9.8±1.1). Even the magnitude of isotopic shifts is progressively following the $C_{NOM}/C_{analyte}$ ratios (see arrow in Figure 5.2a1&a3 and Figure A.4.2 in the supporting information). The observed deviation is, however, not precisely the composite of the background and the peak due to the applied individual background algorithm implemented in the Isodat software: The measured shift for CAF for $C_{NOM}/C_{analyte}$ ratio 100 ($\Delta\delta$ ^{13}C = -3.3‰) is, for example, four times smaller than the theoretically determined isotope shift using the ratio of background area to analyte area (-14.5‰) (see Table A.4.6). This shows that the applied background correction can reduce the influence of NOM but not entirely compensate for it, as already illustrated by Glöckler et al.[50]

The influence of the matrix NOM on the measurement can also be seen in the IRMS chromatograms. A distinct hump-shaped baseline rise is visible in the samples containing NOM (see Figure 5.3). We found a direct correlation ($R^2 \geq 0.999$) between the amount of NOM injected and the background intensity (m/z 44) recorded on the IRMS at the respective analyte retention times for all compounds (see Figure 5.2b). Consequently, the ratio of injected matrix and analyte, $C_{NOM}/C_{analyte}$, seems to be a good proxy of sample purity as proposed by Bakkour et al.[56] and Glöckler et al.[50] Accurate isotope values of DIA were only measured for $C_{NOM}/C_{analyte}$ $\leq$ 10 (Figure 5.2a1 and Figure A.4.2). To further probe for this, we moved the $C_{NOM}/C_{analyte}$ ratio from 100 to 8 using HPLC purification and were thus able to recover the isotope integrity of the analyte (Figure 5.2a1 grey data point). For CAF, a $C_{NOM}/C_{analyte}$ of 10 was not sufficient to resolve the target analyte peak and guarantee accurate isotope analysis (Figure 5.2a3 and Figure A.4.2). Upon comparing these findings with data

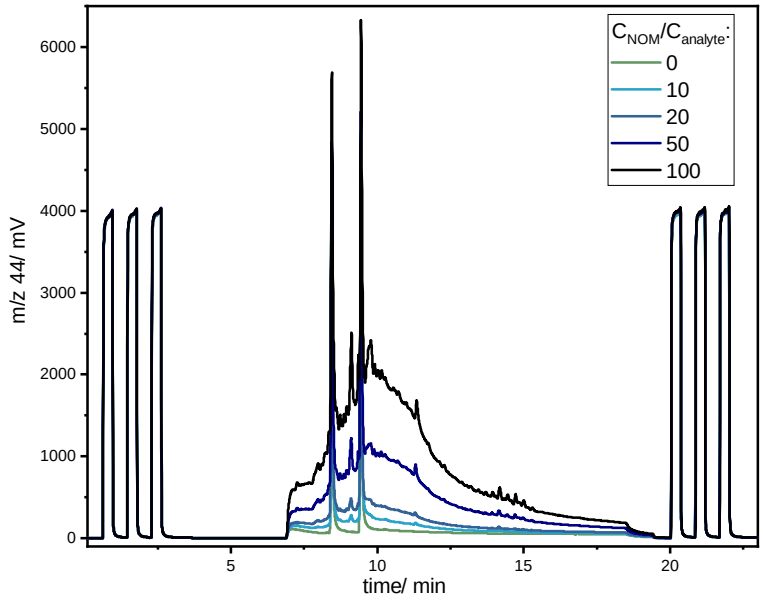

Figure 5.3 GC-IRMS chromatograms of DEA and CAF for different $C_{NOM}/C_{analyte}$ ratios.

published in the existing literature for other analytes, a noticeable range of approximately a $C_{NOM}/C_{analyte}$ ratio of 10 or slightly less emerges.[49,50] The exact $C_{NOM}/C_{analyte}$ ratio guaranteeing accurate isotope analysis varies depending on the analyte, the distance between the signature of the analyte and NOM on the isotopic scale, and the used GC method. This highlights the importance of (i) including standards spanning over a range of isotope signatures in carbon-CSIA method development and (ii) the purity of the sample as a strategy to avoid systematic bias in isotope values. Samples containing NOM in higher amounts therefore warrant sufficient sample purification procedures to guarantee accurate isotope analysis.

5.3.2 Limitations and Enhancement of Preparative Chromatography Revealed by QCM Dry Mass Sensing

To quantitatively assess the limits and possible enhancement of typical preparative chromatography clean-up steps in removing organic matrix from a sample extract, we selected 8 model compounds (CAF, BAM, DIA, DEA, SIM, ATZ, AZOX, BOSC; $\log K_{OW}$ range: -0.07-2.96) present in an extract containing NOM as organic matrix and subjected them to HPLC clean-up using a C_{18} stationary phase (XTerra RP18), a classical phase used in many CSIA applications (see Table A.4.19). Binary solvent mixtures of water and CH_3OH were systematically varied by changing the percentage of CH_3OH in the mobile phase at minute 7.5 and minute 15 thus covering linear, concave, and convex gradients (see illustrative gradients in Figure 5.4a; all gradients in Table A.4.7 and A.4.8). NOM concentrations in the HPLC effluent were acquired using QCM dry mass sensing, whereas analyte retention times were monitored using UV-Visible spectroscopy (UV/Vis) detection at the corresponding maximum absorption wavelength. Figure 5.4b depicts fractions of analytes at the corresponding retention time window where the analyte is completely recovered (coloured vertical bars), whereas the area underneath

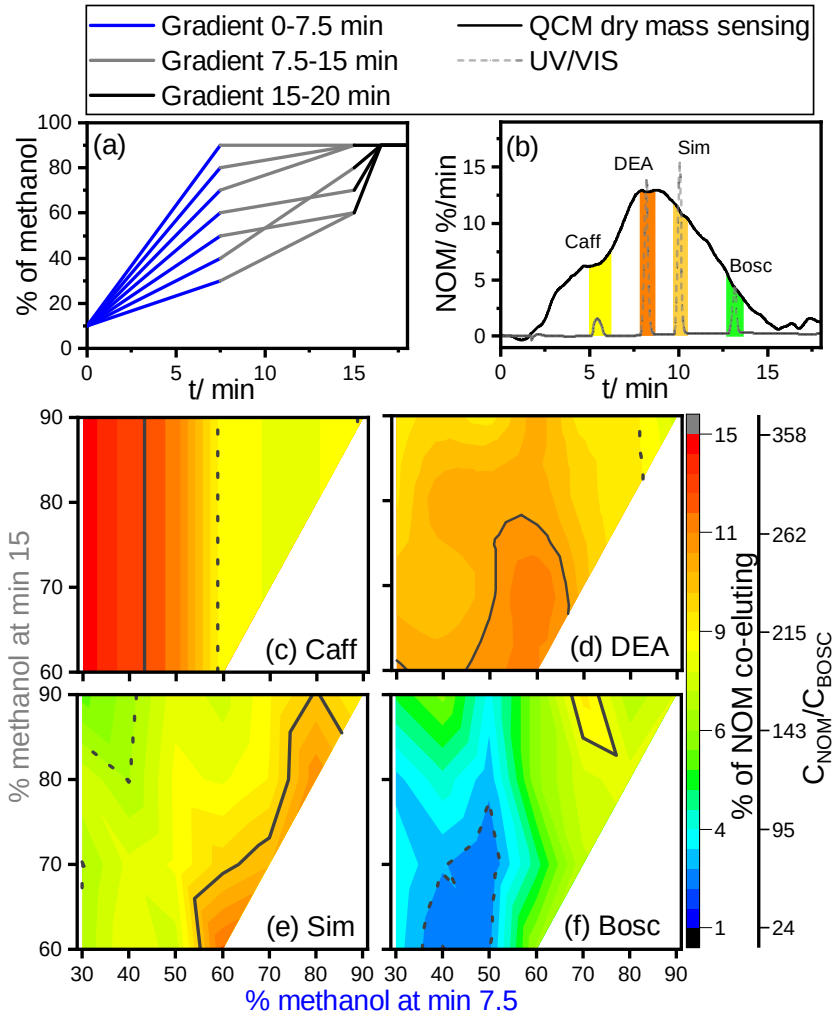

Figure 5.4 (a) Seven out of the 22 measured gradients with varying % of CH_3OH in the mobile phase till minute 7.5 (blue; 30, 40, 50, 60, 70, 80, or 90%) and minute 15 (grey; 60, 70, 80, or 90%). (b) Chromatogram (gradient 10-60-70) shows both the analyte peaks detected using UV/Vis for CAF, DEA, SIM, and BOSC (dotted grey line) and NOM in %/min quantified using QCM dry mass sensing (black line). The amount of co-eluting NOM during the analyte retention time is integrated (colorful areas) and divided by the total amount of NOM measured to receive a number of the percentage of NOM co-eluting with the analyte (corresponding colour). (c-f) The NOM co-elution in % is plotted for the 22 different gradients for 4 analytes ((c): CAF, (d): DEA, (e): SIM, (f): BOSC). The second axis shows the $C_{NOM}/C_{analyte}$ ratio after the purification step corresponding to BOSCs ratio in the original extract of 2383. The minima are encircled using a black dotted line, the maxima using a black solid line.

Table 5.1 Reduction of the $C_{NOM}/C_{analyte}$ ratio during HPLC purification of the Oasis HLB extract of a water sample containing 120 ng/L of each respective analyte and 1.8 mgC/L NOM. The Table displays the $C_{NOM}/C_{analyte}$ (nmol C/nmol C) ratio in the extract (no LC), the reduced ratio for the gradient on XTerra RP18 that showed the highest ($LC_{XTerra\ RP18}$) and the lowest (optim-$LC_{XTerra\ RP18}$) NOM co-extraction, and the lowest (optim-$LC_{Orbit\ 100\ C8}$) co-extraction on Orbit 100 C8. It also shows the gain factor, which is calculated by dividing the $C_{NOM}/C_{analyte}$ ratio before the clean-up ("no LC") by the $C_{NOM}/C_{analyte}$ ratio after the respective clean-up. The matrix removal in % is shown in brackets. The analytes are classified in early-, middle-, and late-eluting substances depending on their retention behaviour during the 22 investigated gradients and listed in the order of their retention time.

	early-eluting			middle-eluting		late-eluting		
	CAF	BAM	DIA	DEA	SIM	ATZ	AZOX	BOSC
logKow	-0.07	0.77	1.50	1.51	2.18	2.61	2.50	2.96
no LC	3034	3393	4343	3909	3601	3370	2292	2383
$LC_{XTerra\ RP18}$	448	347	548	453	417	403	264	207
gain factor	7	10	8	9	9	8	9	12
matrix removal (%)	(85.3)	(89.8)	(87.4)	(88.4)	(88.4)	(88.0)	(88.5)	(91.3)
optim-$LC_{XTerra\ RP18}$	242	215	296	281	192	107	53	47
gain factor	13	16	15	14	19	31	44	51
matrix removal (%)	(92.0)	(93.7)	(93.2)	(92.8)	(94.7)	(96.8)	(97.7)	(98.0)
optim-$LC_{Orbit\ 100\ C8}$	96	156	206	271	129	78	14	**4**
gain factor	32	22	21	14	28	44	167	556
matrix removal (%)	(96.8)	(95.4)	(95.3)	(93.1)	(96.4)	(97.7)	(99.4)	(**99.8**)

represents the percentage of co-eluting NOM in the respective fraction and thus the $C_{NOM}/C_{analyte}$ ratio. Changes of NOM co-eluting in each fraction are shown as heat maps for different gradients in Figure 5.4c-f, where the x-axis represents the percentage of CH_3OH in the mobile phase at minute 7.5 and the left y-axis at minute 15, whereas the colour code represents the percentage of co-eluting NOM as well as $C_{NOM}/C_{analyte}$ ratio at the right y-axis. To reduce the complexity of the figure, data for CAF, DEA, SIM, and BOSC are shown here, whereas the data for BAM, DIA, ATZ, and AZOX are shown in Figure A.4.3 (all NOM co-elution data are summarized in Table A.4.10 and A.4.11).

Gains from an Individual Compound Perspective

A single HPLC purification of an extract of a 5L water sample containing 1.8 mgC/L NOM (post-spiked after the extraction with each respective analyte to correspond to 120 ng/L in the original water sample) could remove between 85-91% of the co-extracted NOM (see Table 5.1, "$LC_{XTerra\ RP18}$ matrix removal"). This corresponds to a remaining percentage of co-eluting NOM in each fraction of between 9-15% of the original NOM concentration (see Figure 5.4c-f solid marked areas). The $C_{NOM}/C_{analyte}$ ratio in the extract could thus be reduced by a factor of 7 to 12 from ratios ranging between 2292 and 4343 to down to between 207 and 548. While these results show the substantial purification potential of HPLC using a typical C_{18} column without any method development, the $C_{NOM}/C_{analyte}$ ratio is still too high for accurate carbon-CSIA ($\leq$10). This highlights the need for optimizing HPLC purification. In fact, screening for 22 gradients using QCM dry mass sensing made it possible to remove an additional 6.7% NOM in the retention window of CAF, 3.7% in the window of DEA, 6.3% of SIM, and

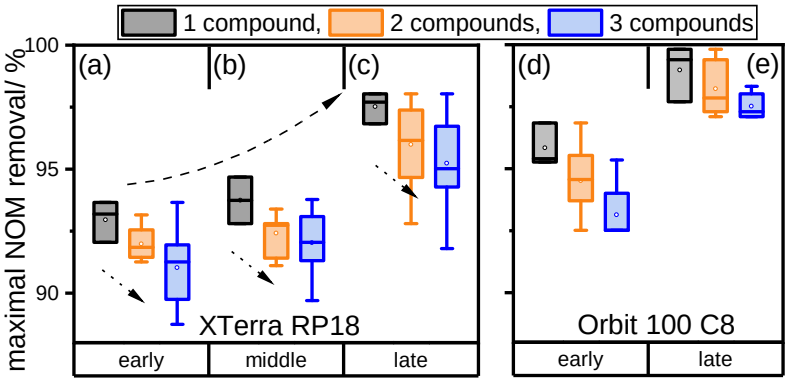

Figure 5.5 Removal of NOM (in %) in the fraction of early-, middle-, or late-eluting compounds during the purification of one individual compound or multiple compounds for both columns. The dashed upward arrow annotates the trend of elution regions early<middle<late, the dotted downward arrow the compound number trend 1>2>3.

6.7% of BOSC (see Figure 5.4c-f, dashed marked areas). These gains are significant considering the associated uncertainties between 0.1% and 1.1% according to triplicate to sextuplicate measurements (see Table A.4.10 and A.4.11). Using the QCM optimized HPLC purification, the $C_{NOM}/C_{analyte}$ ratios could be reduced to between 47 and 296 ("optim-$LC_{XTerra\ RP18}$"), corresponding to gain factors between 13 and 51 compared to no clean-up ("no LC") and to gain factors between 2 to 5 compared to not optimized LC ("$LC_{XTerra\ RP18}$").

An optimized single clean-up on XTerra RP18 leads to larger gain factors for late-eluting compounds (31-51), compared with early- (13-16) and middle-eluting compounds (14-19). These results are meaningful given the shape of the NOM hump that can be influenced more for the late eluting compounds than for the early and middle ones eluting directly with the main part of the NOM hump (see Figure 5.4b). Yet, $C_{NOM}/C_{analyte}$ = 47-296 are significantly above the required value for accurate carbon-CSIA (≤10). This is not surprising given the concentration of the target analytes and NOM in the investigated water sample (1.8 mgC/L NOM, 120 ng/L analyte). This highlights that residuals of NOM of as low as 2% in the collected fraction of such a sample require further optimization, even when recovering 100% of the target analyte. Therefore, we assessed the potential for NOM removal on a different stationary HPLC phase, namely a column Orbit 100 C8, which offers a higher theoretical plate number (see Table A.4.9) for the investigated compounds and, thereby, possesses a higher retention and smaller peak width presumably leading to an even lower NOM co-elution and thus lower $C_{NOM}/C_{analyte}$ ratios. Indeed, it was possible to reach an NOM removal of between 93.1 and 99.8% (see results for all gradients in A.4.12 and A.4.13) leading to gain factors for early- (21-32), middle- (14-28), and late-eluting compounds (167-556) as shown in Table 5.1 "optim-$LC_{Orbit\ 100\ C8}$". Thanks to the QCM, it was therefore possible to remove up to 99.8% of the matrix for BOSC with a single optimized clean-up leading to a $C_{NOM}/C_{analyte}$ ratio = 4, which is smaller than the suggested value of 10.

Trade-Offs between Single- and Multiple-Targets

Purifying more than one compound in a single HPLC purification run is expected to lead to trade-offs in the potential of maximal NOM removal. Therefore, we quantified the maximal NOM removal (lowest percentage of co-eluting NOM depicted in the dashed area of Figure 5.4 and A.4.3) when optimizing HPLC purification for only one compound at a time and compared it with the NOM removal determined for the optimised purification for multiple targets over the whole chromatographic run, covering thereby combinations of early, middle, and late eluting compounds (see Figure 5.5).

Efficiency of HPLC purification deteriorates when aiming for simultaneous purification of two (orange) or three compounds (blue) compared to an individual compound (black) as seen by the maximal NOM removal denoted as dotted downward arrows in Figure 5.5. For (a) early eluting compounds on XTerra RP18, 92.0% NOM can be removed on average when purifying two compounds and 91.0% during the purification of three compared with one (93.0%). The same holds true for (b) middle (1: 93.7%, 2: 92.4%, 3: 92.0%) and (c) late eluting compounds (1: 97.5%, 2: 96.0%, 3: 95.2%). The trend of the NOM removal for individual and multiple compounds is consistent within each elution region following the order early<middle<late (denoted as dashed upward arrow). This picture may vary dependent on the chromatographic behaviour of different matrices, as well as on the exact combination of compounds used (see Table A.4.17 and A.4.18 and Figure 5.1 and A.4.13-A.4.15). For example, the maximal NOM removal determined for late eluting compounds in combination with middle eluting ones (96.7%) is higher in comparison to the simultaneous purification with early eluting compounds (95.3%).

Similar trends were observed on a different column, namely Orbit 100 C8, which further corroborates the acquired results (see Figure 5.5d,e). The data on the middle eluting compounds on Orbit 100 C8 is not shown since we did not determine any variations between the different combinations. Nonetheless, the determined maximal NOM removal on Orbit 100 C8 is higher in comparison with the XTerra RP18 column. In fact, the average NOM removal for three compounds on Orbit 100 C8 ("early": 93.1%, "late": 97.5%, see Figure 5.5d,e) is equal to the individual compound NOM removal on XTerra RP18 ("early": 93.0%, "late": 97.5%, see Figure 5.5a,c), highlighting the importance of column choice. Although the differences in the maximal NOM removal for one, two, or three compounds might seem small, they are significant considering the precision of these measurements (±0.1–1.1%) and their impact on the $C_{NOM}/C_{analyte}$ ratios. This can be illustrated using the example of BOSC, where the $C_{NOM}/C_{analyte}$ ratio changes from 4 for the individual compound to 26 on average for two and to 44 on average for three compounds, thus preventing accurate carbon-CSIA measurements in the latter cases.

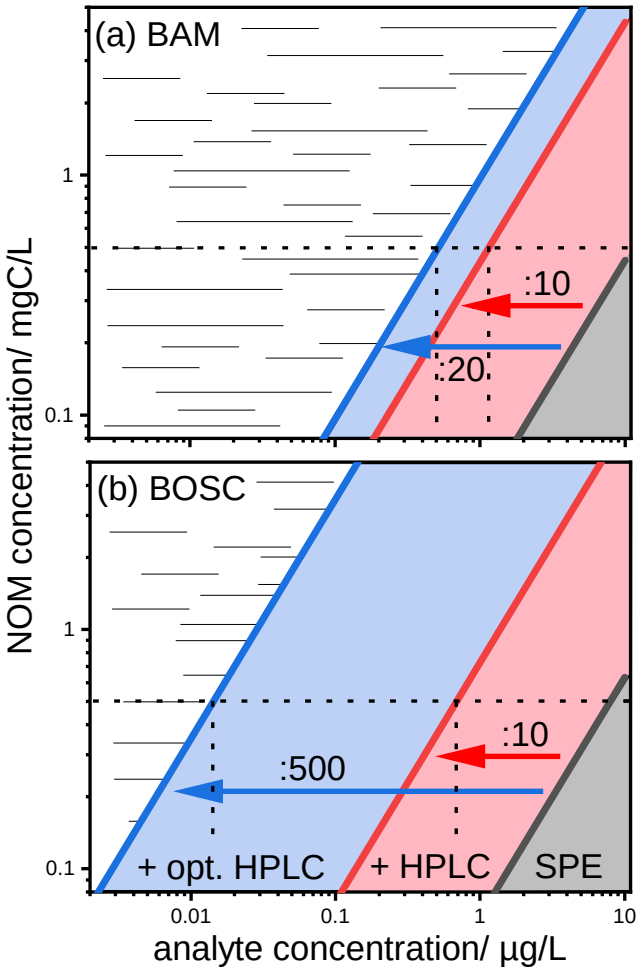

Figure 5.6 Dependence of accurate isotope analysis on the analyte and NOM concentration in the real-world water sample for (a) BAM (early-eluting) and (b) BOSC (late-eluting) for different sample preparation strategies: SPE using Oasis HLB (black), plus an HPLC purification (red), or plus an optimized HPLC purification (blue).

5.4 Conclusion and Analytical Implications

The present work systematically demonstrates that QCM dry mass sensing is a valuable auxiliary tool for optimizing matrix removal during a classical clean-up of extracts prior to carbon-CSIA. In fact, this is the first study to report quantitative efficiencies of RP HPLC clean-up that amounted to matrix removal up to 99.8% upon optimization. On average, the maximal matrix removal within a precision of 1% could be determined by screening 3 to 5 different gradients, including convex, concave, and linear gradients (see Table A.4.14 and A.4.15 and Figures A.4.5-A.4.12), thus demonstrating that a systematic method development with the help of QCM dry mass sensing yields substantial benefits with reasonable efforts.

The discrepancies in gain factors of an HPLC clean-up between early- and late-eluting compounds have analytical implications for carbon-CSIA. This is depicted in Figure 5.6 for one early-eluting compound (BAM, Figure 5.6a) and one late-eluting compound (BOSC, Figure 5.6b), where limits of accurate carbon-CSIA are shown as a function of environmental analyte concentration (x-axis), NOM concentration (y-axis), and efficiency of the HPLC purification (red and blue arrows). While for both model compounds these limits can be shifted by approximately a factor of 10 to lower analyte concentrations using one HPLC purification (red arrow), a factor of up to 500 can be gained instead for a late-eluting compound by optimizing the HPLC purification (blue arrow). In contrast, only a factor of approximately 20 can be gained for an early-eluting compound. These findings are meaningful since the challenge of separating small polar compounds using RP columns is well known.[258–260] Potentially, a column phase engineered for these compounds (e.g., HILIC)[261,262] could result in a better separation of early eluting compounds and NOM and thus a higher NOM removal during purification. To put these findings in a larger context of complete sample preparation for carbon-CSIA, an overall higher removal can become possible when combining the targeted HPLC cleanup presented here with the use of more selective SPE materials (e.g., cyclodextrins)[50] to replace OASIS HLB in the first extraction step, making it possible to measure concentrations ≥ 100 ng/L for BAM and ≥ 3 ng/L for BOSC in a groundwater sample containing 0.5 mgC/L NOM.

The use of NOM elution data for a given matrix is, furthermore, not limited to the 8 model compounds investigated in this study. Combined with software tools that can predict the analyte retention time and peak width,[263–265] it is possible to determine the $C_{NOM}/C_{analyte}$ ratio for any given analyte and thus the feasibility of carbon-CSIA. Creating in the future an openly available database for different samples and matrices can be very useful for researchers and can open the door to training artificial intelligence and prediction tools to assist in the optimization of sample preparation for targeted analysis.

6 Conclusion and Outlook

The overarching goal of this dissertation was to expand the applicability of CSIA to polar, non-volatile compounds present in real-world samples in the low ng/L concentration range. In particular, the research focused on addressing the significant analytical challenges associated with the lack of selectivity in compound-specific isotope analysis (CSIA) sample preparation and the tediousness of these sample preparation workflows. To this end, the present work investigated the effectiveness of strategies to optimize the matrix removal during the purification of sample extract prior to gas chromatography isotope ratio mass spectrometry (GC-IRMS) isotope analysis. This work supplements earlier research efforts addressing the identical analytical issue, wherein substantial efforts were dedicated to introducing new selective extraction/purification techniques to the CSIA sample preparation workflow. The results of this dissertation stress the importance of optimizing the matrix removal during sample purification in a targeted way to enable accurate CSIA of complex real-world samples. In particular, the presented approach of optimizing reversed-phase high-performance liquid chromatography (RP HPLC) purification by online quantifying matrix compounds using quartz crystal microbalance (QCM) dry mass sensing paves the way for (i) faster development of purification methods, (ii) a significantly improved selectivity of chromatographic purification, and (iii) new applications of CSIA for compounds present in complex samples at low to mid ng/L concentrations.

6.1 Implications of Charge of the Sample Matrix on its Sorption on Molecularly Imprinted Polymers

Chapter 2 investigated the influence of the charge of natural organic matter (NOM) on non-specific sorption of NOM during molecularly imprinted solid phase extraction (MISPE) by reducing the charge density of NOM using methylation of acidic functional groups. Breakthrough curves revealed a stronger interaction between the methylated NOM and the MIP, leading to nearly 30% more NOM binding to the MIP. This is most likely the result of smaller electrostatic repulsion between NOM molecules resulting from the significantly reduced charge density. These results demonstrate the importance of studying the underlying intermolecular mechanisms to understand non-specific sorption of matrix compounds on selective sorbent materials like MIPs. Further research should focus on developing techniques to use this electrostatic repulsion to increase the selectivity of MISPE and, thus, matrix removal before CSIA.

6.2 Effectiveness and Limitations of Quartz Crystal Microbalance for Online Quantification of Matrix Compounds during Liquid Chromatography

The central part of the thesis addressed the challenge of developing a detection technique that can quantify matrix components online during liquid chromatography. It was hypothesized that such a detector could help to optimize the separation of the target analyte and the matrix, thus significantly improving the removal of co-extracted sample matrix during the respective chromatographic purification of the sample extract to reduce adverse effects of the sample matrix during the subsequent measurement of the target analyte using GC-MS and GC-IRMS. The present work systematically investigated the possibilities and limitations of using QCM liquid sensing (see chapter 3) and QCM dry mass sensing (see chapters 4 and 5) for this purpose.

6.2.1 Effectiveness and Limitations of QCM Liquid Sensing

To quantify matrix components in the liquid phase using QCM liquid sensing, first, the challenge of finding a suitable coating for the QCM sensor that (i) can extract the entirety of NOM previously extracted from the water sample with a (ii) sufficient capacity had to be tackled. Chapter 3 demonstrates for the first time the successful grafting of a hyper crosslinked divinylbenzene ethylene glycol dimethacrylate (DVB-EGDMA) co-polymer layer onto a QCM sensor using radical polymerization. It was possible to graft the polymer layer with a 200-300 nm thickness inside the dynamic range of QCM measurements.[120,216] Humic acids did sorb onto the grafted co-polymer during sorption experiments leading to a frequency decrease of 18-20 Hz. This is at the higher end of the frequency decrease observed in other studies for a variety of polymer coatings.[131,134,136,143] However, this number is still too low for the purpose of matrix online monitoring. Additionally, it was not possible to regenerate the sorption abilities of the grafted DVB-EGDMA co-polymer using organic solvents. Future research should focus on further increasing the capacity of the grafted polymer layer by (i) increasing the layer thickness while staying inside the QCM‘s dynamic range and (ii) further improving the homogeneity of the grafted polymer layer. Furthermore, future research can build upon the established grafting and characterization procedure to coat the QCM sensor with other co-polymers to gain valuable insights into sorption processes.

6.2.2 Effectiveness and Limitations of QCM Dry Mass Sensing

While there is still a long way to go to monitor matrix compounds online using QCM liquid sensing, QCM dry mass sensing proved to be suitable as a holistic detector for the quantification of complex organic matrices during gradient RP HPLC purification. Chapters 4 and 5 systematically investigated how a QCM can be coupled to a commercial HPLC using a post-column adjustable flow splitter and a microfluidic spray-dryer, developed a measurement and data processing strategy, assessed how it can be used for the quantification of matrix

components during a typical gradient RP HPLC purification, and applied it to different mass spectrometry-based applications. It was possible to overcome challenges of organic solvent gradients (i.e., constantly changing spraying/evaporation behavior) for QCM dry mass sensing by calibrating the system using a constant NaCl concentration in the HPLC eluate. Validating the measurement approach and characterizing the system's upper and lower limit of quantification, precision, and accuracy confirmed the relevance of the approach for a large set of real-world samples in environmental and food chemistry and demonstrated the successful integration of QCM dry mass sensing as auxiliary detector into HPLC purification workflows. Comparing the results acquired with the QCM for a chromatographic application of a complex food sample with the ones obtained with UV-Visible spectroscopy (UV/Vis) detection demonstrated the unsuitability of UV/Vis for such a complex sample. It emphasized again the need for a universal detector like a QCM for the chromatographic separation of target analytes from complex matrices.

Optimizing HPLC purification of an environmental extract using the combined data of UV/Vis detection for the retention of the target analyte and QCM for the retention of matrix compounds led to 93-99.8% NOM being removed from target analytes eluting at retention times spanning over the whole chromatogram. Furthermore, using the data measured with the QCM, it was possible to find optimal HPLC gradients for the simultaneous purification of multiple targets; this, however, led to up to 2.5% less NOM removal. On average, the maximal matrix removal could be determined by screening 3 to 5 different gradients, thus demonstrating that a systematic method development with the help of QCM dry mass sensing yields substantial benefits with reasonable effort.

Applying the QCM as a holistic detector for quantifying complex organic matrices during RP HPLC for subsequent (i) pesticide residue analysis in food using GC-MS and (ii) carbon-CSIA of environmental aquatic micropollutants demonstrated the validity and the applicability of the approach and the benefit this technique can bring to many matrix susceptible analytical applications. (i) In GC-MS residue analysis, significantly different matrix effects (up to 345%) were determined for different chromatographic fractions for several model compounds (DEA, BAM, ATZ, Prop, BOSC). Together with the newly established correlation between the amount of matrix quantified by QCM dry mass sensing and matrix effects measured during the subsequent GC-MS analysis, this shows that QCM dry mass sensing can be a valuable tool to the analyst where HPLC clean-up is routinely performed to reduce adverse effects caused by the sample matrix. (ii) Carbon-CSIA, especially, proved to be highly susceptible to the sample matrix. A direct correlation was found between the mass of NOM injected and the background intensity measured. This matrix background highly affected the accuracy of the isotope measurement, leading to strong isotopic shifts of up to 3.3‰ and becoming greater the higher the amount of matrix in the sample was and the greater the distance of the isotopic signature of the target analyte to that of NOM was. Systematic investigations of the impact of the ratio of injected matrix and analyte, $C_{NOM}/C_{analyte}$, on the accuracy of carbon-CSIA further corroborated the hypothesis and findings of Bakkour et al.[56] and Glöckler et al.[50] that the $C_{NOM}/C_{analyte}$ ratio is a good proxy of sample purity and

that accurate carbon-CSIA necessitates a $C_{NOM}/C_{analyte}$ ratio in the purified sample extract of below 10. This highlights the importance of (i) including standards spanning over a range of isotope signatures in carbon-CSIA method development and (ii) the purity of the sample as a strategy to avoid systematic bias in isotope values. Carbon-CSIA can thus benefit significantly from a sample purification optimized with a semi-universal detector like the QCM, whose purification power can shift the boundaries of accurate carbon-CSIA by up to two orders of magnitude toward lower micropollutant concentrations.

6.3 Perspectives for Micropollutant CSIA in Field Studies

Altogether, the findings of chapters 4 and 5 emphasize the importance (i) of suitable detection techniques for the specific requirements of analytical tasks and (ii) of optimized, highly selective, and automated purification techniques for sample clean-up to use the full potential of CSIA. To put these findings in a larger context of complete sample preparation for carbon-CSIA and to provide the analyst with a more general tool at hand, Table 6.1 summarizes the sample preparation strategies for different NOM and analyte concentration levels expressed as $C_{NOM}/C_{analyte}$ ratios.

For highly contaminated fields (level 1), an extraction using a classical sorbent like Oasis HLB is enough (Ext; NOM removal: 90-95%). For pollutants in the low µg/L range (level 2), using a more selective SPE during the extraction of the water sample can already be the solution to rising amounts of NOM in the extract (Ext^+; NOM removal: 95-99%; i.e., cyclodextrin polymers).[50] While this shows that CSIA for pollutants in the low µg/L range can be achieved using only a selective sample extraction, CSIA of non-volatile organic micropollutants in the ng/L range was limited in the past by the low concentrations of micropollutants in the environment and a lack of suitable sample preparation procedures. As a result, field applications were scarce (see Figure 1.1). This work, together with very recent advancements in CSIA sample preparation, have the potential to change this since field samples with analyte concentrations in the low to mid ng/L region (compare Table 6.1 C_{BAM}, C_{DEA}, and C_{BOSC}) can now be processed. Purifying the SPE extract by adding one HPLC clean-up makes it possible to accurately measure isotope ratios of pollutants present in the sample in mid to high ng/L concentrations (level 3, NOM removal: 99-99.95%) or even in the low to mid ng/L micropollutant concentrations (level 4) if the pollutants were extracted during the first step using a selective SPE material (NOM removal: 99.9-99.99%).

For very low concentrated pollutants (level 5), it might, however, still be necessary to add a second clean-up step (NOM removal: 99.99-99.999%). To this end, procedures that were already successfully used in the field of CSIA, like two-dimensional chromatography or MIPs can be used,[56] or other purification techniques using selective materials like covalent organic frameworks (COFs),[266] or metal organic frameworks (MOFs),[267] which still have to be investigated in the future for their use in CSIA sample preparation. Furthermore, additional advancements on the instrumental end to increase the chromatographic resolution of the hyphenated

Table 6.1 Sample preparation strategies for different NOM and analyte concentration regimes in environmental real-world samples expressed as $C_{NOM}/C_{analyte}$ ratios.

Level	$C_{NOM}/C_{analyte}$ ratio range	C_{BAM}[1]	C_{DEA}[1]	C_{BOSC}[1]	NOM removal in %	Sample Prep. Strategy			
						Ext	Ext^+	HPLC	pur.
1	1-200	>11000	>13000	>8000	90-95	x			
2	200-1000	>2300	>2600	>1600	95-99		x		
3	1000-20000	>500	>900	>15	99-99.95	x		x	
4	3000-100000	>100	>180	>3	99.9-99.99		x	x	
5	30000-1000000	>10	>18	>0.3	99.99-99.999		x	x	x

1: in ng/L for a NOM concentration of 1 mgC/L
Extraction (Ext): analyte recovery: 90-100%, NOM removal: 90-95%.[50]
selective Extraction (Ext^+): analyte recovery: 90-100%, NOM removal: 95-99%.[50]
HPLC: analyte recovery: 90-100%, NOM removal: 93-99%
additional purification (pur.): analyte recovery: 90-100%, NOM removal: 90%

GC and IRMS sensitivity might help close the gap to the level 5 concentrations. There are already strategies available to increase the chromatographic resolution using, for example, longer columns,[51] multidimensional chromatography,[34,52–55] or new reactor design that reduces peak broadening.[268] Alongside with optimized sample preparation procedures, they are expected to boost new applications of CSIA in the future.

All in all, this shows that there are several strategies available to reach level 5. Selectivity optimization alongside automation of procedures is vital for all of them. QCM dry mass sensing paves the way to efficiently develop optimized purification strategies for various purification problems using a large range of liquid chromatographic solid phase materials and modes. Combining the efficient development of selective purification methods using the QCM with the strategy of comparing $C_{matrix}/C_{analyte}$ ratios before and after each chromatographic purification helped to compare two different RP columns objectively for clean-up of an environmental extract for CSIA. In the future, such a selectivity assessment strategy has to be developed/validated for different matrices and applications of CSIA to enable targeted optimization. To extend the applicability of QCM dry mass sensing even further, future research should focus on optimizing the spray-dryer to make it resistant to solvents other than methanol, acetonitrile, or water[269] and to be able to increase the dynamic range of the flow-range to increase the sensitivity of the measuring process. Furthermore, while QCM dry mass sensing was successfully applied to optimize the sample preparation for subsequent isotope analysis using GC-IRMS and residue analysis using GC-MS, it might be potentially useful in the future to other matrix susceptible techniques (i.e., LC-MS)[155] or could even be used to quantify particles (i.e., nanoparticles, micro/nanoplastic).

Last but not least, QCM dry mass sensing enabled online method development and optimization for CSIA sample preparation for environmental extracts, thus taking a big step towards a fully automated method development. The future generation of more data on the behavior of matrix during chromatographic purification using a holistic detector like the QCM could open the door to training artificial intelligence as a method development assistant, getting even closer to the goal of a fully automated, highly selective sample preparation.

A Supporting Information to Introduction Figure 1.1

Table A.1 Publications in CSIA in environmental chemistry are classified as work on new methods to measure a given compound with isotope analysis (method), as a study on the lab scale (lab), or as a field study using real-world samples (field) for several compound classes, namely PAHs (polycyclic aromatic hydrocarbon), pesticides (atrazine, acetochlor, metolachlor, chloridazon, desethylatrazine, desphenylchloridazon, 2,6-dichlorobenzamide, isoproturon, parathion, glyphosate, metalaxyl, bromoxynil, dimetomorph), HCHs (hexachlorocyclohexane), 1H-benzotriazole, BTEX (aromatic hydrocarbons benzene, toluene, ethylbenzene, and xylene), PCB+PCDD (polychlorinated biphenyl, polychlorinated dibenzodioxins), pharmaceuticals (diclofenac, ibuprofen, sulfamethoxazole, sulfonamide), explosives (2,4,6-trinitrotoluene, hexogen, 2,4-dinitrotoluene), fuel oxygenates (tert-butyl methyl ether, ethyl tert-butyl ether, tert-butyl alcohol), and volatile chlorinated aliphatics (trans-1,2-dichloroethene, cis-1,2-dichloroethene, trichloroethene, tetrachloroethene, dichloromethane, chloroform, carbon tetrachloride, 1,2-dichloroethane, 1,1-dichloroethylene, tetrachloromethane). Only publications on micropollutants in water or soil measured with IRMS were considered but no reviews and no exhaust analytics. Source: Kuntze et al.[57] and Web of Science. Publications were considered till 04.10.2023.

Publication	Year	Method/ Lab/ Field
PAH		
Hammer et al.[270]	1998	field
McRae et al.[271]	2000	field
Fabbri et al.[272]	2003	field
Walker et al.[273]	2005	field
Saber et al.[274]	2006	field
Bosch et al.[275]	2015	field
Richnow et al.[276]	2003	field
O'malley et al.[277]	1996	field
Richnow et al.[278]	2003	field
Micić et al.[279]	2007	field
Morasch et al.[280]	2011	field
Mahro et al.[281]	2014	field
Steinbach et al.[282]	2004	field
Blum et al.[283]	2009	field
Griebler et al.[284]	2004	field
Marquès et al.[285]	2016	lab

Blessing et al.[286]	2015	method
Kümmel et al.[287]	2016	lab
Morasch et al.[288]	2007	lab
Li et al.[289]	2009	method
Tolosa et al.[290]	2019	method
Yanik et al.[291]	2003	lab
Zhang et al.[292]	2019	field
Mikolajczuk et al.[293]	2009	method
Lichtfouse et al.[294]	1995	method
Yan et al.[295]	2006	field
Cennerazzo et al.[296]	2017	lab
McRae et al.[297]	1996	lab
McRae et al.[298]	1998	lab
Ou et al.[299]	2010	field
O'malley et al.[300]	1994	field
Kim et al.[301]	2005	method
Bergmann et al.[302]	2011	lab
Buczynska et al.[303]	2014	method
Ternon et al.[304]	2015	method
Kim et al.[305]	2008	field
Smirnov et al.[306]	1998	field
Kim et al.[307]	2006	field
Yang et al.[308]	2020	lab
McRae et al.[309]	2000	field
Vinzelberg et al.[310]	2005	field
Mazéas et al.[311]	1999	field
Zhang et al.[312]	2014	field
Okuda et al.[313]	2002	field
Petrisic et al.[314]	2013	field
O'malley et al.[315]	1997	lab
Zhang et al.[316]	2014	method
Gauchotte-Lindsay et al.[317]	2014	method
Wang et al.[318]	2004	method
McRae et al.[319]	1999	lab

Boyd et al.[320]	2006	method
Marozava et al.[321]	2019	lab
Mazéas et al.[322]	2001	method
Liu et al.[323]	2021	lab
Meckenstock et al.[324]	2004	lab
Mazéas et al.[325]	2002	lab
Jautzy et al.[326]	2013	field
Meckenstock et al.[327]	1999	lab
Morasch et al.[328]	2002	lab
Tolosa et al.[329]	2004	method
Dickhut et al.[330]	2004	lab
Tian et al.[331]	2023	method
van Leeuwen et al.[332]	2022	field

pesticides

Chen et al.[333]	2017	lab
Chen et al.[334]	2019	lab
Penning et al.[335]	2010	lab
Reinnicke et al.[336]	2012	method
Schreglmann et al.[68]	2013	field
Ehrl et al.[337]	2018	lab
Masbou et al.[338]	2018	lab
Ehrl et al.[339]	2018	lab
Torrento et al.[65]	2019	field
Ponsin et al.[340]	2019	method
Meyer et al.[341]	2008	method
Elsayed et al.[342]	2014	lab
Lutz et al.[343]	2017	field
Lihl et al.[344]	2019	method
Alvarez-Zaldívar et al.[253]	field	
Imfeld et al.[345]	2018	lab
Melsbach et al.[346]	2019	method
Schürner et al.[347]	2016	lab
Jin et al.[348]	2016	lab

Wu et al.[349]	2018	lab
Wu et al.[350]	2018	field
Kujawinski et al.[351]	2013	method
Mogusu et al.[352]	2015	method
Hartenbach et al.[353]	2008	lab
Yamamoto et al.[354]	2004	lab
Lutz et al.[355]	2013	lab
Meyer et al.[356]	2009	lab
Penning et al.[357]	2007	method
Reinnicke et al.[358]	2012	lab
Maier et al.[359]	2013	method
Wu et al.[360]	2014	method
Jin et al.[361]	2016	method
Wu et al.[362]	2017	method
Tang et al.[363]	2017	lab
Chen et al.[364]	2019	lab
Melsbach et al.[66]	2020	field
Limon et al.[365]	2020	method
Torabi et al.[366]	2020	lab
Knossow et al.[367]	2020	lab
Shi et al.[368]	2022	lab
Masbou et al.[369]	2018	method
Melsbach et al.[370]	2020	lab
Droz et al.[371]	2021	lab
Drouin et al.[372]	2021	lab
Torrentó et al.[373]	2021	method
Gilevska et al.[374]	2023	field
Gilevska et al.[375]	2022	field
Glöckler et al.[50]	2023	method
Liang et al.[376]	2023	lab
Chen et al.[377]	2022	lab
Li et al.[378]	2022	lab
Arar et al.[379]	2023	lab
Prieto-Espinoza et al.[380]	2022	lab

Kundu et al.[381]	2022	lab
Sun et al.[382]	2022	lab
Marks et al.[236]	2022	method
Meite et al.[383]	2022	lab

HCH

Badea et al.[384]	2011	field
Bashir et al.[385]	2015	field
Chartrand et al.[386]	2015	field
Liu et al.[387]	2017	field
Wu et al.[388]	2019	field
Zhang et al.[389]	2014	lab
Badea et al.[390]	2015	method
Jin et al.[361]	2016	method
Qian et al.[391]	2019	lab
Badea et al.[392]	2009	lab
Bashir et al.[393]	2013	lab
Schilling et al.[394]	2019	lab
Schilling et al.[395]	2019	lab
Ivdra et al.[396]	2014	method
Gui et al.[397]	2015	method
Bashir et al.[398]	2018	lab
Liu et al.[399]	2020	lab
Gao et al.[400]	2022	field
Liu et al.[401]	2022	lab
Liu et al.[402]	2019	lab
Badea et al.[403]	2021	lab
Kannath et al.[404]	2019	method
Ivdra et al.[12]	2017	lab
Liu et al.[405]	2022	field
Zhu et al.[406]	2023	lab
Liu et al.[407]	2022	lab
Gao et al.[400]	2022	field
Liu et al.[408]	2023	field

Aamir et al.[409]	2023	field
1H-benzotriazole		
Bakkour et al.[56]	2018	field
Huntscha et al.[410]	2014	lab
Spahr et al.[411]	2013	method
Wu et al.[412]	2021	lab
BTEX		
Kelley et al.[413]	1997	field
Mancini et al.[414]	2008	field
Lutz et al.[415]	2014	field
Beckley et al.[416]	2016	field
Richnow et al.[417]	1999	field
Stehmeier et al.[418]	1999	field
Bugna et al.[419]	2004	field
Bugna et al.[420]	2005	field
Micić et al.[279]	2007	field
Beller et al.[421]	2008	field
Gelman et al.[422]	2008	field
Mahro et al.[281]	2014	field
Kolhatkar et al.[423]	2017	field
Moshkovich et al.[424]	2018	field
BenIsrael et al.[425]	2019	field
Vieth et al.[426]	2001	field
Mancini et al.[427]	2002	field
Meckenstock et al.[428]	2002	field
Richnow et al.[429]	2002	field
Richnow et al.[276]	2003	field
Richnow et al.[278]	2003	field
Fischer et al.[430]	2004	field
Griebler et al.[284]	2004	field
Peter et al.[431]	2004	field
Steinbach et al.[282]	2004	field

Vieth et al.[432]	2005	field
Fischer et al.[433]	2006	field
Mak et al.[434]	2006	field
Stelzer et al.[435]	2006	field
Fischer et al.[58]	2007	field
Bouchard et al.[436]	2008	field
Batlle-Aguilar et al.[437]	2009	field
Blum et al.[283]	2009	field
Mäurer et al.[438]	2009	field
Prommer et al.[439]	2009	field
De Biase et al.[440]	2011	field
Morasch et al.[280]	2011	field
Rakoczy et al.[441]	2011	field
Van Keer et al.[442]	2012	field
Batlle-Aguilar et al.[443]	2014	field
Ponsin et al.[444]	2015	field
Gilevska et al.[445]	2019	field
McKelvie et al.[446]	2005	field
Feisthauer et al.[447]	2012	field
Xiong et al.[448]	2012	field
Wei et al.[449]	2015	field
Shayan et al.[450]	2018	field
Wei et al.[451]	2018	field
Wanner et al.[452]	2019	field
Imfeld et al.[453]	2014	lab
Ponsin et al.[454]	2017	method
Breukelen et al.[455]	2007	method
Vogt et al.[456]	2008	lab
Fischer et al.[457]	2009	lab
Herrero-Martín et al.[458]	2015	method
Ebongué et al.[459]	2009	method
Dempster et al.[460]	1997	method
Sherwood Lollar et al.[461]	1999	lab
Ahad et al.[462]	2000	lab

Slater et al.[463]	2000	lab
Wang et al.[464]	2003	lab
Harrington et al.[465]	1999	lab
Aeppli et al.[466]	2008	method
Kampara et al.[467]	2008	lab
Tobler et al.[468]	2008	lab
Langenhoff et al.[469]	2009	lab
Seeger et al.[470]	2011	lab
Dorer et al.[471]	2014	method
Jin et al.[472]	2014	lab
Busch-Harris et al.[473]	2008	lab
Jin et al.[474]	2014	lab
Ward et al.[475]	2000	lab
Mancini et al.[476]	2003	lab
Dias et al.[477]	1997	method
Slater et al.[478]	1999	lab
Elsner et al.[479]	2006	method
Morasch et al.[288]	2007	lab
Mancini et al.[414]	2008	lab
Herrmann et al.[480]	2009	lab
Amaral et al.[481]	2010	method
Jechalke et al.[482]	2013	lab
Centler et al.[483]	2013	method
Bouchard et al.[484]	2014	method
Passeport et al.[485]	2014	method
Dorer et al.[486]	2016	lab
Bouchard et al.[487]	2017	method
Morasch et al.[488]	2001	lab
Morasch et al.[489]	2004	lab
Mancini et al.[490]	2006	lab
Qiu et al.[491]	2013	lab
Khan et al.[492]	2018	lab
Klisch et al.[493]	2012	method
Nagel et al.[494]	2011	field

Knöller et al.[495]	2006	lab
Schüth et al.[496]	2003	lab
Sun et al.[497]	2021	lab
Ahad et al.[498]	2008	lab
Teramoto et al.[499]	2020	field
van Leeuwen et al.[332]	2022	field
Müller et al.[500]	2020	field
Passeport et al.[20]	2016	field
Keller et al.[501]	2017	lab
Feng et al.[502]	2021	method
Solano et al.[503]	2018	lab
Gilevska et al.[504]	2021	field
Willach et al.[505]	2020	method
Rostkowski et al.[506]	2021	lab
van Breukelen et al.[507]	2008	method
Hunkeler et al.[508]	2001	lab
Shin et al.[509]	2010	lab
Poulson et al.[510]	2010	lab
Fischer et al.[511]	2008	lab
Kopinke et al.[512]	2005	lab
Rolle et al.[513]	2017	lab
Oba et al.[514]	2008	lab
Rakoczy et al.[515]	2013	lab
Höhener et al.[516]	2012	lab
Bouchard et al.[517]	2008	lab
Jochmann et al.[64]	2006	method
Aüllo et al.[518]	2016	lab
Vieth et al.[519]	2006	lab
Chen et al.[520]	2022	lab
Khan et al.[521]	2022	lab

PCB+PCDD

Horii et al.[522]	2005	method
Vetter et al.[523]	2007	method

Drenzek et al.[524]	2004	lab
Drenzek et al.[525]	2001	lab
Huang et al.[526]	2020	field
Böttcher et al.[527]	2010	field
Liu et al.[528]	2010	lab
Ewald et al.[529]	2007	lab
pharmaceuticals		
Schürner et al.[347]	2016	field
Maier et al.[530]	2014	method
Jin et al.[348]	2016	method
Maier et al.[17]	2016	lab
Birkigt et al.[531]	2015	lab
Gilevska et al.[13]	2015	lab
Willach et al.[532]	2017	lab
Willach et al.[533]	2018	lab
Kujawinski et al.[534]	2012	method
Bennett et al.[535]	2017	field
Ouyang et al.[536]	2022	lab
explosives		
Coffin et al.[537]	2001	field
Amaral et al.[538]	2009	field
Bernstein et al.[539]	2010	field
Moshe et al.[540]	2010	field
Wijker et al.[16]	2013	field
Miyares et al.[541]	1999	field
Pennington et al.[542]	2001	field
Hatzinger et al.[543]	2018	field
Gelman et al.[544]	2011	method
Berg et al.[545]	2007	method
Bernstein et al.[546]	2008	lab
Lott et al.[547]	2015	method
Hofstetter et al.[548]	2008	lab

Tobler et al.[549]	2007	lab
Hartenbach et al.[550]	2006	lab
Ulrich et al.[551]	2018	lab
Tong et al.[552]	2020	lab
Berens et al.[553]	2019	lab
Fuller et al.[554]	2020	field
Smith et al.[555]	2015	lab
Bernstein et al.[556]	2013	lab
Fuller et al.[557]	2016	lab
Ippoliti et al.[558]	2023	lab
Hlohowskyj et al.[559]	2023	lab

fuel oxygenates

Oudijk et al.[560]	2008	field
Day et al.[561]	2003	field
Day et al.[562]	2003	field
Kolhatkar et al.[563]	2002	field
Spence et al.[564]	2005	field
McKelvie et al.[565]	2007	field
Gelman et al.[422]	2008	field
De Biase et al.[440]	2011	field
Thornton et al.[566]	2011	field
Lu et al.[567]	2016	field
Moshkovich et al.[424]	2018	field
van der Waals et al.[568]	2018	field
Kuder et al.[569]	2005	field
Wilson et al.[570]	2005	field
Zwank et al.[571]	2005	field
McKelvie et al.[572]	2007	field
Gafni et al.[573]	2016	field
Berg et al.[574]	2005	field
Lesser et al.[575]	2008	field
Kujawinski et al.[576]	2010	field
Jechalke et al.[577]	2010	field

Fayolle-Guichard et al.[578]	2012	field
Bombach et al.[579]	2015	field
Bastida et al.[580]	2010	lab
Youngster et al.[581]	2010	lab
Hunkeler et al.[582]	2001	lab
Smallwood et al.[583]	2001	method
Wang et al.[464]	2003	lab
Zwank et al.[63]	2003	method
Jochmann et al.[64]	2006	method
Somsamak et al.[584]	2006	lab
Elsner et al.[479]	2006	method
van Breukelen et al.[585]	2007	method
van Breukelen et al.[455]	2007	method
Eweis et al.[586]	2007	lab
Aeppli et al.[466]	2008	method
Busch-Harris et al.[473]	2008	lab
Kuder et al.[587]	2009	lab
Gauchotte et al.[588]	2009	method
Amaral et al.[481]	2010	method
Youngster et al.[589]	2010	lab
Seeger et al.[470]	2011	lab
North et al.[590]	2012	lab
Jin et al.[472]	2014	lab
Herrero-Martín et al.[458]	2015	method
Liu et al.[591]	2016	lab
Rosell et al.[592]	2007	lab
Rosell et al.[593]	2012	lab
Zhang et al.[594]	2015	lab
McKelvie et al.[595]	2009	lab
Schmidt et al.[596]	2004	lab
Heo et al.[597]	2012	lab
McKelvie et al.[598]	2010	lab
Somsamak et al.[599]	2005	lab
Shin et al.[600]	2013	lab

Rosell et al.[601]	2010	lab
Youngster et al.[581]	2010	lab
Elsner et al.[602]	2007	lab
O'Sullivan et al.[603]	2008	lab
Tremblay et al.[604]	2009	method
Bouchard et al.[605]	2022	lab
Ji et al.[606]	2023	lab

volatile chlorinated aliphatics

Hunkeler et al.[607]	2004	field
Blessing et al.[608]	2009	field
Hunkeler et al.[609]	2011	field
McHugh et al.[610]	2011	field
Kaown et al.[15]	2014	field
Filippini et al.[611]	2018	field
Eberts et al.[612]	2008	field
Nijenhuis et al.[613]	2013	field
Badin et al.[614]	2015	field
Beneteau et al.[615]	1999	field
Wang et al.[616]	2010	field
Wang et al.[617]	2013	field
Beckley et al.[416]	2016	field
McKelvie et al.[565]	2007	field
Mundle et al.[618]	2012	field
Damgaard et al.[619]	2013	field
Puigserver et al.[620]	2016	field
Kirchholtes et al.[621]	2004	field
Vanstone et al.[622]	2005	field
Chapman et al.[623]	2007	field
Nijenhuis et al.[624]	2007	field
Imfeld et al.[625]	2008	field
Morrill et al.[626]	2009	field
Courbet et al.[627]	2011	field
Révész et al.[628]	2014	field

Lee et al.[629]	2015	field
Filippini et al.[630]	2016	field
Hallsworth et al.[631]	2017	field
Pierce et al.[632]	2018	field
Schaefer et al.[633]	2018	field
Vogel et al.[634]	2018	field
Blázquez-Pallí et al.[635]	2019	field
Buchner et al.[636]	2019	field
Richards et al.[637]	2019	field
Sturchio et al.[638]	1998	field
Hunkeler et al.[639]	1999	field
Song et al.[640]	2002	field
Kirtland et al.[641]	2003	field
Carreón-Diazconti et al.[642]	2009	field
Kuhn et al.[643]	2009	field
McLoughlin et al.[644]	2014	field
Velimirovic et al.[645]	2014	field
Sonne et al.[646]	2017	field
Wilkin et al.[647]	2018	field
Pooley et al.[648]	2009	field
Elsner et al.[61]	2010	field
Amaral et al.[649]	2011	field
Broholm et al.[650]	2014	field
Hermon et al.[651]	2018	field
Wanner et al.[652]	2018	field
Vieth et al.[653]	2003	field
Morrill et al.[654]	2005	field
Martin et al.[655]	2006	field
Hirschorn et al.[656]	2007	field
Mäurer et al.[438]	2009	field
Patterson et al.[657]	2013	field
Sherwood Lollar et al.[252]	2001	field
Hunkeler et al.[658]	2003	field
Chartrand et al.[659]	2005	field

Hunkeler et al.[660]	2005	field
Abe et al.[661]	2009	field
Hamonts et al.[662]	2012	field
Appelo et al.[663]	2010	field
Torrentó et al.[664]	2014	field
Aeppli et al.[60]	2010	field
Hunkeler et al.[665]	2011	field
Lojkasek-Lima et al.[666]	2012	field
Lojkasek-Lima et al.[667]	2012	field
Wiegert et al.[668]	2012	field
Petitta et al.[669]	2013	field
Palau et al.[59]	2014	field
Audí-Miró et al.[670]	2015	field
Kaown et al.[671]	2016	field
Palau et al.[672]	2016	field
Clark et al.[673]	2017	field
Dogan-Subasi et al.[674]	2017	field
Schiefler et al.[675]	2018	field
Segal et al.[676]	2018	field
Jochmann et al.[64]	2006	method
Imfeld et al.[677]	2008	lab
Cichocka et al.[678]	2008	lab
Haluska et al.[679]	2019	field
van Breukelen et al.[680]	2017	lab
Alvarez-Zaldívar et al.[681]	2016	lab
Schmidt et al.[682]	2014	lab
Kuder et al.[683]	2013	method
Chan et al.[684]	2012	lab
Fletcher et al.[685]	2011	lab
Morrill et al.[686]	2004	method
Harding et al.[687]	2013	lab
Liu et al.[688]	2018	lab
Rosell et al.[689]	2019	lab
Gafni et al.[690]	2019	field

van Breukelen et al.[691]	2005	lab
Vanstone et al.[692]	2008	lab
Hunkeler et al.[693]	2009	method
Fletcher et al.[694]	2009	lab
Amaral et al.[481]	2010	method
Chiang et al.[695]	2012	lab
Wiegert et al.[696]	2013	lab
Shouakar-Stash et al.[697]	2013	method
Wanner et al.[698]	2015	lab
Kret et al.[699]	2015	lab
Wanner et al.[700]	2016	field
Ebert et al.[701]	2017	method
Goli et al.[702]	2017	method
Blázquez-Pallí et al.[703]	2019	lab
Shouakar-Stash et al.[704]	2006	method
Leitner et al.[705]	2017	lab
Zwank et al.[63]	2003	method
Kuder et al.[706]	2013	lab
Rodríguez-Fernández et al.[707]	2017	lab
Wanner et al.[708]	2019	lab
Rodríguez-Fernández et al.[709]	2018	lab
Zwank et al.[710]	2005	lab
Rodríguez-Fernández et al.[711]	2018	field
Mundle et al.[712]	2017	lab
van Breukelen et al.[585]	2007	lab
Chartrand et al.[713]	2007	method
Heckel et al.[714]	2017	method
Slater et al.[478]	1999	lab
Elsner et al.[479]	2006	method
Bouchard et al.[484]	2014	method
Bouchard et al.[487]	2017	method
Ertl et al.[715]	1996	lab
Dayan et al.[716]	1999	lab
Numata et al.[717]	2002	method

Poulson et al.[718]	2002	lab
Slater et al.[719]	2002	lab
Shouakar-Stash et al.[720]	2003	lab
Slater et al.[721]	2003	lab
Chu et al.[722]	2004	lab
Sakaguchi-Söder et al.[723]	2007	lab
Elsner et al.[724]	2008	lab
Liang et al.[725]	2009	lab
Aeppli et al.[726]	2009	lab
Bernstein et al.[727]	2011	lab
Marchesi et al.[728]	2012	lab
Klisch et al.[493]	2012	method
Gan et al.[729]	2013	method
Audí-Miró et al.[730]	2013	lab
Cretnik et al.[731]	2013	lab
Marchesi et al.[732]	2013	lab
Cretnik et al.[733]	2014	lab
Jin et al.[472]	2014	lab
Renpenning et al.[734]	2014	lab
Lee et al.[735]	2015	lab
Buchner et al.[736]	2015	lab
Liu et al.[737]	2016	lab
Liu et al.[738]	2016	lab
Badin et al.[19]	2016	lab
Gafni et al.[739]	2018	lab
Heckel et al.[740]	2018	lab
Yu et al.[741]	2018	lab
Liu et al.[742]	2018	lab
Jian-Ye et al.[743]	2019	method
Thouement et al.[744]	2019	lab
Lihl et al.[344]	2019	method
Gafni et al.[745]	2020	lab
Gui et al.[397]	2015	method
Walaszek et al.[746]	2020	lab

Franke et al.[747]	2020	lab
Franke et al.[748]	2017	lab
Hirschorn et al.[749]	2007	lab
Carpani et al.[750]	2021	field
Heckel et al.[751]	2022	lab
Yankelzon et al.[752]	2020	lab
Palau et al.[753]	2014	method
Head et al.[754]	2020	lab
Hunkeler et al.[755]	2000	lab
Palau et al.[756]	2017	lab
Hirschorn et al.[757]	2004	lab
Hunkeler et al.[758]	2002	lab
Wanner et al.[759]	2017	field
Abe et al.[760]	2009	lab
Soder-Walz et al.[761]	2021	lab
Palau et al.[762]	2017	lab
Hart et al.[763]	2022	field
Liu et al.[764]	2021	lab
Rodríguez-Fernández et al.[707]	2017	lab
Heckel et al.[765]	2017	lab
Liang et al.[766]	2007	lab
Rodríguez-Fernández et al.[709]	2018	lab
Neumann et al.[767]	2009	lab
Elsner et al.[768]	2007	lab
Stewart et al.[769]	2018	lab
Elsner et al.[770]	2004	lab
Breider et al.[771]	2013	lab
Rostkowski et al.[506]	2021	lab
Arnold et al.[772]	2008	lab
Torrentó et al.[773]	2017	lab
Breider et al.[774]	2014	lab
Asfaw et al.[775]	2020	method
Chen et al.[776]	2018	lab
Heckel et al.[777]	2019	lab

Aeppli et al.[778]	2013	lab
Hunkeler et al.[14]	2012	field
Benbow et al.[779]	2008	method
Nikolausz et al.[780]	2006	lab
Torgonskaya et al.[781]	2019	lab
Nadalig et al.[782]	2013	lab
Prieto-Espinoza et al.[783]	2021	lab
Cichocka et al.[784]	2007	lab
Nijenhuis et al.[785]	2005	lab
Büsing et al.[786]	2019	lab
Béranger et al.[787]	2006	lab
Renpenning et al.[788]	2015	lab
Jeannottat et al.[789]	2012	lab
Numata et al.[717]	2002	lab
Palau et al.[790]	2010	field
Thullner et al.[791]	2008	method
Badin et al.[792]	2014	lab
Barth et al.[793]	2002	lab
Jeannottat et al.[794]	2013	lab
Gan et al.[795]	2014	lab
Morrill et al.[796]	2006	lab
Höhener et al.[797]	2015	method
Lihl et al.[798]	2019	lab
Marco-Urrea et al.[799]	2011	lab
Smits et al.[800]	2011	lab
Imfeld et al.[801]	2011	field
Ottosen et al.[802]	2021	field
Damgaard et al.[803]	2013	field
Murray et al.[804]	2019	field
Åkesson et al.[805]	2020	field
Hellal et al.[806]	2020	field
Schwarzbauer et al.[807]	2005	method
Ghezzi et al.[808]	2021	field
Halloran et al.[809]	2021	method

Ottosen et al.[810]	2020	field
Liu et al.[811]	2014	lab
Schmidt et al.[812]	2014	lab
Yu et al.[813]	2014	lab
Bloom et al.[814]	2000	lab
Horst et al.[815]	2020	lab
Schüth et al.[816]	2003	lab
Kopinke et al.[512]	2005	method
Bill et al.[817]	2001	lab
Schüth et al.[496]	2003	lab
Tiehm et al.[818]	2008	lab
Dong et al.[819]	2011	lab
Clingenpeel et al.[820]	2012	lab
Han et al.[821]	2018	lab
Horst et al.[822]	2016	lab
Höhener et al.[516]	2012	lab
Li et al.[823]	2022	lab
Julien et al.[824]	2018	method
Imfeld et al.[825]	2010	lab
Schmidt et al.[826]	2010	lab
Abe et al.[827]	2009	lab
Gilevska et al.[828]	2015	method
Holt et al.[829]	2001	method
Brungard et al.[830]	2003	lab
Heraty et al.[831]	1999	lab
Bouchard et al.[605]	2022	lab
Lincker et al.[832]	2022	lab
Buchner et al.[833]	2022	method
Wienkenjohann et al.[834]	2023	lab
Willmann et al.[835]	2023	lab
Phillips et al.[836]	2022	lab
Asfaw et al.[837]	2023	lab
Cai et al.[838]	2022	lab
Emsbo-Mattingly et al.[839]	2022	field

Yuan et al.[840]	2022	field
Ji et al.[606]	2023	lab

B Supporting Information to Chapter 2

B.1 Chemicals, Materials, and Standard Solutions

All chemicals and materials purchased commercially and used in this work are summarized in Table B.1.

Table B.1 List of reagents, solvents, and analytical standards.

Chemical	Purity/Grade/Type	Supplier
dichloromethane	≥99%	Sigma-Aldrich
formic acid	≥88%	Sigma-Aldrich
hydrochloric acid	ACS reagent, 37%	Sigma-Aldrich
methanol	≥99%	Sigma-Aldrich
sodium chloride	≥99.5%	Fisher Scientific
sodium hydroxide solution	0.1 N	Carl Roth
(trimethylsilyl)diazomethane solution	2.0 M in hexane	Sigma-Aldrich

Ultrapure H_2O (18.2 MΩ cm at 25 °C) was obtained from a Milli-Q® direct reference H_2O purification system from Merck MilliPore (Burlington, USA).

B.2 Methylation: Mechanistic Details

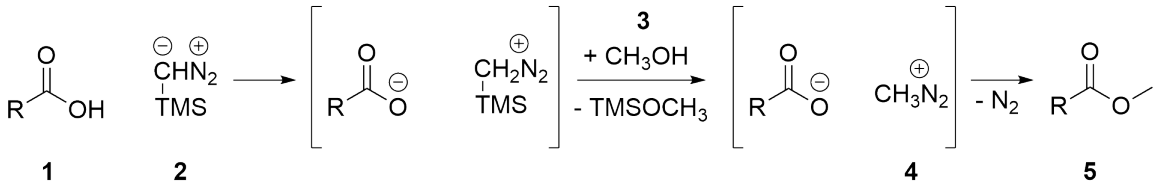

Figure B.1 Reaction mechanism of methylation of NOM carboxylic acid groups (**1**) using TMSD (**2**) according to Kühnel et al.[841] **2** deprotonates the carboxylic acid group of **1** and is subsequently desilylated by the excess of methanol (**3**). The nucleophilic attack of the deprotonated carboxylic acid group at diazomethane (**4**) leads to the release of nitrogen and the final methylated product (**5**).

B.3 Supplementary Data on the Titration

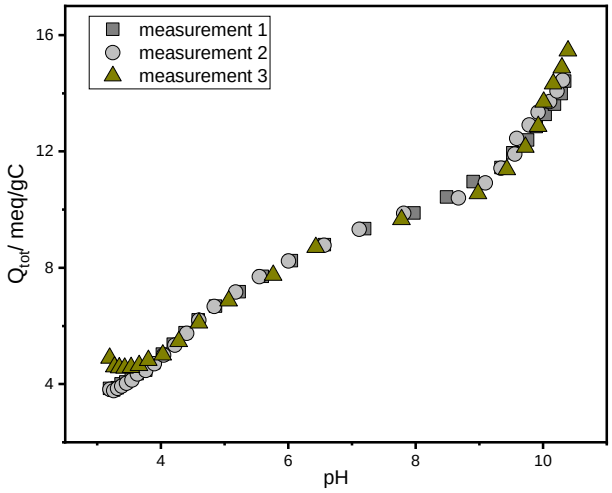

Figure B.2 Triplicate acid-base titration measurements of NOM (3 mgC).

B.4 Supplementary Data on the Breakthrough Curves

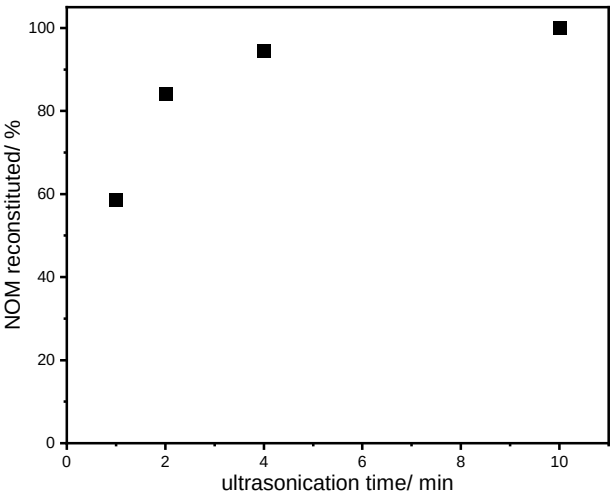

Figure B.3 Validation of time methylated NOM samples have to be ultrasonicated using an ultrasonic lab homogenizer to fully reconstitute all organic compounds in water.

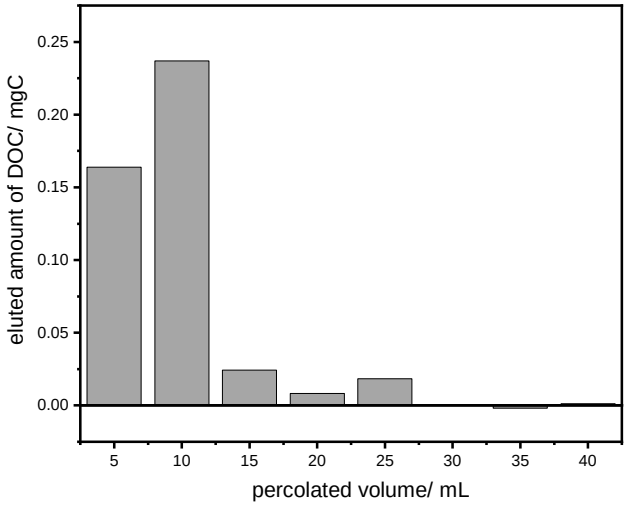

Figure B.4 Breakthrough curves of a control measurement on MISPE. For the control measurement, the same reaction conditions used for methylated NOM were used except of no NOM was included. The gray bars show the amount of DOC in the breakthrough and indicate the amount of contamination in the different fractions originating from the methylation procedure.

C Supporting Information to Chapter 3

C.1 Chemicals, Materials, and Standard Solutions

All chemicals and materials purchased commercially and used in this work are summarized in Table C.1.

Table C.1 List of reagents, solvents, and analytical standards.

Chemical	Purity/Grade/Type	Supplier
1-vinyl-2-pyrrolidone	stabilizer: sodium hydroxide	Sigma-Aldrich
2,2'-azobis(2-methylpropionitrile)	≥98%	Sigma-Aldrich
γ-methacryloxypropyltrimethoxysilane	≥97%	Sigma-Aldrich
acetone	technical grade	in-house supply
acetonitrile	≥99%	Sigma-Aldrich
divinylbenzene	stabilizer: 4-tert-butylpyrocatechol	Sigma-Aldrich
ethylene glycol dimethacryate	stabilizer: hydroquinone monomethyl ether	Sigma-Aldrich
humic acids	technical grade	Sigma-Aldrich
hydrochloric acid	ACS reagent, 37%	Sigma-Aldrich
isopropyl alcohol	≥99%	Sigma-Aldrich
magnesium sulfate	anhydrous, ≥98.0%	Sigma-Aldrich
methanol	≥99%	Sigma-Aldrich
sodium hydroxide solution	1 N	Carl Roth
toluene	≥99%	Sigma-Aldrich
trimethylol-propane trimethacrylate	stabilizer: monomethyl ether hydroquinone	Sigma-Aldrich

Ultrapure H_2O (18.2 MΩ cm at 25 °C) was obtained from a Milli-Q® direct reference H_2O purification system from Merck MilliPore (Burlington, USA).

Before using DVB for the synthesis, the respective monomer was sequentially washed twice with NaOH (1 M) and once with water to remove the stabilizer and. then dried over $MgSO_4$. The stabilizer was removed from EGDMA using a vacuum destillation at 140 °C and 40 mbar. The purified monomers were stored at -80 °C. To purify AIBN, it was recrystallized in methanol and stored at 4 °C.

The carbon content of the above-mentioned humic acids was determined to be 37% ± 3% by measuring a suspension of 0.5 mg humic acids in 1 mL water with a Total Organic Carbon Analyzer (TOC-L, Shimadzu, Germany) and used for mass calculations.

C.2 Sensor Holder

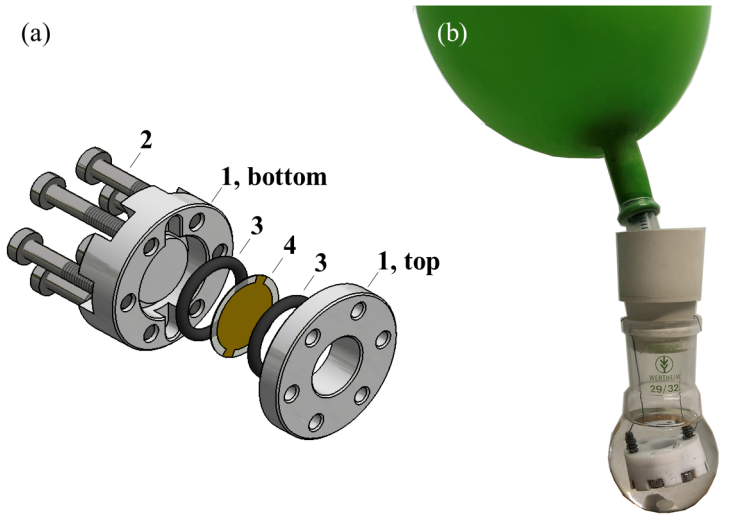

Figure C.1 Sensor holder used during the coating reaction to guarantee only the upper sensor surface being coated. (a) Scheme of the sensor holder: 1: Custom-made teflon sensor holder, 2: Screws, 3: O-rings made of FFKM (11.1 mm x 1.6 mm, Techniparts, Wezep, Netherlands), 4: QCM sensor. (b) Setup during the reaction: The sensor holder is placed in the middle of the flask using wire.

C.3 Data Evaluation

Listing A.4.1 Peak picking for the interval experiments with the shutter in which outliers were eliminated manually.

```
# In[1]:
### RUN ME
import pandas as pd
import scipy.signal as signal
import numpy as np
import scipy
from matplotlib import pyplot as plt
import seaborn as sns
import os

# In[2]:
### RUN ME
def count_experiments(data):
    n = 1
    experiments = {n: {'relative_time': [], 'frequency': []}}
```

```
    for i, row in data.iterrows():
        if (i>0 and data.Relative_time.loc[i] <
        data.Relative_time.loc[i-1]):
            n += 1
            experiments[n] = {'relative_time': [], 'frequency': []}
        experiments[n]['relative_time'].append(row.Relative_time)
        experiments[n]['frequency'].append(row.Resonance_Frequency)
    return n, experiments

def get_peaks(experiment, distance=200, prominence=1):
    peaks, _ = signal.find_peaks(experiment['frequency'],
    prominence=prominence, distance=distance)
    return np.array(experiment['relative_time'])[peaks],
    np.array(experiment['frequency'])[peaks]

def clean_peaks(timepoints_peaks, values_peaks, thrh=20):
    to_delete = []
    for i, val in enumerate(values_peaks):
        if i>0 and i<len(values_peaks)-1 and
        abs(values_peaks[i]-values_peaks[i-1])<=thrh and
        abs(values_peaks[i]-values_peaks[i+1])<=thrh:
            to_delete.append(i)
    values_peaks = np.delete(values_peaks, to_delete)
    timepoints_peaks = np.delete(timepoints_peaks, to_delete)
    return timepoints_peaks, values_peaks

def get_value(param, defult_param):
    if param == '':
        return defult_param
    else:
        return int(param)

# In[3]:
path = os.path.join('~','Desktop', 'Interval',
```

```
'202100830_Interval-100mgC-3.xlsx')
data = pd.read_excel(path, sheet_name='Tabelle2')
data = data.rename(columns={
    'Time (s)': 'Relative_time',
    'Delta F (Hz)': 'Resonance_Frequency'
})
n, experiments = count_experiments(data)
print(f'Based on the timeline there were {n} experiments detected')

# In[4]:
### Compute the picks for the experiment
n = int(input('Choose experiment to plot:'))
distance = input('Approximate min distance between peaks (default=200):')
prominence = input('Prominence value for peaks (default 1):')
threshold = input('Threshold for peaks removal(default 20):')

timepoints_peaks, values_peaks = get_peaks(
    experiment=experiments[n],
    distance=get_value(distance, 200),
    prominence=get_value(prominence, 1)
)
timepoints_peaks, values_peaks = clean_peaks(
    timepoints_peaks=timepoints_peaks,
    values_peaks=values_peaks,
    thrh=get_value(threshold, 20)
)

### Approximate min distance between peaks (default=200): 200
### Prominence value for peaks (default 1):1
### Threshold for peaks removal(default 20):0

# In[5]:
### Plot the results
plt.figure(figsize=(20,10))
```

```
sns.lineplot(x=experiments[n]['relative_time'],
y=experiments[n]["frequency"], ci=None)
sns.scatterplot(x=timepoints_peaks, y=values_peaks, color='r')
plt.ylabel('Resonance Frequency', fontsize=20);
plt.xlabel('Relative Time', fontsize=20);
plt.title(f'Peak Detection in Experiment {n}', fontsize=20);

# In[6]:
### To Save
data = pd.DataFrame(experiments[n])
data['peak_frequency'] = data[['relative_time', 'frequency']].apply(
    lambda x: x[1] if (x[0], x[1]) in
    [(t, v) for (t,v) in zip(timepoints_peaks, values_peaks)] else None,
    axis=1
)

# In[7]:
path_to_save = input(f'Path to save experiment {n}: ')
data[['frequency', 'relative_time', 'peak_frequency']].to_excel(
    path_to_save, index=False
)
```

Listing A.4.2 Linear regression for changes in resonance frequency.

```
import pandas as pd
from scipy.stats import linregress

FILE = "./Date_Name.csv"
COLUMNS = ["t", "F"]

#input t in min and F in Hz

dataset = pd.read_csv(FILE, sep=";")

print(len(dataset))
```

```
for col in COLUMNS:
    dataset[col] = dataset[col].apply(lambda x:
    float(x.replace(",", ".")))

for col in COLUMNS[1:]:
    X = dataset['t']
    y = dataset[col]

    s, i, r, p, std = linregress(X, y)

    print(col)
    print(s *60, std *60)
    print(s *60 *4.42, std *60 *4.42)

#output Hz/h and ng/hcm^2
```

Listing A.4.3 Smoothing of resonance frequency baselines for calculation of the baseline drift.

```
import pandas as pd
import seaborn as sns

FILE = "./Date_Name.csv"
COL = "F"
C = [701]

df = pd.read_csv(FILE, sep=";")

df[COL] = df[COL].apply(lambda x: float(x.replace(",", ".")))

for c in C:
    print(c)
    name = f"{COL}_smoothed_{c}"
    df[name] = df[COL].rolling(c).median()

    df[name] = df[name].apply(lambda x: str(x).replace(".", ","))
```

```
df[COL] = df[COL].apply(lambda x: str(x).replace(".", ","))

df.to_csv("./Date_Name_smooth.csv", sep=";")
```

C.4 Raman Measurement

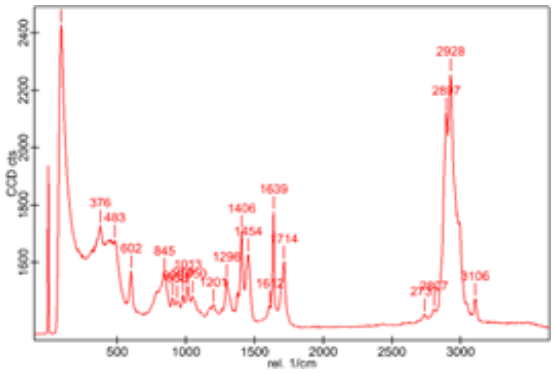

Figure A.4.1 Raman spectrum of a silica QCM sensor coated with a DVB-EGDMA polymer.

C.5 Supplementary Data on Flow Experiments

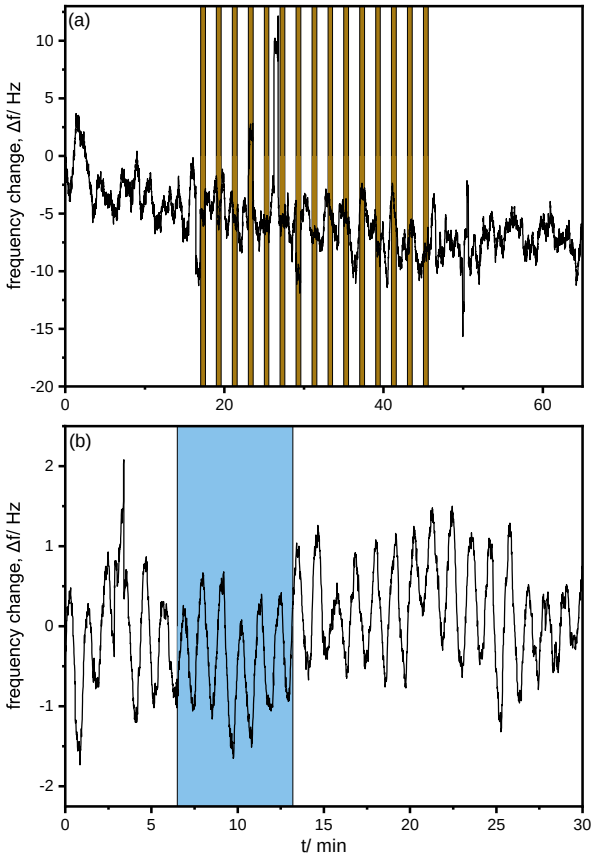

Figure A.4.2 Frequency change (black) during (a) humic acid sorption experiment on an uncoated sensor and (b) water passed over a coated sensor. (a) Humic acid sorption experiment 1 on an uncoated QCM sensor. Water was passed constantly over the sensor with a flow rate of 30 µL/min. Using an injection valve, humic acid solutions were injected during the flow experiments. The brown bars visualize the time when the humic acid solution is passed over the sensor. (b) Water is passed over a coated sensor with a flow rate of 30 µL/min. Using an injection valve, water was injected. The blue bar visualizes the time when the injected water is passed over the sensor.

D Supporting Information to Chapter 4

D.1 Chemicals, Materials, Standard Solutions, and Spray Fabrication

Table A.4.1 List of reagents, solvents, and analytical standards.

Chemical	Purity/Grade	Supplier
QuEChERS extraction		
brown rice (Oryza)	n.a.	Euryza GmbH
disodium hydrogen citrate sesquihydrate	≥99 %	Sigma-Aldrich
magnesium sulfate anhydrous grit	≥98 %	Sigma-Aldrich
sodium chloride	≥99.5 %	Fisher Scientific
trisodium citrate dihydrate	≥99 %	Sigma-Aldrich
Solvents		
acetonitrile	≥99 %	Sigma-Aldrich
isopropanol	≥99 %	Sigma-Aldrich
methanol	≥99 %	Sigma-Aldrich
Analytical Standards		
2,6-dichlorobenzamide (BAM)	PESTANAL®, anal. st.	Sigma-Aldrich
atrazine (Atz)	PESTANAL®, anal. st.	Sigma-Aldrich
boscalid (Bosc)	PESTANAL®, anal. st.	Sigma-Aldrich
desethylatrazine (DEA)	PESTANAL®, anal. st.	Sigma-Aldrich
propargite (Prop)	PESTANAL®, anal. st.	Sigma-Aldrich

n.a. = not available, anal. st. = analytical standard

Ultrapure H_2O (18.2 MΩ cm at 25 °C) was obtained from a Milli-Q® direct reference H_2O purification system from Merck MilliPore (Burlington, USA). Stock solutions of analytical standards (1 g/L) were prepared in CH_3OH and stored at -18 °C.

The microfluidic spray-dryers were fabricated in-house at the Heinz Nixdorf-Chair of Biomedical Electronics at the Center for Translational Cancer Research of the Technical University of Munich (TranslaTUM). Fast and reliable production of microfluidic spray-dryers was achieved using a two-layer soft lithography approach according to a previously published protocol.[152] Microfluidic channels were designed in AutoCAD 2021 (Autodesk GmbH). Negative resists SU8-3025 and SU8-3050 (MicroChem Corp.) were spin-coated and patterned using a maskless laser lithography system (Dilase 250, Kloe, France) on a 3" Si substrate to obtain the negative master mold. The first layer has a thickness of 20 µm and contains the channel for the liquid sample, while the second layer has a thickness of 70 µm and contains the channel for the gas. PDMS (Sylgard 184, Dow

Corning) was mixed at a ratio of 9:1 (w/w), degassed, and cured in the negative SU8 master mold for 60 min at 65 °C. Microfluidic devices were cut along alignment marks using a razor blade, and holes for tubings were punched using a 0.5 mm biopsy punch (World Precision Instruments). Individual PDMS devices were cleaned using isopropanol and acetone and blown dry with nitrogen. PDMS devices were activated using oxygen plasma for 60 s at 30 W (Zepto, Diener electronic GmbH, Germany). A drop of deionized water was applied to the surface to facilitate the alignment of two PDMS devices under a stereo microscope for the final microfluidic device. A permanent bond between PDMS parts is formed by curing the assembled devices for 60 min at 85 °C. The cross-section of the channels for liquid and gas delivery were measured to be 27 × 20 µm^2 (w × h) and 110 × 70 µm^2 (w × h), respectively.

D.2 Determination of Limits of Detection and Quantification

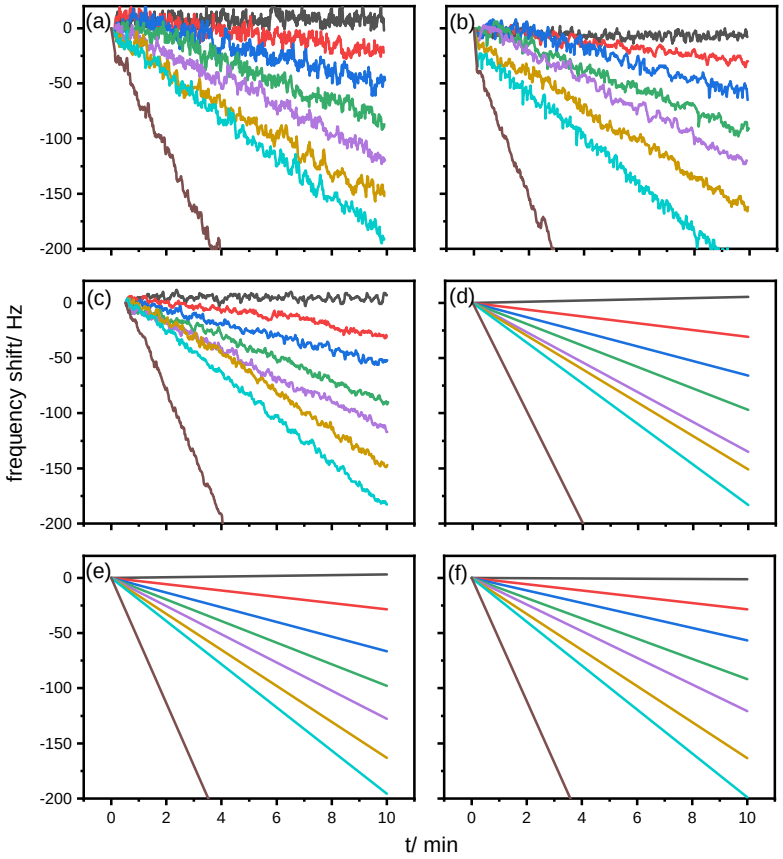

Figure A.4.1 a-c: Frequency raw data of three different CH_3OH/H_2O compositions ((a): 15/85, (b): 50/50, (c): 85/15 (v/v)) containing NaCl in different concentrations (0, 30, 60, 90, 120, 150, 180 and 500 mg/L). d-f: The average slope of quadruplicates of dry mass sensing experiments using different CH_3OH/ H_2O compositions ((d): 15/85, (e): 50/50, (f): 85/15 (v/v)) containing NaCl in different concentrations (0, 30, 60, 90, 120, 150, 180 and 500 mg/L). The slopes were used for the calculation of the LOD and the LOQ.

D.3 TOC Validation

Table A.4.2 HPLC gradient conditions for the TOC validation measurement.

Time/ min	% CH_3OH
0	10
7.5	40
15	80
16.5	90
18	90

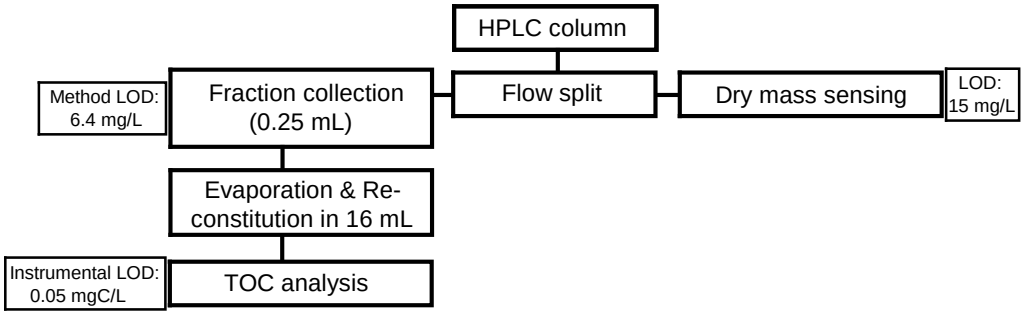

Figure A.4.2 Flow chart of offline TOC measurement of HPLC fractions. The mobile phase is split using a post-column adjustable flow splitter. The high flow goes to a fraction collector; each fraction is collected for 30 seconds (volume: 0.25 mL). The fraction is evaporated and reconstituted in 16 mL H_2O and measured using TOC analysis.

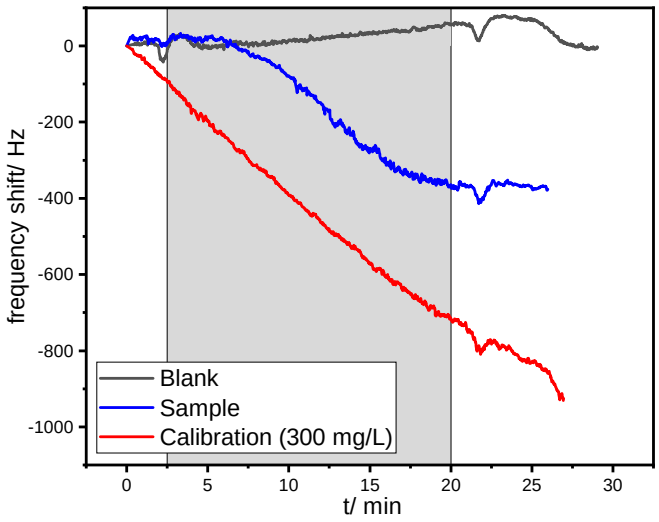

Figure A.4.3 Frequency raw data (blank = black, sample = blue, calibration = red) of the QCM measurement during the TOC validation experiment. The grey bar shows the measurement window (2.5 min dead time).

D.4 HPLC Parameters for Rice Matrix Measurement

Table A.4.3 HPLC gradient conditions for the brown rice measurement.

Time/ min	% CH_3OH
0	10
0.5	10
6	80
13	100
17	100
20	10
22	10

D.5 GC-MS: Measurement Details and Analyte Retention Time

Table A.4.4 SIM parameters for GC-MS analysis and pesticide retention times.

Analyte	Retention Time/ min	Measured Ion m/z
Desethylatrazine	12.0	172.0
2,6-Dichlorobenzamide	12.4	172.9
Atrazine	13.9	200.0
Propargite	16.3	135.1
Boscalid	22.9	140.0

D.6 Correlation of Relative Detector Intensity and Matrix Effect

Table A.4.5 Absolute matrix effect (in %) of five pesticides (in order of their retention time; see Table A.4.4) during GC-MS measurement of LC fractionated brown rice matrix of triplicate sample measurements (standard deviation: ± in %)

fraction	A	B	C	D	E
retention window/ min	6 - 7.5	8.5 - 10	11 - 12.5	12.7 - 14.2	15 - 16.5
			absolute matrix effect/ %		
Desethylatrazine	6.0±7.3	3.8±8.2	9.0±6.3	17±11	130±33
2,6-Dichlorobenzamide	4.1±9.9	-1.1±7.3	5.3±4.4	14±9	101±62
Atrazine	-2.0±5.7	0.8±8.6	3.9±5.9	10±7	110±33
Propargite	-36±7	-31±6	-34±8	-55±11	-83±4
Boscalid	25±8	29±10	23±8	31±11	345±132

D.7 GC-MS Chromatograms for Collected Fractions and Mass Spectrum of Oleic Acid

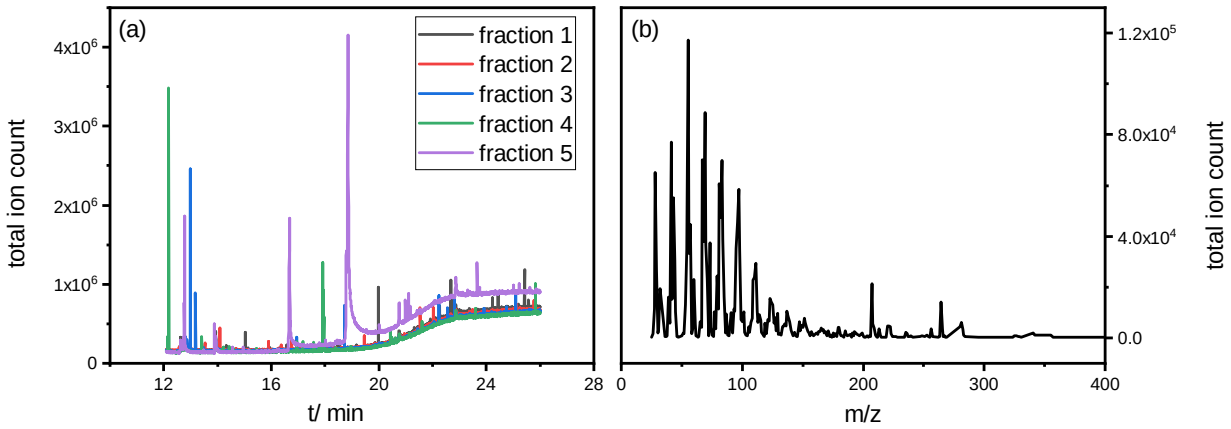

Figure A.4.4 (a) Overlapped GC chromatograms of the five brown rice matrix fractions. GC chromatograms were recorded in full scan mode (0-4000 m/z). There is no data available before minute 12 because of solvent delay. (b) Mass spectrum of the brown rice matrix fraction 5 peak at minute 19. The main component is oleic acid according to the NIST database.

D.8 Matlab Script for QCM Data Processing

```
1
2  clc
3  clear
4
5  para.Projecttitle=('10-80-90');
6  para.Endtime=22;
7  MEOHpercent0min=10;
8  MEOHpercent75min=80;
9  MEOHpercent15min=90;
10 GradientX=[0 7.5 15 16.5 18 19 para.Endtime];
11 GradientY=[MEOHpercent0min MEOHpercent75min MEOHpercent15min 90 90
       10 10];
12
13 figure
14 plot(GradientX,GradientY,'-k')
15 title('Solvent Gradient')
16 xlabel('time /min')
17 ylabel('MeOH %')
```

```
xlim([0 para.Endtime])
ylim([0 100])
%%%%%%%%%%%%%%%%%%%% if no QuEChERS are related QuechersBlank=0,
   otherweise
%%%%%%%%%%%%%%%%%%%% type in any nr.
QuechersBlank=0;
UV without Blank subtraction
namelist=dir('*.txt');
len=length(namelist);

UVfilename='./UV/10_80_90.txt'%namelist(1).name;
% UVfilename="220324_isochratic30percent_NOMextractsample.txt";

[RetentionTime,Intensity]=textread(UVfilename,'%s%s','headerlines'
   ,25);

RetentionTime=strrep(RetentionTime,',','.');

[inx_Time,~,~]=find(contains(RetentionTime,'Time'));
[inx_R,~,~]=find(contains(RetentionTime,'R'));
[inx_Wave,~,~]=find(contains(RetentionTime,'Wave'));

Wavelength=Intensity(inx_Wave);
Starttxt='Bandwidth(nm)';
Endtxt='[PDA';
[inx_Start,~,~]=find(contains(RetentionTime,Starttxt));
inx_Start=inx_Start+3;

[inx_End,~,~]=find(contains(RetentionTime,Endtxt));
inx_End=inx_End-1;
inx_End=inx_End(2:end);
inx_End=[inx_End;length(RetentionTime)];

for i=1:length(Wavelength)
```

```
50
51      UVtime{i}=RetentionTime(inx_Start(i): inx_End(i),1);
52      UVtime{i}= str2double(convertCharsToStrings(UVtime{i}));
53
54      UVintensity{i}=Intensity(inx_Start(i): inx_End(i),1);
55      UVintensity{i}= str2double(convertCharsToStrings(UVintensity{i
            }));
56  end
57  Raw data extraction
58
59  %%figurename must match the sequence of filelist
60  %  figurename={'Blank1', 'Blank2', 'Blank3', 'Calibration01_1','
        Calibration01_2','Calibration01_3', ...
61  % 'Calibration02_1','Calibration02_2','Calibration02_3','
        Sample01_1', 'Sample01_2', 'Sample01_3','Sample02_1', '
        Sample02_2', 'Sample02_3'};
62  para.figurename={'blank1', 'blank2', 'cali1', 'cali2', 'sample1'};
63
64  %%%read the file from QCM
65
66  QCMnamelist=dir('*.txt');
67  len=length(QCMnamelist);
68  n=1;
69  TableTimeDeltaF=[];
70
71  for i=1:len
72      filename{i}=QCMnamelist(i).name;
73
74      [RawF{i},   RawR{i} ,        DeltaF{i}, DeltaR{i},   DeltaMass{
            i},   Thickness{i},   Time{i},        Tag{i}]=textread(
            filename{i},'%s%s%s%s%s%s%s%s','headerlines',16);
75      DeltaF_num{i}=strrep(DeltaF{i},',','.');
76      DeltaF_num{i}=cell2mat(DeltaF_num{i});
```

```
77      %     DeltaF_num{i}=str2double(convertCharsToStrings(
           DeltaF_num{i}));
78      DeltaF_num{i}=str2num(DeltaF_num{i});
79
80      DeltaR_num{i}=strrep(DeltaR{i},',','.');
81      DeltaR_num{i}=cell2mat(DeltaR_num{i});
82      %     DeltaF_num{i}=str2double(convertCharsToStrings(
           DeltaF_num{i}));
83      DeltaR_num{i}=str2num(DeltaR_num{i});
84
85      RawR_num{i}=strrep(RawR{i},',','.');
86      RawR_num{i}=cell2mat(RawR_num{i});
87      %     DeltaF_num{i}=str2double(convertCharsToStrings(
           DeltaF_num{i}));
88      RawR_num{i}=str2num(RawR_num{i});
89
90      Time_num{i}=strrep(Time{i},',','.');
91      Time_num{i}=cell2mat(Time_num{i});
92      % Time_num{i}=str2double(convertCharsToStrings(Time_num{i}));
93      Time_num{i}=str2num(Time_num{i});
94
95      Time_min{i}=Time_num{i}./60;
96
97      % write time and delte freq to excel file.
98
99      T{i}=table(Time_min{i},DeltaF_num{i});
100
101     T{i}.Properties.VariableNames = {'Time_min','DeltaF'};
102
103     TableTimeDeltaF=T{i};
104     excelcolumn={'A2','C2','E2','G2','I2', 'K2', 'M2','O2','Q2', '
           S2', 'U2'};
105
106     excelfilename = [para.Projecttitle 'TableTimeDeltaF.xlsx'];
```

```
107     writetable(TableTimeDeltaF,excelfilename,'Sheet',1,'Range',
            excelcolumn{i})
108
109     [TF{i},S1{i},S2{i}] = ischange(DeltaF_num{i},'linear','
            Threshold',30000);
110 end
111
112 filename
113 add title for excel columns
114
115 for n=1: length(para.figurename)
116
117     excelcolumn={'A1','C1','E1','G1','I1', 'K1', 'M1','O1','Q1', '
            S1', 'U1'};
118
119     excelfilename = [para.Projecttitle 'TableTimeDeltaF.xlsx'];
120     writecell(para.figurename(n),excelfilename,'Sheet',1,'Range',
            excelcolumn{n})
121
122 end
123 Enter the index of blank/calibration/sample!!
124 blank_index=[1:2];
125 calibration_index=[3:4];
126 sample_index= [5];
127 Compare blanks and calibrations via figures
128
129 figure
130 hold on
131 for i=blank_index
132
133     plot(Time_min{i},DeltaF_num{i})
134
135 end
136
```

```
for j=sample_index

    plot(Time_min{j},DeltaF_num{j})

end

hold off

xlim([0,25])
legend([para.figurename(blank_index),para.figurename(sample_index)
   ],"Location",'best')
title('CompareBlank')
figure
hold on
for i=blank_index

    plot(Time_min{i},RawR_num{i})

end

for j=sample_index

    plot(Time_min{j},RawR_num{j})

end

hold off
xlim([0,para.Endtime])
legend([para.figurename(blank_index),para.figurename(sample_index)
   ],"Location",'best')
title('Compare Blanks and Smaple R')
figure

hold on
```

```
169 for i=calibration_index
170
171     plot(Time_min{i},DeltaF_num{i})
172
173 end
174
175 for j=sample_index
176
177     plot(Time_min{j},DeltaF_num{j})
178
179 end
180
181 hold off
182
183 xlim([0,25])
184 legend([para.figurename(calibration_index),para.figurename(
       sample_index)],"Location","best" )
185 title('\DeltaF comparation')
186 ylabel('\DeltaF /Hz')
187 xlabel('time /min')
188
189 xlim([0.0 26])
190 figure
191 hold on
192 for i=calibration_index
193
194     plot(Time_min{i},RawR_num{i})
195
196 end
197
198 for j=sample_index
199
200     plot(Time_min{j},RawR_num{j})
201
```

```
202 end
203
204 hold off
205 xlim([0,para.Endtime])
206 legend([para.figurename(calibration_index),para.figurename(
      sample_index)],"Location",'best')
207 title('R-value comparation')
208 ylabel('R-value /Ohms')
209 xlabel('time /min')
210 Select Blank and Calibration
211 %%%%%%Blank=3 means Blank3
212 %%%%%%Cali=5 means Calibration1; C=5 or 6 or 7 for four blanks and
       three Cali
213 %------select Blank and Calibration
214 Cali=4;
215 Blank=2;
216 Export template file for selected calibration and sample with
      selected blank
217
218 %-------Export template file for selected calibration
219 Caliexcelfilename = [para.Projecttitle 'Template_Calibration.xlsx'
      ];
220
221 writematrix(BLANKfinal_frequency,Caliexcelfilename,'Sheet',1,'
      Range','A1')
222 writematrix(Califinal_frequency,Caliexcelfilename,'Sheet',1,'Range
      ','C1')
223
224 %-------Export template file for Sample
225
226 Samexcelfilename = [para.Projecttitle 'Template_Sample.xlsx'];
227
228 writematrix(BLANKfinal_frequency,Samexcelfilename,'Sheet',1,'Range
      ','A1')
```

```
writematrix(SAMPLEfinal_frequency,Samexcelfilename,'Sheet',1,'Range','C1')
Control subtraction, filtration, derivate calculation
For Calibraition:

%-----------Load data

%Specify path:
path_to_excel_file = Caliexcelfilename;
sheet_name_in_excel = "Sheet1";
data = xlsread(path_to_excel_file, sheet_name_in_excel);

%-----------Compute the difference:
%-----------since timepoints are not aligned the difference is computed between two closest in time points

%define the row
time_control = 1;
frequency_control = 2;
time_calib = 3;
frequency_calib = 4;
control_timepoints = data(:,time_control);
calib_timepoints = data(:,time_calib);
control_freq = data(:,frequency_control);
calib_freq = data(:,frequency_calib);

%Specify path:
path_to_excel_file = Caliexcelfilename;
sheet_name_in_excel = "Sheet1";
data = xlsread(path_to_excel_file, sheet_name_in_excel);

%-----------Compute the difference:
%-----------since timepoints are not aligned the difference is computed between two closest in time points
```

```
260
261 %define the row
262 time_control = 1;
263 frequency_control = 2;
264 time_calib = 3;
265 frequency_calib = 4;
266 control_timepoints = data(:,time_control);
267 calib_timepoints = data(:,time_calib);
268 control_freq = data(:,frequency_control);
269 calib_freq = data(:,frequency_calib);
270
271 %%%%%%%%%%%%%%%%consider the data length of Calibration
272 validEND=sum(~isnan(calib_freq));
273 if validEND>2000
274     validEND=2000;
275 end
276
277 calib_freq=calib_freq(1:validEND);
278 calib_timepoints=calib_timepoints(1:validEND);
279 %searching for the nearest time_control and subtract control
    frequency from
280 %calibration
281
282 %searching for the nearest time_control
283
284 calib = zeros(length(calib_timepoints), 2);
285 for i = 1 : length(calib_timepoints)
286     calib(i, 1) = calib_timepoints(i);
287     [~,Index] = min(abs(control_timepoints-calib_timepoints(i)));
288     calib(i, 2) = calib_freq(i) - control_freq(Index);
289 end
290
291 %------------------calculating derivate
292 %type in approx_step to adjust the timestep in regression
```

```
293
294 approx_step = 100;
295 derivate_data = zeros(length(calib_timepoints) - approx_step,2);
296 for i = 1 : (length(calib_timepoints)-approx_step)
297     approx_timepoint = zeros(approx_step, 1);
298     approx_frequency = zeros(approx_step, 1);
299     for j = 1 : approx_step
300         approx_timepoint(j) = calib(i+j-1, 1);
301         approx_frequency(j) = calib(i+j-1, 2);
302     end
303     X = [ones(size(approx_timepoint)), approx_timepoint];
304     Y = approx_frequency;
305     derivate = X\Y;
306     derivate_data(i, 1) = calib(i + floor(approx_step/2), 1);
307     derivate_data(i, 2) = derivate(2);
308 end
309 position = "C";
310 position_app = position + floor((length(calib_freq)-length(
       derivate_data(:,2)))/2);
311 derivate_data(end,1)
312 %------------Applying filter
313 % odd num only
314 window_length =801;
315 polyorder = 3;
316 filt_calib = sgolayfilt(derivate_data, polyorder, window_length);
317 filt_calib(end,1)
318 figure
319 plot(calib(:, 1), calib(:, 2), '-r', derivate_data(1:end,1),
       derivate_data(1:end,2), '-b')
320 hold on
321 plot(filt_calib(1:end,1), filt_calib(1:end,2),'-k','LineWidth',2)
322 hold off
323 xlim([0 27])
```

```
legend('\DeltaF', '1st Derivate', 'Filtered Derivate','Location',"
   best")
title('Calibration', 'Data processing')
xlabel('time /min')
ylabel({'Frequency /Hz'; '1^st Derivate of \DeltaF'})
plot( derivate_data(:,1), derivate_data(:,2), '-b')
hold on
plot(filt_calib(:,1), filt_calib(:,2),'-k','LineWidth',2)
hold off
ylim([-200 150])
xlim([0 27])
x0=10;
y0=10;
width=1200;
height=400;
set(gcf,'position',[x0,y0,width,height])
For Sample:
path_to_excel_file = Samexcelfilename;
sheet_name_in_excel = "Sheet1";
data = xlsread(path_to_excel_file, sheet_name_in_excel);

%-----------Compute the difference:
%-----------since timepoints are not aligned the difference is
   computed between two closest in time points

%define the row
time_control = 1;
frequency_control = 2;
time_calib = 3;
frequency_calib = 4;
control_timepoints = data(:,time_control);
calib_timepoints = data(:,time_calib);
control_freq = data(:,frequency_control);
calib_freq = data(:,frequency_calib);
```

```
356
357 %searching for the nearest time_control
358
359 calib = zeros(length(calib_timepoints), 2);
360 for i = 1 : length(calib_timepoints)
361     calib(i, 1) = calib_timepoints(i);
362     [~,Index] = min(abs(control_timepoints-calib_timepoints(i)));
363     calib(i, 2) = calib_freq(i) - control_freq(Index);
364 end
365
366 %------------------calculating derivate
367 %type in approx_step to adjust the timestep in regression
368
369 approx_step = 30;
370 derivate_data = zeros(length(calib_timepoints) - approx_step,2);
371 for i = 1 : (length(calib_timepoints)-approx_step)
372     approx_timepoint = zeros(approx_step, 1);
373     approx_frequency = zeros(approx_step, 1);
374     for j = 1 : approx_step
375         approx_timepoint(j) = calib(i+j-1, 1);
376         approx_frequency(j) = calib(i+j-1, 2);
377     end
378     X = [ones(size(approx_timepoint)), approx_timepoint];
379     Y = approx_frequency;
380     derivate = X\Y;
381     derivate_data(i, 1) = calib(i + floor(approx_step/2), 1);
382     derivate_data(i, 2) = derivate(2);
383 end
384 position = "C";
385 position_app = position + floor((length(calib_freq)-length(
       derivate_data(:,2)))/2);
386
387 %------------Applying filter
388 window_length = 301;
```

```
polyorder = 3;
filt_SAMPLE = sgolayfilt(derivate_data, polyorder, window_length);

%------------plot data
figure
plot(calib(:, 1), calib(:, 2), '-r', derivate_data(:,1),
   derivate_data(:,2), '-b')
hold on
plot(filt_SAMPLE(:,1), filt_SAMPLE(:,2),'-k','LineWidth',2)
hold off
xlim([0 27])
legend('\DeltaF', '1st Derivate', 'Filtered Derivate','Location',"
   best")
title('Sample', 'Data processing')
xlabel('time /min')
ylabel({'Frequency /Hz'; '1^st Derivate of \DeltaF'})
%------------zoom

plot( derivate_data(:,1), derivate_data(:,2), '-b')
hold on
plot(filt_SAMPLE(:,1), filt_SAMPLE(:,2),'-k','LineWidth',2)
hold off
ylim([-200 150])
xlim([0 20])
x0=10;
y0=10;
width=1200;
height=400;
set(gcf,'position',[x0,y0,width,height])
%----------------saving data to the file
%first row is time
%second row is calb.frequency

head = {'time_calib', 'frequency_calib'};
```

```
file_name = "Sample_Frequency-filtered.xlsx";
if exist(file_name, 'file') == 1
    delete(file_name);
end
writematrix(calib, file_name, 'range', 'A2');
writematrix("time_calib",file_name, 'range', 'A1');
writematrix("frequency_calib",file_name, 'range', 'B1');
writematrix("filtered gravity", file_name, 'range', 'C1');
writematrix(derivate_data(:, 2), file_name, 'range', position_app)
Correction of time (shift, cut off)
df_dm=0.1415;

%-------input timeshift
timeshift=-2.50;


shifted_filt_calibtime=filt_calib(:,1)+timeshift;

shifted_filt_SAMPLEtime=filt_SAMPLE(:,1)+timeshift;

%////////cut off the negative timeframe

cutted_shifted_filt_calibtime=shifted_filt_calibtime(
   shifted_filt_calibtime>0 & shifted_filt_calibtime<20);

cutted_shifted_filt_SAMPLEtime=shifted_filt_SAMPLEtime(
   shifted_filt_SAMPLEtime>0 & shifted_filt_SAMPLEtime<20);

cutted_shifted_filt_calibfreq=filt_calib(:,2);
cutted_shifted_filt_calibfreq=cutted_shifted_filt_calibfreq(
   shifted_filt_calibtime>0 & shifted_filt_calibtime<20);

cutted_shifted_filt_SAMPLEfreq=filt_SAMPLE(:,2);
```

```
451 cutted_shifted_filt_SAMPLEfreq=cutted_shifted_filt_SAMPLEfreq(
       shifted_filt_SAMPLEtime>0 & shifted_filt_SAMPLEtime<20);
452
453 figure
454 plot(cutted_shifted_filt_SAMPLEtime,cutted_shifted_filt_SAMPLEfreq
       )
455 Gradient construction: run if HPLC with Gradient
456 GRADIENT.startMEOH=0.111;
457
458 %%%%%%%%%%%%%%%%%% y=mx+b
459 GRADIENT.m1=5.2952;
460 GRADIENT.m2=3.7;
461 GRADIENT.m3=11.1;
462
463 GRADIENT.t1=8.4524;
464 GRADIENT.t2=26;
465 GRADIENT.t3=-77.6;
466
467 %-------input sample concentrations in H2O and MeOH
468
469 GRADIENT.sample_meoh=300;
470 GRADIENT.sample_h2o=300;
471
472 gradientcomposition=zeros(length(cutted_shifted_filt_calibtime),1)
       ;
473 gradientcomposition(cutted_shifted_filt_calibtime<=0.5)= GRADIENT.
       startMEOH;
474 gradientcomposition(cutted_shifted_filt_calibtime>0.5 &
       cutted_shifted_filt_calibtime<=11)=(
       cutted_shifted_filt_calibtime(cutted_shifted_filt_calibtime>0.5
        & cutted_shifted_filt_calibtime<=11).* GRADIENT.m1 + GRADIENT.
       t1)/100;
475 gradientcomposition(cutted_shifted_filt_calibtime>11 &
       cutted_shifted_filt_calibtime<=14)=(
```

```
    cutted_shifted_filt_calibtime(cutted_shifted_filt_calibtime>11
    & cutted_shifted_filt_calibtime<=14).* GRADIENT.m2 + GRADIENT.
    t2)/100;
476 gradientcomposition(cutted_shifted_filt_calibtime>14 &
    cutted_shifted_filt_calibtime<=16) = (
    cutted_shifted_filt_calibtime(cutted_shifted_filt_calibtime>14
    & cutted_shifted_filt_calibtime<=16).* GRADIENT.m3 + GRADIENT.
    t3)./100;
477 gradientcomposition(cutted_shifted_filt_calibtime>16) = 1;
478
479 plot(cutted_shifted_filt_calibtime,gradientcomposition)
480 figure
481 yyaxis left
482 plot(cutted_shifted_filt_calibtime,gradientcomposition.*90)
483 ylim([0 100])
484
485 yyaxis right
486 plot(CaliDF(:,1), CaliDF(:,2));
487
488 legend('Solvent Gradient','Calibration \DeltaF','Location',"south
    ")
489 xlim([0 20])
490 concentration_sprayed=ones(length(cutted_shifted_filt_calibtime)
    ,1);
491
492 concentration_sprayed=gradientcomposition.*GRADIENT.sample_meoh +
    (1-gradientcomposition).* GRADIENT.sample_h2o;
493
494 figure
495 plot(cutted_shifted_filt_calibtime,concentration_sprayed)
496 Calculation of sprayed concentration
497
498 Isocratic: Run if isocratic, input the solvent composition of MeOH
499
```

```
500 %  Isocratic!!+++++++++calculation of sprayed conc.
501 %%% deactive  if with Gradient
502 % GRADIENT.sample_meoh=290.6055516;
503 % GRADIENT.sample_h2o=290.2358244;
504 %
505 % gradient_HPLC=0.3333;
506 %
507 % concentration_sprayed=GRADIENT.sample_meoh.*gradient_HPLC+
       GRADIENT.sample_h2o.*(1-gradient_HPLC);
508 sample concentration calculated
509 if length(cutted_shifted_filt_calibfreq)< length(
       cutted_shifted_filt_SAMPLEfreq)
510     cutted_shifted_filt_SAMPLEfreq=cutted_shifted_filt_SAMPLEfreq
          (1:length(cutted_shifted_filt_calibfreq));
511     cutted_shifted_filt_SAMPLEtime=cutted_shifted_filt_SAMPLEtime
          (1:length(cutted_shifted_filt_calibfreq));
512     concentration_sprayed=concentration_sprayed(1:length(
          cutted_shifted_filt_calibfreq));
513 else
514     cutted_shifted_filt_calibfreq=cutted_shifted_filt_calibfreq(1:
          length(cutted_shifted_filt_SAMPLEfreq));
515     cutted_shifted_filt_calibfreq=cutted_shifted_filt_calibfreq(1:
          length(cutted_shifted_filt_SAMPLEtime));
516     concentration_sprayed=concentration_sprayed(1:length(
          cutted_shifted_filt_SAMPLEfreq));
517 end
518
519 %--------------------sample concentration calculated
520
521 concentration_sample_passedColumn=cutted_shifted_filt_SAMPLEfreq./
       cutted_shifted_filt_calibfreq.*concentration_sprayed;
522
523 %/////////plot
524
```

```
525 %%%%%%Mass Calculation
526
527 para.MassInteEndtime=20;
528
529 validtimeframe=cutted_shifted_filt_SAMPLEtime>=0 &
       cutted_shifted_filt_SAMPLEtime<=para.MassInteEndtime &
       concentration_sample_passedColumn>=0;
530
531 SprayTotalMass=trapz(cutted_shifted_filt_SAMPLEtime(validtimeframe
       ),concentration_sample_passedColumn(validtimeframe))/2000
532 SprayTotalMass = 1.9785
533 TheoInjectedNOM=1.80;
534 MassBalance=SprayTotalMass/TheoInjectedNOM
535 FinalResult=table(cutted_shifted_filt_SAMPLEtime,
       concentration_sample_passedColumn);
536
537 % % % % % % % % % % % % % % % % % % % % export excel
538
539 FinalResult=table(cutted_shifted_filt_SAMPLEtime,
       concentration_sample_passedColumn);
540
541 FinalResult.Properties.VariableNames = {'Time_min','Mass Conc. /
       mg/L'};
542
543 TableFinalResult=FinalResult;
544 excelcolumn={'A2','C2','E2','G2','I2', 'K2', 'M2','O2','Q2', 'S2',
        'U2','W2', 'Y2'};
545
546 excelfilename = [para.Projecttitle 'TableFinalResult.xlsx'];
547 writetable(TableFinalResult,excelfilename,'Sheet',1,'Range',
       excelcolumn{1})
548
549 f = figure;
550 u = f.Units;
```

```
f.Units = 'normalized';

% % legend([p1 p3],{'First','Third'})

xlim([0,20])

g_1=gca;

plot_1=plot(cutted_shifted_filt_SAMPLEtime,
   concentration_sample_passedColumn, 'LineWidth',2,"Color",'k');
ylim ([-10,700])
xlim([0,20])
g_1.YColor='k';
xlabel('Time /min');
% legend('QCM')

Y1=ylabel('Mass /mg');   label
xlim_1=get(g_1,'xlim');
ylim_1=get(g_1,'ylim');

pos_2=get(g_1,'position');
g_2=axes('Position',pos_2,'Color','none','XTick',[],'YAxisLocation
   ','right');
Y2=ylabel('UV-Vis');   label
g_2.YColor='k';
hold on;
plot_2=plot(UVtime{1}, UVintensity{1},'-','LineWidth',1,"Color",'
   #0072BD');

xlim([0,20])
% ylim ([0,100])
pos_1=g_1.Position;
pos_1(1)=pos_1(1)-0.03;
pos_1(3)=pos_1(3)*0.9;
```

```
582
583 g_3=axes('Position',pos_1,'Color','none','XTick',[],'YTick',[]);
584 set([g_1;g_2;g_3],'position',pos_1);
585 hold on;
586
587 plot_3=plot(GradientX,GradientY,'-','LineWidth',1,"Color", '#
      D95319');
588 % legend('Gradient: MeOH %')
589
590 xlim([0,20])
591 ylim ([0,100])
592 pos_4=pos_1;
593 pos_4(3)=pos_4(3)+0.1;
594 g_4=axes('Position',pos_4,'Color','none','XTick',[],'YLim',[0
      100],'YTick',[0:10:100],'YAxisLocation','right');
595
596 Y3=ylabel('MeOH %');  label
597 legend([plot_1,plot_2, plot_3], {'QCM','220nm PestMix','Gradient:
      MeOH %'}, 'Location', "northwest","Box","off")
598
599 g_4.YColor='k';
600 grid off;
601 title(para.Projecttitle)
602 %%%%%%%%%%%%%%%%%%%%PestMix peak time
603 Peaktime=[];
604 Peaktime(1,:)=[6.258  6.883];
605 Peaktime(2,:)=[6.700  7.317];
606 Peaktime(3,:)=[6.983  7.575];
607 Peaktime(4,:)=[8.125  8.675];
608 Peaktime(5,:)=[9.183  9.750];
609 Peaktime(6,:)=[9.908  10.433];
610 Peaktime(7,:)=[10.125  10.783];
611 Peaktime(8,:)=[10.367  10.908];
612
```

```
613 for i=1:length(Peaktime)
614     Peak_Starttime=Peaktime(i,1);
615     Peak_Endtime=Peaktime(i,2);
616     Peaktimedata=cutted_shifted_filt_SAMPLEtime>=Peak_Starttime&
           cutted_shifted_filt_SAMPLEtime<=Peak_Endtime;
617     Spray_Peak_NOMMass(i)=trapz(cutted_shifted_filt_SAMPLEtime(
           Peaktimedata),concentration_sample_passedColumn(
           Peaktimedata))/2000;
618
619 end
620 Spray_Peak_NOMMass
621 RelNOM_Peak=Spray_Peak_NOMMass/SprayTotalMass*100
```

E Supporting Information to Chapter 5

E.1 Chemicals, Materials, and Standard Solutions

All chemicals and materials purchased commercially and used in this work are summarized in Table A.4.1. Additional information on the selected model analytes can be found in Table A.4.2.

Table A.4.1 List of reagents, solvents, and analytical standards.

Chemical	Purity/Grade	Supplier
2,6-dichlorobenzamide (BAM)	PESTANAL®, anal. st.	Sigma-Aldrich
atrazine (ATZ)	PESTANAL®, anal. st.	Sigma-Aldrich
azoxystrobin (AZOX)	PESTANAL®, anal. st.	Sigma-Aldrich
boscalid (BOSC)	PESTANAL®, anal. st.	Sigma-Aldrich
caffeine (CAF), USGS63		USGS
desethylatrazine (DEA)	PESTANAL®, anal. st.	Sigma-Aldrich
desisopropylatrazine (DIA)	PESTANAL®, anal. st.	Sigma-Aldrich
methanol	≥99%	Sigma-Aldrich
simazine (SIM)	PESTANAL®, anal. st.	Sigma-Aldrich
sodium chloride	≥99.5%	Fisher Scientific

anal. st. = analytical standard

Ultrapure H_2O (18.2 MΩ cm at 25 °C) was obtained from a Milli-Q® direct reference H_2O purification system from Merck MilliPore (Burlington, USA). Stock solutions of analytical standards (1 g/L) were prepared in CH_3OH and stored at -18 °C.

Table A.4.2 Additional information on the selected model analytes including the chemical formula, the isotope signature of the specific batch used, the molecular weight, the $\log K_{OW}$ and the charge at pH7.

Name	Formula	Isotope Signature	Molecular Weight [g/mol]	$\log K_{OW}$ [-]	Charge pH 7 [-]
BAM	$C_7H_5Cl_2NO$	n.a.	190.02	0.77	n
ATZ	$C_8H_{14}ClN_5$	-29,56	215.68	2.61	n
AZOX	$C_{22}H_{17}N_3O_5$	n.a.	403.4	2.50	n
BOSC	$C_{18}H_{12}Cl_2N_2O$	n.a.	343.2	2.96	n
CAF	$C_8H_{10}N_4O_2$	-1,17	194.19	-0.07	n
DEA	$C_6H_{10}ClN_5$	-29,39	187.63	1.51	n
DIA	$C_5H_8ClN_5$	-36,78	173.60	1.50	n
SIM	$C_7H_{12}ClN_5$	n.a.	201.66	2.18	n

n.a. = not available, n = neutral.

E.2 Extraction of Riverine NOM

Surface water samples (Wiesäckerbach, latitude 48.269009, longitude 11.667976, Garching, Germany) were filtered using glass microfiber filter membranes (1.2 µm particle retention, 47 mm diameter, Whatman, UK). NOM was extracted using Oasis HLB SPE material (Waters, 200 mg, 6 cc) and an automated SPE system (Smart Prep Extractor, Horizon Technology, USA). The extraction was performed using conventional SPE conditions at 5 mL/min. The Oasis HLB cartridges were dried overnight under vacuum and eluted using 5 mL of CH_3OH. The eluates were combined, reduced under a gentle stream of nitrogen at 30 °C, and stored at -18 °C. TOC analysis (TOC-L, Shimadzu, Japan) was used to determine the carbon content of the eluate. Elemental analysis (EURO-EA, HEKATech, Germany) was used to determine the percentage of carbon in the extracted NOM (see Table A.4.3).

Table A.4.3 Elemental analysis of NOM extracted from Wiesäckerbach using Oasis HLB.

Element	Content in %
Carbon	51.20
Hydrogen	6.56
Nitrogen	2.02
Sulfur	0.51
Oxygen	39.71

E.3 Compound Specific Isotope Analysis: Method Detection Limits, $\Delta\partial^{13}C$ Data, and Chromatogram Background Data

Table A.4.4 HPLC gradient used for purifying NOM sample prior to GC-c-IRMS measurement.

t/ min				
0	7.5	15	16.5	18
% of CH_3OH				
10	90	90	90	90

Table A.4.5 Method detection limits (nmol C) for GC-IRMS measurements determined according to the moving mean procedure with an uncertainty limit of ±0.5‰ and the corresponding analyte amplitude at m/z 44 in mV.

Analyte	MQL nmol C on column	Amplitude/ mV
ATZ	1	818 ± 24
DIA	2	1172 ± 156
DEA	3	2489 ± 78
CAF	4	3643 ± 71

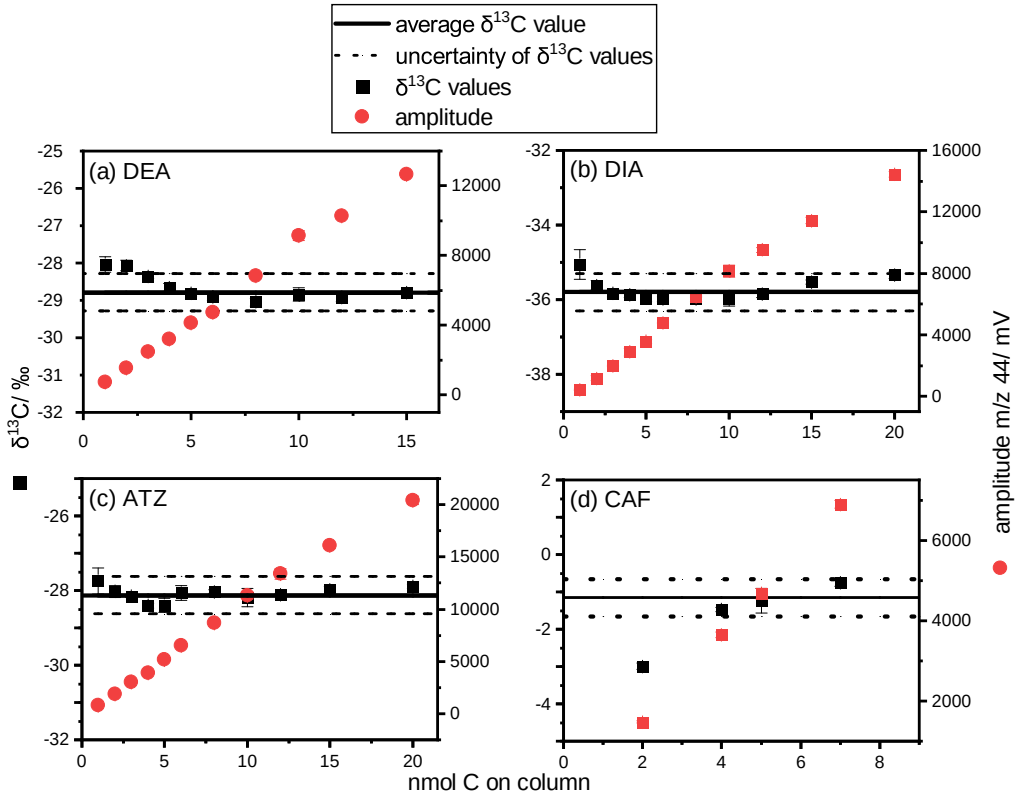

Figure A.4.1 Determination of Method detection limits (nmol C) for GC-IRMS measurements with an uncertainty limit of ±0.5‰ (dotted lines) for four analytes: (a) DEA, (b) DIA, (c) ATZ, and (d) CAF. The measured $\partial^{13}C$ values are shown in black, and the respective peak amplitude in red (m/z 44 in mV). Isotope values and amplitudes are arithmetic means of at least triplicate measurements with their respective standard deviation.

Table A.4.6 Determined ratio of background area to analyte area in the GC-IRMS chromatogram is shown as matrix fraction (f_{matrix}) in %. Using this ratio, theoretically determined isotope shifts were calculated ($\Delta\partial^{13}C_{calc}$ in ‰) using the isotope value of the analyte and NOM ($\partial^{13}C \approx 27\pm1$). The experimentally determined isotope shifts are shown for comparison as $\Delta\partial^{13}C_{exp}$ in ‰.

compound	NOM/analyte ratio	f_{matrix} [%]	$\Delta\partial^{13}C_{calc}$ [‰]	$\Delta\partial^{13}C_{exp}$ [‰]
DIA	10	17.8 ± 0.5	1.74 ± 0.05	0.43 ± 0.23
	20	26 ± 4	2.54 ± 0.39	0.58 ± 0.07
	50	42 ± 6	4.11 ± 0.59	0.99 ± 0.42
	100	54 ± 8	5.18 ± 0.78	1.33 ± 0.60
DEA	10	11.1 ± 0.1	0.26 ± 0.00	0.18 ± 0.20
	20	20 ± 1	0.47 ± 0.01	-0.04 ± 0.19
	50	36 ± 2	0.87 ± 0.05	-0.08 ± 0.45
	100	48 ± 7	1.15 ± 0.17	-0.44 ± 0.20
ATZ	10	9.5 ± 0.2	0.24 ± 0.00	0.46 ± 0.40
	20	15.6 ± 0.4	0.40 ± 0.01	0.34 ± 0.16
	50	33 ± 3	0.84 ± 0.07	0.40 ± 0.30
	100	49 ± 2	1.25 ± 0.05	0.42 ± 0.38
CAF	10	20 ± 1	-5.17 ± 0.23	-1.02 ± 0.44
	20	22 ± 1	-5.79 ± 0.16	-0.79 ± 0.09
	50	40 ± 4	-10.34 ± 1.03	-1.89 ± 0.23
	100	56 ± 11	-14.48 ± 2.84	-3.30 ± 0.78

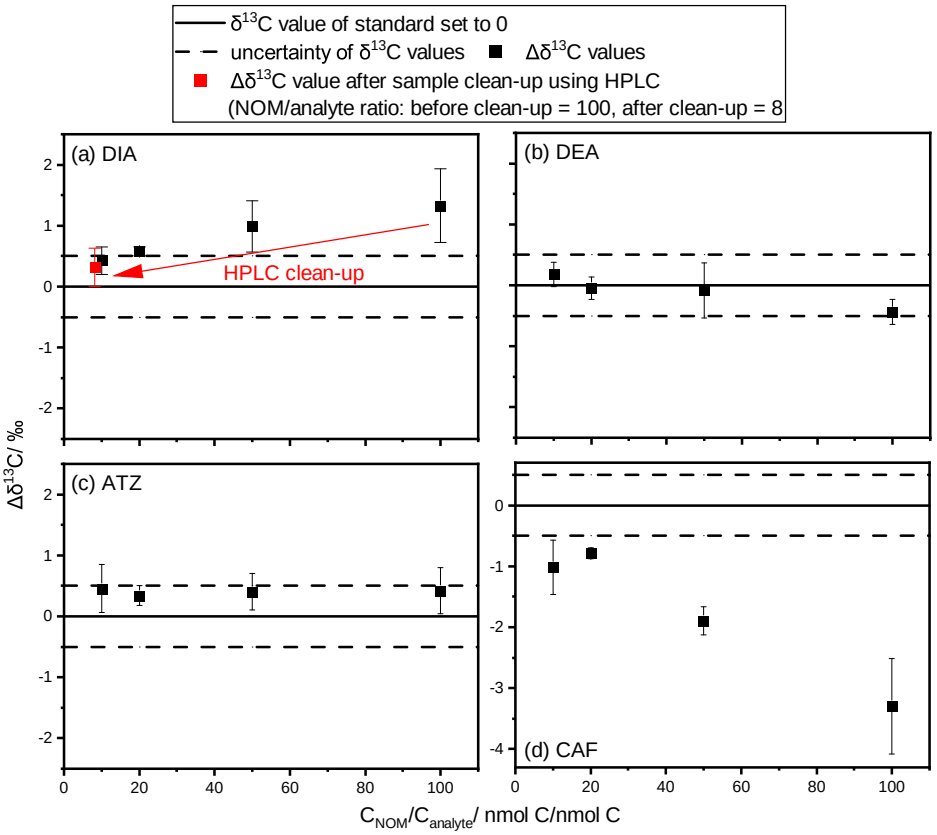

Figure A.4.2 Deviations of carbon isotope values ($\Delta\delta^{13}C$ in black) of (a) DIA, (b) DEA, (c) ATZ, and (d) CAF during the measurement of samples containing NOM in different amounts (NOM/analyte ratios: 10, 20, 50, 100) from the values of standard measurements. The dotted black lines show the uncertainty limit of carbon isotope analysis using GC-IRMS (±0.5‰). The error bars resemble the 95% confidence interval of triplicate measurements. The red data point shows a measurement after an HPLC clean-up using 10-60-90 gradient and column 1 of a sample containing NOM/analyte ratio 100 with an expected final NOM/analyte ratio of 8 after the clean-up.

E.4 Details on HPLC Gradients and QCM Dry Mass Sensing Results

Table A.4.7 22 HPLC gradients used to optimize separation of analytes and NOM on XTerra RP18. Mobile phase consists of methanol and water.

t/ min				
0	7.5	15	16.5	18
% of methanol				
10	30	60	90	90
10	30	70	90	90
10	30	80	90	90
10	30	90	90	90
10	40	60	90	90
10	40	70	90	90
10	40	80	90	90
10	40	90	90	90
10	50	60	90	90
10	50	70	90	90
10	50	80	90	90
10	50	90	90	90
10	60	60	90	90
10	60	70	90	90
10	60	80	90	90
10	60	90	90	90
10	70	70	90	90
10	70	80	90	90
10	70	90	90	90
10	80	80	90	90
10	80	90	90	90
10	90	90	90	90

Table A.4.8 7 HPLC gradients used to optimize separation of analytes and NOM on Orbit 100 C8. Mobile phase consists of methanol and water.

t/ min				
0	7.5	15	16.5	18
% of methanol				
10	30	60	90	90
10	40	80	90	90
10	50	60	90	90
10	60	70	90	90
10	70	90	90	90
10	80	90	90	90
10	90	90	90	90

Table A.4.9 Theoretical plate number for gradient 10-70-90.

	CAF	BAM	DIA	DEA	SIM	ATZ	AZOX	BOSC
XTerra RP18	822	800	2061	5639	11294	13795	28775	27699
Orbit 100 C8	10384	10605	15990	28947	41653	49415	50835	54224

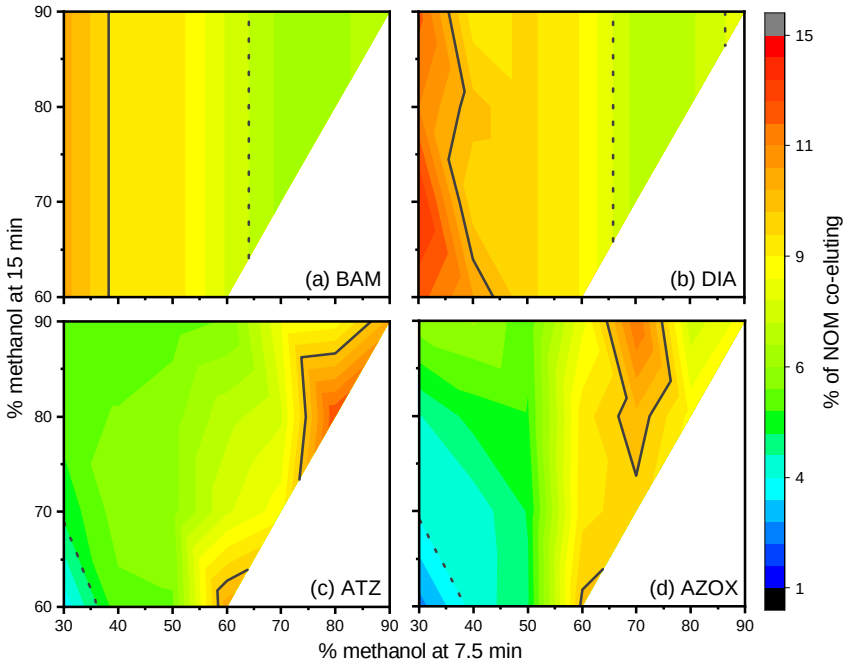

Figure A.4.3 The NOM co-elution in % on XTerra RP18 column is plotted for the 22 different gradients for 4 analytes ((a): BAM, (b): DIA, (c): ATZ, (d): AZOX). The x-axis represents the % of methanol at minute 7.5 during the HPLC clean-up and the y-axis % of methanol at minute 15.

Table A.4.10 NOM co-elution in % shown for 22 HPLC gradients on XTerra RP18. Gradient: first number represents % of methanol at min 0, second number at min 7.5, and third number at min 15.

Gradient	CAF	BAM	DIA	DEA
10-30-60	14.8 ± 0.8	10.2 ± 0.8	11.7	10.6
10-30-70	14.8 ± 0.8	10.2 ± 0.8	12.6	9.8
10-30-80	14.8 ± 0.8	10.2 ± 0.8	11.0	8.9
10-30-90	14.8 ± 0.8	10.2 ± 0.8	11.7	8.6
10-40-60	12.3 ± 1.0	8.7 ± 0.7	10.5	10.2
10-40-70	12.3 ± 1.0	8.7 ± 0.7	9.2	9.6
10-40-80	12.3 ± 1.0	8.7 ± 0.7	9.7 ± 0.3	10.5 ± 0.9
10-40-90	12.3 ± 1.0	8.7 ± 0.7	8.8	9.3
10-50-60	11.3 ± 0.7	8.8 ± 0.7	9.1 ± 0.8	10.9 ± 0.5
10-50-70	11.3 ± 0.7	8.8 ± 0.7	9.1 ± 0.8	10.3
10-50-80	11.3 ± 0.7	8.8 ± 0.7	9.1 ± 0.8	10.2
10-50-90	11.3 ± 0.7	8.8 ± 0.7	9.1 ± 0.8	8.7
10-60-60	8.2 ± 0.1	7.5 ± 0.2	8.5 ± 1.1	11.0
10-60-70	8.2 ± 0.1	7.5 ± 0.2	8.5 ± 1.1	11.6
10-60-80	8.2 ± 0.1	7.5 ± 0.2	8.5 ± 1.1	10.4
10-60-90	8.2 ± 0.1	7.5 ± 0.2	8.5 ± 1.1	10.3
10-70-70	8.0 ± 0.8	6.5 ± 0.6	6.8 ± 0.8	9.7
10-70-80	8.0 ± 0.8	6.5 ± 0.6	6.8 ± 0.8	9.2
10-70-90	8.0 ± 0.8	6.5 ± 0.6	6.8 ± 0.8	8.6
10-80-80	8.0 ± 0.5	6.4 ± 0.5	6.9 ± 0.6	8.7 ± 0.9
10-80-90	8.0 ± 0.5	6.4 ± 0.5	6.9 ± 0.6	8.7 ± 0.9
10-90-90	8.6	6.8	7.8	7.2

Table A.4.11 NOM co-elution in % shown for 22 HPLC gradients on XTerra RP18. Gradient: first number represents % of methanol at min 0, second number at min 7.5, and third number at min 15.

Gradient	SIM	ATZ	AZOX	BOSC
10-30-60	6.6	3.2	2.3	3.2
10-30-70	6.5	4.6	3.6	3.4
10-30-80	7.4	5.2	4.0	2.8
10-30-90	5.3	5.0	5.8	4.6
10-40-60	8.0	5.3	3.7	2.0
10-40-70	7.6	5.8	3.7	2.6
10-40-80	6.5 ± 0.6	5.6 ± 0.6	4.7 ± 0.3	3.8 ± 0.3
10-40-90	6.2	5.0	6.1	5.7
10-50-60	7.2 ± 0.7	5.4 ± 0.4	4.4 ± 0.8	2.4 ± 0.4
10-50-70	8.1	5.8	4.5	2.0
10-50-80	8.1	5.8	5.0	2.7
10-50-90	7.8	5.3	5.2	3.3
10-60-60	11.6	10.3	9.6	6.1
10-60-70	9.3	7.4	8.8	4.3
10-60-80	7.9	6.8	8.8	5.9
10-60-90	7.3	5.6	7.9	5.8
10-70-70	10.0	8.3	9.3	6.9
10-70-80	8.5	7.4	9.9	7.4
10-70-90	8.4	8.0	11.5	8.7
10-80-80	10.9	12.0	8.3	7.7
10-80-90	9.6 ± 0.4	8.2 ± 0.5	7.2 ± 0.6	6.6 ± 0.7
10-90-90	8.3	10.2	8.2	7.6

Table A.4.12 NOM co-elution in % shown for 7 HPLC gradients on Orbit 100 C8. Gradient: first number represents % of methanol at min 0, second number at min 7.5, and third number at min 15.

Gradient	CAF	BAM	DIA	DEA
10-30-60	7.4	7.5	8.8	6.9
10-40-80	5.0	6.0	5.7	7.2
10-50-60	4.5	6.3	7.2	13.2
10-60-70	4.6	6.0	6.5	7.7
10-70-90	4.7	5.5	5.3	7.6
10-80-90	3.2	4.6	5.1	7.0
10-90-90	4.9	4.9	4.7	7.9

Table A.4.13 NOM co-elution in % shown for 7 HPLC gradients on Orbit 100 C8. Gradient: first number represents % of methanol at min 0, second number at min 7.5, and third number at min 15.

Gradient	SIM	ATZ	AZOX	BOSC
10-30-60	3.6	2.9	2.7	1.9
10-40-80	6.3	5.1	3.5	2.7
10-50-60	8.9	2.3	0.6	0.2
10-60-70	10.0	6.8	2.5	1.7
10-70-90	8.0	6.0	10.4	6.8
10-80-90	8.1	6.9	8.3	6.6
10-90-90	9.0	8.2	7.6	5.9

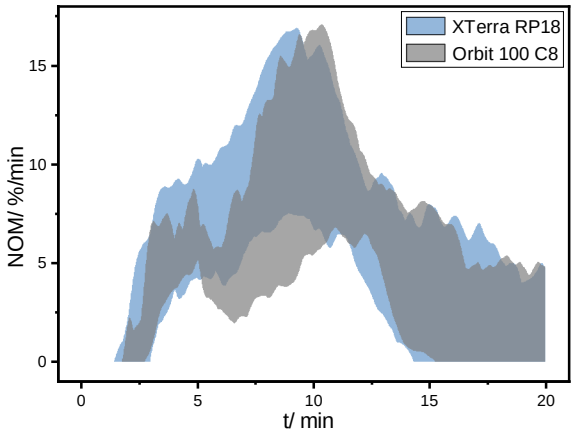

Figure A.4.4 Comparison of NOM retention on XTerra RP18 (blue) and Orbit 100 C8 (grey). The bands resemble all measured NOM values (in %/min) between the maximal and the minimal value determined for 22 gradients in case of column 1 (XTerra RP18 Column, 150×3.0 mm, 3.5 µm, pore size 125 Å) and 7 gradients in case of column 2 (Orbit 100 C8 Column, 150×3.0 mm, 3.5 µm, pore size 100 Å).

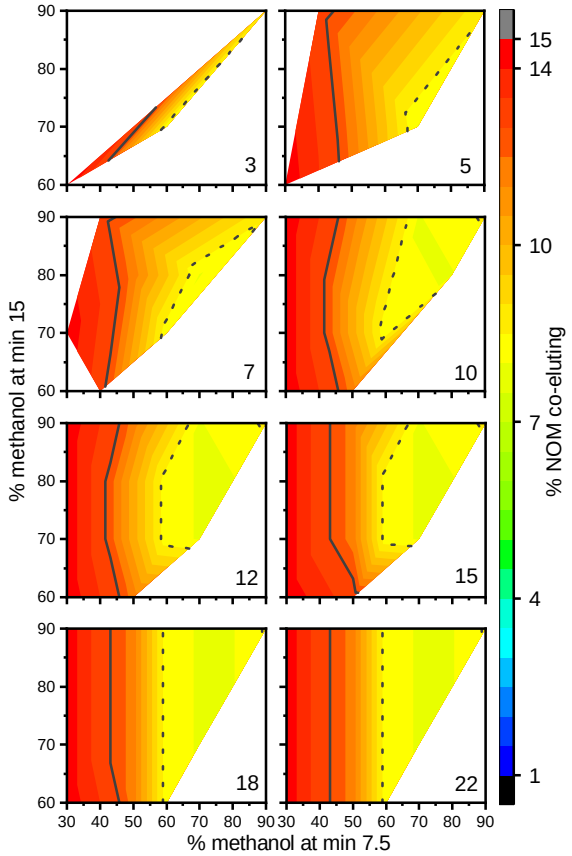

Figure A.4.5 Gradient screening of CAF using 3, 5, 7, 10, 12, 15, 18, or 22 different gradients on XTerra RP18.

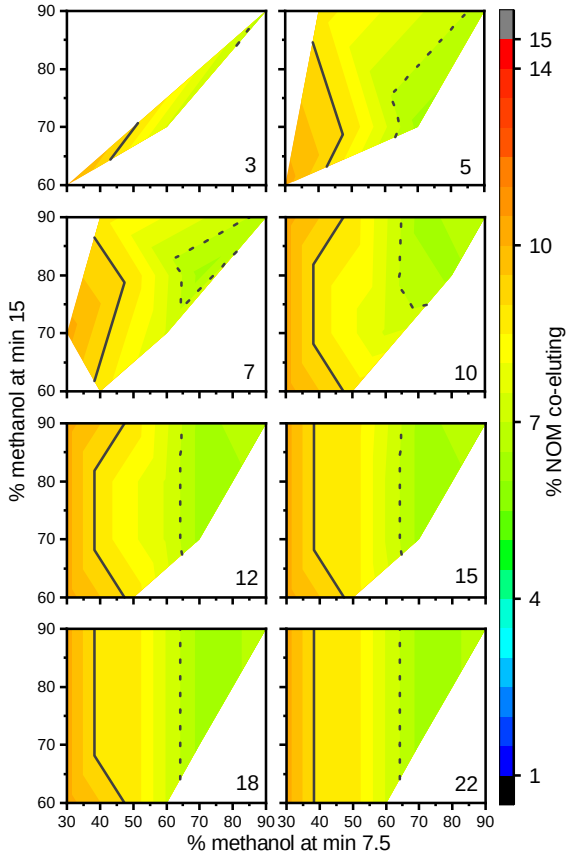

Figure A.4.6 Gradient screening of BAM using 3, 5, 7, 10, 12, 15, 18, or 22 different gradients on XTerra RP18.

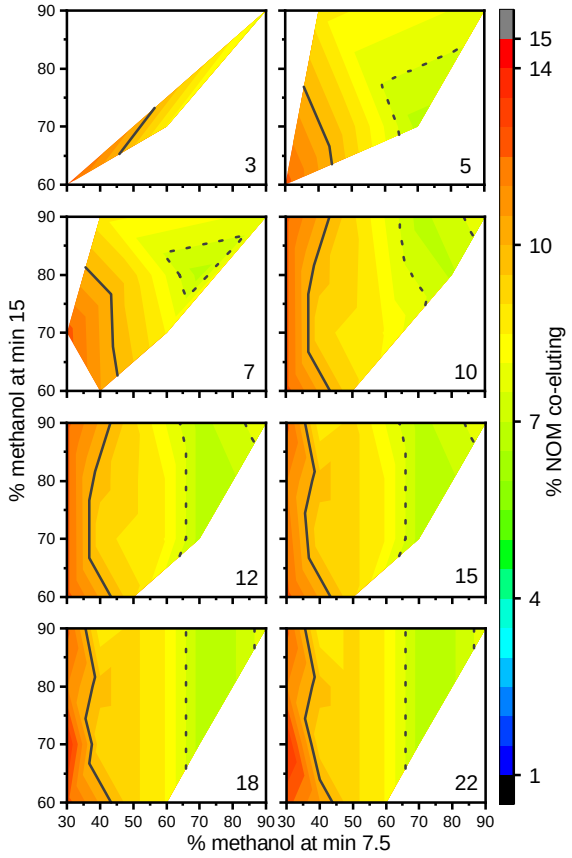

Figure A.4.7 Gradient screening of DIA using 3, 5, 7, 10, 12, 15, 18, or 22 different gradients on XTerra RP18.

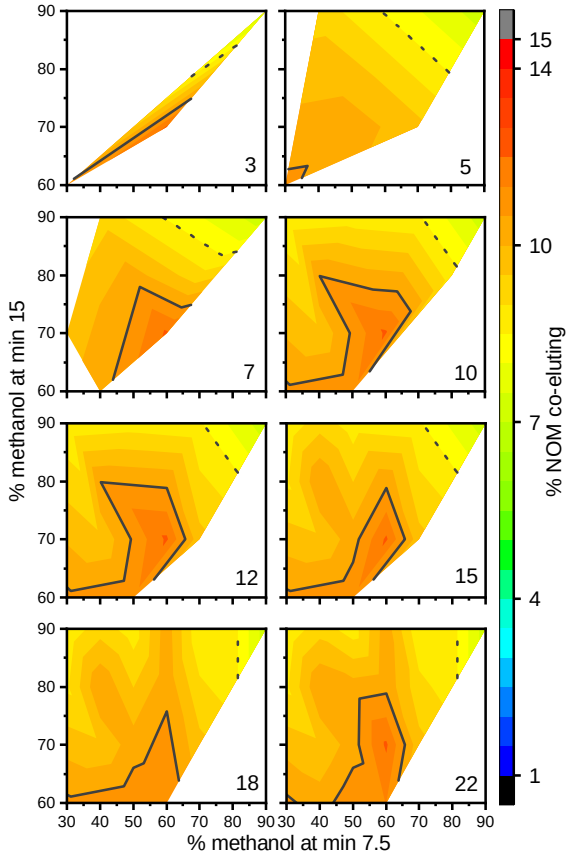

Figure A.4.8 Gradient screening of DEA using 3, 5, 7, 10, 12, 15, 18, or 22 different gradients on XTerra RP18.

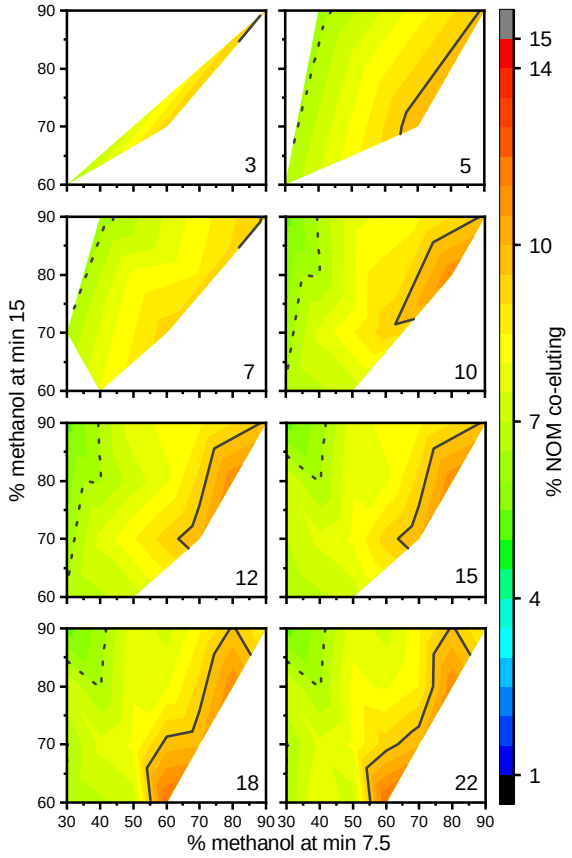

Figure A.4.9 Gradient screening of SIM using 3, 5, 7, 10, 12, 15, 18, or 22 different gradients on XTerra RP18.

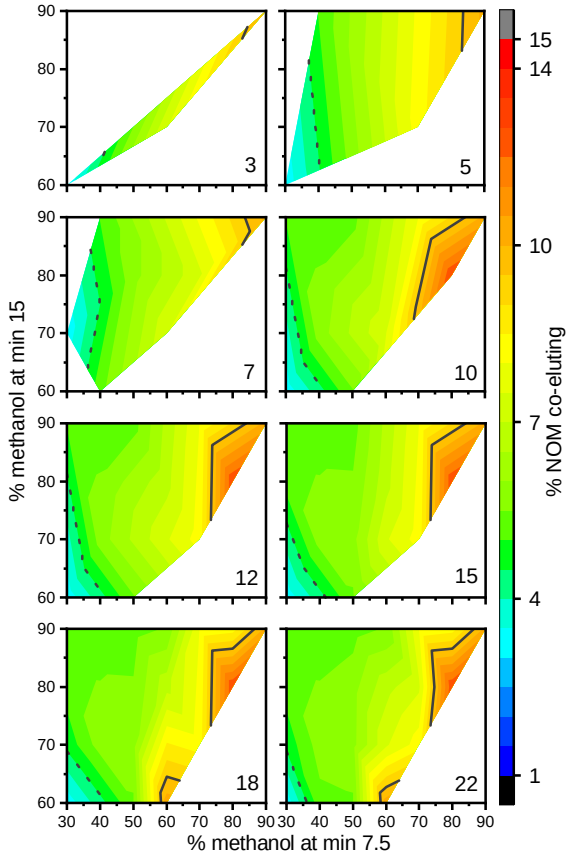

Figure A.4.10 Gradient screening of ATZ using 3, 5, 7, 10, 12, 15, 18, or 22 different gradients on XTerra RP18.

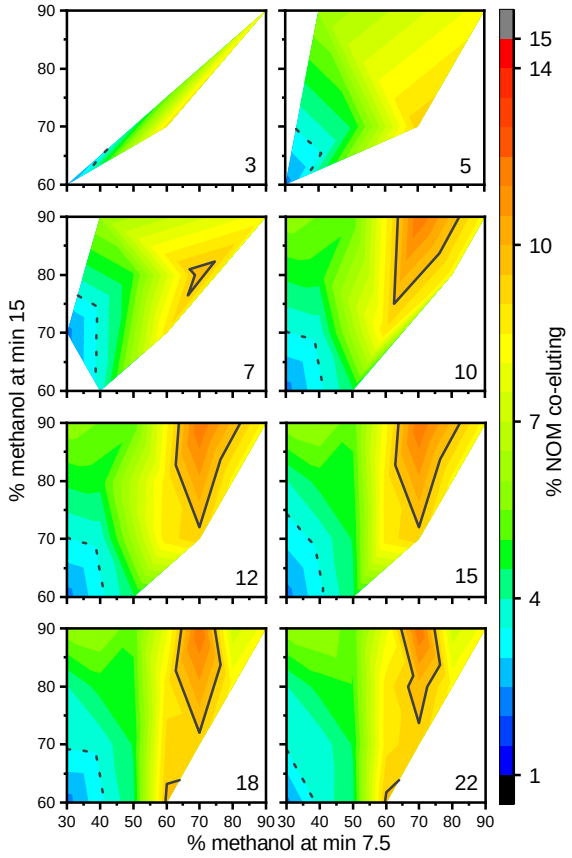

Figure A.4.11 Gradient screening of AZOX using 3, 5, 7, 10, 12, 15, 18, or 22 different gradients on XTerra RP18.

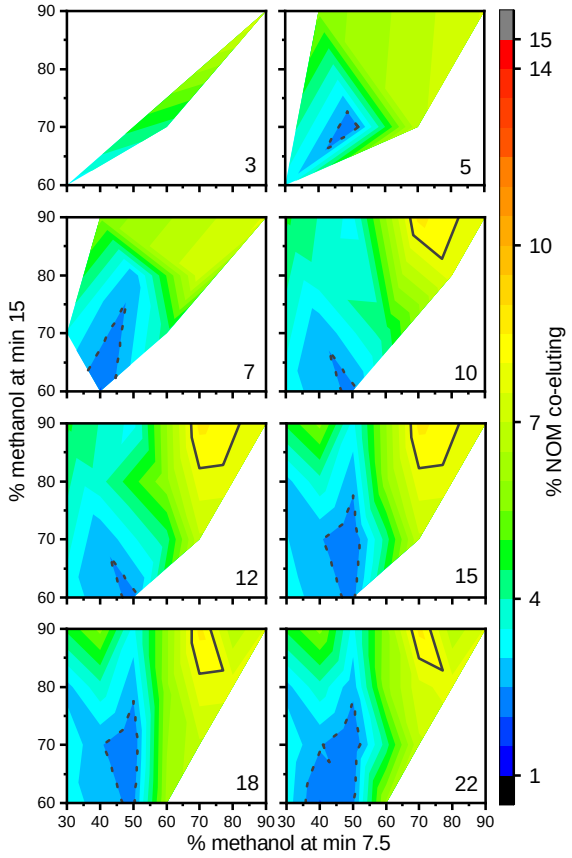

Figure A.4.12 Gradient screening of BOSC using 3, 5, 7, 10, 12, 15, 18, or 22 different gradients on XTerra RP18.

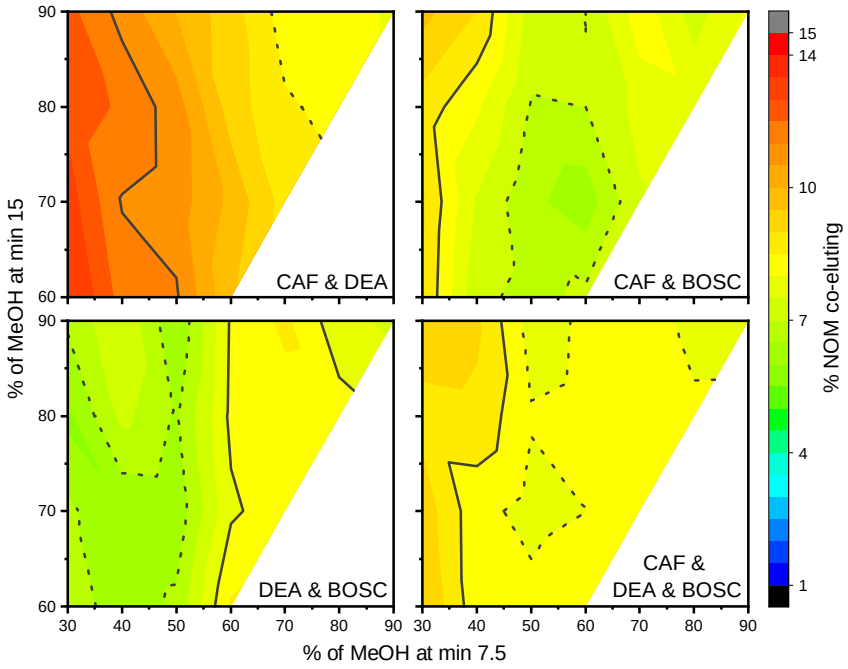

Figure A.4.13 NOM co-elution average for HPLC purification on XTerra RP18 of two or three compounds (early eluting: CAF, middle eluting: DEA, late eluting: BOSC).

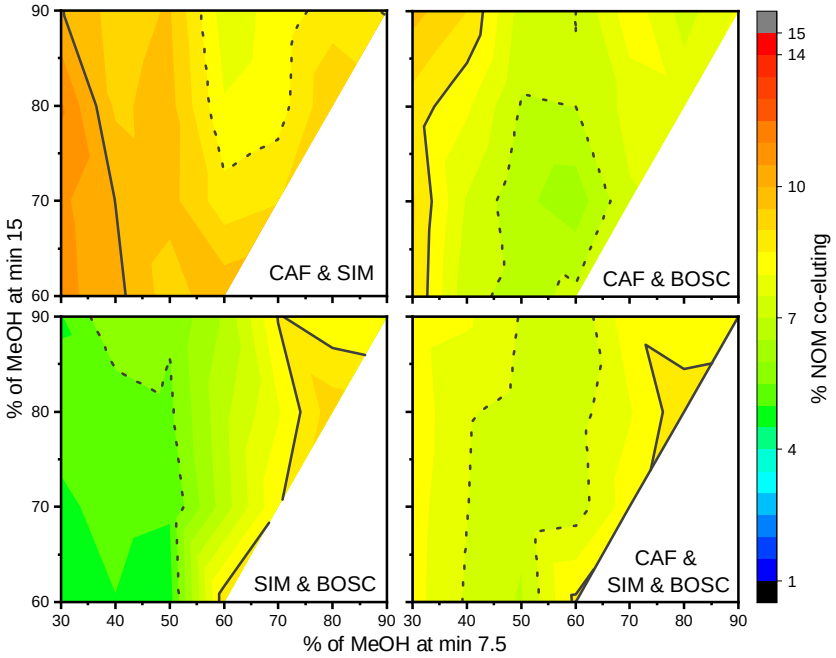

Figure A.4.14 NOM co-elution average for HPLC purification on XTerra RP18 of two or three compounds (early eluting: CAF, middle eluting: SIM, late eluting: BOSC).

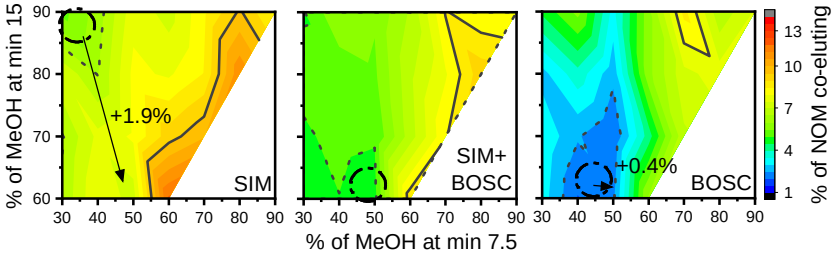

Figure A.4.15 Gradient screening for the individual compounds SIM and BOSC and their NOM co-elution average for HPLC purification on XTerra RP18 of both compounds at the same time (SIM+BOSC). The optimal gradient with the lowest NOM co-elution is encircled both for the individual compound purification (SIM, BOSC, gradient$_i$) and multiple compound purification (SIM+BOSC, gradient$_m$). The arrows show the difference between the optimal gradient$_i$ and the optimal gradient$_m$, the number next to the arrows the difference of NOM co-elution in % between gradient$_i$ and gradient$_m$.

Table A.4.14 Minimal NOM co-elution on XTerra RP18 column dependent on the number of gradients screened (from 3 to 22 gradients). All gradient mixes include convex, concave, and linear gradients. The number of gradients that is sufficient to find the optimal conditions within a precision of 1% is marked bold.

Number of Gradients	CAF	BAM	DIA	DEA
3	**8.2**	**6.8**	7.8	**7.2**
5	8.0	6.4	**6.8**	7.2
7	8.0	6.4	6.8	7.2
10	8.0	6.4	6.8	7.2
12	8.0	6.4	6.8	7.2
15	8.0	6.4	6.8	7.2
18	8.0	6.4	6.8	7.2
22	8.0	6.4	6.8	7.2

Table A.4.15 Minimal NOM co-elution on XTerra RP18 column dependent on the number of gradients screened (from 3 to 22 gradients). All gradient mixes include convex, concave, and linear gradients. The number of gradients that is sufficient to find the optimal conditions within a precision of 1% is marked bold.

Number of Gradients	SIM	ATZ	AZOX	BOSC
3	6.6	**3.2**	**2.3**	3.2
5	**6.2**	3.2	2.3	**2.0**
7	6.2	3.2	2.3	2.0
10	5.3	3.2	2.3	2.4
12	5.3	3.2	2.3	2.4
15	5.3	3.2	2.3	2.0
18	5.3	3.2	2.3	2.0
22	5.3	3.2	2.3	2.0

Table A.4.16 Analyte recovery in % during HPLC purification.

DIA	DEA	ATZ	BOSC
91.4±4.8	86.2±0.1	84.9±3.1	89.2±4.3

Table A.4.17 Higher NOM co-extraction during an optimized multi compound HPLC purification on XTerra RP18 in comparison to the optimized HPLC purification for a single compound is shown as optimization loss in % NOM (loss/ %). The different compounds are classified into early, middle, and late eluting.

compound			loss/%		
early	middle	late	early	middle	late
CAF	DEA		0.6	0	
CAF	SIM		0.2	2.0	
BAM	DEA		0.5	0	
BAM	SIM		1.1	2.0	
CAF		ATZ	0.2		2.4
CAF		AZOX	0		4.9
CAF		BOSC	0.2		2.3
BAM		ATZ	1.1		2.4
BAM		AZOX	2.4		1.4
BAM		BOSC	2.4		0
	DEA	ATZ		1.4	1.9
	DEA	AZOX		1.7	1.7
	DEA	BOSC		1.7	0.9
	SIM	ATZ		1.3	0
	SIM	AZOX		1.3	0
	SIM	BOSC		1.9	0.4
BAM	DEA	ATZ	0	1.4	4.8
BAM	DEA	ATZ	2.4	2.1	1.8
BAM	DEA	ATZ	2.5	1.5	2.1
BAM	DEA	AZOX	2.4	2.4	1.4
BAM	DEA	AZOX	2.5	1.5	2.9
BAM	DEA	AZOX	0.5	0	5.9
BAM	SIM	ATZ	3.9	1.3	0
BAM	SIM	ATZ	2.4	0.9	1.8
BAM	SIM	ATZ	1.1	2.0	2.4
BAM	SIM	AZOX	3.9	1.3	0
BAM	SIM	AZOX	2.4	1.2	2.4
CAF	DEA	BOSC	3.3	1.5	1.4
CAF	DEA	BOSC	0	1.5	4.7
CAF	DEA	BOSC	3.3	3.1	0
CAF	SIM	BOSC	3.3	1.9	0.4
CAF	SIM	BOSC	0.2	2.0	3.9

Table A.4.18 Higher NOM co-extraction during an optimized multi compound HPLC purification on Orbit 100 C8 in comparison to the optimized HPLC purification for a single compound is shown as optimization loss in % NOM (loss/ %). The different compounds are classified into early, middle, and late eluting.

compound			loss/%		
early	middle	late	early	middle	late
CAF	DEA		0	0.1	
CAF	SIM		4.3	0	
BAM	DEA		0	0.1	
BAM	SIM		2.9	0	
CAF		ATZ	1.3		0
CAF		AZOX	1.3		0
CAF		BOSC	1.3		0
BAM		ATZ	1.7		0
BAM		AZOX	1.7		0
BAM		BOSC	1.7		0
	DEA	ATZ		0	0.6
	DEA	AZOX		0	2.1
	DEA	BOSC		0	1.8
	SIM	ATZ		0	0.6
	SIM	AZOX		0	2.1
	SIM	BOSC		0	1.8
BAM	DEA	ATZ	2.9	0	0.6
BAM	DEA	AZOX	2.9	0	2.1
BAM	DEA	AZOX	1.4	0.8	1.9
BAM	SIM	ATZ	2.9	0	0.6
BAM	SIM	AZOX	2.9	0	2.1
CAF	DEA	BOSC	1.5	0.8	1.5
CAF	SIM	BOSC	4.3	0	1.8

Table A.4.19 Overview of columns used in the field of CSIA during HPLC purification of compounds present in different sample matrices.

publication	compounds	matrix	column
Schreglmann et al.[68]	pesticides	water	ODS (30) Ultracarb
Piper et al.[28]	steroids	urine	LiChrospher 100 RP18
Melsbach et al.[66]	pesticides	water	Synergi Hydro-RP
Tripp et al.[75]	amino acids	bones	Waters Symmetry or Supelco Discovery HS F5
Lalonde et al.[76]	steroids	urine	Zorbax Eclipse XDB Phenyl column and Zorbax Eclipse XDB-C18 columns
Swalethorp et al.[77]	amino acids	fish	Primesep A
Yun et al.[78]	pesticides	plants	Zorbax Eclips XDB C18
Cheng et al.[79]	hexabromocyclododecane	no	Zorbax SB-C18
Shrivastava et al.[842]	steroids	urine	LiChroCART
Akamatsu et al.[262]	glucose	sake	VG50-4E
Murata et al.[843]	aroma compounds	green tea	CAPCELLPAK ODS
Zhu et al.[844]	decabrominated diphenyl ether	no	Zorbax Eclipse Plus-C18
Iannella et al.[845]	prednisolone or prednisone	pharmaceutical formulation	ACE® C18
Saccon et al.[846]	phenols	air	Supelco Supelcosil^{TM} LC-18
Broek et al.[847]	amino acids	proteinaceous samples	SiELC Primesep A
Drenzek et al.[524]	PCBs	bacteria culture	Chrompack Chromsep Omnipher 5 C18

Abbreviations

Γ	Bandwidth of the resonance
γ-MAPS	γ-Methacryloxypropyltrimethoxysilane
Δf	Resonance frequency change
AIBN	2,2'-Azobis(2-methylpropionitrile
ATZ	Atrazine
AZOX	Azoxystrobin
BAM	2,6-dichlorobenzamide
BOSC	Boscalid
BTEX	Benzene, toluene, ethylbenzene, and xylene
C	Mass sensitivity coefficient
CAD	Charged aerosol detector
CAF	Caffeine
COF	Covalent organic framework
CSIA	Compound-specific isotope analysis
D	Dissipation
DAD	Diode array detector
DCM	Dichloromethane
DEA	Desethylatrazine
D_{hyd}	Hydraulic diameter
DIA	Desisopropylatrazine

EDX Energy dispersive X-ray mapping

EGDMA Ethylene glycol dimethacrylate

ELSD Evaporative light-scattering detector

f_0 Fundamental frequency

FTIR Fourier-transform infrared

GC-c-IRMS Gas chromatography combustion isotope ratio mass spectrometry

HCH Hexachlorocyclohexane

HPLC High-performance liquid chromatography

IAC Immunoaffinity chromatography

IEC Ion-exchange chromatography

LLE Liquid-liquid extraction

LOD Limits of detection

LOQ Limits of quantification

MAA Methacrylic acid

ME% Matrix effect in percent

MeOH Methanol

MIPs Molecularly imprinted polymers

MISPE Molecularly imprinted solid phase extraction

MOF Metal organic framework

MQL Method detection limits

NOM Natural organic matter

NVP N-vinylpyrrolidone

PAH Polycyclic aromatic hydrocarbon

PCB Polychlorinated biphenyl

PCDD Polychlorinated dibenzodioxins

PDMS Polydimethylsiloxane

Prop Propargite

PS-DVB Polystyrene-divinylbenzene

P&T Purge and trap

PTFE Polytetrafluorethylene

QCM Quartz crystal microbalance

QCM-D QCM with dissipation measurement

QCM-R QCM with resistance measurement

RAFT Reversible addition-fragmentation chain-transfer

RP Reversed-phase

SEM Scanning electron microscopy imaging

SIM Simazine

SPE Solid phase extraction

TMSD Trimethylsilyl diazomethane

TOC Total organic carbon

UV/Vis UV-Visible spectrometry

Bibliography

[1] T. C. Schmidt, L. Zwank, M. Elsner, M. Berg, R. U. Meckenstock, S. B. Haderlein, Compound-specific stable isotope analysis of organic contaminants in natural environments: a critical review of the state of the art, prospects, and future challenges, Analytical and Bioanalytical Chemistry 378 (2004) 283–300.

[2] M. Elsner, M. A. Jochmann, T. B. Hofstetter, D. Hunkeler, A. Bernstein, T. C. Schmidt, A. Schimmelmann, Current challenges in compound-specific stable isotope analysis of environmental organic contaminants, Analytical and Bioanalytical Chemistry 403 (2012) 2471–2491.

[3] M. Elsner, G. Imfeld, Compound-specific isotope analysis (csia) of micropollutants in the environment - current developments and future challenges., Current opinion in biotechnology 41 (2016) 60–72.

[4] M. Blessing, M. A. Jochmann, T. C. Schmidt, Pitfalls in compound-specific isotope analysis of environmental samples, Analytical and Bioanalytical Chemistry 390 (2008) 591–603.

[5] M. Blessing, N. Baran, A review on environmental isotope analysis of aquatic micropollutants: Recent advances, pitfalls and perspectives, TrAC Trends in Analytical Chemistry 157 (2022).

[6] C. Neubauer, K. Kantnerová, A. Lamothe, J. Savarino, A. Hilkert, D. Juchelka, K. Hinrichs, M. Elvert, V. B. Heuer, M. Elsner, R. Bakkour, M. Julien, M. Öztoprak, S. Schouten, S. Hattori, T. Dittmar, Discovering nature's fingerprints: Isotope ratio analysis on bioanalytical mass spectrometers., Journal of the American Society for Mass Spectrometry 34 (2023) 525–537.

[7] Z. Muccio, G. P. Jackson, Isotope ratio mass spectrometry., The Analyst 134 (2009) 213–222.

[8] A. F. Diefendorf, E. J. Freimuth, Extracting the most from terrestrial plant-derived n-alkyl lipids and their carbon isotopes from the sedimentary record: A review, Organic Geochemistry 103 (2017) 1–21.

[9] H. Liu, J. Nie, Y. Liu, S. A. Wadood, K. M. Rogers, Y. Yuan, R. Gan, A review of recent compound-specific isotope analysis studies applied to food authentication., Food chemistry 415 (2023).

[10] H. G. Close, Compound-specific isotope geochemistry in the ocean., Annual review of marine science 11 (2019) 27–56.

[11] S. Spahr, J. Bolotin, J. Schleucher, I. Ehlers, U. von Gunten, T. B. Hofstetter, Compound-specific carbon, nitrogen, and hydrogen isotope analysis of n-nitrosodimethylamine in aqueous solutions., Analytical chemistry 87 (2015) 2916–2924.

[12] N. Ivdra, A. Fischer, S. Herrero-Martín, T. Giunta, M. Bonifacie, H. H. Richnow, Carbon, hydrogen and chlorine stable isotope fingerprinting for forensic investigations of hexachlorocyclohexanes., Environmental science & technology 51 (2017) 446–454.

[13] T. Gilevska, M. Gehre, H. H. Richnow, Multidimensional isotope analysis of carbon, hydrogen and oxygen as tool for identification of the origin of ibuprofen., Journal of pharmaceutical and biomedical analysis 115 (2015) 410–417.

[14] D. Hunkeler, T. Laier, F. Breider, O. S. Jacobsen, Demonstrating a natural origin of chloroform in groundwater using stable carbon isotopes., Environmental science & technology 46 (2012) 6096–6101.

[15] D. Kaown, O. Shouakar-Stash, J. Yang, Y. Hyun, K. K. Lee, Identification of multiple sources of groundwater contamination by dual isotopes, Groundwater 52 (2014).

[16] R. S. Wijker, J. Bolotin, S. F. Nishino, J. C. Spain, T. B. Hofstetter, Using compound-specific isotope analysis to assess biodegradation of nitroaromatic explosives in the subsurface., Environmental science & technology 47 (2013) 6872–6883.

[17] M. P. Maier, C. Prasse, S. G. Pati, S. Nitsche, Z. Li, M. Radke, A. H. Meyer, T. B. Hofstetter, T. A. Ternes, M. Elsner, Exploring trends of c and n isotope fractionation to trace transformation reactions of diclofenac in natural and engineered systems., Environmental science & technology 50 (2016) 10933–10942.

[18] M. A. S. Ratti, S. Canonica, K. McNeill, J. Bolotin, T. B. Hofstetter, Isotope fractionation associated with the photochemical dechlorination of chloroanilines., Environmental science & technology 49 (2015) 9797–9806.

[19] A. Badin, M. M. Broholm, C. S. Jacobsen, J. Palau, P. Dennis, D. Hunkeler, Identification of abiotic and biotic reductive dechlorination in a chlorinated ethene plume after thermal source remediation by means of isotopic and molecular biology tools., Journal of contaminant hydrology 192 (2016) 1–19.

[20] E. Passeport, R. C. Landis, G. Lacrampe-Couloume, E. J. Lutz, E. E. Mack, K. A. West, S. A. Morgan, B. S. Lollar, Sediment monitored natural recovery evidenced by compound specific isotope analysis and high-resolution pore water sampling., Environmental science & technology 50 (2016) 12197–12204.

[21] W. Meier-Augenstein, Applied gas chromatography coupled to isotope ratio mass spectrometry., Journal of chromatography. A 842 (1999) 351–371.

[22] D. E. Matthews, J. M. Hayes, Isotope-ratio-monitoring gas chromatography-mass spectrometry, Analytical Chemistry 50 (1978) 1465–1473.

[23] A. Barrie, J. Bricout, J. Koziet, Gas chromatography—stable isotope ratio analysis at natural abundance levels, Journal of Mass Spectrometry 11 (1984) 583–588.

[24] J. T. Brenna, T. N. Corso, H. J. Tobias, R. J. Caimi, High-precision continuous-flow isotope ratio mass spectrometry., Mass spectrometry reviews 16 (1997) 227–258.

[25] M. Moini, F. P. Abramson, A moving belt device to couple high-performance liquid chromatography and chemical reaction interface mass spectrometry., Biological mass spectrometry 20 (1991) 308–312.

[26] O. Seki, T. Nakatsuka, H. Shibata, K. Kawamura, A compound-specific n-alkane δ13c and δd approach for assessing source and delivery processes of terrestrial organic matter within a forested watershed in northern japan, Geochimica et Cosmochimica Acta 74 (2010) 599–613.

[27] I. S. Castañeda, J. P. Werne, T. C. Johnson, T. R. Filley, Late quaternary vegetation history of southeast africa: The molecular isotopic record from lake malawi, Palaeogeography, Palaeoclimatology, Palaeoecology 275 (2009) 100–112.

[28] T. Piper, U. Mareck, H. Geyer, U. Flenker, M. Thevis, P. Platen, W. Schänzer, Determination of 13c/12c ratios of endogenous urinary steroids: method validation, reference population and application to doping control purposes., Rapid communications in mass spectrometry 22 (2008) 2161–2175.

[29] F. A. de Oliveira, A. Casilli, T. Piper, T. da Silva, C. A. da Silva, R. V. S. da Silva, M. A. D. Sasso, G. R. D. S. G. Salgueiro, M. C. Padilha, H. M. G. Pereira, M. Thevis, F. R. de Aquino Neto, Implementation and performance of the gas chromatography/combustion/isotope ratio mass spectrometry-based method for the confirmatory analysis of endogenous anabolic steroids during the rio de janeiro olympic and paralympic games 2016., Analytical chemistry 91 (2019) 11747–11756.

[30] T. B. Hofstetter, R. P. Schwarzenbach, S. M. Bernasconi, Assessing transformation processes of organic compounds using stable isotope fractionation., Environmental science & technology 42 (2008) 7737–7743.

[31] T. C. Schmidt, M. A. Jochmann, Origin and fate of organic compounds in water: characterization by compound-specific stable isotope analysis., Annual review of analytical chemistry 5 (2012) 133–155.

[32] M. Elsner, L. Zwank, D. Hunkeler, R. P. Schwarzenbach, A new concept linking observable stable isotope fractionation to transformation pathways of organic pollutants., Environmental science & technology 39 (2005) 6896–6916.

[33] T. B. Hofstetter, M. Berg, Analytical techniques for assessing transformation processes of organic contaminants by compound-specific stable isotope analyses, TrAC Trends in Analytical Chemistry 30 (2011) 618–627.

[34] D. Sciarrone, A. Schepis, M. Zoccali, P. Donato, F. Vita, D. M. T. Creti, A. Alpi, L. Mondello, Multidimensional gas chromatography coupled to combustion-isotope ratio mass spectrometry/quadrupole ms with a low-bleed ionic liquid secondary column for the authentication of truffles and products containing truffle., Analytical chemistry 90 (2018) 6610–6617.

[35] X. Zhang, D. Han, X. Chen, X. Zhao, J. Cheng, Y. Liu, Combined use of fatty acid profile and fatty acid δ13c fingerprinting for origin traceability of scallops (patinopecten yessoensis, chlamys farreri, and argopecten irradians)., Food chemistry 298 (2019).

[36] J. E. Spangenberg, N. Ogrinc, Authentication of vegetable oils by bulk and molecular carbon isotope analyses with emphasis on olive oil and pumpkin seed oil., Journal of agricultural and food chemistry 49 (2001) 1534–1540.

[37] A. L. Sessions, Isotope-ratio detection for gas chromatography., Journal of separation science 29 (2006) 1946–1961.

[38] M. Núñez, F. Borrull, E. Pocurull, N. Fontanals, Sample treatment for the determination of emerging organic contaminants in aquatic organisms, Trends in Analytical Chemistry 97 (2017) 136–145.

[39] M. P. Ricci, D. A. Merritt, K. H. Freeman, J. M. Hayes, Acquisition and processing of data for isotope-ratio-monitoring mass spectrometry., Organic geochemistry 21 (1994) 561–571.

[40] L. Ellis, A. L. Fincannon, Analytical improvements in irm-gc/ms analyses: Advanced techniques in tube furnace design and sample preparation, Organic Geochemistry 29 (1998) 1101–1117.

[41] K. J. Goodman, J. T. Brenna, Curve fitting for restoration of accuracy for overlapping peaks in gas chromatography/combustion isotope ratio mass spectrometry., Analytical chemistry 66 (1994) 1294–1301.

[42] J. Zrostlíková, J. Hajslová, J. Poustka, P. Begany, Alternative calibration approaches to compensate the effect of co-extracted matrix components in liquid chromatography-electrospray ionisation tandem mass spectrometry analysis of pesticide residues in plant materials., Journal of chromatography. A 973 (2002) 13–26.

[43] M. Vahl, A. Graven, R. K. Juhler, Analysis of chlormequat residues in grain using liquid chromatography-mass spectrometry (lc-ms/ms), Fresenius' Journal of Analytical Chemistry 361 (1998) 817–820.

[44] B. K. Choi, A. I. Gusev, D. M. Hercules, Postcolumn introduction of an internal standard for quantitative lc-ms analysis, Analytical Chemistry 71 (1999) 4107–4110.

[45] M. Gros, M. Petrovíc, D. Barceló, Development of a multi-residue analytical methodology based on liquid chromatography-tandem mass spectrometry (lc-ms/ms) for screening and trace level determination of pharmaceuticals in surface and wastewaters., Talanta 70 (2006) 678–690.

[46] M. Anastassiades, S. J. Lehotay, D. Stajnbaher, F. J. Schenck, Fast and easy multiresidue method employing acetonitrile extraction/partitioning and "dispersive solid-phase extraction" for the determination of pesticide residues in produce., Journal of AOAC International 86 (2003) 412–431.

[47] K. Maštovská, S. J. Lehotay, M. Anastassiades, Combination of analyte protectants to overcome matrix effects in routine gc analysis of pesticide residues in food matrixes., Analytical chemistry 77 (2005) 8129–8137.

[48] M. Sulyok, F. Berthiller, R. Krska, R. Schuhmacher, Development and validation of a liquid chromatography/tandem mass spectrometric method for the determination of 39 mycotoxins in wheat and maize., Rapid communications in mass spectrometry 20 (2006) 2649–2659.

[49] R. Bakkour, Molecularly-imprinted polymers for compound-specific isotope analysis of polar organic micropollutants in aquatic environments., in: Doctoral Thesis (No. 24753), 2018.

[50] D. Glöckler, C. Wabnitz, M. Elsner, R. Bakkour, Avoiding interferences in advance: Cyclodextrin polymers to enhance selectivity in extraction of organic micropollutants for carbon isotope analysis., Analytical chemistry 95 (2023) 7839–7848.

[51] H. Kawashima, M. Murakami, Measurement of the stable carbon isotope ratio of atmospheric volatile organic compounds using chromatography, combustion, and isotope ratio mass spectrometry coupled with thermal desorption, Atmospheric Environment 89 (2014) 140–147.

[52] H. J. Tobias, G. L. Sacks, Y. Zhang, J. T. Brenna, Comprehensive two-dimensional gas chromatography combustion isotope ratio mass spectrometry., Analytical chemistry 80 (2008) 8613–8621.

[53] H. J. Tobias, Y. Zhang, R. J. Auchus, J. T. Brenna, Detection of synthetic testosterone use by novel comprehensive two-dimensional gas chromatography combustion-isotope ratio mass spectrometry., Analytical chemistry 83 (2011) 7158–7165.

[54] J. Zimmermann, P. Wanner, D. Hunkeler, Compound-specific carbon isotope analysis of volatile organic compounds in complex soil extracts using purge and trap concentration coupled to heart-cutting two-dimensional gas chromatography-isotope ratio mass spectrometry., Journal of chromatography. A 1655 (2021).

[55] A. D. Brailsford, I. Gavrilović, R. Ansell, D. A. Cowan, A. T. Kicman, Two-dimensional gas chromatography with heart-cutting for isotope ratio mass spectrometry analysis of steroids in doping control., Drug testing and analysis 4 (2012) 962–969.

[56] R. Bakkour, J. Bolotin, B. Sellergren, T. B. Hofstetter, Molecularly imprinted polymers for compound-specific isotope analysis of polar organic micropollutants in aquatic environments., Analytical chemistry 90 (2018) 7292–7301.

[57] K. Kuntze, H. Eisenmann, H. H. Richnow, A. Fischer, Compound-specific stable isotope analysis (csia) for evaluating degradation of organic pollutants: An overview of field case studies, Anaerobic Utilization of Hydrocarbons, Oils, and Lipids (2019).

[58] A. Fischer, K. Theuerkorn, N. Stelzer, M. Gehre, M. Thullner, H. H. Richnow, Applicability of stable isotope fractionation analysis for the characterization of benzene biodegradation in a btex-contaminated aquifer., Environmental science & technology 41 (2007) 3689–3696.

[59] J. Palau, M. Marchesi, J. C. C. Chambon, R. Aravena, À. Canals, P. J. Binning, P. L. Bjerg, N. Otero, A. Soler, Multi-isotope (carbon and chlorine) analysis for fingerprinting and site characterization at a fractured bedrock aquifer contaminated by chlorinated ethenes., The Science of the total environment 475 (2014) 61–70.

[60] C. Aeppli, T. B. Hofstetter, H. I. F. Amaral, R. Kipfer, R. P. Schwarzenbach, M. Berg, Quantifying in situ transformation rates of chlorinated ethenes by combining compound-specific stable isotope analysis, groundwater dating, and carbon isotope mass balances., Environmental science & technology 44 (2010) 3705–3711.

[61] M. Elsner, G. L. Couloume, S. A. Mancini, L. Burns, B. S. Lollar, Carbon isotope analysis to evaluate nanoscale fe(o) treatment at a chlorohydrocarbon contaminated site, Groundwater Monitoring & Remediation 30 (2010).

[62] R. P. Schwarzenbach, B. I. Escher, K. Fenner, T. B. Hofstetter, C. A. Johnson, U. von Gunten, B. Wehrli, The challenge of micropollutants in aquatic systems, Science 313 (2006) 1072–1077.

[63] L. Zwank, M. Berg, T. C. Schmidt, S. B. Haderlein, Compound-specific carbon isotope analysis of volatile organic compounds in the low-microgram per liter range., Analytical chemistry 75 (2003) 5575–5583.

[64] M. A. Jochmann, M. Blessing, S. B. Haderlein, T. C. Schmidt, A new approach to determine method detection limits for compound-specific isotope analysis of volatile organic compounds., Rapid communications in mass spectrometry 20 (2006) 3639–3648.

[65] C. Torrentó, R. Bakkour, G. Glauser, A. Melsbach, V. Ponsin, T. B. Hofstetter, M. Elsner, D. Hunkeler, Solid-phase extraction method for stable isotope analysis of pesticides from large volume environmental water samples., The Analyst 144 (2019) 2898–2908.

[66] A. Melsbach, D. Pittois, M. Bayerle, M. Daubmeier, A. H. Meyer, K. Hölzer, T. Gallé, M. Elsner, Isotope fractionation of micropollutants during large-volume extraction: heads-up from a critical method evaluation for atrazine, desethylatrazine and 2,6-dichlorobenzamide at low ng/l concentrations in groundwater, Isotopes in Environmental and Health Studies 57 (2020) 35–52.

[67] D. A. Merritt, J. M. Hayes, Factors controlling precision and accuracy in isotope-ratio-monitoring mass spectrometry., Analytical chemistry 66 (1994) 2336–2347.

[68] K. Schreglmann, M. Hoeche, S. Steinbeiss, S. Reinnicke, M. Elsner, Carbon and nitrogen isotope analysis of atrazine and desethylatrazine at sub-microgram per liter concentrations in groundwater, Analytical and Bioanalytical Chemistry 405 (2013) 2857–2867.

[69] A. Andrade-Eiroa, M. Canle, V. Leroy-Cancellieri, V. Cerdà, Solid phase extraction of organic compounds: a critical review. part i, Trends in Analytical Chemistry 80 (2016) 641–654.

[70] M. Paolini, L. Ziller, K. H. Laursen, S. Husted, F. Camin, Compound-specific δ^{15}n and δ^{15}c analyses of amino acids for potential discrimination between organically and conventionally grown wheat., Journal of agricultural and food chemistry 63 (2015) 5841–5850.

[71] V. V. Galy, T. I. Eglinton, C. France-Lanord, S. P. Sylva, The provenance of vegetation and environmental signatures encoded in vascular plant biomarkers carried by the ganges–brahmaputra rivers, Earth and Planetary Science Letters 304 (2010) 1–12.

[72] F. Kenig, B. N. Popp, R. E. Summons, Preparative hplc with ultrastable-y zeolite for compound-specific carbon isotopic analyses, Organic Geochemistry 31 (2000) 1087–1094.

[73] M. C. Graham, R. W. Allan, A. E. Fallick, J. G. Farmer, Investigation of extraction and clean-up procedures used in the quantification and stable isotopic characterisation of pahs in contaminated urban soils., The Science of the total environment 360 (2006) 81–89.

[74] S. Yamamoto, K. Kawamura, O. Seki, P. A. Meyers, Y. Zheng, W. Zhou, Environmental influences over the last 16 ka on compound-specific δ13c variations of leaf wax n-alkanes in the hani peat deposit from northeast china, Chemical Geology 277 (2010) 261–268.

[75] J. A. Tripp, J. S. O. McCullagh, R. E. M. Hedges, Preparative separation of underivatized amino acids for compound-specific stable isotope analysis and radiocarbon dating of hydrolyzed bone collagen., Journal of separation science 29 (2006) 41–48.

[76] K. Lalonde, A. Barber, C. Ayotte, Two-dimensional hplc purification of underivatized urinary testosterone and metabolites for compound specific stable carbon isotope analysis., Drug testing and analysis 13 (2020) 558–570.

[77] R. Swalethorp, L. I. Aluwihare, A. R. Thompson, M. D. Ohman, M. R. Landry, Errors associated with compound specific δ15n analysis of amino acids in preserved fish samples purified by high pressure liquid chromatography, bioRxiv 18 (2019) 259–270.

[78] H. Y. Yun, E.-J. Won, J. Choi, Y. Cho, D. J. Lim, I.-S. Kim, K. Shin, Stable isotope analysis of residual pesticides via high performance liquid chromatography and elemental analyzer–isotope ratio mass spectrometry, Molecules 27 (2022).

[79] G. Cheng, S. Gao, Y. Gao, Z. Yu, P. Peng, Compound-specific stable carbon isotope analysis of hexabromocyclododecane diastereoisomers using gas chromatography-isotope ratio mass spectrometry., Rapid communications in mass spectrometry 33 (2019) 1318–1323.

[80] E. M. Thurman, Organic Geochemistry of Natural Waters, Kluwer Academic Publishers, 1985.

[81] M. Putz, T. Piper, M. Dubois, P. Delahaut, M. Thevis, Analysis of endogenous steroids in urine by means of multi-immunoaffinity chromatography and isotope ratio mass spectrometry for sports drug testing, Analytical and Bioanalytical Chemistry 411 (2019) 7563–7571.

[82] D. Glöckler, M. Harir, P. Schmitt-Kopplin, M. Elsner, R. Bakkour, Selectivity of β-cyclodextrin polymer toward aquatic contaminants: Insights from ultrahigh-resolution mass spectrometry of dissolved organic matter., Analytical chemistry (2023).

[83] D. Glöckler, M. Harir, P. Schmitt-Kopplin, M. Elsner, R. Bakkour, Discriminative behavior of cyclodextrin polymers against dissolved organic matter: Role of cavity size and sorbate properties., Analytical chemistry (2023).

[84] B. Sellergren, Imprinted polymers with memory for small molecules, proteins, or crystals, Angewandte Chemie 39 (2000) 1031–1037.

[85] B. Sellergren, Noncovalent molecular imprinting: antibody-like molecular recognition in polymeric network materials, Trends in Analytical Chemistry 16 (1997) 310–320.

[86] B. Sellergren, Polymer- and template-related factors influencing the efficiency in molecularly imprinted solid-phase extractions, Trends in Analytical Chemistry 18 (1999) 164–174.

[87] E. Turiel, A. Martín-Esteban, Molecularly imprinted polymers for sample preparation: a review., Analytica chimica acta 668 (2010) 87–99.

[88] A. Martín-Esteban, Molecularly-imprinted polymers as a versatile, highly selective tool in sample preparation, Trends in Analytical Chemistry 45 (2013) 169–181.

[89] L. Chen, X. Wang, W. Lu, X. Wu, J. Li, Molecular imprinting: perspectives and applications., Chemical Society reviews 45 (2016) 2137–2211.

[90] G. Vasapollo, R. D. Sole, L. Mergola, M. R. Lazzoi, A. Scardino, S. Scorrano, G. Mele, Molecularly imprinted polymers: Present and future prospective, International Journal of Molecular Sciences 12 (2011) 5908 – 5945.

[91] D. Xiao, Y. Jiang, Y. Bi, Molecularly imprinted polymers for the detection of illegal drugs and additives: a review, Microchimica Acta 185 (2018) 1–20.

[92] J. B. Ferreira, C. de Jesus Macrino, L. A. F. Dinali, J. F. A. Filho, C. F. Silva, K. B. Borges, W. Romão, Molecularly imprinted polymers as a selective sorbent for forensic applications in biological samples—a review, Analytical and Bioanalytical Chemistry 413 (2021) 6013 – 6036.

[93] Z. Song, J. Li, W. Lu, B. Li, G. Yang, Y. Bi, M. Arabi, X. Wang, J. Ma, L. Chen, Molecularly imprinted polymers based materials and their applications in chromatographic and electrophoretic separations, TrAC Trends in Analytical Chemistry (2021).

[94] X. Huang, H. Zou, X. Chen, Q. Luo, L. Kong, Molecularly imprinted monolithic stationary phases for liquid chromatographic separation of enantiomers and diastereomers., Journal of chromatography A 984 (2003) 273–282.

[95] B. Sellergren, Imprinted chiral stationary phases in high-performance liquid chromatography., Journal of chromatography A 906 (2001) 227–252.

[96] X. Ni, X. Tang, D. Wang, J. Zhang, L. Zhao, J. Gao, H. He, P. Dramou, Research progress of sensors based on molecularly imprinted polymers in analytical and biomedical analysis., Journal of pharmaceutical and biomedical analysis 235 (2023).

[97] Y. Saylan, S. Akgönüllü, H. Yavuz, S. Ünal, A. Denizli, Molecularly imprinted polymer based sensors for medical applications, Sensors 19 (2019).

[98] C. Malitesta, , I. Losito, P. G. Zambonin, Molecularly imprinted electrosynthesized polymers: new materials for biomimetic sensors., Analytical chemistry 71 (1999) 1366–1370.

[99] S. A. Zaidi, Molecular imprinted polymers as drug delivery vehicles, Drug Delivery 23 (2016) 2262–2271.

[100] D. A. Cunliffe, A. F. Kirby, C. Alexander, Molecularly imprinted drug delivery systems., Advanced drug delivery reviews 57 (2005) 1836–1853.

[101] B. Sellergren, C. J. Allender, Molecularly imprinted polymers: a bridge to advanced drug delivery., Advanced drug delivery reviews 57 (2005) 1733–1741.

[102] R. J. Umpleby, G. T. Rushton, R. N. Shah, A. M. Rampey, J. C. Bradshaw, J. K. Berch, K. D. Shimizu, Recognition directed site-selective chemical modification of molecularly imprinted polymers, Macromolecules 34 (2001) 8446–8452.

[103] Z. Zhang, J. Hu, Selective removal of estrogenic compounds by molecular imprinted polymer (mip)., Water research 42 (2008) 4101–4108.

[104] M. Arabi, A. Ostovan, A. R. Bagheri, X. Guo, L. Wang, J. Li, X. Wang, B. Li, L. Chen, Strategies of molecular imprinting-based solid-phase extraction prior to chromatographic analysis, TrAC Trends in Analytical Chemistry 128 (2020).

[105] M. Gast, S. Kühner, H. Sobek, P. Walther, B. Mizaikoff, Enhanced selectivity by passivation: Molecular imprints for viruses with exceptional binding properties., Analytical chemistry 90 (2018) 5576–5585.

[106] A. Flores, D. A. Cunliffe, M. J. Whitcombe, E. N. Vulfson, Imprinted polymers prepared by aqueous suspension polymerization, Journal of Applied Polymer Science 77 (2000) 1841–1850.

[107] K. F. Lim, C. I. Holdsworth, Effect of formulation on the binding efficiency and selectivity of precipitation molecularly imprinted polymers, Molecules 23 (2018).

[108] A. Murray, B. Örmeci, Competitive effects of humic acid and wastewater on adsorption of methylene blue dye by activated carbon and non-imprinted polymers., Journal of environmental sciences 66 (2017) 310–317.

[109] G. Newcombe, Charge vs. porosity — some influences on the adsorption of natural organic matter (nom) by activated carbon, Water Science and Technology 40 (1999) 191–198.

[110] L. F. Angeles, D. S. Aga, Catching the elusive persistent and mobile organic compounds: Novel sample preparation and advanced analytical techniques, Trends in Environmental Analytical Chemistry 25 (2020).

[111] S. Knoll, T. Rösch, C. Huhn, Trends in sample preparation and separation methods for the analysis of very polar and ionic compounds in environmental water and biota samples, Analytical and Bioanalytical Chemistry 412 (2020) 6149–6165.

[112] M. Nasiri, H. Ahmadzadeh, A. Amiri, Sample preparation and extraction methods for pesticides in aquatic environments: A review, Trends in Analytical Chemistry 123 (2020) 115772.

[113] P. Žuvela, M. Skoczylas, J. J. Liu, T. Bączek, R. Kaliszan, M. W. Wong, B. Buszewski, K. Héberger, Column characterization and selection systems in reversed-phase high-performance liquid chromatography., Chemical reviews 119 (2019) 3674–3729.

[114] A. Matilainen, E. T. Gjessing, T. Lahtinen, L. Hed, A. Bhatnagar, M. Sillanpää, An overview of the methods used in the characterisation of natural organic matter (nom) in relation to drinking water treatment., Chemosphere 83 (2011) 1431–1442.

[115] N. Her, G. Amy, D. M. McKnight, J. Sohn, Y. Yoon, Characterization of dom as a function of mw by fluorescence eem and hplc-sec using uva, doc, and fluorescence detection., Water research 37 (2003) 4295–4303.

[116] I. N. Acworth, D. Thomas, Charged aerosol detection and evaporative light scattering detection – fundamental differences affecting analytical performance, Planta Medica 80 (2014).

[117] T. Vehovec, A. Obreza, Review of operating principle and applications of the charged aerosol detector., Journal of chromatography. A 1217 (2010) 1549–1556.

[118] A. de Villiers, T. Górecki, F. Lynen, R. Szucs, P. A. T. Sandra, Improving the universal response of evaporative light scattering detection by mobile phase compensation., Journal of chromatography. A 1161 (2007) 183–191.

[119] I. Reviakine, D. Johannsmann, R. P. Richter, Hearing what you cannot see and visualizing what you hear: interpreting quartz crystal microbalance data from solvated interfaces., Analytical chemistry 83 (2011) 8838–8848.

[120] D. Johannsmann, The Quartz Crystal Microbalance in Soft Matter Research, Springer, 2015.

[121] G. Sauerbrey, Verwendung von schwingquarzen zur wägung dünner schichten und zur mikrowägung, Zeitschrift für Physik 155 (1959) 206–222.

[122] D. Johannsmann, A. Langhoff, C. Leppin, Studying soft interfaces with shear waves: Principles and applications of the quartz crystal microbalance (qcm), Sensors 21 (2021).

[123] A. Arnau, A review of interface electronic systems for at-cut quartz crystal microbalance applications in liquids, Sensors 8 (2008) 370–411.

[124] Y. Montagut, J. V. García, Y. Jiménez, C. March, Á. Montoya, A. Arnau, Frequency-shift vs phase-shift characterization of in-liquid quartz crystal microbalance applications., The Review of scientific instruments 82 (2011).

[125] M. Rodahl, F. Höök, A. Krozer, P. Brzezinski, B. Kasemo, Quartz crystal microbalance setup for frequency and q-factor measurements in gaseous and liquid environments, Review of Scientific Instruments 66 (1995) 3924–3930.

[126] O. Shekhah, J. Liu, R. A. Fischer, C. Wöll, Mof thin films: existing and future applications., Chemical Society reviews 40 (2011) 1081–1106.

[127] C. K. O'Sullivan, G. G. Guilbault, Commercial quartz crystal microbalances-theory and applications, Biosensors and Bioelectronics 14 (1999) 663–670.

[128] R. E. Speight, M. A. Cooper, A survey of the 2010 quartz crystal microbalance literature, Journal of Molecular Recognition 25 (2012).

[129] S. K. Vashist, P. Vashist, Recent advances in quartz crystal microbalance-based sensors, J. Sensors 2011 (2011) 1–13.

[130] K. A. Marx, Quartz crystal microbalance: a useful tool for studying thin polymer films and complex biomolecular systems at the solution-surface interface., Biomacromolecules 4 (2003) 1099–1120.

[131] W. Li, P. Liao, T. Oldham, Y. Jiang, C. Pan, S. Yuan, J. D. Fortner, Real-time evaluation of natural organic matter deposition processes onto model environmental surfaces., Water research 129 (2018) 231–239.

[132] M. Yan, C. Liu, D. Wang, J. Ni, J. Cheng, Characterization of adsorption of humic acid onto alumina using quartz crystal microbalance with dissipation., Langmuir 27 (2011) 9860–9865.

[133] M. Yan, D. Wang, J. Xie, C. Liu, J. Cheng, C. W. K. Chow, J. van Leeuwen, Investigation of the adsorption characteristics of natural organic matter from typical chinese surface waters onto alumina using quartz crystal microbalance with dissipation., Journal of hazardous materials 215 (2012) 115–121.

[134] M. Eita, In situ study of the adsorption of humic acid on the surface of aluminium oxide by qcm-d reveals novel features, Soft Matter 7 (2011) 709–715.

[135] M. Eita, Insight into the adsorption of humic acid/gd3+ complex on the surface of al2o3 studied in situ by qcm-d and ex situ by ellipsometry and xps, Soft Matter 7 (2011) 7424–7430.

[136] X. Wang, D. Huang, B. Cheng, L. Wang, New insight into the adsorption behaviour of effluent organic matter on organic–inorganic ultrafiltration membranes: a combined qcm-d and afm study, Royal Society Open Science 5 (2018).

[137] J. E. Tomaszewski, R. P. Schwarzenbach, M. Sander, Protein encapsulation by humic substances., Environmental science & technology 45 (2011) 6003–6010.

[138] O. S. Furman, S. Usenko, B. L. T. Lau, Relative importance of the humic and fulvic fractions of natural organic matter in the aggregation and deposition of silver nanoparticles., Environmental science & technology 47 (2013) 1349–1356.

[139] T. H. Nguyen, M. Elimelech, Adsorption of plasmid dna to a natural organic matter-coated silica surface: kinetics, conformation, and reversibility., Langmuir : the ACS journal of surfaces and colloids 23 (2007) 3273–3279.

[140] T. H. Nguyen, K. L. Chen, Role of divalent cations in plasmid dna adsorption to natural organic matter-coated silica surface., Environmental science & technology 41 (2007) 5370–5375.

[141] J. E. Tomaszewski, M. Madliger, J. A. Pedersen, R. P. Schwarzenbach, M. Sander, Adsorption of insecticidal cry1ab protein to humic substances. 2. influence of humic and fulvic acid charge and polarity characteristics., Environmental science & technology 46 (2012) 9932–9940.

[142] M. Sander, J. E. Tomaszewski, M. Madliger, R. P. Schwarzenbach, Adsorption of insecticidal cry1ab protein to humic substances. 1. experimental approach and mechanistic aspects., Environmental science & technology 46 (2012) 9923–9931.

[143] A. Armanious, M. Aeppli, M. Sander, Dissolved organic matter adsorption to model surfaces: adlayer formation, properties, and dynamics at the nanoscale., Environmental science & technology 48 (2014) 9420–9429.

[144] T. Zeng, C. J. Wilson, W. A. Mitch, Effect of chemical oxidation on the sorption tendency of dissolved organic matter to a model hydrophobic surface., Environmental science & technology 48 (2014) 5118–5126.

[145] N. Fontanals, M. Galià, R. M. Marcé, F. Borrull, Comparison of hydrophilic polymeric sorbents for on-line solid-phase extraction of polar compounds from aqueous samples, Chromatographia 60 (2004) 511–515.

[146] N. Fontanals, M. Galià, P. A. G. Cormack, R. M. Marcé, D. Sherrington, F. Borrull, Evaluation of a new hypercrosslinked polymer as a sorbent for solid-phase extraction of polar compounds., Journal of chromatography. A 1075 (2005) 51–56.

[147] N. Fontanals, R. M. Marcé, F. Borrull, New materials in sorptive extraction techniques for polar compounds., Journal of chromatography. A 1152 (2007) 14–31.

[148] A. Andrade-Eiroa, M. Canle, V. Leroy-Cancellieri, V. Cerdà, Solid-phase extraction of organic compounds: A critical review. part ii, Trends in Analytical Chemistry 80 (2016) 655–667.

[149] C. F. Poole, Solid-Phase Extraction, Elsevier, 2020.

[150] W. W. Schulz, W. H. King, A universal mass detector for liquid chromatography, Journal of Chromatographic Science 11 (1973) 343–348.

[151] T. Müller, D. A. White, T. P. J. Knowles, Dry-mass sensing for microfluidics, Applied Physics Letters 105 (2014).

[152] T. Kartanas, V. P. Ostanin, P. K. Challa, R. Daly, J. Charmet, T. P. J. Knowles, Enhanced quality factor label-free biosensing with micro-cantilevers integrated into microfluidic systems., Analytical chemistry 89 (2017) 11929–11936.

[153] T. Kartanas, A. Levin, Z. Toprakcioglu, T. Scheidt, T. A. Hakala, J. Charmet, T. P. J. Knowles, Label-free protein analysis using liquid chromatography with gravimetric detection., Analytical chemistry 93 (2021) 2848–2853.

[154] L. Zhang, S. Liu, X. Cui, C. Pan, A. Zhang, F. Chen, A review of sample preparation methods for the pesticide residue analysis in foods, Central European Journal of Chemistry 10 (2012) 900–925.

[155] J. Hajslová, J. Zrostlíková, Matrix effects in (ultra)trace analysis of pesticide residues in food and biotic matrices., Journal of chromatography. A 1000 (2003) 181–197.

[156] K. Ridgway, S. P. Lalljie, R. M. Smith, Sample preparation techniques for the determination of trace residues and contaminants in foods., Journal of chromatography. A 1153 (2007) 36–53.

[157] D. A. Lambropoulou, T. A. Albanis, Methods of sample preparation for determination of pesticide residues in food matrices by chromatography–mass spectrometry-based techniques: a review, Analytical and Bioanalytical Chemistry 389 (2007) 1663–1683.

[158] Q. He, J. Liang, L.-X. Chen, S. Chen, H. li Zheng, H.-X. Liu, H.-J. Zhang, Removal of the environmental pollutant carbamazepine using molecular imprinted adsorbents: Molecular simulation, adsorption properties, and mechanisms., Water research 168 (2019).

[159] J. Dai, M. M. F. de Cortalezzi, Influence of ph, ionic strength and natural organic matter concentration on a mip-fluorescent sensor for the quantification of dnt in water, Heliyon 5 (2019).

[160] Z. Salahshoor, K.-V. Ho, S.-Y. Hsu, A. H. Hossain, K. M. Trauth, C.-H. Lin, M. M. Fidalgo, Detection of atrazine and its metabolites in natural water samples using photonic molecularly imprinted sensors, Molecules 27 (2022).

[161] J. A. Leenheer, J. P. Croué, Peer reviewed: Characterizing aquatic dissolved organic matter, Environmental Science & Technology 37 (2003) 18–26.

[162] M. A. Edwards, M. M. Benjamin, J. N. Ryan, Role of organic acidity in sorption of natural organic matter (nom) to oxide surfaces, Colloids and Surfaces A: Physicochemical and Engineering Aspects 107 (1996) 297–307.

[163] R. York, N. G. A. Bell, Molecular tagging for molecular characterization of natural organic matter., Environmental science & technology 54 (2020) 3051–3063.

[164] J. Smilek, P. Sedlacek, M. Kalina, M. Klucakova, On the role of humic acids' carboxyl groups in the binding of charged organic compounds., Chemosphere 138 (2015) 503–510.

[165] https://humic-substances.org/acidic-functional-groups-of-ihss-samples/, accessed: 2023-12-07 (2023).

[166] J. D. Ritchie, E. M. Perdue, Proton-binding study of standard and reference fulvic acids, humic acids, and natural organic matter, Geochimica et Cosmochimica Acta 67 (2003) 85–96.

[167] C. W. Davies, Ion Association, Butterworths, 1962.

[168] E. B. H. Santos, V. I. Esteves, J. Rodrigues, A. C. Duarte, Humic substances' proton-binding equilibria: assessment of errors and limitations of potentiometric data, Analytica Chimica Acta 392 (1999) 333–341.

[169] I. M. Arsenie, H. Borén, B. Allard, Determination of the carboxyl content in humic substances by methylation., The Science of the total environment 116 (1992) 213–220.

[170] A. Presser, A. Hüfner, Trimethylsilyldiazomethane – a mild and efficient reagent for the methylation of carboxylic acids and alcohols in natural products, Monatshefte für Chemie / Chemical Monthly 135 (2004) 1015–1022.

[171] R. L. Wershaw, D. J. Pinckney, Methylation of humic acid fractions, Science 199 (1978) 906 – 907.

[172] F. H. Chi, G. Amy, Kinetic study on the sorption of dissolved natural organic matter onto different aquifer materials: the effects of hydrophobicity and functional groups., Journal of colloid and interface science 274 (2004) 380–391.

[173] M. H. Abraham, W. E. Acree, A. J. Leo, D. Hoekman, Partition of compounds from water and from air into the wet and dry monohalobenzenes, New Journal of Chemistry 33 (2009) 1685–1692.

[174] M. Boukadida, A. Anene, N. Jaoued-Grayaa, Y. Chevalier, S. Hbaieb, Choice of the functional monomer of molecularly imprinted polymers: Does it rely on strong acid-base or hydrogen bonding interactions?, Colloid and Interface Science Communications (2022).

[175] K. Golker, B. C. G. Karlsson, J. G. Wiklander, A. M. Rosengren, I. A. Nicholls, Hydrogen bond diversity in the pre-polymerization stage contributes to morphology and mip-template recognition – maa versus mma, European Polymer Journal 66 (2015) 558–568.

[176] T. H. Nguyen, K.-U. Goss, W. P. Ball, Polyparameter linear free energy relationships for estimating the equilibrium partition of organic compounds between water and the natural organic matter in soils and sediments., Environmental science & technology 39 (2005) 913–924.

[177] R. Schwarzenbach, P. Gschwend, D. M. Imboden, Sorption i: General introduction and sorption processes involving organic matter, in: Environmental Organic Chemistry, 1993.

[178] G. Newcombe, M. Drikas, Adsorption of nom onto activated carbon: Electrostatic and non-electrostatic effects, Carbon 35 (1997) 1239–1250.

[179] J. C. Westall, H. H. Chen, W. Zhang, B. J. Brownawell, Sorption of linear alkylbenzenesulfonates on sediment materials, Environmental Science & Technology 33 (1999) 3110–3118.

[180] M. G. Stapleton, D. L. Sparks, S. K. Dentel, Sorption of pentachlorophenol to hdtma-clay as a function of ionic strength and ph., Environmental science & technology 28 (1994) 2330–2335.

[181] M. H. Abraham, A. Ibrahim, W. E. Acree, Partition of compounds from gas to water and from gas to physiological saline at 310 k: Linear free energy relationships, Fluid Phase Equilibria 251 (2007) 93–109.

[182] M. von Lützow, I. Kögel-Knabner, K. Ekschmitt, E. Matzner, G. Guggenberger, B. Marschner, H. Flessa, Stabilization of organic matter in temperate soils: mechanisms and their relevance under different soil conditions – a review, European Journal of Soil Science 57 (2006) 426–445.

[183] K. Eusterhues, C. Rumpel, M. Kleber, I. Kögel-Knabner, Stabilisation of soil organic matter by interactions with minerals as revealed by mineral dissolution and oxidative degradation, Organic Geochemistry 34 (2003) 1591–1600.

[184] K. Kaiser, W. Zech, Competitive sorption of dissolved organic matter fractions to soils and related mineral phases, Soil Science Society of America Journal 61 (1997) 64–69.

[185] B. Gu, J. Schmitt, Z. Chen, L. Liang, J. F. McCarthy, Adsorption and desorption of natural organic matter on iron oxide: mechanisms and models., Environmental science & technology 28 (1994) 38–46.

[186] I. Chowdhury, D. M. Cwiertny, S. L. Walker, Combined factors influencing the aggregation and deposition of nano-tio2 in the presence of humic acid and bacteria., Environmental science & technology 46 (2012) 6968–6976.

[187] C. Pan, L. D. Troyer, P. Liao, J. G. Catalano, W. Li, D. E. Giammar, Effect of humic acid on the removal of chromium(vi) and the production of solids in iron electrocoagulation., Environmental science & technology 51 (2017) 6308–6318.

[188] A. Philippe, G. E. Schaumann, Interactions of dissolved organic matter with natural and engineered inorganic colloids: a review., Environmental science & technology 48 (2014) 8946–8962.

[189] D. Rana, T. Matsuura, Surface modifications for antifouling membranes., Chemical reviews 110 (2010) 2448–2471.

[190] N. Her, G. Amy, J. W. Chung, J. Yoon, Y. Yoon, Characterizing dissolved organic matter and evaluating associated nanofiltration membrane fouling., Chemosphere 70 (2008) 495–502.

[191] S. T. McBeath, N. J. D. Graham, Degradation of perfluorooctane sulfonate via in situ electro-generated ferrate and permanganate oxidants in nom-rich source waters, Environmental Science: Water Research & Technology 7 (2021) 1778–1790.

[192] E. M. Murphy, J. M. Zachara, S. C. Smith, Influence of mineral-bound humic substances on the sorption of hydrophobic organic compounds, Environmental Science & Technology 24 (1990) 1507–1516.

[193] P. Mazzei, A. Piccolo, Interactions between natural organic matter and organic pollutants as revealed by nmr spectroscopy, Magnetic Resonance in Chemistry 53 (2015) 667–678.

[194] P. H. Santschi, J. J. Lenhart, B. D. Honeyman, Heterogeneous processes affecting trace contaminant distribution in estuaries: The role of natural organic matter, Marine Chemistry 58 (1997) 99–125.

[195] J. J. Pignatello, Dynamic interactions of natural organic matter and organic compounds, Journal of Soils and Sediments 12 (2012) 1241–1256.

[196] I. Kristiana, J. Tan, C. A. Joll, A. Heitz, U. von Gunten, J. W. A. Charrois, Formation of n-nitrosamines from chlorination and chloramination of molecular weight fractions of natural organic matter., Water research 47 (2013) 535–546.

[197] A. Matilainen, M. Vepsäläinen, M. Sillanpää, Natural organic matter removal by coagulation during drinking water treatment: a review., Advances in colloid and interface science 159 (2010) 189–197.

[198] A. W. P. Vermeer, W. H. van Riemsdijk, L. K. Koopal, Adsorption of humic acid to mineral particles. 1. specific and electrostatic interactions, Langmuir 14 (1998) 2810–2819.

[199] M. J. Avena, L. K. Koopal, Kinetics of humic acid adsorption at solid-water interfaces, Environmental Science & Technology 33 (1999) 2739–2744.

[200] K. Namjesnik-Dejanovic, S. E. Cabaniss, Reverse-phase hplc method for measuring polarity distributions of natural organic matter., Environmental science & technology 38 (2004) 1108–1114.

[201] A. P. Gamerdinger, R. S. Achin, R. W. Traxler, Approximating the impact of sorption on biodegradation kinetics in soil-water systems, Soil Science Society of America Journal 61 (1997) 1618–1626.

[202] D. Violleau, H. Essis-Tome, H. Habarou, J. P. Croué, M. Pontie, Fouling studies of a polyamide nanofiltration membrane by selected natural organic matter: an analytical approach, Desalination 173 (2005) 223–238.

[203] J. Mo, Q. Yang, N. Zhang, W. Zhang, Y. Zheng, Z. Zhang, A review on agro-industrial waste (aiw) derived adsorbents for water and wastewater treatment., Journal of environmental management 227 (2018) 395–405.

[204] W. Zhang, L. Ding, J. Luo, M. Y. Jaffrin, B. Tang, Membrane fouling in photocatalytic membrane reactors (pmrs) for water and wastewater treatment: A critical review, Chemical Engineering Journal 302 (2016) 446–458.

[205] O. V. Borisova, O. V. Borisova, L. Billon, R. P. Richter, E. Reimhult, O. V. Borisov, ph- and electro-responsive properties of poly(acrylic acid) and poly(acrylic acid)-block-poly(acrylic acid-grad-styrene) brushes studied by quartz crystal microbalance with dissipation monitoring., Langmuir : the ACS journal of surfaces and colloids 31 (2015) 7684–7694.

[206] M. Stamm, Grafting on Solid Surfaces: “Grafting to” and “Grafting from” Methods, Springer, 2008.

[207] Y. Nakayama, T. Matsuda, In situ observation of dithiocarbamate-based surface photograft copolymerization using quartz crystal microbalance, Macromolecules 32 (1999) 5405–5410.

[208] G. Dunér, E. Thormann, A. Dėdinaitė, Quartz crystal microbalance with dissipation (qcm-d) studies of the viscoelastic response from a continuously growing grafted polyelectrolyte layer., Journal of colloid and interface science 408 (2013) 229–234.

[209] C. Sugnaux, H. Klok, Glucose-sensitive qcm-sensors via direct surface raft polymerization., Macromolecular rapid communications 35 (2014) 1402–1407.

[210] M. Bartholin, G. Boissier, J. Dubois, Styrene-divinylbenzene copolymers, 3. revisited ir analysis, Macromolecular Chemistry and Physics 182 (1981) 2075–2085.

[211] L. Li, H. Song, X. Chen, Enhancement of thermal stability of poly(divinylbenzene) microspheres, Materials Letters 62 (2008) 179–182.

[212] E. Partouche, S. Margel, Carbonization of pan grafted uniform crosslinked polystyrene microspheres, Carbon 46 (2008) 796–805.

[213] G. G. de Lima, J. K. Elter, B. S. Chee, W. L. E. Magalhães, D. M. Devine, M. J. D. Nugent, M. J. C. de Sá, A tough and novel dual-response paa/p(nipaam-co-pegdma) ipn hydrogels with ceramics by photopolymerization for consolidation of bone fragments following fracture, Biomedical Materials 14 (2019).

[214] M. B. Moran, G. C. Martin, The laser raman spectrum of polyethylene glycol dimethacrylate), Journal of Macromolecular Science, Part A 19 (1983) 611–618.

[215] X. Shi, G. Chen, L. Xu, C. Kang, L. Guihai, H. Luo, Y. Zhou, M. S. Dargusch, G. Pan, Achieving ultralow surface roughness and high material removal rate in fused silica via a novel acid sio2 slurry and its chemical-mechanical polishing mechanism, Applied Surface Science 500 (2020).

[216] W. Bücking, B. Du, A. Turshatov, A. M. König, I. Reviakine, B. Bode, D. Johannsmann, Quartz crystal microbalance based on torsional piezoelectric resonators., The Review of scientific instruments 78 (2007).

[217] K. Yang, D. Lin, B. Xing, Interactions of humic acid with nanosized inorganic oxides., Langmuir 25 (2009) 3571–3576.

[218] A. D. Site, Factors affecting sorption of organic compounds in natural sorbent/water systems and sorption coefficients for selected pollutants. a review, Journal of Physical and Chemical Reference Data 30 (2001) 187–439.

[219] M. Tassi, J. D. Vos, S. Chatterjee, F. Sobott, J. Bones, S. Eeltink, Advances in native high-performance liquid chromatography and intact mass spectrometry for the characterization of biopharmaceutical products., Journal of separation science 41 (2018) 125–144.

[220] Z. Xie, Q. Feng, S. Zhang, Y. Yan, C. Deng, C. Ding, Advances in proteomics sample preparation and enrichment for phosphorylation and glycosylation analysis., Proteomics (2022) e2200070.

[221] A. Beyer, M. K. Biziuk, Applications of sample preparation techniques in the analysis of pesticides and pcbs in food., Food chemistry 108 (2008) 669–680.

[222] H. Rapp-Wright, G. L. McEneff, B. Murphy, S. Gamble, R. M. Morgan, M. S. Beardah, L. P. Barron, Suspect screening and quantification of trace organic explosives in wastewater using solid phase extraction and liquid chromatography-high resolution accurate mass spectrometry., Journal of hazardous materials 329 (2017) 11–21.

[223] J. S. da Silva Burato, D. A. V. Medina, A. L. de Toffoli, E. V. S. Maciel, F. M. Lanças, Recent advances and trends in miniaturized sample preparation techniques., Journal of separation science 43 (2019) 202–225.

[224] J. Płotka-Wasylka, N. Szczepańska, M. de la Guardia, J. Namieśnik, Miniaturized solid-phase extraction techniques, Trends in Analytical Chemistry 73 (2015) 19–38.

[225] C. M. R. Ribeiro, A. R. L. Ribeiro, A. S. Maia, V. M. F. Gonçalves, M. E. Tiritan, New trends in sample preparation techniques for environmental analysis, Critical Reviews in Analytical Chemistry 44 (2014) 142–185.

[226] A. C. Moser, D. S. Hage, Immunoaffinity chromatography: an introduction to applications and recent developments., Bioanalysis 2 (2010) 769–790.

[227] Z. Gu, C. Yang, N. Chang, X. Yan, Metal-organic frameworks for analytical chemistry: from sample collection to chromatographic separation., Accounts of chemical research 45 (2012) 734–745.

[228] K. Sugitate, S. Nakamura, N. Orikata, K. Mizukoshi, M. Nakamura, A. Toriba, K. Hayakawa, Search of components causing matrix effects on gc/ms for pesticide analysis in food, Journal of Pesticide Science 37 (2012) 156–163.

[229] C. Wabnitz, W. Chen, M. Elsner, R. Bakkour, Quartz crystal microbalance as a holistic detector for quantifying complex organic matrices during liquid chromatography: 2. compound-specific isotope analysis, Analytical Chemistry 96 (2024) 7436 – 7443.

[230] Din 32645: Chemical analysis-decision limit, detection limit and determination limit under repeatability conditions-terms, methods, evaluation (Nov. 2008).

[231] P. Payá, M. Anastassiades, D. Mack, I. Sigalova, B. Tasdelen, J. Oliva, A. Barba, Analysis of pesticide residues using the quick easy cheap effective rugged and safe (quechers) pesticide multiresidue method in combination with gas and liquid chromatography and tandem mass spectrometric detection, Analytical and Bioanalytical Chemistry 389 (2007) 1697–1714.

[232] D. L. Buhrman, P. I. Price, P. J. Rudewiczcor, Quantitation of sr 27417 in human plasma using electrospray liquid chromatography-tandem mass spectrometry: A study of ion suppression, Journal of the American Society for Mass Spectrometry 7 (1996) 1099–1105.

[233] B. K. Matuszewski, M. L. Constanzer, C. M. Chavez-Eng, Strategies for the assessment of matrix effect in quantitative bioanalytical methods based on hplc-ms/ms., Analytical chemistry 75 (2003) 3019–3030.

[234] S. Z. Mikhail, W. Kimel, Densities and viscosities of methanol-water mixtures., Journal of Chemical & Engineering Data 6 (1961) 533–537.

[235] https://www.hplc-asi.com/flow-splitters/, accessed: 2022-12-02 (2022).

[236] R. G. H. Marks, M. A. Jochmann, W. A. Brand, T. C. Schmidt, How to couple lc-irms with hrms - a proof-of-concept study., Analytical chemistry 94 (2022) 2981–2987.

[237] C. Gunnarson, T. Lauer, H. Willenbring, E. J. Larson, M. Dittmann, K. Broeckhoven, D. R. Stoll, Implications of dispersion in connecting capillaries for separation systems involving post-column flow splitting., Journal of chromatography. A 1639 (2021) 461893.

[238] T. Kartanas, R. Rodrigues, T. Müller, T. W. Herling, T. P. J. Knowles, J. Charmet, 3d microfluidics spray nozzle for sample processing and materials deposition, AIP Conference Proceedings 2092 (2019).

[239] T. Kartanas, Z. Toprakcioglu, T. A. Hakala, A. Levin, T. W. Herling, R. Daly, J. Charmet, T. P. J. Knowles, Mechanism of droplet-formation in a supersonic microfluidic spray device, Applied Physics Letters 116 (2020) 153702.

[240] H. Hu, , R. G. Larson, Evaporation of a sessile droplet on a substrate, Journal of Physical Chemistry B 106 (2002) 1334–1344.

[241] S. J. Martin, G. C. Frye, K. O. Wessendorf, Sensing liquid properties with thickness-shear mode resonators, Sensors and Actuators A-physical 44 (1994) 209–218.

[242] S. Sandron, A. Rojas, R. . Wilson, N. W. Davies, P. R. Haddad, R. A. Shellie, P. N. Nesterenko, B. P. Kelleher, B. Paull, Chromatographic methods for the isolation, separation and characterisation of dissolved organic matter., Environmental science. Processes & impacts 17 (2015) 1531–1567.

[243] F. C. Wu, R. D. Evans, P. Dillon, High-performance liquid chromatographic fractionation and characterization of fulvic acid, Analytica Chimica Acta 464 (2002) 47–55.

[244] N. Kawasaki, K. Matsushige, K. Komatsu, A. Kohzu, F. W. Nara, F. Ogishi, M. Yahata, H. Mikami, T. Goto, A. Imai, Fast and precise method for hplc-size exclusion chromatography with uv and toc (ndir) detection: importance of multiple detectors to evaluate the characteristics of dissolved organic matter., Water research 45 (2011) 6240–6248.

[245] D. F. Swinehart, The beer-lambert law, Journal of Chemical Education 39 (1962) 333.

[246] G. V. Korshin, C. W. K. Chow, R. Fabris, M. Drikas, Absorbance spectroscopy-based examination of effects of coagulation on the reactivity of fractions of natural organic matter with varying apparent molecular weights., Water research 43 (2009) 1541–1548.

[247] X. Zhao, Y. He, J. Chen, J.-Y. Zhang, L. Chen, B. Wang, C. Wu, Y. Yuan, Identification and direct determination of fatty acids profile in oleic acid by hplc-cad and ms-it-tof., Journal of pharmaceutical and biomedical analysis 204 (2021) 114238.

[248] Z. Wu, Q. Zhang, N. Li, Y. Pu, B. Wang, T. Zhang, Comparison of critical methods developed for fatty acid analysis: A review., Journal of separation science 40 (2017) 288–298.

[249] S. Uclés, A. Lozano, A. Sosa, P. P. Vázquez, A. Valverde, A. R. Fernández-Alba, Matrix interference evaluation employing gc and lc coupled to triple quadrupole tandem mass spectrometry., Talanta 174 (2017) 72–81.

[250] M. Anastassiades, K. Maštovská, S. J. Lehotay, Evaluation of analyte protectants to improve gas chromatographic analysis of pesticides., Journal of chromatography. A 1015 (2003) 163–184.

[251] M. Thullner, F. Centler, H. H. Richnow, A. Fischer, Quantification of organic pollutant degradation in contaminated aquifers using compound specific stable isotope analysis – review of recent developments, Organic Geochemistry 42 (2012) 1440–1460.

[252] B. S. Lollar, G. F. Slater, B. E. Sleep, M. E. Witt, G. M. Klecka, M. R. Harkness, J. L. Spivack, Stable carbon isotope evidence for intrinsic bioremediation of tetrachloroethene and trichloroethene at area 6, dover air force base., Environmental science & technology 35 (2001) 261–269.

[253] P. Alvarez-Zaldívar, S. Payraudeau, F. Meite, J. Masbou, G. Imfeld, Pesticide degradation and export losses at the catchment scale: Insights from compound-specific isotope analysis (csia)., Water research 139 (2018) 198–207.

[254] C. Wabnitz, A. Canavan, W. Chen, M. Reisbeck, R. Bakkour, Quartz crystal microbalance as a holistic detector for quantifying complex organic matrices during liquid chromatography: 1. coupling, characterization, and validation, Analytical Chemistry 96 (2024) 7429 – 7435.

[255] T. B. Coplen, Guidelines and recommended terms for expression of stable-isotope-ratio and gas-ratio measurement results., Rapid communications in mass spectrometry 25 (2011) 2538–2560.

[256] R. A. Werner, W. A. Brand, Referencing strategies and techniques in stable isotope ratio analysis., Rapid communications in mass spectrometry 15 (2001) 501–519.

[257] M. H. O'Leary, Carbon isotopes in photosynthesis: Fractionation techniques may reveal new aspects of carbon dynamics in plants, BioScience 38 (1988) 328–336.

[258] B. Buszewski, S. Noga, Hydrophilic interaction liquid chromatography (hilic)—a powerful separation technique, Analytical and Bioanalytical Chemistry 402 (2011) 231–247.

[259] P. Hemström, K. Irgum, Hydrophilic interaction chromatography., Journal of separation science 29 (2006) 1784–1821.

[260] Y. Guo, S. Gaiki, Retention behavior of small polar compounds on polar stationary phases in hydrophilic interaction chromatography., Journal of chromatography. A 1074 (2005) 71–80.

[261] G. Kahsay, H. Song, A. V. Schepdael, D. Cabooter, E. Adams, Hydrophilic interaction chromatography (hilic) in the analysis of antibiotics., Journal of pharmaceutical and biomedical analysis 87 (2014) 142–154.

[262] F. Akamatsu, Y. Igi, A. Fujita, Separation and purification of glucose in sake for carbon stable isotope analysis, Food Analytical Methods 13 (2020) 885–891.

[263] X. Domingo-Almenara, C. Guijas, E. M. Billings, J. R. Montenegro-Burke, W. Uritboonthai, A. E. Aisporna, E. Chen, H. P. Benton, G. Siuzdak, The metlin small molecule dataset for machine learning-based retention time prediction, Nature Communications 10 (2019).

[264] M. J. den Uijl, P. J. Schoenmakers, G. K. Schulte, D. R. Stoll, M. R. van Bommel, B. W. Pirok, Measuring and using scanning-gradient data for use in method optimization for liquid chromatography., Journal of chromatography. A 1636 (2020).

[265] R. Bouwmeester, L. Martens, S. Degroeve, Comprehensive and empirical evaluation of machine learning algorithms for small molecule lc retention time prediction., Analytical chemistry 91 (2019) 3694–3703.

[266] H. Qian, C. Yang, W.-L. Wang, C. Yang, X. Yan, Advances in covalent organic frameworks in separation science., Journal of chromatography. A 1542 (2018) 1–18.

[267] B. Hashemi, P. Zohrabi, N. Raza, K. Kim, Metal-organic frameworks as advanced sorbents for the extraction and determination of pollutants from environmental, biological, and food media., Trends in Analytical Chemistry 97 (2017) 65–82.

[268] A. A. Baczynski, P. J. Polissar, D. Juchelka, J. B. Schwieters, A. Hilkert, R. E. Summons, K. H. Freeman, Picomolar-scale compound-specific isotope analyses., Rapid communications in mass spectrometry 32 (2018) 730–738.

[269] J. N. Lee, C. Park, G. M. Whitesides, Solvent compatibility of poly(dimethylsiloxane)-based microfluidic devices., Analytical chemistry 75 (2003) 6544–6554.

[270] B. T. Hammer, C. A. Kelley, R. Coffin, L. A. Cifuentes, J. G. Mueller, δ13c values of polycyclic aromatic hydrocarbons collected from two creosote-contaminated sites, Chemical Geology 152 (1998) 43–58.

[271] C. McRae, C. gong Sun, C. F. McMillan, C. E. Snape, A. E. Fallick, Sourcing of fossil fuel-derived pah in the environment, Polycyclic Aromatic Compounds 20 (2000) 97–109.

[272] D. Fabbri, I. Vassura, C. gong Sun, C. E. Snape, C. McRae, A. E. Fallick, Source apportionment of polycyclic aromatic hydrocarbons in a coastal lagoon by molecular and isotopic characterisation, Marine Chemistry 84 (2003) 123–135.

[273] S. E. Walker, R. M. Dickhut, C. J. Chisholm-Brause, S. P. Sylva, C. M. Reddy, Molecular and isotopic identification of pah sources in a highly industrialized urban estuary, Organic Geochemistry 36 (2005) 619–632.

[274] D. L. Saber, D. M. Mauro, T. Sirivedhin, Environmental forensics investigation in sediments near a former manufactured gas plant site, Environmental Forensics 7 (2006) 65–75.

[275] C. Bosch, A. Andersson, M. Krusa, C. Bandh, I. Hovorková, J. Klánová, T. D. J. Knowles, R. D. Pancost, R. P. Evershed, Ö. Gustafsson, Source apportionment of polycyclic aromatic hydrocarbons in central european soils with compound-specific triple isotopes (δ(13)c, δ(14)c, and δ(2)h)., Environmental science & technology 49 (2015) 7657–7665.

[276] H. H. Richnow, R. U. Meckenstock, L. A. Reitzel, A. Baun, A. Ledin, T. H. Christensen, In situ biodegradation determined by carbon isotope fractionation of aromatic hydrocarbons in an anaerobic landfill leachate plume (vejen, denmark)., Journal of contaminant hydrology 64 (2003) 59–72.

[277] V. P. O'malley, T. A. Abrajano, J. Hellou, Stable carbon isotopic apportionment of individual polycyclic aromatic hydrocarbons in st. john's harbour, newfoundland, Environmental Science & Technology 30 (1996) 634–639.

[278] H. H. Richnow, E. Annweiler, W. Michaelis, R. U. Meckenstock, Microbial in situ degradation of aromatic hydrocarbons in a contaminated aquifer monitored by carbon isotope fractionation., Journal of contaminant hydrology 65 (2003) 101–120.

[279] V. Micić, K. Straub, P. Blum, A. Kappler, Natural attenuation of naphthalene and benzene at a former gasworks site, Water Science & Technology: Water Supply 7 (2007) 145–153.

[280] B. Morasch, D. Hunkeler, J. Zopfi, B. Temime, P. Höhener, Intrinsic biodegradation potential of aromatic hydrocarbons in an alluvial aquifer–potentials and limits of signature metabolite analysis and two stable isotope-based techniques., Water research 45 (2011) 4459–4469.

[281] B. Mahro, A. Berghoff, A. Berning, C. Wortmann, A. Moller, Comparative assessment of laboratory and field-based methods to monitor natural attenuation processes in the contaminated groundwater of a former coking plant site, Environmental Engineering and Management Journal 13 (2014) 583–596.

[282] A. Steinbach, R. P. Seifert, E. Annweiler, W. Michaelis, Hydrogen and carbon isotope fractionation during anaerobic biodegradation of aromatic hydrocarbons–a field study., Environmental science & technology 38 (2004) 609–616.

[283] P. Blum, D. Hunkeler, M. Weede, C. Beyer, P. Grathwohl, B. Morasch, Quantification of biodegradation for o-xylene and naphthalene using first order decay models, michaelis-menten kinetics and stable carbon isotopes., Journal of contaminant hydrology 105 (2009) 118–130.

[284] C. Griebler, M. Safinowski, A. Vieth, H. H. Richnow, R. U. Meckenstock, Combined application of stable carbon isotope analysis and specific metabolites determination for assessing in situ degradation of aromatic hydrocarbons in a tar oil-contaminated aquifer., Environmental science & technology 38 (2004) 617–631.

[285] M. Marquès, M. Mari, C. Audí-Miró, J. Sierra, A. Soler, M. Nadal, J. L. Domingo, Photodegradation of polycyclic aromatic hydrocarbons in soils under a climate change base scenario., Chemosphere 148 (2016) 495–503.

[286] M. Blessing, M. A. Jochmann, S. B. Haderlein, T. C. Schmidt, Optimization of a large-volume injection method for compound-specific isotope analysis of polycyclic aromatic compounds at trace concentrations., Rapid communications in mass spectrometry : RCM 29 (2015) 2349–2360.

[287] S. Kümmel, R. Starke, G. Chen, F. Musat, H. H. Richnow, C. Vogt, Hydrogen isotope fractionation as a tool to identify aerobic and anaerobic pah biodegradation., Environmental science & technology 50 (2016) 3091–3100.

[288] B. Morasch, P. Höhener, D. Hunkeler, Evidence for in situ degradation of mono-and polyaromatic hydrocarbons in alluvial sediments based on microcosm experiments with 13c-labeled contaminants., Environmental pollution 148 (2007) 739–748.

[289] Y. Li, Y. Xiong, J. Fang, L. Wang, Q. Liang, Application of hollow fiber liquid-phase microextraction in identification of oil spill sources., Journal of chromatography. A 1216 (2009) 6155–6161.

[290] I. Tolosa, C. Guitart, M. Mesa-Albernas, C. P. Funkey, R. Cassi, Re-evaluation assessment of a large volume sampling (lvs) system for the determination of petroleum hydrocarbons and their stable carbon isotopes in deep-sea waters, Analytical Methods (2019).

[291] P. J. Yanik, T. H. O'donnell, S. A. Macko, Y. Qian, M. C. Kennicutt, The isotopic compositions of selected crude oil pahs during biodegradation, Organic Geochemistry 34 (2003) 291–304.

[292] R. Zhang, T. Li, J. M. Russell, F. Zhang, X. Xiao, Y. Cheng, Z. Liu, M. Guan, Q. Han, Source apportionment of polycyclic aromatic hydrocarbons in continental shelf of the east china sea with dual compound-specific isotopes (δ13c and δ2h)., The Science of the total environment (2019).

[293] A. Mikołajczuk, B. Geypens, M. Berglund, P. D. P. Taylor, Use of a temperature-programmable injector coupled to gas chromatography-combustion-isotope ratio mass spectrometry for compound-specific carbon isotopic analysis of polycyclic aromatic hydrocarbons., Rapid communications in mass spectrometry 23 (2009) 2421–2427.

[294] E. Lichtfouse, H. Budzinski, 13 c analysis of molecular organic substances, a novel breakthrough in analytical sciences, Analusis 23 (1995) 364–369.

[295] B. Yan, T. A. Abrajano, R. F. Bopp, L. A. Benedict, D. A. Chaky, E. F. Perry, J. Song, D. P. Keane, Combined application of δ13c and molecular ratios in sediment cores for pah source apportionment in the new york/new jersey harbor complex, Organic Geochemistry 37 (2006) 674–687.

[296] J. Cennerazzo, A. de Junet, J. Audinot, C. Leyval, Dynamics of pahs and derived organic compounds in a soil-plant mesocosm spiked with 13c-phenanthrene., Chemosphere 168 (2017) 1619–1627.

[297] C. McRae, G. D. Love, I. P. Murray, C. E. Snape, A. E. Fallick, Potential of gas chromatography isotope ratio mass spectrometry to source polycyclic aromatic hydrocarbon emissions, Analytical Communications 33 (1996) 331–333.

[298] C. McRae, C. E. Snape, A. E. Fallick, Variations in the stable isotope ratios of specific aromatic and aliphatic hydrocarbons from coal conversion processes, Analyst 123 (1998) 1519–1523.

[299] D.-N. Ou, M. Liu, S. bo Cheng, L. jun Hou, S. Xu, L. li Wang, Identification of the sources of polycyclic aromatic hydrocarbons based on molecular and isotopic characterization from the yangtze estuarine and nearby coastal areas, Journal of Geographical Sciences 20 (2010) 283–294.

[300] V. P. O'malley, T. A. Abrajano, J. Hellou, Determination of the 13c12c ratios of individual pah from environmental samples: can pah sources be apportioned?, Organic Geochemistry 21 (1994) 809–822.

[301] M. Kim, M. C. Kennicutt, Y. Qian, Polycyclic aromatic hydrocarbon purification procedures for compound specific isotope analysis., Environmental science & technology 39 (2005) 6770–6.

[302] F. D. Bergmann, N. A. Laban, A. H. Meyer, M. Elsner, R. U. Meckenstock, Dual (c, h) isotope fractionation in anaerobic low molecular weight (poly)aromatic hydrocarbon (pah) degradation: potential for field studies and mechanistic implications., Environmental science & technology 45 (2011) 6947–6953.

[303] A. Buczyńska, B. Geypens, R. E. V. Grieken, K. D. Wael, Large-volume injection combined with gas chromatography/isotope ratio mass spectrometry for the analysis of polycyclic aromatic hydrocarbons., Rapid communications in mass spectrometry : RCM 28 (2014) 200–208.

[304] E. Ternon, I. Tolosa, Comprehensive analytical methodology to determine hydrocarbons in marine waters using extraction disks coupled to glass fiber filters and compound-specific isotope analyses., Journal of chromatography. A 1404 (2015) 10–20.

[305] M. Kim, M. C. Kennicutt, Y. Qian, Source characterization using compound composition and stable carbon isotope ratio of pahs in sediments from lakes, harbor, and shipping waterway., The Science of the total environment 389 (2008) 367–377.

[306] A. D. Smirnov, T. A. Abrajano, A. Y. . Smirnov, A. Stark, Distribution and sources of polycyclic aromatic hydrocarbons in the sediments of lake erie, part 1. spatial distribution, transport, and deposition, Organic Geochemistry 29 (1998) 1813–1828.

[307] M. Kim, M. C. Kennicutt, Y. Qian, Molecular and stable carbon isotopic characterization of pah contaminants at mcmurdo station, antarctica., Marine pollution bulletin 52 (2006) 1585–1590.

[308] J. Yang, P. Sun, X. Zhang, X. Wei, Y. Huang, W. Du, A. Qadeer, M. Liu, Y. Huang, Source apportionment of pahs in roadside agricultural soils of a megacity using positive matrix factorization receptor model and compound-specific carbon isotope analysis., Journal of hazardous materials 403 (2020).

[309] C. McRae, C. E. Snape, C. gong Sun, D. Fabbri, D. Tartari, C. Trombini, A. E. Fallick, Use of compound-specific stable isotope analysis to source anthropogenic natural gas-derived polycyclic aromatic hydrocarbons in a lagoon sediment, Environmental Science & Technology 34 (2000) 4684–4686.

[310] G. Vinzelberg, J. Schwarzbauer, R. Littke, Groundwater contamination by chlorinated naphthalenes and related substances caused by activities of a former military base., Chemosphere 61 (2005) 770–782.

[311] L. Mazéas, H. Budzinski, Quantification of petrogenic pah in marine sediment using molecular stable carbon isotopic ratio measurement, Analusis 27 (1999) 200–202.

[312] X. Zhang, Y. Xu, J. Ruan, S. Ding, X. Huang, Origin, distribution and environmental significance of perylene in okinawa trough since last glaciation maximum, Organic Geochemistry 76 (2014) 288–294.

[313] T. Okuda, H. Kumata, H. Naraoka, R. Ishiwatari, H. Takada, Vertical distributions and δ13c isotopic compositions of pahs in chidorigafuchi moat sediment, japan, Organic Geochemistry 33 (2002) 843–848.

[314] M. G. Petrisic, G. Muri, N. Ogrinc, Source identification and sedimentary record of polycyclic aromatic hydrocarbons in lake bled (nw slovenia) using stable carbon isotopes., Environmental science & technology 47 (2013) 1280–1286.

[315] V. P. O'malley, R. A. Burke, W. S. Schlotzhauer, Using gc–ms/combustion/irms to determine the 13c/12c ratios of individual hydrocarbons produced from the combustion of biomass materials—application to biomass burning, Organic Geochemistry 27 (1997) 567–581.

[316] L. Zhang, Y. Zhang, F. Liu, J. Liu, Compound-specific carbon isotope analysis of polycyclic aromatic hydrocarbons in water using solid-phase extraction coupled with gc/c-irms, Asian Journal of Chemistry 26 (2014) 906–910.

[317] C. Gauchotte-Lindsay, L. A. McGregor, A. Assal, R. Thomas, R. M. Kalin, Highlighting the effects of co-eluting interferences on compound-specific stable isotope analysis of polycyclic aromatic hydrocarbons by using comprehensive two-dimensional gas chromatography, ChemPlusChem 79 (2014) 804–812.

[318] Y. Wang, Y. Huang, J. N. Huckins, J. D. Petty, Compound-specific carbon and hydrogen isotope analysis of sub-parts per billion level waterborne petroleum hydrocarbons., Environmental science & technology 38 (2004) 3689–3697.

[319] C. McRae, C. gong Sun, C. E. Snape, A. E. Fallick, D. A. Taylor, δ13c values of coal-derived pahs from different processes and their application to source apportionment, Organic Geochemistry 30 (1999) 881–889.

[320] T. J. Boyd, C. L. Osburn, K. J. Johnson, K. B. Birgl, R. Coffin, Compound-specific isotope analysis coupled with multivariate statistics to source-apportion hydrocarbon mixtures., Environmental science & technology 40 (2006) 1916–1924.

[321] S. Marozava, A. H. Meyer, A. P. de Mora, M. Gharasoo, L. Zhuo, H. Wang, O. A. Cirpka, R. U. Meckenstock, M. Elsner, Mass transfer limitation during slow anaerobic biodegradation of 2-methylnaphthalene., Environmental science & technology (2019).

[322] L. Mazéas, H. Budzinski, Polycyclic aromatic hydrocarbon 13c/12c ratio measurement in petroleum and marine sediments application to standard reference materials and a sediment suspected of contamination from the erika oil spill., Journal of chromatography. A 923 (2001) 165–176.

[323] H. Liu, M. li Wu, H. Gao, N. Yi, X. Duan, Hydrocarbon transformation pathways and soil organic carbon stability in the biostimulation of oil-contaminated soil: Implications of 13c natural abundance., The Science of the total environment 788 (2021).

[324] R. U. Meckenstock, M. Safinowski, C. Griebler, Anaerobic degradation of polycyclic aromatic hydrocarbons., FEMS microbiology ecology 49 (2004) 27–36.

[325] L. Mazéas, H. Budzinski, N. Raymond, Absence of stable carbon isotope fractionation of saturated and polycyclic aromatic hydrocarbons during aerobic bacterial biodegradation, Organic Geochemistry 33 (2002) 1259–1272.

[326] J. J. Jautzy, J. M. E. Ahad, C. Gobeil, M. M. Savard, Century-long source apportionment of pahs in athabasca oil sands region lakes using diagnostic ratios and compound-specific carbon isotope signatures., Environmental science & technology 47 (2013) 6155–6163.

[327] R. U. Meckenstock, B. Morasch, R. Warthmann, B. Schink, E. Annweiler, W. Michaelis, H. H. Richnow, 13c/12c isotope fractionation of aromatic hydrocarbons during microbial degradation., Environmental microbiology 1 (1999) 409–414.

[328] B. Morasch, H. H. Richnow, B. Schink, A. Vieth, R. U. Meckenstock, Carbon and hydrogen stable isotope fractionation during aerobic bacterial degradation of aromatic hydrocarbons, Applied and Environmental Microbiology 68 (2002) 5191–5194.

[329] I. Tolosa, S. J. de Mora, Isolation of neutral and acidic lipid biomarker classes for compound-specific-carbon isotope analysis by means of solvent extraction and normal-phase high-performance liquid chromatography., Journal of chromatography. A 1045 (2004) 71–84.

[330] R. M. Dickhut, T. V. Padma, A. Cincinelli, Fractionation of stable isotope-labeled organic pollutants as a potential tracer of atmospheric transport processes., Environmental science & technology 38 (2004) 3871–3876.

[331] B. Tian, S. Gao, Z. Zhu, X. Zeng, Y. Liang, Z. Yu, P. Peng, Two-dimensional gas chromatography coupled to isotope ratio mass spectrometry for determining high molecular weight polycyclic aromatic hydrocarbons in sediments., Journal of chromatography. A 1693 (2023).

[332] J. A. van Leeuwen, J. Gerritse, N. Hartog, S. Ertl, J. R. Parsons, S. M. Hassanizadeh, Anaerobic degradation of benzene and other aromatic hydrocarbons in a tar-derived plume: Nitrate versus iron reducing conditions., Journal of contaminant hydrology 248 (2022).

[333] S. Chen, P. Yang, J. R. kumar, Y. Liu, L. Ma, Inconsistent carbon and nitrogen isotope fractionation in the biotransformation of atrazine by ensifer sp. cx-t and sinorihizobium sp. k., International Biodeterioration & Biodegradation 125 (2017) 170–176.

[334] S. Chen, K. Zhang, R. K. Jha, L. Ma, Impact of atrazine concentration on bioavailability and apparent isotope fractionation in gram-negative rhizobium sp. cx-z., Environmental pollution (2019).

[335] H. Penning, S. R. Sørensen, A. H. Meyer, J. Aamand, M. Elsner, C, n, and h isotope fractionation of the herbicide isoproturon reflects different microbial transformation pathways., Environmental science & technology 44 (2010) 2372–2378.

[336] S. Reinnicke, D. Juchelka, S. Steinbeiss, A. H. Meyer, A. Hilkert, M. Elsner, Gas chromatography/isotope ratio mass spectrometry of recalcitrant target compounds: performance of different combustion reactors and strategies for standardization., Rapid communications in mass spectrometry : RCM 26 (2012) 1053–1060.

[337] B. N. Ehrl, M. Gharasoo, M. Elsner, Isotope fractionation pinpoints membrane permeability as a barrier to atrazine biodegradation in gram-negative polaromonas sp. nea-c, Environmental Science & Technology 52 (2018) 4137–4144.

[338] J. Masbou, G. Drouin, S. Payraudeau, G. Imfeld, Carbon and nitrogen stable isotope fractionation during abiotic hydrolysis of pesticides., Chemosphere 213 (2018) 368–376.

[339] B. N. Ehrl, K. Kundu, M. Gharasoo, S. Marozava, M. Elsner, Rate-limiting mass transfer in micropollutant degradation revealed by isotope fractionation in chemostat, Environmental Science & Technology 53 (2018) 1197–1205.

[340] V. Ponsin, C. Torrentó, C. Lihl, M. Elsner, D. Hunkeler, Compound-specific chlorine isotope analysis of the herbicides atrazine, acetochlor and metolachlor., Analytical chemistry (2019).

[341] A. H. Meyer, H. Penning, H. Lowag, M. Elsner, Precise and accurate compound specific carbon and nitrogen isotope analysis of atrazine: critical role of combustion oven conditions., Environmental science & technology 42 (2008) 7757–7763.

[342] O. Elsayed, E. Maillard, S. Vuilleumier, I. Nijenhuis, H. H. Richnow, G. Imfeld, Using compound-specific isotope analysis to assess the degradation of chloroacetanilide herbicides in lab-scale wetlands., Chemosphere 99 (2014) 89–95.

[343] S. R. Lutz, Y. van der Velde, O. Elsayed, G. Imfeld, M. Lefrancq, S. Payraudeau, B. M. van Breukelen, Pesticide fate on catchment scale: conceptual modelling of stream csia data, Hydrology and Earth System Sciences 21 (2017) 5243–5261.

[344] C. Lihl, J. Renpenning, S. Kümmel, F. Gelman, H. K. V. Schürner, M. Daubmeier, B. Heckel, A. Melsbach, A. Bernstein, O. Shouakar-Stash, M. Gehre, M. Elsner, Towards improved accuracy in chlorine isotope analysis: synthesis routes for in-house standards and characterization via complementary mass spectrometry methods., Analytical chemistry (2019).

[345] G. Imfeld, L. Besaury, B. Maucourt, S. Donadello, N. Baran, S. Vuilleumier, Toward integrative bacterial monitoring of metolachlor toxicity in groundwater, Frontiers in Microbiology 9 (2018).

[346] A. Melsbach, V. Ponsin, C. Torrentó, C. Lihl, T. B. Hofstetter, D. Hunkeler, M. Elsner, 13c- and 15n-isotope analysis of desphenylchloridazon by liquid chromatography-isotope-ratio mass spectrometry and derivatization gas chromatography-isotope-ratio mass spectrometry., Analytical chemistry 91 (2019) 3412–3420.

[347] H. K. V. Schürner, M. P. Maier, D. Eckert, R. Brejcha, C.-C. Neumann, C. Stumpp, O. A. Cirpka, M. Elsner, Compound-specific stable isotope fractionation of pesticides and pharmaceuticals in a mesoscale aquifer model., Environmental science & technology 50 (2016) 5729–5739.

[348] B. Jin, M. Rolle, Position-specific isotope modeling of organic micropollutants transformation through different reaction pathways., Environmental pollution 210 (2016) 94–103.

[349] L. Wu, B. Chládková, O. J. Lechtenfeld, S. Lian, J. Schindelka, H. Herrmann, H. H. Richnow, Characterizing chemical transformation of organophosphorus compounds by 13c and 2h stable isotope analysis., The Science of the total environment 615 (2018) 20–28.

[350] L. Wu, D. Verma, M. Bondgaard, A. Melvej, C. Vogt, S. Subudhi, H. H. Richnow, Carbon and hydrogen isotope analysis of parathion for characterizing its natural attenuation by hydrolysis at a contaminated site., Water research 143 (2018) 146–154.

[351] D. M. Kujawinski, J. B. Wolbert, L. Zhang, M. A. Jochmann, D. Widory, N. Baran, T. C. Schmidt, Carbon isotope ratio measurements of glyphosate and ampa by liquid chromatography coupled to isotope ratio mass spectrometry, Analytical and Bioanalytical Chemistry 405 (2013) 2869–2878.

[352] E. O. Mogusu, J. B. Wolbert, D. M. Kujawinski, M. A. Jochmann, M. Elsner, Dual element (15n/14n, 13c/12c) isotope analysis of glyphosate and ampa by derivatization-gas chromatography isotope ratio mass spectrometry (gc/irms) combined with lc/irms, Analytical and Bioanalytical Chemistry 407 (2015) 5249–5260.

[353] A. E. Hartenbach, T. B. Hofstetter, P. R. Tentscher, S. Canonica, M. Berg, R. P. Schwarzenbach, Carbon, hydrogen, and nitrogen isotope fractionation during light-induced transformations of atrazine., Environmental science & technology 42 (2008) 7751–7756.

[354] Y. Yamamoto, F. Tanaka, S. Fujihara, T. Matsumaru, Carbon isotope fractionation during chlorothalonil dissipation in an upland soil, Journal of Pesticide Science 29 (2004) 53–56.

[355] S. R. Lutz, H. van Meerveld, M. J. Waterloo, H. P. Broers, B. M. van Breukelen, A model-based assessment of the potential use of compound-specific stable isotope analysis in river monitoring of diffuse pesticide pollution, Hydrology and Earth System Sciences 17 (2013) 4505–4524.

[356] A. H. Meyer, H. Penning, M. Elsner, C and n isotope fractionation suggests similar mechanisms of microbial atrazine transformation despite involvement of different enzymes (atza and trzn)., Environmental science & technology 43 (2009) 8079–8085.

[357] H. Penning, M. Elsner, Intramolecular carbon and nitrogen isotope analysis by quantitative dry fragmentation of the phenylurea herbicide isoproturon in a combined injector/capillary reactor prior to gc separation., Analytical chemistry 79 21 (2007) 8399–8405.

[358] S. Reinnicke, A. Simonsen, S. R. Sørensen, J. Aamand, M. Elsner, C and n isotope fractionation during biodegradation of the pesticide metabolite 2,6-dichlorobenzamide (bam): potential for environmental assessments., Environmental science & technology 46 (2012) 1447–1454.

[359] M. P. Maier, S. Qiu, M. Elsner, Enantioselective stable isotope analysis (esia) of polar herbicides, Analytical and Bioanalytical Chemistry 405 (2013) 2825–2831.

[360] L. Wu, J. Yao, P. Trebse, N. Zhang, H. H. Richnow, Compound specific isotope analysis of organophosphorus pesticides., Chemosphere 111 (2014) 458–463.

[361] B. Jin, M. Rolle, Joint interpretation of enantiomer and stable isotope fractionation for chiral pesticides degradation., Water research 105 (2016) 178–186.

[362] L. Wu, S. Kümmel, H. H. Richnow, Validation of gc–irms techniques for δ13c and δ2h csia of organophosphorus compounds and their potential for studying the mode of hydrolysis in the environment, Analytical and Bioanalytical Chemistry 409 (2017) 2581–2590.

[363] X. yan Tang, Y. Yang, W. da Huang, M. B. McBride, J. Guo, R. Tao, Y. Dai, Transformation of chlorpyrifos in integrated recirculating constructed wetlands (ircws) as revealed by compound-specific stable isotope (csia) and microbial community structure analysis., Bioresource technology 233 (2017) 264–270.

[364] S. Chen, K. Zhang, R. K. Jha, C. Chen, H. H. Yu, Y. Liu, L. Ma, Isotope fractionation in atrazine degradation reveals rate-limiting, energy-dependent transport across the cell membrane of gram-negative rhizobium sp. cx-z., Environmental pollution 248 (2019) 857–864.

[365] A. W. Limon, M. Moingt, D. Widory, The carbon stable isotope compositions of glyphosate and ampa: improved analytical sensitivity and first application to environmental water matrices., Rapid communications in mass spectrometry : RCM (2020).

[366] E. Torabi, C. Wiegert, B. Guyot, S. Vuilleumier, G. Imfeld, Dissipation of s-metolachlor and butachlor in agricultural soils and responses of bacterial communities: Insights from compound-specific isotope and biomolecular analyses., Journal of environmental sciences 92 (2020) 163–175.

[367] N. Knossow, H. Siebner, A. Bernstein, Isotope analysis method for the herbicide bromoxynil and its application to study photo-degradation processes., Journal of hazardous materials 388 (2020) 122036.

[368] J. Shi, Z. Zhang, R. Yang, Quantitative assessment of degradation degree of metalaxyl in soil and plant by compound-specific isotope analysis, Water, Air, & Soil Pollution 233 (2022).

[369] J. Masbou, F. Meite, B. Guyot, G. Imfeld, Enantiomer-specific stable carbon isotope analysis (esia) to evaluate degradation of the chiral fungicide metalaxyl in soils., Journal of hazardous materials 353 (2018) 99–107.

[370] A. Melsbach, D. Pittois, M. Bayerle, M. Daubmeier, A. H. Meyer, K. Hölzer, T. Gallé, M. Elsner, Isotope fractionation of micropollutants during large-volume extraction: heads-up from a critical method evaluation for atrazine, desethylatrazine and 2,6-dichlorobenzamide at low ng/l concentrations in groundwater, Isotopes in Environmental and Health Studies 57 (2020) 35 – 52.

[371] B. Droz, G. Drouin, L. Maurer, C. Villette, S. Payraudeau, G. Imfeld, Phase transfer and biodegradation of pesticides in water-sediment systems explored by compound-specific isotope analysis and conceptual modeling., Environmental science & technology (2021).

[372] G. Drouin, B. Droz, F. Leresche, S. Payraudeau, J. Masbou, G. Imfeld, Direct and indirect photodegradation of atrazine and s-metolachlor in agriculturally impacted surface water and associated c and n isotope fractionation., Environmental science. Processes & impacts (2021).

[373] C. Torrentó, V. Ponsin, C. Lihl, T. B. Hofstetter, N. Baran, M. Elsner, D. Hunkeler, Triple-element compound-specific stable isotope analysis (3d-csia): Added value of cl isotope ratios to assess herbicide degradation., Environmental science & technology (2021).

[374] T. Gilevska, S. Payraudeau, G. Imfeld, Evaluating pesticide degradation in artificial wetlands with compound-specific isotope analysis: A case study with the fungicide dimethomorph., The Science of the total environment (2023).

[375] T. Gilevska, J. Masbou, B. Baumlin, B. Chaumet, C. Chaumont, S. Payraudeau, J. Tournebize, A. Probst, J. Probst, G. Imfeld, Do pesticides degrade in surface water receiving runoff from agricultural catchments? combining passive samplers (pocis) and compound-specific isotope analysis., The Science of the total environment (2022).

[376] E. Liang, T. Huang, J. Li, T. Wang, Degradation pathways of atrazine by electrochemical oxidation at different current densities: Identifications from compound-specific isotope analysis and dft calculation., Environmental pollution (2023).

[377] S.-G. Chen, L. Ma, Y. Wang, Kinetic isotope effects of c and n indicate different transformation mechanisms between atza- and trzn-harboring strains in dechlorination of atrazine, Biodegradation 33 (2022) 207 – 221.

[378] J. Li, E. Liang, T. Huang, X. Zhao, T. Wang, Insights into atrazine degradation by thermally activated persulfate: Evidence from dual c-h isotope analysis and dft simulations, Chemical Engineering Journal (2022).

[379] M. S. Arar, R. Bakkour, M. Elsner, A. Bernstein, Microbial hydrolysis of atrazine in contaminated groundwater., Chemosphere (2023).

[380] M. Prieto-Espinoza, R. D. chiara, B. Belfort, S. Weill, G. Imfeld, Reactive transport of micropollutants in laboratory aquifers undergoing transient exposure periods., The Science of the total environment (2022).

[381] K. Kundu, A. Melsbach, B. Heckel, S. Schneidemann, D. Kanapathi, S. Marozava, J. Merl-Pham, M. Elsner, Linking increased isotope fractionation at low concentrations to enzyme activity regulation: 4-cl phenol degradation by arthrobacter chlorophenolicus a6, Environmental Science & Technology 56 (2022) 3021–3032.

[382] F. Sun, A. Mellage, Z. Wang, R. Bakkour, C. Griebler, M. Thullner, O. A. Cirpka, M. Elsner, Toward improved bioremediation strategies: Response of bam-degradation activity to concentration and flow changes in an inoculated bench-scale sediment tank, Environmental Science & Technology 56 (2022) 4050–4061.

[383] F. Meite, M. Granet, G. Imfeld, Ageing of copper, zinc and synthetic pesticides in particle-size and chemical fractions of agricultural soils., The Science of the total environment (2022).

[384] S.-L. Badea, C. Vogt, M. Gehre, A. Fischer, A. F. Danet, H. H. Richnow, Development of an enantiomer-specific stable carbon isotope analysis (esia) method for assessing the fate of α-hexachlorocyclo-hexane in the environment., Rapid communications in mass spectrometry : RCM 25 (2011) 1363–1372.

[385] S. Bashir, K. L. Hitzfeld, M. Gehre, H. H. Richnow, A. Fischer, Evaluating degradation of hexachlorcyclohexane (hch) isomers within a contaminated aquifer using compound-specific stable carbon isotope analysis (csia)., Water research 71 (2015) 187–196.

[386] M. M. G. Chartrand, E. Passeport, C. Rose, G. Lacrampe-Couloume, T. F. Bidleman, L. M. Jantunen, B. S. Lollar, Compound specific isotope analysis of hexachlorocyclohexane isomers: a method for source fingerprinting and field investigation of in situ biodegradation., Rapid communications in mass spectrometry 29 (2015) 505–514.

[387] Y. Liu, S. Bashir, R. Stollberg, R. Trabitzsch, H. Weiss, H. Paschke, I. Nijenhuis, H. H. Richnow, Compound specific and enantioselective stable isotope analysis as tools to monitor transformation of hexachlorocyclohexane (hch) in a complex aquifer system., Environmental science & technology 51 (2017) 8909–8916.

[388] L. Wu, Y. Liu, X. Liu, A. Bajaj, M. Sharma, R. Lal, H. H. Richnow, Isotope fractionation approach to characterize the reactive transport processes governing the fate of hexachlorocyclohexanes at a contaminated site in india., Environment international 132 (2019).

[389] N. Zhang, S. Bashir, J. Qin, J. Schindelka, A. Fischer, I. Nijenhuis, H. Herrmann, L. Y. Wick, H. H. Richnow, Compound specific stable isotope analysis (csia) to characterize transformation mechanisms of α-hexachlorocyclohexane., Journal of hazardous materials 280 (2014) 750–757.

[390] S.-L. Badea, A. F. Danet, Enantioselective stable isotope analysis (esia) - a new concept to evaluate the environmental fate of chiral organic contaminants., The Science of the total environment 514 (2015) 459–466.

[391] Y. Qian, K. Chen, Y. Liu, J. Li, Assessment of hexachlorcyclohexane biodegradation in contaminated soil by compound-specific stable isotope analysis., Environmental pollution 254 (2019).

[392] S.-L. Badea, C. Vogt, S. Weber, A. F. Danet, H. H. Richnow, Stable isotope fractionation of gamma-hexachlorocyclohexane (lindane) during reductive dechlorination by two strains of sulfate-reducing bacteria., Environmental science & technology 43 (2009) 3155–3161.

[393] S. Bashir, A. Fischer, I. Nijenhuis, H. H. Richnow, Enantioselective carbon stable isotope fractionation of hexachlorocyclohexane during aerobic biodegradation by sphingobium spp., Environmental science & technology 47 (2013) 11432–11439.

[394] I. E. Schilling, R. Hess, J. Bolotin, R. Lal, T. B. Hofstetter, H.-P. E. Kohler, Kinetic isotope effects of the enzymatic transformation of γ-hexachlorocyclohexane by the lindane dehydrochlorinase variants lina1 and lina2., Environmental science & technology 53 (2019) 2353–2363.

[395] I. E. Schilling, C. E. Bopp, R. Lal, H.-P. E. Kohler, T. B. Hofstetter, Assessing aerobic biotransformation of hexachlorocyclohexane isomers by compound-specific isotope analysis., Environmental science & technology (2019).

[396] N. Ivdra, S. Herrero-Martín, A. Fischer, Validation of user- and environmentally friendly extraction and clean-up methods for compound-specific stable carbon isotope analysis of organochlorine pesticides and their metabolites in soils., Journal of chromatography. A 1355 (2014) 36–45.

[397] J. Gui, Z. Chen, Y. tao Zhang, L. Zhang, F.-T. Liu, Novel approach to stable chlorine isotope analysis using gas chromatography-negative chemical ionization mass spectrometry, Analytical Letters 48 (2015) 605–616.

[398] S. Bashir, K. Kuntze, C. Vogt, I. Nijenhuis, Anaerobic biotransformation of hexachlorocyclohexane isomers by dehalococcoides species and an enrichment culture, Biodegradation 29 (2018) 409–418.

[399] Y. Liu, J. Liu, J. Renpenning, I. Nijenhuis, H. H. Richnow, Dual c-cl isotope analysis for characterizing the reductive dechlorination of α- and γ- hexachlorocyclohexane by two dehalococcoides mccartyi strains and an enrichment culture., Environmental science & technology (2020).

[400] C. Gao, Y. Wang, Y. Q. Xia, H. Liu, W. Cheng, Y. L. Xie, Y. Yang, Stable carbon isotope analysis of hexachlorocyclohexanes by liquid–liquid extraction gas chromatography isotope ratio mass spectrometry: Method evaluation and applications, Molecules 27 (2022).

[401] X. Liu, L. Wu, S. Kümmel, H. H. Richnow, Stable isotope fractionation associated with the synthesis of hexachlorocyclohexane isomers for characterizing sources., Chemosphere (2022).

[402] Y. Liu, L. Wu, P. Kohli, R. Kumar, H. Stryhanyuk, I. Nijenhuis, R. Lal, H. H. Richnow, Enantiomer and carbon isotope fractionation of α-hexachlorocyclohexane by sphingobium indicum strain b90a and the corresponding enzymes., Environmental science & technology (2019).

[403] S.-L. Badea, D. I. Stegăruș, V. C. Niculescu, S. Enache, A. Soare, R. E. Ionete, D. Gori, P. Höhener, Dehalogenation of α-hexachlorocyclohexane by iron sulfide nanoparticles: Study of reaction mechanism with stable carbon isotopes and ph variations., The Science of the total environment 801 (2021).

[404] S. Kannath, P. Adamczyk, L. Wu, H. H. Richnow, A. Dybala-Defratyka, Can alkaline hydrolysis of γ-hch serve as a model reaction to study its aerobic enzymatic dehydrochlorination by lina?, International Journal of Molecular Sciences 20 (2019).

[405] X. Liu, A. Yang, S. Kümmel, H. H. Richnow, Uptake and metabolization of hch isomers in trees examined over an annual growth period by compound-specific isotope analysis and enantiomer fractionation., Environmental science & technology (2022).

[406] M. Zhu, Y. Liu, J. Xu, Y. He, Compound-specific stable isotope analysis for characterization of the transformation of γ-hch induced by biochar., Chemosphere (2023).

[407] Y. Liu, J. Fu, L. Wu, S. Kümmel, I. Nijenhuis, H. H. Richnow, Characterization of hexachlorocyclohexane isomer dehydrochlorination by lina1 and lina2 using multi-element compound-specific stable isotope analysis., Environmental science & technology (2022).

[408] X. Liu, S. Kümmel, S. Trapp, H. H. Richnow, Uptake and transformation of hexachlorocyclohexane isomers (hchs) in tree growth rings at a contaminated field site, Environmental Science & Technology 57 (2023) 8776–8784.

[409] M. Aamir, Z. Guo, J. Yu, L. Zhao, D. Xu, X. Sun, C. Xu, L. Niu, W. Liu, Integrating compound-specific stable isotope and enantiomer-specific analysis to characterize the isomeric and enantiomeric signatures of hexachlorocyclohexanes (hchs) in paddy soils., Journal of hazardous materials 459 (2023).

[410] S. Huntscha, T. B. Hofstetter, E. L. Schymanski, S. Spahr, J. Hollender, Biotransformation of benzotriazoles: insights from transformation product identification and compound-specific isotope analysis., Environmental science & technology 48 (2014) 4435–4443.

[411] S. Spahr, S. Huntscha, J. Bolotin, M. P. Maier, M. Elsner, J. Hollender, T. B. Hofstetter, Compound-specific isotope analysis of benzotriazole and its derivatives, Analytical and Bioanalytical Chemistry 405 (2013) 2843–2856.

[412] L. Wu, S. Suchana, R. Flick, S. Kümmel, H. H. Richnow, E. Passeport, Carbon, hydrogen and nitrogen stable isotope fractionation allow characterizing the reaction mechanisms of 1h-benzotriazole aqueous phototransformation., Water research 203 (2021).

[413] C. A. Kelley, B. T. Hammer, R. Coffin, Concentrations and stable isotope values of btex in gasoline-contaminated groundwater, Environmental Science & Technology 31 (1997) 2469–2472.

[414] S. A. Mancini, G. Lacrampe-Couloume, B. S. Lollar, Source differentiation for benzene and chlorobenzene groundwater contamination: A field application of stable carbon and hydrogen isotope analyses, Environmental Forensics 9 (2008) 177 – 186.

[415] S. R. Lutz, B. M. van Breukelen, Combined source apportionment and degradation quantification of organic pollutants with csia: 2. model validation and application., Environmental science & technology 48 (2014) 6229–6236.

[416] L. M. Beckley, T. E. McHugh, P. R. Philp, Utility of compound-specific isotope analysis for vapor intrusion investigations, Groundwater Monitoring & Remediation 36 (2016).

[417] H. H. Richnow, R. U. Meckenstock, Isotopen-geochemisches konzept zur in-situ erfassung des biologischen abbaus in kontaminiertem grundwasser, TerraTech 8 (1999) 38–41.

[418] L. Stehmeier, M. Francis, T. Jack, E. Diegor, L. Winsor, T. Abrajano, Field and in vitro evidence for in-situ bioremediation using compound-specific c-13/c-12 ratio monitoring., Org Geochem 30 (1999) 821–833.

[419] G. C. Bugna, J. P. Chanton, C. A. Kelley, T. B. Stauffer, W. G. Macintyre, E. L. Libelo, A field test of δ13c as a tracer of aerobic hydrocarbon degradation, Organic Geochemistry 35 (2004) 123–135.

[420] G. C. Bugna, J. P. Chanton, T. B. Stauffer, W. G. Macintyre, E. L. Libelo, Partitioning microbial respiration between jet fuel and native organic matter in an organic-rich long time-contaminated aquifer., Chemosphere 60 2 (2005) 177–87.

[421] H. R. Beller, S. R. Kane, T. C. Legler, J. R. McKelvie, B. S. Lollar, F. Pearson, L. M. Balser, D. M. Mackay, Comparative assessments of benzene, toluene, and xylene natural attenuation by quantitative polymerase chain reaction analysis of a catabolic gene, signature metabolites, and compound-specific isotope analysis., Environmental science & technology 42 (2008) 6065–6072.

[422] F. Gelman, R. Binstock, Natural attenuation of mtbe and btex compounds in a petroleum contaminated shallow coastal aquifer, Environmental Chemistry Letters 6 (2008) 259–262.

[423] R. V. Kolhatkar, M. Schnobrich, Land application of sulfate salts for enhanced natural attenuation of benzene in groundwater: A case study, Groundwater Monitoring & Remediation 37 (2017).

[424] E. Moshkovich, Z. Ronen, F. Gelman, O. Dahan, In situ bioremediation of a gasoline-contaminated vadose zone: Implications from direct observations, Vadose Zone Journal 17 (2018).

[425] M. BenIsrael, P. Wanner, R. Aravena, B. L. Parker, E. A. Haack, D. T. Tsao, K. E. Dunfield, Toluene biodegradation in the vadose zone of a poplar phytoremediation system identified using metagenomics and toluene-specific stable carbon isotope analysis, International Journal of Phytoremediation 21 (2019) 60 – 69.

[426] A. Vieth, B. Morasch, R. U. Meckenstock, H. H. Richnow, Charakterisierung des biologischen abbaus von btex im grundwasser über isotopenfraktionierung – feldstudien, TerraTech 5 (2001) 37–41.

[427] S. A. Mancini, G. Lacrampe-Couloume, H. Jonker, B. M. van Breukelen, J. Groen, F. Volkering, B. S. Lollar, Hydrogen isotopic enrichment: an indicator of biodegradation at a petroleum hydrocarbon contaminated field site., Environmental science & technology 36 (2002) 2464–2470.

[428] R. U. Meckenstock, B. Morasch, M. Kästner, A. Vieth, H. H. Richnow, Assessment of bacterial degradation of aromatic hydrocarbons in the environment by analysis of stable carbon isotope fractionation, Water, Air and Soil Pollution: Focus 2 (2002) 141–152.

[429] H. H. Richnow, A. Vieth, M. Kästner, M. Gehre, R. U. Meckenstock, Isotope fractionation of toluene: A perspective to characterise microbial in situ degradation, The Scientific World Journal 2 (2002) 1227 – 1234.

[430] A. Fischer, A. Vieth, K. Knöller, T. Wachter, A. Dahmke, H.-H. Richnow, Charakterisierung des mikrobiellen schadstoffabbaus mithilfe von isotopenchemischen methoden, Grundwasser 9 (2004) 159–172.

[431] A. S. Peter, A. Steinbach, R. Liedl, T. Ptak, W. Michaelis, G. Teutsch, Assessing microbial degradation of o-xylene at field-scale from the reduction in mass flow rate combined with compound-specific isotope analyses., Journal of contaminant hydrology 71 (2004) 127–154.

[432] A. Vieth, M. Kästner, M. Schirmer, H. Weiss, S. H. Gödeke, R. U. Meckenstock, H. H. Richnow, Monitoring in situ biodegradation of benzene and toluene by stable carbon isotope fractionation, Environmental Toxicology and Chemistry 24 (2005).

[433] A. Fischer, J. Bauer, R. U. Meckenstock, W. Stichler, C. Griebler, P. Maloszewski, M. Kästner, H. H. Richnow, A multitracer test proving the reliability of stable isotope fractionation analysis for assessing anaerobic degradation in a btex contaminated aquifer, Environ Sci Technol 40 (2006) 4245–4252.

[434] K. S. Mak, C. Griebler, R. U. Meckenstock, R. Liedl, A. S. Peter, Combined application of conservative transport modelling and compound-specific carbon isotope analyses to assess in situ attenuation of benzene, toluene, and o-xylene., Journal of contaminant hydrology 88 (2006) 306–320.

[435] N. Stelzer, A. Fischer, H.-H. Richnow, M. Kästner, Analyse des anaeroben benzolabbaus: Vergleich von in-situ-mikrokosmen, elektronenakzeptorbilanzen und isotopenfraktionierungsprozessen, Grundwasser 11 (2006) 247–258.

[436] D. Bouchard, D. Hunkeler, P. Gaganis, R. Aravena, P. Höhener, M. M. Broholm, P. Kjeldsen, Carbon isotope fractionation during diffusion and biodegradation of petroleum hydrocarbons in the unsaturated zone: field experiment at vaerløse airbase, denmark, and modeling., Environmental science & technology 42 (2008) 596–601.

[437] J. Batlle-Aguilar, S. Brouyère, A. Dassargues, B. Morasch, D. Hunkeler, P. Höhener, L. Diels, K. Vanbroekhoven, P. Seuntjens, H. Halen, Benzene dispersion and natural attenuation in an alluvial aquifer with strong interactions with surface water, Journal of Hydrology 369 (2009) 305–317.

[438] D. Mäurer, H. Stupp, D. Heinrichs, T. Haupt, H. Eisenmann, Strategien zur behandlung des ckw-btex-grundwasserschadens deponie rondenbarg., altlasten spektrum 5 (2009) 225–232.

[439] H. Prommer, B. Anneser, M. Rolle, F. Einsiedl, C. Griebler, Biogeochemical and isotopic gradients in a btex/pah contaminant plume: model-based interpretation of a high-resolution field data set., Environmental science & technology 43 (2009) 8206–8212.

[440] C. D. Biase, D. L. Reger, A. Schmidt, S. Jechalke, N. Reiche, P. M. Martinez-Lavanchy, M. Rosell, M. van Afferden, U. Maier, S. E. Oswald, M. Thullner, Treatment of volatile organic contaminants in a vertical flow filter: Relevance of different removal processes, Ecological Engineering 37 (2011) 1292–1303.

[441] J. Rakoczy, B. Remy, C. Vogt, H. H. Richnow, A bench-scale constructed wetland as a model to characterize benzene biodegradation processes in freshwater wetlands., Environmental science & technology 45 (2011) 10036–10044.

[442] I. V. Keer, J. Bronders, J. Verhack, J. Schwarzbauer, R. Swennen, Limitations in the use of compound-specific stable isotope analysis to understand the behaviour of a complex btex groundwater contamination near brussels (belgium), Environmental Earth Sciences 66 (2012) 457–470.

[443] J. Batlle-Aguilar, B. Morasch, D. Hunkeler, S. Brouyère, Benzene dynamics and biodegradation in alluvial aquifers affected by river fluctuations, Groundwater 52 (2014).

[444] V. Ponsin, J. Maier, Y. Guelorget, D. Hunkeler, D. Bouchard, H. Villavicencio, P. Höhener, Documentation of time-scales for onset of natural attenuation in an aquifer treated by a crude-oil recovery system., The Science of the total environment 512-513 (2015) 62–73.

[445] T. Gilevska, E. Passeport, M. Shayan, E. S. Seger, E. J. Lutz, K. A. West, S. A. Morgan, E. E. Mack, B. S. Lollar, Determination of in situ biodegradation rates via a novel high resolution isotopic approach in contaminated sediments., Water research 149 (2019) 632–639.

[446] J. R. McKelvie, J. E. Lindstrom, H. R. Beller, S. A. Richmond, B. S. Lollar, Analysis of anaerobic btx biodegradation in a subarctic aquifer using isotopes and benzylsuccinates., Journal of contaminant hydrology 81 (2005) 167–186.

[447] S. Feisthauer, M. Seidel, P. Bombach, S. Traube, K. Knöller, M. Wånge, S. Fachmann, H. H. Richnow, Characterization of the relationship between microbial degradation processes at a hydrocarbon contaminated site using isotopic methods., Journal of contaminant hydrology 133 (2012) 17–29.

[448] W. Xiong, C. Mathies, K. Bradshaw, T. Carlson, K. Tang, Y. Wang, Benzene removal by a novel modification of enhanced anaerobic biostimulation., Water research 46 (2012) 4721–4731.

[449] M. Wei, J. Rakoczy, C. Vogt, F. Harnisch, R. Schumann, H. H. Richnow, Enhancement and monitoring of pollutant removal in a constructed wetland by microbial electrochemical technology., Bioresource technology 196 (2015) 490–499.

[450] M. Shayan, N. R. Thomson, R. Aravena, J. F. Barker, E. L. Madsen, M. Marchesi, C. M. DeRito, D. Bouchard, T. E. Buscheck, R. V. Kolhatkar, E. J. Daniels, Integrated plume treatment using persulfate coupled with microbial sulfate reduction, Groundwater Monitoring & Remediation 38 (2018).

[451] Y. Wei, N. Thomson, M. Marchesi, J. Barker, E. Madsen, R. Kolhatkar, T. Buscheck, D. Hunkeler, C. DeRito, Infiltration of sulfate to enhance sulfate-reducing biodegradation of petroleum hydrocarbons., Ground Water Monit Remed 38 (2018) 73–87.

[452] P. Wanner, R. Aravena, J. Fernandes, M. BenIsrael, E. A. Haack, D. T. Tsao, K. E. Dunfield, B. L. Parker, Assessing toluene biodegradation under temporally varying redox conditions in a fractured bedrock aquifer using stable isotope methods., Water research 165 (2019).

[453] G. Imfeld, F.-D. Kopinke, A. Fischer, H. H. Richnow, Carbon and hydrogen isotope fractionation of benzene and toluene during hydrophobic sorption in multistep batch experiments., Chemosphere 107 (2014) 454–461.

[454] V. Ponsin, T. E. Buscheck, D. Hunkeler, Heart-cutting two-dimensional gas chromatography-isotope ratio mass spectrometry analysis of monoaromatic hydrocarbons in complex groundwater and gas-phase samples., Journal of chromatography. A 1492 (2017) 117–128.

[455] B. M. van Breukelen, Quantifying the degradation and dilution contribution to natural attenuation of contaminants by means of an open system rayleigh equation, Environmental Science & Technology 41 (2007) 4980–4985.

[456] C. Vogt, E. Cyrus, I. Herklotz, D. Schlosser, A. Bahr, S. Herrmann, H. H. Richnow, A. Fischer, Evaluation of toluene degradation pathways by two-dimensional stable isotope fractionation., Environmental science & technology 42 (2008) 7793–800.

[457] A. Fischer, M. Gehre, J. Breitfeld, H. H. Richnow, C. Vogt, Carbon and hydrogen isotope fractionation of benzene during biodegradation under sulfate-reducing conditions: a laboratory to field site approach., Rapid communications in mass spectrometry : RCM 23 (2009) 2439–2447.

[458] S. Herrero-Martín, I. Nijenhuis, H. H. Richnow, M. Gehre, Coupling of a headspace autosampler with a programmed temperature vaporizer for stable carbon and hydrogen isotope analysis of volatile organic compounds at microgram per liter concentrations., Analytical chemistry 87 (2015) 951–959.

[459] V. W. Ebongué, B. Geypens, M. Berglund, P. D. P. Taylor, Headspace solid phase microextraction – gc/c-irms for δ13cvpdb measurements of mono-aromatic hydrocarbons using ea-irms calibration, Isotopes in Environmental and Health Studies 45 (2009) 53 – 58.

[460] H. S. Dempster, B. S. Lollar, S. Feenstra, Tracing organic contaminants in groundwater: A new methodology using compound-specific isotopic analysis, Environmental Science & Technology 31 (1997) 3193–3197.

[461] B. S. Lollar, G. F. Slater, J. M. E. Ahad, B. E. Sleep, J. L. Spivack, M. J. Brennan, P. MacKenzie, Contrasting carbon isotope fractionation during biodegradation of trichloroethylene and toluene: Implications for intrinsic bioremediation, Organic Geochemistry 30 (1999) 813–820.

[462] J. M. E. Ahad, B. S. Lollar, E. A. Edwards, G. F. Slater, B. E. Sleep, Carbon isotope fractionation during anaerobic biodegradation of toluene: Implications for intrinsic bioremediation, Environmental Science & Technology 34 (2000) 892–896.

[463] G. F. Slater, J. M. E. Ahad, B. S. Lollar, ‡, R. Allen-King, B. E. Sleep, Carbon isotope effects resulting from equilibrium sorption of dissolved vocs., Analytical chemistry 72 (2000) 5669–5672.

[464] Y. Wang, Y. Huang, Hydrogen isotopic fractionation of petroleum hydrocarbons during vaporization: implications for assessing artificial and natural remediation of petroleum contamination, Applied Geochemistry 18 (2003) 1641–1651.

[465] R. R. Harrington, S. R. Poulson, J. I. Drever, P. J. S. Colberg, E. F. Kelly, Carbon isotope systematics of monoaromatic hydrocarbons: vaporization and adsorption experiments, Organic Geochemistry 30 (1999) 765–775.

[466] C. Aeppli, M. Berg, T. B. Hofstetter, R. Kipfer, R. P. Schwarzenbach, Simultaneous quantification of polar and non-polar volatile organic compounds in water samples by direct aqueous injection-gas chromatography/mass spectrometry., Journal of chromatography. A 1181 (2008) 116–124.

[467] M. Kampara, M. Thullner, H. H. Richnow, H. Harms, L. Y. Wick, Impact of bioavailability restrictions on microbially induced stable isotope fractionation. 2. experimental evidence., Environmental science & technology 42 (2008) 6552–6558.

[468] N. B. Tobler, T. B. Hofstetter, R. P. Schwarzenbach, Carbon and hydrogen isotope fractionation during anaerobic toluene oxidation by geobacter metallireducens with different fe(iii) phases as terminal electron acceptors., Environmental science & technology 42 (2008) 7786–7792.

[469] A. A. M. Langenhoff, H. H. Richnow, J. Gerritse, Benzene degradation at a site amended with nitrate or chlorate, Bioremediation Journal 13 (2009) 180 – 187.

[470] E. M. Seeger, P. Kuschk, H. Fazekas, P. Grathwohl, M. Kaestner, Bioremediation of benzene-, mtbe- and ammonia-contaminated groundwater with pilot-scale constructed wetlands., Environmental pollution 159 (2011) 3769–3776.

[471] C. Dorer, P. Höhener, N. Hedwig, H. H. Richnow, C. Vogt, Rayleigh-based concept to tackle strong hydrogen fractionation in dual isotope analysis-the example of ethylbenzene degradation by aromatoleum aromaticum., Environmental science & technology 48 (2014) 5788–5797.

[472] B. Jin, M. Rolle, T. Li, S. B. Haderlein, Diffusive fractionation of btex and chlorinated ethenes in aqueous solution: quantification of spatial isotope gradients., Environmental science & technology 48 (2014) 6141–6150.

[473] J. L. Busch-Harris, K. L. Sublette, K. P. Roberts, C. Landrum, A. D. Peacock, G. Davis, D. M. Ogles, W. E. Holmes, D. J. Harris, C. Ota, X. Yang, A. G. Kolhatkar, Bio-traps coupled with molecular biological methods and stable isotope probing demonstrate the in situ biodegradation potential of mtbe and tba in gasoline-contaminated aquifers, Groundwater Monitoring & Remediation 28 (2008).

[474] B. Jin, M. Rolle, Mechanistic approach to multi-element isotope modeling of organic contaminant degradation., Chemosphere 95 (2014) 131–139.

[475] J. A. Ward, J. M. E. Ahad, G. Lacrampe-Couloume, G. F. Slater, E. A. Edwards, B. S. Lollar, Hydrogen isotope fractionation during methanogenic degradation of toluene: Potential for direct verification of bioremediation, Environmental Science & Technology 34 (2000) 4577–4581.

[476] S. A. Mancini, A. C. Ulrich, G. Lacrampe-Couloume, B. E. Sleep, E. A. Edwards, B. S. Lollar, Carbon and hydrogen isotopic fractionation during anaerobic biodegradation of benzene, Applied and Environmental Microbiology 69 (2003) 191 – 198.

[477] R. F. Dias, K. H. Freeman, Carbon isotope analyses of semivolatile organic compounds in aqueous media using solid-phase microextraction and isotope ratio monitoring gc/ms., Analytical chemistry 69 (1997) 944–950.

[478] G. F. Slater, H. S. Dempster, B. S. Lollar, J. M. E. Ahad, Headspace analysis: A new application for isotopic characterization of dissolved organic contaminants, Environmental Science & Technology 33 (1999) 190–194.

[479] M. Elsner, G. L. Couloume, B. S. Lollar, Freezing to preserve groundwater samples and improve headspace quantification limits of water-soluble organic contaminants for carbon isotope analysis., Analytical chemistry 78 (2006) 7528–7534.

[480] S. Herrmann, C. Vogt, A. Fischer, A. Kuppardt, H. H. Richnow, Characterization of anaerobic xylene biodegradation by two-dimensional isotope fractionation analysis., Environmental microbiology reports 1 (2009) 535–544.

[481] H. I. F. Amaral, M. Berg, M. S. Brennwald, M. Hofer, R. Kipfer, (13)c/(12)c analysis of ultra-trace amounts of volatile organic contaminants in groundwater by vacuum extraction., Environmental science & technology 44 (2010) 1023–1029.

[482] S. Jechalke, A. G. Franchini, F. Bastida, P. Bombach, M. Rosell, J. Seifert, M. von Bergen, C. Vogt, H. H. Richnow, Analysis of structure, function, and activity of a benzene-degrading microbial community., FEMS microbiology ecology 85 (2013) 14–26.

[483] F. Centler, F. Heße, M. Thullner, Estimating pathway-specific contributions to biodegradation in aquifers based on dual isotope analysis: theoretical analysis and reactive transport simulations., Journal of contaminant hydrology 152 (2013) 97–116.

[484] D. Bouchard, D. Hunkeler, Solvent-based dissolution method to sample gas-phase volatile organic compounds for compound-specific isotope analysis., Journal of chromatography. A 1325 (2014) 16–22.

[485] E. Passeport, R. C. Landis, S. O. C. Mundle, K. Chu, E. E. Mack, E. J. Lutz, B. S. Lollar, Diffusion sampler for compound specific carbon isotope analysis of dissolved hydrocarbon contaminants., Environmental science & technology 48 (2014) 9582–9590.

[486] C. Dorer, C. Vogt, T. R. Neu, H. Stryhanyuk, H. H. Richnow, Characterization of toluene and ethylbenzene biodegradation under nitrate-, iron(iii)- and manganese(iv)-reducing conditions by compound-specific isotope analysis., Environmental pollution 211 (2016) 271–281.

[487] D. Bouchard, P. Wanner, H. Luo, P. W. McLoughlin, J. K. Henderson, R. J. Pirkle, D. Hunkeler, Optimization of the solvent-based dissolution method to sample volatile organic compound vapors for compound-specific isotope analysis., Journal of chromatography. A 1520 (2017) 23–34.

[488] B. Morasch, H. H. Richnow, B. Schink, R. U. Meckenstock, Stable hydrogen and carbon isotope fractionation during microbial toluene degradation: Mechanistic and environmental aspects, Applied and Environmental Microbiology 67 (2001) 4842 – 4849.

[489] B. Morasch, H. H. Richnow, A. Vieth, B. Schink, R. U. Meckenstock, Stable isotope fractionation caused by glycyl radical enzymes during bacterial degradation of aromatic compounds, Applied and Environmental Microbiology 70 (2004) 2935 – 2940.

[490] S. A. Mancini, S. K. Hirschorn, M. Elsner, G. Lacrampe-Couloume, B. E. Sleep, E. A. Edwards, B. S. Lollar, Effects of trace element concentration on enzyme controlled stable isotope fractionation during aerobic biodegradation of toluene., Environmental science & technology 40 (2006) 7675–7681.

[491] S. Qiu, D. Eckert, O. A. Cirpka, M. Huenniger, P. S. K. Knappett, P. Maloszewski, R. U. Meckenstock, C. Griebler, M. Elsner, Direct experimental evidence of non-first order degradation kinetics and sorption-induced isotopic fractionation in a mesoscale aquifer: 13c/12c analysis of a transient toluene pulse., Environmental science & technology 47 (2013) 6892–6899.

[492] A. M. Khan, L. Y. Wick, M. Thullner, Applying the rayleigh approach for stable isotope-based analysis of voc biodegradation in diffusion-dominated systems., Environmental science & technology 52 (2018) 7785–7795.

[493] M. A. Klisch, T. Kuder, R. P. Philp, T. E. McHugh, Validation of adsorbents for sample preconcentration in compound-specific isotope analysis of common vapor intrusion pollutants., Journal of chromatography. A 1270 (2012) 20–27.

[494] A. Nagel, H. Strauss, M. Stephan, C. Achten, Nachweis von natural attenuation mittels isotopenuntersuchungen an einem ehemaligen kokereistandort, Grundwasser 16 (2011) 235–245.

[495] K. Knöller, C. Vogt, H. H. Richnow, S. M. Weise, Sulfur and oxygen isotope fractionation during benzene, toluene, ethyl benzene, and xylene degradation by sulfate-reducing bacteria., Environmental science & technology 40 (2006) 3879–3885.

[496] C. Schüth, H. Taubald, N. Bolaño, K. Maciejczyk, Carbon and hydrogen isotope effects during sorption of organic contaminants on carbonaceous materials., Journal of contaminant hydrology 64 (2003) 269–281.

[497] F. Sun, J. Peters, M. Thullner, O. A. Cirpka, M. Elsner, Magnitude of diffusion- and transverse dispersion-induced isotope fractionation of organic compounds in aqueous systems, Environmental Science & Technology 55 (2021) 4772 – 4782.

[498] J. M. E. Ahad, G. F. Slater, Carbon isotope effects associated with fenton-like degradation of toluene: potential for differentiation of abiotic and biotic degradation., The Science of the total environment 401 (2008) 194–198.

[499] E. H. Teramoto, C. Vogt, M. P. M. Baessa, L. Polese, A. U. Soriano, H. K. Chang, H. H. Richnow, Dynamics of hydrocarbon mineralization characterized by isotopic analysis at a jet-fuel-contaminated site in subtropical climate., Journal of contaminant hydrology 234 (2020).

[500] C. Müller, K. Knöller, R. Lucas, S. Kleinsteuber, R. Trabitzsch, H. Weiss, R. Stollberg, H. H. Richnow, C. Vogt, Benzene degradation in contaminated aquifers: Enhancing natural attenuation by injecting nitrate., Journal of contaminant hydrology 238 (2020).

[501] A. H. Keller, S. Kleinsteuber, C. Vogt, Anaerobic benzene mineralization by nitrate-reducing and sulfate-reducing microbial consortia enriched from the same site: Comparison of community composition and degradation characteristics, Microbial Ecology 75 (2017) 941 – 953.

[502] J.-R. Feng, H.-G. Ni, A modified method to calculate dual-isotope slopes for the natural attenuation of organic pollutants in the environment, Environmental Science and Pollution Research 28 (2021) 30399–30408.

[503] F. M. Solano, M. Marchesi, N. R. Thomson, D. Bouchard, R. Aravena, Carbon and hydrogen isotope fractionation of benzene, toluene, and o-xylene during chemical oxidation by persulfate, Groundwater Monitoring & Remediation 38 (2018).

[504] T. Gilevska, A. S. Ojeda, S. Kümmel, M. Gehre, E. S. Seger, K. West, S. A. Morgan, E. E. Mack, B. S. Lollar, Multi-element isotopic evidence for monochlorobenzene and benzene degradation under anaerobic conditions in contaminated sediments., Water research 207 (2021).

[505] S. Willach, H. V. Lutze, H. Somnitz, J. Terhalle, N. Stojanović, M. Lüling, M. A. Jochmann, T. B. Hofstetter, T. C. Schmidt, Carbon isotope fractionation of substituted benzene analogs during oxidation with ozone and hydroxyl radicals: How should experimental data be interpreted?, Environmental science & technology (2020).

[506] M. Rostkowski, H. K. V. Schürner, A. E. Sowińska, L. Vasquez, M. Przydacz, M. Elsner, A. Dybala-Defratyka, Isotope effects on the vaporization of organic compounds from an aqueous solution–insight from experiment and computations, The Journal of Physical Chemistry. B 125 (2021) 13868 – 13885.

[507] B. M. van Breukelen, H. Prommer, Beyond the rayleigh equation: reactive transport modeling of isotope fractionation effects to improve quantification of biodegradation., Environmental science & technology 42 (2008) 2457–2463.

[508] D. Hunkeler, N. Andersen, R. Aravena, S. M. Bernasconi, B. J. Butler, Hydrogen and carbon isotope fractionation during aerobic biodegradation of benzene., Environmental science & technology 35 (2001) 3462–3467.

[509] W.-J. Shin, K.-S. Lee, Carbon isotope fractionation of benzene and toluene by progressive evaporation., Rapid communications in mass spectrometry : RCM 24 (2010) 1636–1640.

[510] S. R. Poulson, H. Naraoka, Carbon isotope fractionation during degradation of benzene, trichloroethene, and tetrachloroethene under ultraviolet light, Geochemical Journal 40 (2006) 291–296.

[511] A. Fischer, I. Herklotz, S. Herrmann, M. Thullner, S. A. B. Weelink, A. J. M. Stams, M. Schlömann, H. H. Richnow, C. Vogt, Combined carbon and hydrogen isotope fractionation investigations for elucidating benzene biodegradation pathways., Environmental science & technology 42 (2008) 4356–4363.

[512] F.-D. Kopinke, A. Georgi, M. Voskamp, H. H. Richnow, Carbon isotope fractionation of organic contaminants due to retardation on humic substances: implications for natural attenuation studies in aquifers., Environmental science & technology 39 (2005) 6052–6062.

[513] M. Rolle, B. Jin, Normal and inverse diffusive isotope fractionation of deuterated toluene and benzene in aqueous systems, Environmental Science and Technology Letters 4 (2017) 298–304.

[514] Y. Oba, H. Naraoka, Carbon and hydrogen isotopic fractionation of low molecular weight organic compounds during ultraviolet degradation, Organic Geochemistry 39 (2008) 501–509.

[515] J. Rakoczy, S. Feisthauer, K. Wasmund, P. Bombach, T. R. Neu, C. Vogt, H. H. Richnow, Benzene and sulfide removal from groundwater treated in a microbial fuel cell, Biotechnology and Bioengineering 110 (2013).

[516] P. Höhener, X. Yu, Stable carbon and hydrogen isotope fractionation of dissolved organic groundwater pollutants by equilibrium sorption., Journal of contaminant hydrology 129-130 (2012) 54–61.

[517] D. Bouchard, P. Höhener, D. Hunkeler, Carbon isotope fractionation during volatilization of petroleum hydrocarbons and diffusion across a porous medium: a column experiment., Environmental science & technology 42 (2008) 7801–7806.

[518] T. Aüllo, S. Berlendis, J. F. Lascourreges, D. Dessort, D. Duclerc, S. Saint-Laurent, B. Schraauwers, J. C. Mas, D. Patriarche, C. Boesinger, M. Magot, A. Ranchou-Peyruse, New bio-indicators for long term natural attenuation of monoaromatic compounds in deep terrestrial aquifers, Frontiers in Microbiology 7 (2016).

[519] A. Vieth, H. Wilkes, Deciphering biodegradation effects on light hydrocarbons in crude oils using their stable carbon isotopic composition: A case study from the gullfaks oil field, offshore norway, Geochimica et Cosmochimica Acta 70 (2006) 651–665.

[520] T. Chen, Y. Wu, J. nan Wang, C. Philippe, Assessing the biodegradation of btex and stress response in a bio-permeable reactive barrier using compound-specific isotope analysis, International Journal of Environmental Research and Public Health 19 (2022).

[521] A. M. Khan, M. Gharasoo, L. Y. Wick, M. Thullner, Phase-specific stable isotope fractionation effects during combined gas-liquid phase exchange and biodegradation., Environmental pollution (2022).

[522] Y. Horii, K. Kannan, G. Petrick, T. Gamo, J. Falandysz, N. Yamashita, Congener-specific carbon isotopic analysis of technical pcb and pcn mixtures using two-dimensional gas chromatography-isotope ratio mass spectrometry., Environmental science & technology 39 (2005) 4206–4212.

[523] W. Vetter, S. Gaul, J. Melcher, Improved quality control in gas chromatography interfaced to stable isotope ratio mass spectrometry by application of derivative chromatography., Analytica chimica acta 590 (2007) 49–54.

[524] N. J. Drenzek, T. I. Eglinton, C. O. Wirsen, N. C. Sturchio, L. J. Heraty, K. R. Sowers, Q. Wu, H. D. May, C. M. Reddy, Invariant chlorine isotopic signatures during microbial pcb reductive dechlorination., Environmental pollution 128 (2004) 445–448.

[525] N. J. Drenzek, T. I. Eglinton, C. O. Wirsen, H. D. May, Q. Wu, K. R. Sowers, C. M. Reddy, The absence and application of stable carbon isotopic fractionation during the reductive dechlorination of polychlorinated biphenyls., Environmental science & technology 35 (2001) 3310–3313.

[526] C. Huang, Y. Zeng, X. Luo, Z. Ren, Q. Lu, Y. Tian, S. Gao, S. Wang, S. Harrad, B. Mai, Tracing the sources and microbial degradation of pcbs in field sediments by a multiple-line-of-evidence approach including compound-specific stable isotope analysis., Water research 182 (2020).

[527] M. E. Böttcher, M. Voss, D. E. Schulz-Bull, R. Schneider, T. Leipe, K. Knöller, Environmental changes in the pearl river estuary (china) as reflected by light stable isotopes and organic contaminants, Journal of Marine Systems 82 (2010).

[528] F. Liu, D. Cichocka, I. Nijenhuis, H. H. Richnow, D. E. Fennell, Carbon isotope fractionation during dechlorination of 1,2,3,4-tetrachlorodibenzo-p-dioxin by a dehalococcoides-containing culture., Chemosphere 80 (2010) 1113–1119.

[529] E. Ewald, A. Wagner, I. Nijenhuis, H. H. Richnow, U. Lechner, Microbial dehalogenation of trichlorinated dibenzo-p-dioxins by a dehalococcoides-containing mixed culture is coupled to carbon isotope fractionation., Environmental science & technology 41 (2007) 7744–7751.

[530] M. P. Maier, S. D. Corte, S. Nitsche, T. Spaett, N. Boon, M. Elsner, C & n isotope analysis of diclofenac to distinguish oxidative and reductive transformation and to track commercial products., Environmental science & technology 48 (2014) 2312–2320.

[531] J. Birkigt, T. Gilevska, B. Ricken, H. H. Richnow, D. Vione, P. F.-X. Corvini, I. Nijenhuis, D. Cichocka, Carbon stable isotope fractionation of sulfamethoxazole during biodegradation by microbacterium sp. strain br1 and upon direct photolysis., Environmental science & technology 49 (2015) 6029–6036.

[532] S. Willach, H. V. Lutze, K. Eckey, K. Löppenberg, M. Lüling, J. Terhalle, J. B. Wolbert, M. A. Jochmann, U. Karst, T. C. Schmidt, Degradation of sulfamethoxazole using ozone and chlorine dioxide - compound-specific stable isotope analysis, transformation product analysis and mechanistic aspects., Water research 122 (2017) 280–289.

[533] S. Willach, H. V. Lutze, K. Eckey, K. Löppenberg, M. Lüling, J. B. Wolbert, D. M. Kujawinski, M. A. Jochmann, U. Karst, T. C. Schmidt, Direct photolysis of sulfamethoxazole using various irradiation sources and wavelength ranges-insights from degradation product analysis and compound-specific stable isotope analysis., Environmental science & technology 52 (2018) 1225–1233.

[534] D. M. Kujawinski, L. Zhang, T. C. Schmidt, M. A. Jochmann, When other separation techniques fail: compound-specific carbon isotope ratio analysis of sulfonamide containing pharmaceuticals by high-temperature-liquid chromatography-isotope ratio mass spectrometry., Analytical chemistry 84 (2012) 7656–7663.

[535] K. A. Bennett, S. D. Kelly, X. Tang, B. J. Reid, Potential for natural and enhanced attenuation of sulphanilamide in a contaminated chalk aquifer., Journal of environmental sciences 62 (2017) 39–48.

[536] W. Ouyang, S. Kümmel, L. Adrian, Y. guan Zhu, H. H. Richnow, Carbon and hydrogen stable isotope fractionation of sulfamethoxazole during anaerobic transformation catalyzed by desulfovibrio vulgaris hildenborough., Chemosphere 311 (2022).

[537] R. Coffin, P. H. Miyares, C. A. Kelley, L. A. Cifuentes, C. M. Reynolds, Stable carbon and nitrogen isotope analysis of tnt: Two-dimensional source identification, Environmental Toxicology and Chemistry 20 (2001).

[538] H. I. F. Amaral, J. Fernandes, M. Berg, R. P. Schwarzenbach, R. Kipfer, Assessing tnt and dnt groundwater contamination by compound-specific isotope analysis and 3h-3he groundwater dating: a case study in portugal., Chemosphere 77 (2009) 805–812.

[539] A. Bernstein, E. M. Adar, Z. Ronen, H. Lowag, W. Stichler, R. U. Meckenstock, Quantifying rdx biodegradation in groundwater using delta15n isotope analysis., Journal of contaminant hydrology 111 (2010) 25–35.

[540] S. B. Moshe, Z. Ronen, O. Dahan, A. Bernstein, N. Weisbrod, F. Gelman, E. M. Adar, Isotopic evidence and quantification assessment of in situ rdx biodegradation in the deep unsaturated zone, Soil Biology & Biochemistry 42 (2010) 1253–1262.

[541] P. H. Miyares, C. M. Reynolds, J. C. Pennington, R. Coffin, T. F. Jenkins, L. A. Cifuentes, Using stable isotopes of carbon and nitrogen as in-situ tracers for monitoring the natural attenuation of explosives, in: Using Stable Isotopes of Carbon and Nitrogen as In-Situ Tracers for Monitoring the Natural Attenuation of Explosives, 1999.

[542] J. C. Pennington, J. M. Brannon, D. Gunnison, D. W. Harrelson, M. Zakikhani, P. H. Miyares, T. F. Jenkins, J. U. Clarke, C. A. Hayes, D. Ringleberg, E. Perkins, H. L. Fredrickson, Monitored natural attenuation of explosives, Soil and Sediment Contamination: An International Journal 10 (2001) 45 – 70.

[543] P. B. Hatzinger, M. E. Fuller, N. C. Sturchio, J. K. Böhlke, Validation of stable isotope ratio analysis to document the biodegradation and natural attenuation of rdx, estcp project er-201208, in: Validation of stable isotope ratio analysis to document the biodegradation and natural attenuation of RDX, ESTCP Project ER-201208, 2018.

[544] F. Gelman, A. Kotlyar, D. Chiguala, Z. Ronen, Precise and accurate compound-specific carbon and nitrogen isotope analysis of rdx by gc-irms, International Journal of Environmental Analytical Chemistry 91 (2011) 1392 – 1400.

[545] M. Berg, J. Bolotin, T. B. Hofstetter, Compound-specific nitrogen and carbon isotope analysis of nitroaromatic compounds in aqueous samples using solid-phase microextraction coupled to gc/irms., Analytical chemistry 79 (2007) 2386–2393.

[546] A. Bernstein, Z. Ronen, E. M. Adar, R. Nativ, H. Lowag, W. Stichler, R. U. Meckenstock, Compound-specific isotope analysis of rdx and stable isotope fractionation during aerobic and anaerobic biodegradation., Environmental science & technology 42 (2008) 7772–7777.

[547] M. J. Lott, J. D. Howa, L. A. Chesson, J. R. Ehleringer, Improved accuracy and precision in δ15 nair measurements of explosives, urea, and inorganic nitrates by elemental analyzer/isotope ratio mass spectrometry using thermal decomposition., Rapid communications in mass spectrometry : RCM 29 (2015) 1381–1388.

[548] T. B. Hofstetter, J. C. Spain, S. F. Nishino, J. Bolotin, R. P. Schwarzenbach, Identifying competing aerobic nitrobenzene biodegradation pathways by compound-specific isotope analysis., Environmental science & technology 42 (2008) 4764–4770.

[549] N. B. Tobler, T. B. Hofstetter, R. P. Schwarzenbach, Assessing iron-mediated oxidation of toluene and reduction of nitroaromatic contaminants in anoxic environments using compound-specific isotope analysis., Environmental science & technology 41 (2007) 7773–7780.

[550] A. E. Hartenbach, T. B. Hofstetter, M. Berg, J. Bolotin, R. P. Schwarzenbach, Using nitrogen isotope fractionation to assess abiotic reduction of nitroaromatic compounds., Environmental science & technology 40 (2006) 7710–7716.

[551] B. A. Ulrich, M. L. Palatucci, J. Bolotin, J. C. Spain, T. B. Hofstetter, Different mechanisms of alkaline and enzymatic hydrolysis of the insensitive munition component 2,4-dinitroanisole lead to identical products, Environmental Science & Technology Letters (2018).

[552] Y. Tong, M. J. Berens, B. A. Ulrich, J. Bolotin, J. H. Strehlau, T. B. Hofstetter, W. A. Arnold, Exploring the utility of compound-specific isotope analysis for assessing ferrous iron-mediated reduction of rdx in the subsurface., Environmental science & technology (2020).

[553] M. J. Berens, B. A. Ulrich, J. H. Strehlau, T. B. Hofstetter, W. A. Arnold, Mineral identity, natural organic matter, and repeated contaminant exposures do not affect the carbon and nitrogen isotope fractionation of 2,4-dinitroanisole during abiotic reduction., Environmental science. Processes & impacts 21 (2019) 51–62.

[554] M. E. Fuller, P. G. K. van Groos, M. Jarrett, K. H. Kucharzyk, A. T. Minard-Smith, L. J. Heraty, N. C. Sturchio, Application of a multiple lines of evidence approach to document natural attenuation of hexahydro-1,3,5-trinitro-1,3,5-triazine (rdx) in groundwater., Chemosphere 250 (2020).

[555] R. W. Smith, C. R. Tobias, P. Vlahos, C. Cooper, M. Ballentine, T. Ariyarathna, S. Fallis, T. J. Groshens, Mineralization of rdx-derived nitrogen to n2 via denitrification in coastal marine sediments., Environmental science & technology 49 (2015) 2180–2187.

[556] A. Bernstein, Z. Ronen, F. Gelman, Insight on rdx degradation mechanism by rhodococcus strains using 13c and 15n kinetic isotope effects., Environmental science & technology 47 (2013) 479–484.

[557] M. E. Fuller, L. J. Heraty, C. W. Condee, S. Vainberg, N. C. Sturchio, J. K. Böhlke, P. B. Hatzinger, Relating carbon and nitrogen isotope effects to reaction mechanisms during aerobic or anaerobic degradation of rdx (hexahydro-1,3,5-trinitro-1,3,5-triazine) by pure bacterial cultures, Applied and Environmental Microbiology 82 (2016) 3297 – 3309.

[558] P. Ippoliti, J. Werlich, C. Fuglsby, C. T. Yarnes, C. P. Saunders, J. R. Dettman, Linking ammonium nitrate-aluminum (an-al) post-blast residues to pre-blast explosive materials using isotope ratio and trace elemental analysis for source attribution, Journal of Forensic Sciences 68 (2023) 407 – 415.

[559] S. R. Hlohowskyj, K. Kew, L. A. Stern, C. R. Yamnitz, Forensic discrimination of smokeless powders using carbon and nitrogen isotope ratios., Journal of the American Society for Mass Spectrometry (2023).

[560] G. Oudijk, Compound-specific stable carbon isotope analysis of mtbe in groundwater contamination fingerprinting studies: The use of hydrogeologic principles to assess its validity, Environmental Forensics 9 (2008) 40 – 54.

[561] M. J. Day, T. A. Gulliver, Rate of natural attenuation of tert-butyl alcohol at a chemical plant, Soil and Sediment Contamination: An International Journal 12 (2003) 119 – 138.

[562] M. J. Day, R. Aravena, D. Hunkeler, T. A. Gulliver, Application of carbon isotopes to document biodegradation of t-butyl alcohol under field conditions, Contam Soil Sediment Water (2002) 88–92.

[563] R. V. Kolhatkar, T. Kuder, P. R. Philp, J. Allen, J. T. Wilson, Use of compound-specific stable carbon isotope analyses to demonstrate anaerobic biodegradation of mtbe in groundwater at a gasoline release site., Environmental science & technology 36 (2002) 5139–5146.

[564] M. J. Spence, S. H. Bottrell, S. F. Thornton, H. H. Richnow, K. H. Spence, Hydrochemical and isotopic effects associated with petroleum fuel biodegradation pathways in a chalk aquifer., Journal of contaminant hydrology 79 (2005) 67–88.

[565] J. R. McKelvie, S. K. Hirschorn, G. Lacrampe-Couloume, J. E. Lindstrom, J. F. Braddock, K. T. Finneran, D. A. Trego, B. S. Lollar, Evaluation of tce and mtbe in situ biodegradation: Integrating stable isotope, metabolic intermediate, and microbial lines of evidence, Groundwater Monitoring & Remediation 27 (2007).

[566] S. F. Thornton, S. H. Bottrell, K. H. Spence, R. W. Pickup, M. J. Spence, N. W. Shah, H. Mallinson, H. H. Richnow, Assessment of mtbe biodegradation in contaminated groundwater using 13c and 14c analysis: Field and laboratory microcosm studies, Applied Geochemistry 26 (2011) 828–837.

[567] J. Lu, F. S. Muramoto, P. R. Philp, T. Kuder, Monitoring in situ biodegradation of mtbe using multiple rounds of compound-specific stable carbon isotope analysis, Groundwater Monitoring & Remediation 36 (2016).

[568] M. J. van der Waals, C. F. N. Pijls, A. J. C. Sinke, A. A. M. Langenhoff, H. Smidt, J. Gerritse, Anaerobic degradation of a mixture of mtbe, etbe, tba, and benzene under different redox conditions, Applied Microbiology and Biotechnology 102 (2018) 3387 – 3397.

[569] T. Kuder, J. T. Wilson, P. M. Kaiser, R. V. Kolhatkar, P. R. Philp, J. Allen, Enrichment of stable carbon and hydrogen isotopes during anaerobic biodegradation of mtbe: microcosm and field evidence., Environmental science & technology 39 (2005) 213–220.

[570] J. T. Wilson, R. V. Kolhatkar, T. Kuder, P. R. Philp, S. J. Daugherty, Stable isotope analysis of mtbe to evaluate the source of tba in ground water, Groundwater Monitoring & Remediation 25 (2005).

[571] L. Zwank, M. Berg, M. Elsner, T. C. Schmidt, R. P. Schwarzenbach, S. B. Haderlein, New evaluation scheme for two-dimensional isotope analysis to decipher biodegradation processes: application to groundwater contamination by mtbe., Environmental science & technology 39 (2005) 1018–1029.

[572] J. R. McKelvie, D. M. Mackay, N. R. de Sieyes, G. Lacrampe-Couloume, B. S. Lollar, Quantifying mtbe biodegradation in the vandenberg air force base ethanol release study using stable carbon isotopes., Journal of contaminant hydrology 94 (2007) 157–165.

[573] A. Gafni, R. Rosenzweig, F. Gelman, Z. Ronen, Anaerobic biodegradation of mtbe in a field site above the israeli coastal aquifer: evidence from δ13c compound-specific isotope analysis, Journal of Chemical Technology & Biotechnology 91 (2016) 1638–1645.

[574] M. Berg, L. Zwank, J. Bolotin, C. Aeppli, A. Häner, M. Möller, C. Munz, U. Ziegler, Einzelstoff-isotopenanalyse zur beurteilung des abbauverhaltens von methyl- tert-butylether (mtbe) an einem altlastenstandort, Altlasten Spektrum 1 (2005) 20–26.

[575] L. E. Lesser, P. C. Johnson, R. Aravena, G. E. Spinnler, C. L. Bruce, J. P. Salanitro, An evaluation of compound-specific isotope analyses for assessing the biodegradation of mtbe at port hueneme, ca., Environmental science & technology 42 (2008) 6637–6643.

[576] D. M. Kujawinski, M. Stephan, M. A. Jochmann, K. Krajenke, J. Haas, T. C. Schmidt, Stable carbon and hydrogen isotope analysis of methyl tert-butyl ether and tert-amyl methyl ether by purge and trap-gas chromatography-isotope ratio mass spectrometry: method evaluation and application., Journal of environmental monitoring : JEM 12 (2010) 347–354.

[577] S. Jechalke, M. Rosell, P. M. Martinez-Lavanchy, P. Pérez-Leiva, T. Rohwerder, C. Vogt, H. H. Richnow, Linking low-level stable isotope fractionation to expression of the cytochrome p450 monooxygenase-encoding ethb gene for elucidation of methyl tert-butyl ether biodegradation in aerated treatment pond systems, Applied and Environmental Microbiology 77 (2010) 1086 – 1096.

[578] F. Fayolle-Guichard, J. Durand, M. Cheucle, M. Rosell, R. J. Michelland, J.-P. Tracol, F. L. Roux, G. Grundman, O. Atteia, H. H. Richnow, A. Dumestre, Y. Benoit, Study of an aquifer contaminated by ethyl tert-butyl ether (etbe): site characterization and on-site bioremediation., Journal of hazardous materials 201-202 (2012) 236–243.

[579] P. Bombach, N. Nägele, M. Rosell, H. H. Richnow, A. Fischer, Evaluation of ethyl tert-butyl ether biodegradation in a contaminated aquifer by compound-specific isotope analysis and in situ microcosms., Journal of hazardous materials 286 (2015) 100–106.

[580] F. Bastida, M. Rosell, A. G. Franchini, J. Seifert, S. Finsterbusch, N. Jehmlich, S. Jechalke, M. von Bergen, H. H. Richnow, Elucidating mtbe degradation in a mixed consortium using a multidisciplinary approach., FEMS microbiology ecology 73 (2010) 370–384.

[581] L. K. G. Youngster, M. Rosell, H. H. Richnow, M. M. Häggblom, Assessment of mtbe biodegradation pathways by two-dimensional isotope analysis in mixed bacterial consortia under different redox conditions, Applied Microbiology and Biotechnology 88 (2010) 309–317.

[582] D. Hunkeler, B. J. Butler, R. Aravena, J. F. Barker, Monitoring biodegradation of methyl tert-butyl ether (mtbe) using compound-specific carbon isotope analysis., Environmental science & technology 35 (2001) 676–681.

[583] B. J. Smallwood, R. P. Philp, T. W. Burgoyne, J. Allen, The use of stable isotopes to differentiate specific source markers for mtbe, Environmental Forensics 2 (2001) 215 – 221.

[584] P. Somsamak, H. H. Richnow, M. M. Häggblom, Carbon isotope fractionation during anaerobic degradation of methyl tert-butyl ether under sulfate-reducing and methanogenic conditions, Applied and Environmental Microbiology 72 (2006) 1157 – 1163.

[585] B. M. van Breukelen, Extending the rayleigh equation to allow competing isotope fractionating pathways to improve quantification of biodegradation, Environmental Science & Technology 41 (2007) 4004–4010.

[586] J. B. Eweis, E. M. Labolle, D. A. Benson, G. E. Fogg, Role of volatilization in changing tba and mtbe concentrations at mtbe-contaminated sites., Environmental science & technology 41 (2007) 6822–6827.

[587] T. Kuder, P. R. Philp, J. Allen, Effects of volatilization on carbon and hydrogen isotope ratios of mtbe., Environmental science & technology 43 6 (2009) 1763–8.

[588] C. Gauchotte, G. O'Sullivan, S. Davis, R. M. Kalin, Development of an advanced on-line position-specific stable carbon isotope system and application to methyl tert-butyl ether., Rapid communications in mass spectrometry : RCM 23 (2009) 3183–3193.

[589] L. K. G. Youngster, L. J. Kerkhof, M. M. Häggblom, Community characterization of anaerobic methyl tert-butyl ether (mtbe)-degrading enrichment cultures., FEMS microbiology ecology 72 (2010) 279–288.

[590] K. P. North, D. M. Mackay, M. D. Annable, K. L. Sublette, G. B. Davis, R. B. Holland, D. Petersen, K. M. Scow, An ex situ evaluation of tba- and mtbe-baited bio-traps., Water research 46 (2012) 3879–3888.

[591] T. Liu, H. Ahn, W. Sun, L. R. McGuinness, L. J. Kerkhof, M. M. Häggblom, Identification of a ruminococcaceae species as the methyl tert-butyl ether (mtbe) degrading bacterium in a methanogenic consortium., Environmental science & technology 50 (2016) 1455–1464.

[592] M. Rosell, D. Barceló, T. Rohwerder, U. Breuer, M. Gehre, H. H. Richnow, Variations in 13c/12c and d/h enrichment factors of aerobic bacterial fuel oxygenate degradation., Environmental science & technology 41 (2007) 2036–2043.

[593] M. Rosell, R. Gonzalez-Olmos, T. Rohwerder, K. Rusevova, A. Georgi, F.-D. Kopinke, H. H. Richnow, Critical evaluation of the 2d-csia scheme for distinguishing fuel oxygenate degradation reaction mechanisms., Environmental science & technology 46 (2012) 4757–4766.

[594] N. Zhang, J. Schindelka, H. Herrmann, C. George, M. Rosell, S. Herrero-Martín, P. Klán, H. H. Richnow, Investigation of humic substance photosensitized reactions via carbon and hydrogen isotope fractionation., Environmental science & technology 49 (2015) 233–242.

[595] J. R. McKelvie, M. R. Hyman, M. Elsner, C. A. Smith, D. Aslett, G. Lacrampe-Couloume, B. S. Lollar, Isotopic fractionation of methyl tert-butyl ether suggests different initial reaction mechanisms during aerobic biodegradation., Environmental science & technology 43 (2009) 2793–2799.

[596] T. C. Schmidt, M. Schirmer, H. Weiss, S. B. Haderlein, Microbial degradation of methyl tert-butyl ether and tert-butyl alcohol in the subsurface., Journal of contaminant hydrology 70 (2004) 173–203.

[597] S. Heo, W.-J. Shin, S.-W. Lee, Y.-S. Bong, K.-S. Lee, Using stable isotope analysis to discriminate gasoline on the basis of its origin., Rapid communications in mass spectrometry 26 (2012) 517–522.

[598] J. R. McKelvie, M. Elsner, A. J. Simpson, B. S. Lollar, M. J. Simpson, Quantitative site-specific (2)h nmr investigation of mtbe: potential for assessing contaminant sources and fate., Environmental science & technology 44 (2010) 1062–1068.

[599] P. Somsamak, H. H. Richnow, M. M. Häggblom, Carbon isotopic fractionation during anaerobic biotransformation of methyl tert-butyl ether and tert-amyl methyl ether., Environmental science & technology 39 (2005) 103–109.

[600] W.-J. Shin, S.-W. Lee, S. Heo, K.-S. Lee, Stable isotopic fingerprinting for identification of the methyl tert-butyl ether (mtbe) manufacturer, Environmental Forensics 14 (2013) 36 – 41.

[601] M. Rosell, S. Finsterbusch, S. Jechalke, T. Hübschmann, C. Vogt, H. H. Richnow, Evaluation of the effects of low oxygen concentration on stable isotope fractionation during aerobic mtbe biodegradation., Environmental science & technology 44 (2010) 309–315.

[602] M. Elsner, J. McKelvie, G. L. Couloume, B. S. Lollar, Insight into methyl tert-butyl ether (mtbe) stable isotope fractionation from abiotic reference experiments, Environ. Sci. Technol. 41 (2007) 5693–5700.

[603] G. O'Sullivan, R. M. Kalin, Investigation of the range of carbon and hydrogen isotopes within a global set of gasolines, Environmental Forensics 9 (2008) 166 – 176.

[604] P. Tremblay, M. M. Savard, A. S. Smirnoff, R. Paquin, Membrane permeation continuous-flow isotope ratio mass spectrometry for on-line carbon isotope ratio determination., Rapid communications in mass spectrometry : RCM 23 14 (2009) 2213–20.

[605] D. Bouchard, P. Höhener, D. Gori, D. Hunkeler, T. E. Buscheck, Stable carbon and hydrogen isotope fractionation of volatile organic compounds caused by vapor-liquid equilibrium., Chemosphere (2022).

[606] L. Ji, H. Zhang, W. Ding, R. Song, Y. Han, H. Yu, P. Paneth, Theoretical kinetic isotope effects in establishing the precise biodegradation mechanisms of organic pollutants., Environmental science & technology (2023).

[607] D. Hunkeler, N. Chollet, X. Pittet, R. Aravena, J. A. Cherry, B. L. Parker, Effect of source variability and transport processes on carbon isotope ratios of tce and pce in two sandy aquifers., Journal of contaminant hydrology 74 (2004) 265–822.

[608] M. Blessing, T. C. Schmidt, R. Dinkel, S. B. Haderlein, Delineation of multiple chlorinated ethene sources in an industrialized area–a forensic field study using compound-specific isotope analysis., Environmental science & technology 43 (2009) 2701–2707.

[609] D. Hunkeler, R. Aravena, O. Shouakar-Stash, N. Weisbrod, A. Nasser, L. Netzer, D. Ronen, Carbon and chlorine isotope ratios of chlorinated ethenes migrating through a thick unsaturated zone of a sandy aquifer., Environmental science & technology 45 (2011) 8247–8253.

[610] T. E. McHugh, T. Kuder, S. L. Fiorenza, K. A. Gorder, E. M. Dettenmaier, P. R. Philp, Application of csia to distinguish between vapor intrusion and indoor sources of vocs., Environmental science & technology 45 (2011) 5952–5958.

[611] M. F. Filippini, I. Nijenhuis, S. Kümmel, V. Chiarini, G. F. Crosta, H. H. Richnow, A. Gargini, Multi-element compound specific stable isotope analysis of chlorinated aliphatic contaminants derived from chlorinated pitches., The Science of the total environment 640-641 (2018) 153–162.

[612] S. M. Eberts, C. L. Braun, S. A. Jones, Compound-specific isotope analysis: Questioning the origins of a trichloroethene plume, Environmental Forensics 9 (2008) 85 – 95.

[613] I. Nijenhuis, M. Schmidt, E. Pellegatti, E. Paramatti, H. H. Richnow, A. Gargini, A stable isotope approach for source apportionment of chlorinated ethene plumes at a complex multi-contamination events urban site., Journal of contaminant hydrology 153 (2013) 92–105.

[614] A. Badin, M. Schirmer, C. Wermeille, D. Hunkeler, Perchlorethen-quellendifferenzierung mittels kohlenstoff-chlor-isotopenanalyse: Felduntersuchungen zur beurteilung der variabilität der isotopensignatur, Grundwasser 20 (2015) 263–270.

[615] K. Beneteau, R. Aravena, S. K. Frape, Isotopic characterization of chlorinated solvents—laboratory and field results, Organic Geochemistry 30 (1999) 739–753.

[616] Y. Y. Wang, G. J. Smith, Advanced site diagnostic tool 3d-csia for in situ remediation., Remediation Journal 21 (2010) 79–96.

[617] Y. Y. Wang, Chlorinated hydrocarbon–contaminated site investigation with optimized 3d-csia approach, Remediation Journal 23 (2013) 111–120.

[618] S. O. C. Mundle, T. Johnson, G. Lacrampe-Couloume, A. P. de Mora, M. Duhamel, E. A. Edwards, M. L. McMaster, E. E. Cox, K. M. Révész, B. S. Lollar, Monitoring biodegradation of ethene and bioremediation of chlorinated ethenes at a contaminated site using compound-specific isotope analysis (csia)., Environmental science & technology 46 (2012) 1731–1738.

[619] I. N. Damgaard, P. L. Bjerg, J. Bælum, C. Scheutz, D. Hunkeler, C. S. Jacobsen, N. Tuxen, M. M. Broholm, Identification of chlorinated solvents degradation zones in clay till by high resolution chemical, microbial and compound specific isotope analysis., Journal of contaminant hydrology 146 (2013) 37–50.

[620] D. Puigserver, J. M. Nieto, M. Grifoll, J. Vila, A. Cortés, M. Viladevall, B. L. Parker, J. M. Carmona, Temporal hydrochemical and microbial variations in microcosm experiments from sites contaminated with chloromethanes under biostimulation with lactic acid, Bioremediation Journal 20 (2016) 54 – 70.

[621] H. J. Kirchholtes, M. Bauer, U. Schollenberger, S. Spitzberg, W. Ufrecht, Untersuchung eines lhkw-schadens im festgestein unter berücksichtigung von natural attenuation—ergebnisse und folgerungen aus einer feldstudie, Grundwasser 9 (2004) 119–126.

[622] N. Vanstone, A. Przepiora, J. L. Vogan, G. Lacrampe-Couloume, B. G. Powers, E. Perez, S. A. Mabury, B. S. Lollar, Monitoring trichloroethene remediation at an iron permeable reactive barrier using stable carbon isotopic analysis., Journal of contaminant hydrology 78 (2005) 313–325.

[623] S. W. Chapman, B. L. Parker, J. A. Cherry, R. Aravena, D. Hunkeler, Groundwater-surface water interaction and its role on tce groundwater plume attenuation., Journal of contaminant hydrology 91 (2007) 203–232.

[624] I. Nijenhuis, M. Nikolausz, A. Köth, T. Felföldi, H. Weiss, J. Drangmeister, J. Grossmann, M. Kästner, H. H. Richnow, Assessment of the natural attenuation of chlorinated ethenes in an anaerobic contaminated aquifer in the bitterfeld/wolfen area using stable isotope techniques, microcosm studies and molecular biomarkers., Chemosphere 67 (2007) 300–311.

[625] G. Imfeld, I. Nijenhuis, M. Nikolausz, S. Zeiger, H. Paschke, J. Drangmeister, J. Grossmann, H. H. Richnow, S. Weber, Assessment of in situ degradation of chlorinated ethenes and bacterial community structure in a complex contaminated groundwater system., Water research 42 (2008) 871–882.

[626] P. L. Morrill, B. E. Sleep, D. Seepersad, M. L. McMaster, E. D. Hood, C. A. Lebrón, D. W. Major, E. A. Edwards, B. S. Lollar, Variations in expression of carbon isotope fractionation of chlorinated ethenes during biologically enhanced pce dissolution close to a source zone., Journal of contaminant hydrology 110 (2009) 60–71.

[627] C. Courbet, A. Rivière, S. Jeannottat, S. Rinaldi, D. Hunkeler, H. Bendjoudi, G. de Marsily, Complementing approaches to demonstrate chlorinated solvent biodegradation in a complex pollution plume: Mass balance, pcr and compound-specific stable isotope analysis., Journal of contaminant hydrology 126 (2011) 315–329.

[628] K. M. Révész, B. S. Lollar, J. D. Kirshtein, C. R. Tiedeman, T. E. Imbrigiotta, D. J. Goode, A. M. Shapiro, M. A. Voytek, P. J. Lacombe, E. Busenberg, Integration of stable carbon isotope, microbial community, dissolved hydrogen gas, and 2hh2o tracer data to assess bioaugmentation for chlorinated ethene degradation in fractured rocks., Journal of contaminant hydrology 156 (2014) 62–77.

[629] S.-S. Lee, D. Kaown, K. K. Lee, Evaluation of the fate and transport of chlorinated ethenes in a complex groundwater system discharging to a stream in wonju, korea., Journal of contaminant hydrology 182 (2015) 231–243.

[630] M. F. Filippini, A. Amorosi, B. Campo, S. Herrero-Martín, I. Nijenhuis, B. L. Parker, A. Gargini, Origin of vc-only plumes from naturally enhanced dechlorination in a peat-rich hydrogeologic setting., Journal of contaminant hydrology 192 (2016) 129–139.

[631] J. E. Hallsworth, S. Atashgahi, Y. Lu, Y. Zheng, E. Saccenti, M. Suárez-Diez, J. Ramiro-García, H. Eisenmann, M. Elsner, A. J. Stams, D. Springael, W. Dejonghe, H. Smidt, Geochemical and microbial community determinants of reductive dechlorination at a site biostimulated with glycerol, Environmental Microbiology 19 (2017) 968–981.

[632] A. A. Pierce, S. W. Chapman, L. K. Zimmerman, J. C. Hurley, R. Aravena, J. A. Cherry, B. L. Parker, Dfn-m field characterization of sandstone for a process-based site conceptual model and numerical simulations of tce transport with degradation., Journal of contaminant hydrology 212 (2018) 96–114.

[633] C. E. Schaefer, D. R. Lippincott, H. Klammler, K. Hatfield, Evidence of rock matrix back-diffusion and abiotic dechlorination using a field testing approach., Journal of contaminant hydrology 209 (2018) 33–41.

[634] M. Vogel, I. Nijenhuis, J. R. Lloyd, C. Boothman, M. Pöritz, K. Mackenzie, Combined chemical and microbiological degradation of tetrachloroethene during the application of carbo-iron at a contaminated field site., The Science of the total environment 628-629 (2018) 1027–1036.

[635] N. Blázquez-Pallí, M. Rosell, J. Varias, M. Bosch, A. Soler, T. Vicent, E. Marco-Urrea, Multi-method assessment of the intrinsic biodegradation potential of an aquifer contaminated with chlorinated ethenes at an industrial area in barcelona (spain)., Environmental pollution 244 (2019) 165–173.

[636] D. Buchner, M. Schweikhart, S. Behrens, T. Schöndorf, C. Laskov, S. B. Haderlein, Sanierung eines pce-schadens in einem makroskopisch oxischen grundwasserleiter durch stimulation anaerober dehalogenierender bakterien, Grundwasser 24 (2019) 51–63.

[637] P. M. Richards, Y.-R. Liang, R. L. Johnson, T. E. Mattes, Cryogenic soil coring reveals coexistence of aerobic and anaerobic vinyl chloride degrading bacteria in a chlorinated ethene contaminated aquifer., Water research 157 (2019) 281–291.

[638] N. C. Sturchio, J. L. Clausen, L. J. Heraty, L. Huang, B. D. Holt, T. A. Abrajano, Chlorine isotope investigation of natural attenuation of trichloroethene in an aerobic aquifer, Environmental Science & Technology 32 (1998) 3037–3042.

[639] D. Hunkeler, R. Aravena, B. J. Butler, Monitoring microbial dechlorination of tetrachloroethene (pce) in groundwater using compound-specific stable carbon isotope ratios: Microcosm and field studies, Environmental Science & Technology 33 (1999) 2733–2738.

[640] D. L. Song, M. E. Conrad, K. S. Sorenson, L. Alvarez-Cohen, Stable carbon isotope fractionation during enhanced in situ bioremediation of trichloroethene., Environmental science & technology 36 (2002) 2262–2268.

[641] B. C. Kirtland, C. M. Aelion, P. A. Stone, D. Hunkeler, Isotopic and geochemical assessment of in situ biodegradation of chlorinated hydrocarbons., Environmental science & technology 37 (2003) 4205–4212.

[642] C. Carreón-Diazconti, J. Santamaría, J. Berkompas, J. A. Field, M. L. Brusseau, Assessment of in situ reductive dechlorination using compound-specific stable isotopes, functional gene pcr, and geochemical data., Environmental science & technology 43 (2009) 4301–4307.

[643] T. Kuhn, K. Hamonts, J. A. van Dijk, H. Kalka, W. Stichler, D. Springael, W. Dejonghe, R. U. Meckenstock, Assessment of the intrinsic bioremediation capacity of an eutrophic river sediment polluted by discharging chlorinated aliphatic hydrocarbons: a compound-specific isotope approach., Environmental science & technology 43 (2009) 5263–5269.

[644] P. W. McLoughlin, A. D. Peacock, R. J. Pirkle, J. T. Wilson, R. W. McCracken, Csia of tce and daughter products with multiple sources, multiple attenuation mechanisms, and low ethene, Remediation Journal 25 (2014) 11–21.

[645] M. Velimirovic, T. Tosco, M. Uyttebroek, M. Luna, F. Gastone, C. de Boer, N. Klaas, H. Sapion, H. Eisenmann, P. olof Larsson, J. Braun, R. Sethi, L. Bastiaens, Field assessment of guar gum stabilized microscale zerovalent iron particles for in-situ remediation of 1,1,1-trichloroethane., Journal of contaminant hydrology 164 (2014) 88–99.

[646] A. T. Sonne, U. S. McKnight, V. K. Rønde, P. L. Bjerg, Assessing the chemical contamination dynamics in a mixed land use stream system., Water research 125 (2017) 141–151.

[647] R. T. Wilkin, T. R. Lee, M. Sexton, S. D. Acree, R. W. Puls, D. W. Blowes, C. Kalinowski, J. M. Tilton, L. L. Woods, Geochemical and isotope study of trichloroethene degradation in a zero-valent iron permeable reactive barrier: A twenty-two-year performance evaluation., Environmental science & technology 53 (2018) 296–306.

[648] K. E. Pooley, M. Blessing, T. C. Schmidt, S. B. Haderlein, K. T. B. MacQuarrie, H. Prommer, Aerobic biodegradation of chlorinated ethenes in a fractured bedrock aquifer: quantitative assessment by compound-specific isotope analysis (csia) and reactive transport modeling., Environmental science & technology 43 (2009) 7458–7464.

[649] H. I. F. Amaral, C. Aeppli, R. Kipfer, M. Berg, Assessing the transformation of chlorinated ethenes in aquifers with limited potential for natural attenuation: added values of compound-specific carbon isotope analysis and groundwater dating., Chemosphere 85 (2011) 774–781.

[650] M. M. Broholm, D. Hunkeler, N. Tuxen, S. Jeannottat, C. Scheutz, Stable carbon isotope analysis to distinguish biotic and abiotic degradation of 1,1,1-trichloroethane in groundwater sediments., Chemosphere 108 (2014) 265–273.

[651] L. Hermon, J. Denonfoux, J. Hellal, C. Joulian, S. Ferreira, S. Vuilleumier, G. Imfeld, Dichloromethane biodegradation in multi-contaminated groundwater: Insights from biomolecular and compound-specific isotope analyses., Water research 142 (2018) 217–226.

[652] P. Wanner, B. L. Parker, S. W. Chapman, G. da Penha Lima, G. da Penha Lima, A. Gilmore, E. E. Mack, R. Aravena, R. Aravena, Identification of degradation pathways of chlorohydrocarbons in saturated low-permeability sediments using compound-specific isotope analysis., Environmental science & technology 52 (2018) 7296–7306.

[653] A. Vieth, J. Müller, G. Strauch, M. Kästner, M. Gehre, R. U. Meckenstock, H. H. Richnow, In-situ biodegradation of tetrachloroethene and trichloroethene in contaminated aquifers monitored by stable isotope fractionation, Isotopes in Environmental and Health Studies 39 (2003) 113 – 124.

[654] P. L. Morrill, G. Lacrampe-Couloume, G. F. Slater, B. E. Sleep, E. A. Edwards, M. L. McMaster, D. W. Major, B. S. Lollar, Quantifying chlorinated ethene degradation during reductive dechlorination at kelly afb using stable carbon isotopes., Journal of contaminant hydrology 76 (2005) 279–293.

[655] H. Martin, M. Heidinger, S. Ertl, L. Eichinger, A. Tiehm, K. Schmidt, U. Karch, J. Leve, 13c isotopenuntersuchungen zur bestimmung von natural attenuation – abgrenzung und charakterisierung eines ckw-schadens am standort frankenthal, TerraTech 3 (2006) 14–17.

[656] S. K. Hirschorn, A. Grostern, G. Lacrampe-Couloume, E. A. Edwards, L. Mackinnon, C. Repta, D. W. Major, B. S. Lollar, Quantification of biotransformation of chlorinated hydrocarbons in a biostimulation study: added value via stable carbon isotope analysis., Journal of contaminant hydrology 94 (2007) 249–260.

[657] B. M. Patterson, R. Aravena, G. B. Davis, A. Furness, T. P. Bastow, D. Bouchard, Multiple lines of evidence to demonstrate vinyl chloride aerobic biodegradation in the vadose zone, and factors controlling rates., Journal of contaminant hydrology 153 (2013) 69–77.

[658] D. Hunkeler, R. Aravena, B. L. Parker, J. A. Cherry, X. Diao, Monitoring oxidation of chlorinated ethenes by permanganate in groundwater using stable isotopes: laboratory and field studies., Environmental science & technology 37 (2003) 798–804.

[659] M. M. G. Chartrand, P. L. Morrill, G. Lacrampe-Couloume, B. S. Lollar, Stable isotope evidence for biodegradation of chlorinated ethenes at a fractured bedrock site., Environmental science & technology 39 (2005) 4848–4856.

[660] D. Hunkeler, R. Aravena, K. Berry-Spark, E. E. Cox, Assessment of degradation pathways in an aquifer with mixed chlorinated hydrocarbon contamination using stable isotope analysis., Environmental science & technology 39 (2005) 5975–5981.

[661] Y. Abe, R. Aravena, J. Zopfi, B. L. Parker, D. Hunkeler, Evaluating the fate of chlorinated ethenes in streambed sediments by combining stable isotope, geochemical and microbial methods., Journal of contaminant hydrology 107 (2009) 10–21.

[662] K. Hamonts, T. Kuhn, J. Vos, M. Maesen, H. Kalka, H. Smidt, D. Springael, R. U. Meckenstock, W. Dejonghe, Temporal variations in natural attenuation of chlorinated aliphatic hydrocarbons in eutrophic river sediments impacted by a contaminated groundwater plume., Water research 46 (2012) 1873–1888.

[663] T. Appelo, M. Rolle, A reactive multicomponent transport model for saturated porous media long-term impacts on groundwater and reductive dechlorination following bioremediation in a highly characterized trichloroethene dnapl source area, Ground Water 48 (2010) 627–632.

[664] C. Torrentó, C. Audí-Miró, G. Bordeleau, M. Marchesi, M. Rosell, N. Otero, A. Soler, The use of alkaline hydrolysis as a novel strategy for chloroform remediation: the feasibility of using construction wastes and evaluation of carbon isotopic fractionation., Environmental science & technology 48 (2014) 1869–1877.

[665] D. Hunkeler, Y. Abe, M. M. Broholm, S. Jeannottat, C. Westergaard, C. S. Jacobsen, R. Aravena, P. L. Bjerg, Assessing chlorinated ethene degradation in a large scale contaminant plume by dual carbon-chlorine isotope analysis and quantitative pcr., Journal of contaminant hydrology 119 (2011) 69–79.

[666] P. Lojkasek-Lima, R. Aravena, B. L. Parker, J. A. Cherry, Fingerprinting tce in a bedrock aquifer using compound-specific isotope analysis, Groundwater 50 (2012).

[667] P. Lojkasek-Lima, R. Aravena, O. Shouakar-Stash, S. K. Frape, M. Marchesi, S. L. Fiorenza, J. L. Vogan, Evaluating tce abiotic and biotic degradation pathways in a permeable reactive barrier using compound specific isotope analysis, Groundwater Monitoring & Remediation 32 (2012).

[668] C. Wiegert, C. Aeppli, T. D. J. Knowles, H. Holmstrand, R. P. Evershed, R. D. Pancost, J. Macháckova, Ö. Gustafsson, Dual carbon-chlorine stable isotope investigation of sources and fate of chlorinated ethenes in contaminated groundwater., Environmental science & technology 46 (2012) 10918–10925.

[669] M. Petitta, E. Pacioni, C. Sbarbati, G. Corvatta, M. F. Fanelli, R. Aravena, Hydrodynamic and isotopic characterization of a site contaminated by chlorinated solvents: Chienti river valley, central italy, Applied Geochemistry 32 (2013) 164–174.

[670] C. Audí-Miró, S. Cretnik, C. Torrentó, M. Rosell, O. Shouakar-Stash, N. Otero, J. Palau, M. Elsner, A. Soler, C, cl and h compound-specific isotope analysis to assess natural versus fe(0) barrier-induced degradation of chlorinated ethenes at a contaminated site., Journal of hazardous materials 299 (2015) 747–754.

[671] D. Kaown, S.-C. Jun, R. Kim, S. Woosik, K. K. Lee, Characterization of a site contaminated by chlorinated ethenes and ethanes using multi-analysis, Environmental Earth Sciences 75 (2016) 1–13.

[672] J. Palau, P. Jamin, A. Badin, N. Vanhecke, B. Haerens, S. Brouyère, D. Hunkeler, Use of dual carbon-chlorine isotope analysis to assess the degradation pathways of 1,1,1-trichloroethane in groundwater., Water research 92 (2016) 235–243.

[673] J. A. Clark, R. L. Stotler, S. K. Frape, W. A. Illman, Compound-specific isotope analyses to assess tce biodegradation in a fractured dolomitic aquifer, Groundwater 55 (2017).

[674] E. Doğan-Subaşı, M. Elsner, S. Qiu, S. Cretnik, S. Atashgahi, O. Shouakar-Stash, N. Boon, W. Dejonghe, L. Bastiaens, Contrasting dual (c, cl) isotope fractionation offers potential to distinguish reductive chloroethene transformation from breakdown by permanganate., The Science of the total environment 596-597 (2017) 169–177.

[675] A. A. Schiefler, D. J. Tobler, N. D. Overheu, N. Tuxen, Extent of natural attenuation of chlorinated ethenes at a contaminated site in denmark, Energy Procedia (2018).

[676] D. C. Segal, T. Kuder, R. V. Kolhatkar, Assessment of anaerobic biodegradation of bis(2-chloroethyl) ether in groundwater using carbon and chlorine compound-specific isotope analysis., The Science of the total environment 625 (2018) 696–705.

[677] G. Imfeld, C. E. Aragonés, S. Zeiger, C. V. von Eckstaedt, H. Paschke, R. Trabitzsch, H. Weiss, H. H. Richnow, Tracking in situ biodegradation of 1,2-dichloroethenes in a model wetland., Environmental science & technology 42 (2008) 7924–7930.

[678] D. Cichocka, G. Imfeld, H. H. Richnow, I. Nijenhuis, Variability in microbial carbon isotope fractionation of tetra- and trichloroethene upon reductive dechlorination., Chemosphere 71 (2008) 639–648.

[679] A. A. Haluska, C. E. Schaefer, J.-S. Cho, G. M. Lavorgna, M. D. Annable, Long-term mass flux assessment of a dnapl source area treated using bioremediation., Journal of contaminant hydrology (2019).

[680] B. M. van Breukelen, H. A. A. Thouement, P. E. Stack, M. Vanderford, P. R. Philp, T. Kuder, Modeling 3d-csia data: Carbon, chlorine, and hydrogen isotope fractionation during reductive dechlorination of tce to ethene., Journal of contaminant hydrology 204 (2017) 79–89.

[681] P. Alvarez-Zaldívar, F. Centler, U. Maier, M. Thullner, G. Imfeld, Biogeochemical modelling of in situ biodegradation and stable isotope fractionation of intermediate chloroethenes in a horizontal subsurface flow wetland, Ecological Engineering 90 (2016) 170–179.

[682] M. Schmidt, S. Lege, I. Nijenhuis, Comparison of 1,2-dichloroethane, dichloroethene and vinyl chloride carbon stable isotope fractionation during dechlorination by two dehalococcoides strains., Water research 52 (2014) 146–154.

[683] T. Kuder, P. R. Philp, Demonstration of compound-specific isotope analysis of hydrogen isotope ratios in chlorinated ethenes., Environmental science & technology 47 (2013) 1461–1467.

[684] C. C. H. Chan, S. O. C. Mundle, T. Eckert, X. Liang, S. Tang, G. Lacrampe-Couloume, E. A. Edwards, B. S. Lollar, Large carbon isotope fractionation during biodegradation of chloroform by dehalobacter cultures., Environmental science & technology 46 (2012) 10154–10160.

[685] K. E. Fletcher, I. Nijenhuis, H. H. Richnow, F. E. Löffler, Stable carbon isotope enrichment factors for cis-1,2-dichloroethene and vinyl chloride reductive dechlorination by dehalococcoides., Environmental science & technology 45 (2011) 2951–2957.

[686] P. L. Morrill, G. Lacrampe-Couloume, B. S. Lollar, Dynamic headspace: a single-step extraction for isotopic analysis of microg/l concentrations of dissolved chlorinated ethenes., Rapid communications in mass spectrometry : RCM 18 (2004) 595–600.

[687] K. C. Harding, P. K. H. Lee, M. Bill, T. E. Buscheck, M. E. Conrad, L. Alvarez-Cohen, Effects of varying growth conditions on stable carbon isotope fractionation of trichloroethene (tce) by tcea-containing dehalococcoides mccartyi strains., Environmental science & technology 47 (2013) 12342–12350.

[688] Y. Liu, A. guo Zhou, Y. Gan, X. Li, Roles of hydroxyl and sulfate radicals in degradation of trichloroethene by persulfate activated with fe2+ and zero-valent iron: Insights from carbon isotope fractionation., Journal of hazardous materials 344 (2018) 98–103.

[689] M. Rosell, J. Palau, S. H. Mortan, G. Caminal, A. Soler, O. Shouakar-Stash, E. Marco-Urrea, Dual carbon - chlorine isotope fractionation during dichloroelimination of 1,1,2-trichloroethane by an enrichment culture containing dehalogenimonas sp., The Science of the total environment 648 (2019) 422–429.

[690] A. Gafni, H. Siebner, A. Bernstein, Potential for co-metabolic oxidation of tce and evidence for its occurrence in a large-scale aquifer survey., Water research 171 (2019).

[691] B. M. van Breukelen, D. Hunkeler, F. Volkering, Quantification of sequential chlorinated ethene degradation by use of a reactive transport model incorporating isotope fractionation., Environmental science & technology 39 (2005) 4189–4197.

[692] N. Vanstone, M. Elsner, G. Lacrampe-Couloume, S. A. Mabury, B. S. Lollar, Potential for identifying abiotic chloroalkane degradation mechanisms using carbon isotopic fractionation., Environmental science & technology 42 (2008) 126–132.

[693] D. Hunkeler, B. M. van Breukelen, M. Elsner, Modeling chlorine isotope trends during sequential transformation of chlorinated ethenes., Environmental science & technology 43 (2009) 6750–6756.

[694] K. E. Fletcher, F. E. Löffler, H. H. Richnow, I. Nijenhuis, Stable carbon isotope fractionation of 1,2-dichloropropane during dichloroelimination by dehalococcoides populations., Environmental science & technology 43 (2009) 6915–6919.

[695] S.-Y. D. Chiang, R. Mora, W. H. Diguiseppi, G. Davis, K. L. Sublette, P. B. Gedalanga, S. Mahendra, Characterizing the intrinsic bioremediation potential of 1,4-dioxane and trichloroethene using innovative environmental diagnostic tools., Journal of environmental monitoring : JEM 14 (2012) 2317–2326.

[696] C. Wiegert, M. Mandalakis, T. D. J. Knowles, P. Polymenakou, C. Aeppli, J. Macháckova, H. Holmstrand, R. P. Evershed, R. D. Pancost, O. Gustafsson, Carbon and chlorine isotope fractionation during microbial degradation of tetra- and trichloroethene., Environmental science & technology 47 (2013) 6449–6456.

[697] O. Shouakar-Stash, R. J. Drimmie, Online methodology for determining compound-specific hydrogen stable isotope ratios of trichloroethene and 1,2-cis-dichloroethene by continuous-flow isotope ratio mass spectrometry., Rapid communications in mass spectrometry : RCM 27 (2013) 1335–1344.

[698] P. Wanner, D. Hunkeler, Carbon and chlorine isotopologue fractionation of chlorinated hydrocarbons during diffusion in water and low permeability sediments, Geochimica et Cosmochimica Acta 157 (2015) 198–212.

[699] E. Kret, A. Kiecak, G. Malina, I. Nijenhuis, A. Postawa, Identification of tce and pce sorption and biodegradation parameters in a sandy aquifer for fate and transport modelling: batch and column studies, Environmental Science and Pollution Research International 22 (2015) 9877 – 9888.

[700] P. Wanner, B. L. Parker, S. W. Chapman, R. Aravena, D. Hunkeler, Quantification of degradation of chlorinated hydrocarbons in saturated low permeability sediments using compound-specific isotope analysis., Environmental science & technology 50 (2016) 5622–5630.

[701] K. Ebert, C. Laskov, M. Elsner, S. B. Haderlein, Calibration bias of experimentally determined chlorine isotope enrichment factors: the need for a two-point calibration in compound-specific chlorine isotope analysis., Rapid communications in mass spectrometry : RCM 31 (2017) 68–74.

[702] O. C. Goli, T. Górecki, H. T. E. Mugammar, M. Marchesi, R. Aravena, Evaluation of the suitability of the waterloo membrane sampler for sample preconcentration before compound-specific isotope analysis, Environmental Technology and Innovation 7 (2017) 141–151.

[703] N. Blázquez-Pallí, O. Shouakar-Stash, J. Palau, A. Trueba-Santiso, J. Varias, M. Bosch, A. Soler, T. Vicent, E. Marco-Urrea, M. Rosell, Use of dual element isotope analysis and microcosm studies to determine the origin and potential anaerobic biodegradation of dichloromethane in two multi-contaminated aquifers, Science of The Total Environment (2019).

[704] O. Shouakar-Stash, R. J. Drimmie, M. Zhang, S. K. Frape, Compound-specific chlorine isotope ratios of tce, pce and dce isomers by direct injection using cf-irms, Applied Geochemistry 21 (2006) 766–781.

[705] S. Leitner, T. G. Reichenauer, A. Watzinger, Determination of carbon isotope enrichment factors of cis-dichloroethene after precursor amendment., Rapid communications in mass spectrometry 31 (2017) 1699–1708.

[706] T. Kuder, B. M. van Breukelen, M. Vanderford, P. R. Philp, 3d-csia: carbon, chlorine, and hydrogen isotope fractionation in transformation of tce to ethene by a dehalococcoides culture., Environmental science & technology 47 (2013) 9668–9677.

[707] D. Rodríguez-Fernández, C. Torrentó, M. Guivernau, M. Vinas, D. Hunkeler, A. Soler, C. Domènech, M. Rosell, Vitamin b12 effects on chlorinated methanes-degrading microcosms: Dual isotope and metabolically active microbial populations assessment., The Science of the total environment 621 (2017) 1615–1625.

[708] P. Wanner, D. Hunkeler, Molecular dynamic simulations of carbon and chlorine isotopologue fractionation of chlorohydrocarbons during diffusion in liquid water, Environmental Science & Technology Letters (2019).

[709] D. Rodríguez-Fernández, B. Heckel, C. Torrentó, A. H. Meyer, M. Elsner, D. Hunkeler, A. Soler, M. Rosell, C. Domènech, Dual element (ccl) isotope approach to distinguish abiotic reactions of chlorinated methanes by fe(0) and by fe(ii) on iron minerals at neutral and alkaline ph., Chemosphere 206 (2018) 447–456.

[710] L. Zwank, M. Elsner, A. Aeberhard, R. P. Schwarzenbach, S. B. Haderlein, Carbon isotope fractionation in the reductive dehalogenation of carbon tetrachloride at iron (hydr)oxide and iron sulfide minerals., Environmental science & technology 39 (2005) 5634–5641.

[711] D. Rodríguez-Fernández, C. Torrentó, J. Palau, M. Marchesi, A. Soler, D. Hunkeler, C. Domènech, M. Rosell, Unravelling long-term source removal effects and chlorinated methanes natural attenuation processes by c and cl stable isotopic patterns at a complex field site., The Science of the total environment 645 (2018) 286–296.

[712] S. O. C. Mundle, J. C. Spain, G. Lacrampe-Couloume, S. F. Nishino, B. S. Lollar, Branched pathways in the degradation of cdce by cytochrome p450 in polaromonas sp. js666., The Science of the total environment 605 (2017) 99–105.

[713] M. M. G. Chartrand, S. K. Hirschorn, G. Lacrampe-Couloume, B. S. Lollar, Compound-specific hydrogen isotope analysis of 1,2-dichloroethane: potential for delineating source and fate of chlorinated hydrocarbon contaminants in groundwater, Rapid Communications in Mass Spectrometry 21 (2007) 1841–1847.

[714] B. Heckel, D. Rodríguez-Fernández, C. Torrentó, A. H. Meyer, J. Palau, C. Domènech, M. Rosell, A. Soler, D. Hunkeler, M. Elsner, Compound-specific chlorine isotope analysis of tetrachloromethane and trichloromethane by gas chromatography-isotope ratio mass spectrometry vs gas chromatography-quadrupole mass spectrometry: Method development and evaluation of precision and trueness., Analytical chemistry 89 (2017) 3411–3420.

[715] S. Ertl, F. Seibel, L. Eichinger, F. H. Frimmel, A. Kettrup, Determination of the 13c/12c isotope ratio of organic compounds for the biological degradation of tetrachloroethene (pce) and trichloroethene (tce), Acta Hydrochimica Et Hydrobiologica 24 (1996) 16–21.

[716] H. Dayan, T. A. Abrajano, N. C. Sturchio, L. Winsor, Carbon isotopic fractionation during reductive dehalogenation of chlorinated ethenes by metallic iron, Organic Geochemistry 30 (1999) 755–763.

[717] M. Numata, N. Nakamura, H. Koshikawa, Y. Terashima, Chlorine stable isotope measurements of chlorinated aliphatic hydrocarbons by thermal ionization mass spectrometry, Analytica Chimica Acta 455 (2002) 1–9.

[718] S. R. Poulson, H. Naraoka, Carbon isotope fractionation during permanganate oxidation of chlorinated ethylenes (cdce, tce, pce)., Environmental science & technology 36 (2002) 3270–3274.

[719] G. F. Slater, B. S. Lollar, R. A. King, S. F. O'Hannesin, Isotopic fractionation during reductive dechlorination of trichloroethene by zero-valent iron: influence of surface treatment., Chemosphere 49 (2002) 587–596.

[720] O. Shouakar-Stash, S. K. Frape, R. J. Drimmie, Stable hydrogen, carbon and chlorine isotope measurements of selected chlorinated organic solvents., Journal of contaminant hydrology 60 (2003) 211–228.

[721] G. F. Slater, B. S. Lollar, S. Lesage, S. Brown, Carbon isotope fractionation of pce and tce during dechlorination by vitamin b12, Groundwater Monitoring & Remediation 23 (2003).

[722] K. H. Chu, S. Mahendra, D. L. Song, M. E. Conrad, L. Alvarez-Cohen, Stable carbon isotope fractionation during aerobic biodegradation of chlorinated ethenes., Environmental science & technology 38 (2004) 3126–3130.

[723] K. Sakaguchi-Söder, J. Jager, H. Grund, F. Matthäus, C. Schüth, Monitoring and evaluation of dechlorination processes using compound-specific chlorine isotope analysis., Rapid communications in mass spectrometry 21 (2007) 3077–3084.

[724] M. Elsner, D. Hunkeler, Evaluating chlorine isotope effects from isotope ratios and mass spectra of polychlorinated molecules., Analytical chemistry 80 (2008) 4731–4740.

[725] X. Liang, R. P. Philp, E. C. Butler, Kinetic and isotope analyses of tetrachloroethylene and trichloroethylene degradation by model fe(ii)-bearing minerals., Chemosphere 75 (2009) 63–69.

[726] C. Aeppli, M. Berg, O. A. Cirpka, C. Holliger, R. P. Schwarzenbach, T. B. Hofstetter, Influence of mass-transfer limitations on carbon isotope fractionation during microbial dechlorination of trichloroethene., Environmental science & technology 43 (2009) 8813–8820.

[727] A. Bernstein, O. Shouakar-Stash, K. Ebert, C. Laskov, D. Hunkeler, S. Jeannottat, K. Sakaguchi-Söder, J. Laaks, M. A. Jochmann, S. Cretnik, J. Jager, S. B. Haderlein, T. C. Schmidt, R. Aravena, M. Elsner, Compound-specific chlorine isotope analysis: a comparison of gas chromatography/isotope ratio mass spectrometry and gas chromatography/quadrupole mass spectrometry methods in an interlaboratory study., Analytical chemistry 83 (2011) 7624–7634.

[728] M. Marchesi, R. Aravena, K. Sra, N. R. Thomson, N. Otero, A. Soler, S. A. Mancini, Carbon isotope fractionation of chlorinated ethenes during oxidation by fe2+ activated persulfate., The Science of the total environment 433 (2012) 318–322.

[729] Y. Gan, T. Yu, A. guo Zhou, Y. Liu, C. fu Liu, A technique for carbon and chlorine isotope analyses of chlorinated aliphatic hydrocarbons in groundwater, Journal of Earth Science 24 (2013) 274–281.

[730] C. Audí-Miró, S. Cretnik, N. Otero, J. Palau, O. Shouakar-Stash, A. Soler, M. Elsner, Cl and c isotope analysis to assess the effectiveness of chlorinated ethene degradation by zero-valent iron: Evidence from dual element and product isotope values, Applied Geochemistry 32 (2013) 175–183.

[731] S. Cretnik, K. A. Thoreson, A. Bernstein, K. Ebert, D. Buchner, C. Laskov, S. B. Haderlein, O. Shouakar-Stash, S. Kliegman, K. McNeill, M. Elsner, Reductive dechlorination of tce by chemical model systems in comparison to dehalogenating bacteria: insights from dual element isotope analysis (13c/12c, 37cl/35cl)., Environmental science & technology 47 (2013) 6855–6863.

[732] M. Marchesi, N. R. Thomson, R. Aravena, K. Sra, N. Otero, A. Soler, Carbon isotope fractionation of 1,1,1-trichloroethane during base-catalyzed persulfate treatment., Journal of hazardous materials 260 (2013) 61–66.

[733] S. Cretnik, A. Bernstein, O. Shouakar-Stash, F. E. Löffler, M. Elsner, Chlorine isotope effects from isotope ratio mass spectrometry suggest intramolecular c-cl bond competition in trichloroethene (tce) reductive dehalogenation, Molecules 19 (2014) 6450 – 6473.

[734] J. Renpenning, S. F. Keller, S. Cretnik, O. Shouakar-Stash, M. Elsner, T. Schubert, I. Nijenhuis, Combined c and cl isotope effects indicate differences between corrinoids and enzyme (sulfurospirillum multivorans pcea) in reductive dehalogenation of tetrachloroethene, but not trichloroethene., Environmental science & technology 48 (2014) 11837–11845.

[735] M. K. O. Lee, E. Wells, Y. K. Wong, J. C. Koenig, L. Adrian, H. H. Richnow, M. Manefield, Relative contributions of dehalobacter and zerovalent iron in the degradation of chlorinated methanes., Environmental science & technology 49 (2015) 4481–4489.

[736] D. Buchner, S. F. Behrens, C. Laskov, S. B. Haderlein, Resiliency of stable isotope fractionation (δ(13)c and δ(37)cl) of trichloroethene to bacterial growth physiology and expression of key enzymes., Environmental science & technology 49 (2015) 13230–13237.

[737] Y. Liu, A. guo Zhou, Y. Gan, X. Li, Variability in carbon isotope fractionation of trichloroethene during degradation by persulfate activated with zero-valent iron: Effects of inorganic anions., The Science of the total environment 548-549 (2016) 1–5.

[738] Y. Liu, A. guo Zhou, Y. Gan, X. Li, Effects of inorganic anions on carbon isotope fractionation during fenton-like degradation of trichloroethene., Journal of hazardous materials 308 (2016) 187–191.

[739] A. Gafni, C. Lihl, F. Gelman, M. Elsner, A. Bernstein, δ13c and δ37cl isotope fractionation to characterize aerobic vs anaerobic degradation of trichloroethylene, Environmental Science and Technology Letters 5 (2018) 202–208.

[740] B. Heckel, K. McNeill, M. Elsner, Chlorinated ethene reactivity with vitamin b12 is governed by cobalamin chloroethylcarbanions as crossroads of competing pathways, ACS Catalysis 8 (2018) 3054–3066.

[741] R. Yu, R. G. Andrachek, L. G. Lehmicke, D. L. Freedman, Remediation of chlorinated ethenes in fractured sandstone by natural and enhanced biotic and abiotic processes: A crushed rock microcosm study., The Science of the total environment 626 (2018) 497–506.

[742] N. Liu, L. Ding, H. Li, P. Zhang, J. Zheng, C.-H. Weng, Stable carbon isotope fractionation of chlorinated ethenes by a microbial consortium containing multiple dechlorinating genes., Bioresource technology 261 (2018) 133–141.

[743] G. Jian-Ye, Z. Jing, Z. Chen-Ling, C. Zong-Yu, L. Fei, C. Huan-Wen, Approach to compound-specific isotope analysis of chlorine with reaction mass spectrometry and its exploration, Chinese Journal of Analytical Chemistry 47 (2019) 237–243.

[744] H. A. A. Thouement, T. Kuder, T. J. Heimovaara, B. M. van Breukelen, Do csia data from aquifers inform on natural degradation of chlorinated ethenes in aquitards?, Journal of contaminant hydrology 226 (2019).

[745] A. Gafni, F. Gelman, Z. Ronen, A. Bernstein, Variable carbon and chlorine isotope fractionation in tce co-metabolic oxidation., Chemosphere 242 (2020).

[746] M. Walaszek, L. Cary, G. Billon, M. Blessing, A. Bouvet-Swialkowski, M. George, J. Criquet, J. R. Mossmann, Dynamics of chlorinated aliphatic hydrocarbons in the chalk aquifer of northern france., The Science of the total environment (2020).

[747] S. Franke, K. Seidel, L. Adrian, I. Nijenhuis, Dual element (c/cl) isotope analysis indicates distinct mechanisms of reductive dehalogenation of chlorinated ethenes and dichloroethane in dehalococcoides mccartyi strain btf08 with defined reductive dehalogenase inventories, Frontiers in Microbiology 11 (2020).

[748] S. Franke, C. Lihl, J. Renpenning, M. Elsner, I. Nijenhuis, Triple-element compound-specific stable isotope analysis of 1,2-dichloroethane for characterization of the underlying dehalogenation reaction in two dehalococcoides mccartyi strains, FEMS Microbiology Ecology 93 (2017).

[749] S. K. Hirschorn, M. J. A. Dinglasan-Panlilio, E. A. Edwards, G. Lacrampe-Couloume, B. S. Lollar, Isotope analysis as a natural reaction probe to determine mechanisms of biodegradation of 1,2-dichloroethane., Environmental microbiology 9 (2007) 1651–1657.

[750] G. Carpani, M. Marchesi, I. Pietrini, L. Alberti, L. Zaninetta, O. Shouakar-Stash, F. de Ferra, 1,2-dca natural attenuation evaluation in groundwater: Insight by dual isotope 13c/37cl and molecular analysis approach, Water (2021).

[751] B. Heckel, M. Elsner, Exploring mechanisms of biotic chlorinated alkane reduction: Evidence of nucleophilic substitution (sn2) with vitamin b12., Environmental science & technology (2022).

[752] I. Yankelzon, T. Englman, A. Bernstein, H. Siebner, Z. Ronen, F. Gelman, Multi-elemental c-br-cl isotope analysis for characterizing biotic and abiotic transformations of 1-bromo-2-chloroethane (bce), Environmental Science and Pollution Research 27 (2020) 22749–22757.

[753] J. Palau, S. Cretnik, O. Shouakar-Stash, M. Höche, M. Elsner, D. Hunkeler, C and cl isotope fractionation of 1,2-dichloroethane displays unique δ^{13}c/δ^{3}cl patterns for pathway identification and reveals surprising c-cl bond involvement in microbial oxidation., Environmental science & technology 48 (2014) 9430–9437.

[754] N. A. Head, J. I. Gerhard, A. M. Inglis, A. N. Garcia, A. I. Chowdhury, D. A. Reynolds, C. de Boer, A. Sidebottom, L. M. Austrins, J. Eimers, D. M. O'Carroll, Field test of electrokinetically-delivered thermally activated persulfate for remediation of chlorinated solvents in clay., Water research 183 (2020).

[755] D. Hunkeler, R. Aravena, Evidence of substantial carbon isotope fractionation among substrate, inorganic carbon, and biomass during aerobic mineralization of 1,2-dichloroethane byxanthobacter autotrophicus, Applied and Environmental Microbiology 66 (2000) 4870 – 4876.

[756] J. Palau, O. Shouakar-Stash, S. H. Mortan, R. Yu, M. Rosell, E. Marco-Urrea, D. L. Freedman, R. Aravena, A. Soler, D. Hunkeler, Hydrogen isotope fractionation during the biodegradation of 1,2-dichloroethane: Potential for pathway identification using a multi-element (c, cl, and h) isotope approach., Environmental science & technology 51 (2017) 10526–10535.

[757] S. K. Hirschorn, M. J. A. Dinglasan, M. Elsner, S. A. Mancini, G. Lacrampe-Couloume, E. A. Edwards, B. S. Lollar, Pathway dependent isotopic fractionation during aerobic biodegradation of 1,2-dichloroethane., Environmental science & technology 38 (2004) 4775–4781.

[758] D. Hunkeler, R. Aravena, E. E. Cox, Carbon isotopes as a tool to evaluate the origin and fate of vinyl chloride: laboratory experiments and modeling of isotope evolution., Environmental science & technology 36 (2002) 3378–3384.

[759] P. Wanner, B. L. Parker, S. W. Chapman, R. Aravena, D. Hunkeler, Does sorption influence isotope ratios of chlorinated hydrocarbons under field conditions, Applied Geochemistry 84 (2017) 348–359.

[760] Y. Abe, J. Zopfi, D. Hunkeler, Effect of molecule size on carbon isotope fractionation during biodegradation of chlorinated alkanes by xanthobacter autotrophicus gj10, Isotopes in Environmental and Health Studies 45 (2009) 18 – 26.

[761] J. M. Soder-Walz, C. Torrentó, C. Algora, K. Wasmund, P. G. Cortés, A. Soler, T. Vicent, M. Rosell, E. Marco-Urrea, Trichloromethane dechlorination by a novel dehalobacter sp. strain 8m reveals a third contrasting c and cl isotope fractionation pattern within this genus., The Science of the total environment (2021).

[762] J. Palau, R. Yu, S. H. Mortan, O. Shouakar-Stash, M. Rosell, D. L. Freedman, C. Sbarbati, S. L. Fiorenza, R. Aravena, E. Marco-Urrea, M. Elsner, A. Soler, D. Hunkeler, Distinct dual c-cl isotope fractionation patterns during anaerobic biodegradation of 1,2-dichloroethane: Potential to characterize microbial degradation in the field., Environmental science & technology 51 (2017) 2685–2694.

[763] S. T. Hart, R. A. Bertolo, M. S. Agostini, R. Feig, P. Lojkasek-Lima, J. C. R. Gouvea, F. S. Barreto, R. Aravena, Hydrogeochemical and isotopic evaluation of voc commingled plumes in a weathered fractured bedrock aquifer treated with thermal and bioremediation., Journal of contaminant hydrology 245 (2022).

[764] Y. Liu, Y. Zhang, A. guo Zhou, M. Li, Insights into carbon isotope fractionation on trichloroethene degradation in base activated persulfate process: The role of multiple reactive oxygen species., The Science of the total environment 800 (2021).

[765] B. Heckel, S. Cretnik, S. Kliegman, O. Shouakar-Stash, K. McNeill, M. Elsner, Reductive outer-sphere single electron transfer is an exception rather than the rule in natural and engineered chlorinated ethene dehalogenation., Environmental science & technology 51 (2017) 9663–9673.

[766] X. Liang, Y. Dong, T. Kuder, L. R. Krumholz, R. P. Philp, E. C. Butler, Distinguishing abiotic and biotic transformation of tetrachloroethylene and trichloroethylene by stable carbon isotope fractionation., Environmental science & technology 41 (2007) 7094–7100.

[767] A. Neumann, T. B. Hofstetter, M. Skarpeli-Liati, R. P. Schwarzenbach, Reduction of polychlorinated ethanes and carbon tetrachloride by structural fe(ii) in smectites., Environmental science & technology 43 (2009) 4082–4089.

[768] M. Elsner, D. M. Cwiertny, A. L. Roberts, B. S. Lollar, 1,1,2,2-tetrachloroethane reactions with oh-, cr(ii), granular iron, and a copper-iron bimetal: insights from product formation and associated carbon isotope fractionation., Environmental science & technology 41 (2007) 4111–4117.

[769] S. M. Stewart, T. B. Hofstetter, P. Joshi, C. A. Gorski, Linking thermodynamics to pollutant reduction kinetics by fe2+ bound to iron oxides., Environmental science & technology 52 (2018) 5600–5609.

[770] M. Elsner, S. B. Haderlein, T. Kellerhals, S. Luzi, L. Zwank, W. Angst, R. P. Schwarzenbach, Mechanisms and products of surface-mediated reductive dehalogenation of carbon tetrachloride by fe(ii) on goethite., Environmental science & technology 38 (2004) 2058–2066.

[771] F. Breider, C. N. Albers, D. Hunkeler, Assessing the role of trichloroacetyl-containing compounds in the natural formation of chloroform using stable carbon isotopes analysis., Chemosphere 90 (2013) 441–448.

[772] W. A. Arnold, J. Bolotin, U. von Gunten, T. B. Hofstetter, Evaluation of functional groups responsible for chloroform formation during water chlorination using compound specific isotope analysis., Environmental science & technology 42 (2008) 7778–7785.

[773] C. Torrentó, J. Palau, D. Rodríguez-Fernández, B. Heckel, A. H. Meyer, C. Domènech, M. Rosell, A. Soler, M. Elsner, D. Hunkeler, Carbon and chlorine isotope fractionation patterns associated with different engineered chloroform transformation reactions., Environmental science & technology 51 (2017) 6174–6184.

[774] F. Breider, D. Hunkeler, Mechanistic insights into the formation of chloroform from natural organic matter using stable carbon isotope analysis, Geochimica et Cosmochimica Acta 125 (2014) 85–95.

[775] B. A. Asfaw, K. Sakaguchi-Söder, A. Bernstein, H. Siebner, C. Schüth, Optimization of compound-specific chlorine stable isotope analysis of chloroform using taguchi design of experiments., Rapid communications in mass spectrometry (2020).

[776] G. Chen, O. Shouakar-Stash, O. Shouakar-Stash, E. Phillips, S. D. Justicia-Leon, T. Gilevska, B. S. Lollar, E. E. Mack, E. S. Seger, F. E. Löffler, F. E. Löffler, Dual carbon-chlorine isotope analysis indicates distinct anaerobic dichloromethane degradation pathways in two members of peptococcaceae., Environmental science & technology 52 (2018) 8607–8616.

[777] B. Heckel, E. Phillips, E. A. Edwards, B. S. Lollar, M. Elsner, M. Manefield, M. J. Lee, Reductive dehalogenation of trichloromethane by two different dehalobacter restrictus strains reveal opposing dual element isotope effects., Environmental science & technology 53 (2019) 2332–2343.

[778] C. Aeppli, D. Bastviken, P. S. Andersson, O. Gustafsson, Chlorine isotope effects and composition of naturally produced organochlorines from chloroperoxidases, flavin-dependent halogenases, and in forest soil., Environmental science & technology 47 (2013) 6864–6871.

[779] T. Benbow, R. Frew, A. R. Hayman, Validation of a rapid and simple method for the preparation of aqueous organic compounds prior to compound specific isotope analysis, Organic Geochemistry 39 (2008) 1690–1702.

[780] M. Nikolausz, I. Nijenhuis, K. Ziller, H. H. Richnow, M. Kästner, Stable carbon isotope fractionation during degradation of dichloromethane by methylotrophic bacteria., Environmental microbiology 8 (2006) 156–164.

[781] M. L. Torgonskaya, A. M. Zyakun, Y. A. Trotsenko, K. S. Laurinavichius, S. Kümmel, S. Vuilleumier, H. H. Richnow, Individual stages of bacterial dichloromethane degradation mapped by carbon and chlorine stable isotope analysis., Journal of environmental sciences 78 (2019) 147–160.

[782] T. Nadalig, M. Greule, F. Bringel, S. Vuilleumier, F. Keppler, Hydrogen and carbon isotope fractionation during degradation of chloromethane by methylotrophic bacteria, MicrobiologyOpen 2 (2013) 893 – 900.

[783] M. Prieto-Espinoza, S. Weill, B. Belfort, E. E. L. Muller, J. Masbou, F. Lehmann, S. Vuilleumier, G. Imfeld, Water table fluctuations affect dichloromethane biodegradation in lab-scale aquifers contaminated with organohalides., Water research 203 (2021).

[784] D. Cichocka, M. Siegert, G. Imfeld, J. Andert, K. Beck, G. Diekert, H. H. Richnow, I. Nijenhuis, Factors controlling the carbon isotope fractionation of tetra- and trichloroethene during reductive dechlorination by sulfurospirillum ssp. and desulfitobacterium sp. strain pce-s., FEMS microbiology ecology 62 (2007) 98–107.

[785] I. Nijenhuis, J. Andert, K. Beck, M. Kästner, G. Diekert, H. H. Richnow, Stable isotope fractionation of tetrachloroethene during reductive dechlorination by sulfurospirillum multivorans and desulfitobacterium sp. strain pce-s and abiotic reactions with cyanocobalamin, Applied and Environmental Microbiology 71 (2005) 3413 – 3419.

[786] J. Büsing, D. Buchner, S. F. Behrens, S. B. Haderlein, Deciphering the variability of stable isotope (c, cl) fractionation of tetrachloroethene biotransformation by desulfitobacterium strains carrying different reductive dehalogenases enzymes., Environmental science & technology (2019).

[787] S. C. Béranger, B. E. Sleep, B. S. Lollar, A. J. Brown, Isotopic fractionation of tetrachloroethene undergoing biodegradation supported by endogenous decay, Journal of Environmental Engineering 132 (2006) 725–735.

[788] J. Renpenning, I. Rapp, I. Nijenhuis, Substrate hydrophobicity and cell composition influence the extent of rate limitation and masking of isotope fractionation during microbial reductive dehalogenation of chlorinated ethenes., Environmental science & technology 49 (2015) 4293–4301.

[789] S. Jeannottat, D. Hunkeler, Chlorine and carbon isotopes fractionation during volatilization and diffusive transport of trichloroethene in the unsaturated zone., Environmental science & technology 46 (2012) 3169–3176.

[790] J. Palau, A. Soler, À. Canals, R. Aravena, Use of environmental isotopes (13c, 15n, and 18o) for evaluating sources and fate of nitrate and tetrachloroethene in an alluvial aquifer, Environmental Forensics 11 (2010) 237–247.

[791] M. Thullner, M. Kampara, H. H. Richnow, H. Harms, L. Y. Wick, Impact of bioavailability restrictions on microbially induced stable isotope fractionation. 1. theoretical calculation., Environmental science & technology 42 (2008) 6544–6551.

[792] A. Badin, G. F. Buttet, J. Maillard, C. Holliger, D. Hunkeler, Multiple dual c-cl isotope patterns associated with reductive dechlorination of tetrachloroethene., Environmental science & technology 48 (2014) 9179–9186.

[793] J. A. C. Barth, G. F. Slater, C. Schüth, M. Bill, A. Downey, M. J. Larkin, R. M. Kalin, Carbon isotope fractionation during aerobic biodegradation of trichloroethene by burkholderia cepacia g4: a tool to map degradation mechanisms, Applied and Environmental Microbiology 68 (2002) 1728 – 1734.

[794] S. Jeannottat, D. Hunkeler, Can soil gas vocs be related to groundwater plumes based on their isotope signature?, Environmental science & technology 47 (2013) 12115–12122.

[795] Y. Gan, T. Yu, A. guo Zhou, Y. Liu, K. Yu, L. Han, Variability in the carbon isotope fractionation of trichloroethene on its reductive dechlorination by vitamin b12., Environmental science. Processes & impacts 16 (2014) 1882–1888.

[796] P. L. Morrill, B. E. Sleep, G. F. Slater, E. A. Edwards, B. S. Lollar, Evaluation of isotopic enrichment factors for the biodegradation of chlorinated ethenes using a parameter estimation model: toward an improved quantification of biodegradation., Environmental science & technology 40 (2006) 3886–3892.

[797] P. Höhener, M. Elsner, H. Eisenmann, O. Atteia, Improved constraints on in situ rates and on quantification of complete chloroethene degradation from stable carbon isotope mass balances in groundwater plumes., Journal of contaminant hydrology 182 (2015) 173–182.

[798] C. Lihl, L. M. Douglas, S. Franke, A. P. de Mora, A. H. Meyer, M. Daubmeier, E. A. Edwards, I. Nijenhuis, B. S. Lollar, M. Elsner, Mechanistic dichotomy in bacterial trichloroethene dechlorination revealed by carbon and chlorine isotope effects., Environmental science & technology 53 (2019) 4245–4254.

[799] E. Marco-Urrea, I. Nijenhuis, L. Adrian, Transformation and carbon isotope fractionation of tetra- and trichloroethene to trans-dichloroethene by dehalococcoides sp. strain cbdb1., Environmental science & technology 45 (2011) 1555–1562.

[800] T. H. M. Smits, A. Assal, D. Hunkeler, C. Holliger, Anaerobic degradation of vinyl chloride in aquifer microcosms., Journal of environmental quality 40 (2011) 915–922.

[801] G. Imfeld, H. Pieper, N. Shani, P. Rossi, M. Nikolausz, I. Nijenhuis, H. Paschke, H. Weiss, H. H. Richnow, Characterization of groundwater microbial communities, dechlorinating bacteria, and in situ biodegradation of chloroethenes along a vertical gradient, Water, Air, & Soil Pollution 221 (2011) 107–122.

[802] C. B. Ottosen, P. L. Bjerg, D. Hunkeler, J. Zimmermann, N. Tuxen, D. Harrekilde, L. R. Bennedsen, G. Leonard, L. Brabæk, I. L. Kristensen, M. M. Broholm, Assessment of chlorinated ethenes degradation after field scale injection of activated carbon and bioamendments: Application of isotopic and microbial analyses., Journal of contaminant hydrology 240 (2021).

[803] I. N. Damgaard, P. L. Bjerg, C. S. Jacobsen, A. Tsitonaki, H. Kerrn-Jespersen, M. M. Broholm, Performance of full-scale enhanced reductive dechlorination in clay till, Groundwater Monitoring & Remediation 33 (2013).

[804] A. M. Murray, C. B. Ottosen, J. Maillard, C. Holliger, A. Johansen, L. Brabæk, I. L. Kristensen, J. Zimmermann, D. Hunkeler, M. M. Broholm, Chlorinated ethene plume evolution after source thermal remediation: Determination of degradation rates and mechanisms., Journal of contaminant hydrology (2019).

[805] S. Åkesson, C. J. Sparrenbom, C. J. Paul, R. E. Jansson, H. Holmstrand, Characterizing natural degradation of tetrachloroethene (pce) using a multidisciplinary approach, Ambio 50 (2020) 1074 – 1088.

[806] J. Hellal, C. Joulian, C. Urien, S. Ferreira, J. Denonfoux, L. Hermon, S. Vuilleumier, G. Imfeld, Chlorinated ethene biodegradation and associated bacterial taxa in multi-polluted groundwater: Insights from biomolecular markers and stable isotope analysis., The Science of the total environment (2020).

[807] J. Schwarzbauer, L. Dsikowitzky, S. Heim, R. Littke, Determination of 13c/12c-ratios of anthropogenic organic contaminants in river water samples by gc-irmms, International Journal of Environmental Analytical Chemistry 85 (2005) 349 – 364.

[808] D. Ghezzi, M. F. Filippini, M. Cappelletti, A. Firrincieli, D. Zannoni, A. Gargini, S. Fedi, Molecular characterization of microbial communities in a peat-rich aquifer system contaminated with chlorinated aliphatic compounds, Environmental Science and Pollution Research 28 (2021) 23017 – 23035.

[809] L. J. S. Halloran, F. Vakili, P. Wanner, O. Shouakar-Stash, D. Hunkeler, Sorption- and diffusion-induced isotopic fractionation in chloroethenes., The Science of the total environment 788 (2021).

[810] C. B. Ottosen, V. K. Rønde, U. S. McKnight, M. D. Annable, M. M. Broholm, J. F. Devlin, P. L. Bjerg, Natural attenuation of a chlorinated ethene plume discharging to a stream: Integrated assessment of hydrogeological, chemical and microbial interactions., Water research 186 (2020).

[811] Y. Liu, Y. Gan, A. guo Zhou, C. fu Liu, X. Li, T. Yu, Carbon and chlorine isotope fractionation during fenton-like degradation of trichloroethene., Chemosphere 107 (2014) 94–100.

[812] K. R. Schmidt, S. Gaza, A. D. Voropaev, S. Ertl, A. Tiehm, Aerobic biodegradation of trichloroethene without auxiliary substrates., Water research 59 (2014) 112–118.

[813] T. Yu, Y. Gan, A. guo Zhou, K. Yu, Y. Liu, Investigation of stable c and cl isotope effects of trichloroethene and tetrachloroethylene during evaporation at different temperatures, Journal of Earth Science 25 (2014) 735–740.

[814] Y. Bloom, R. Aravena, D. Hunkeler, E. A. Edwards, S. K. Frape, Carbon isotope fractionation during microbial dechlorination of trichloroethene, cis-1,2-dichloroethene, and vinyl chloride: Implications for assessment of natural attenuation, Environmental Science & Technology 34 (2000) 2768–2772.

[815] A. Horst, G. Lacrampe-Couloume, Isotope fractionation (2h/1h, 13c/12c, 37cl/35cl) in trichloromethane and trichloroethene caused by partitioning between gas phase and water., Environmental science. Processes & impacts (2020).

[816] C. Schüth, M. Bill, J. A. C. Barth, G. F. Slater, R. M. Kalin, Carbon isotope fractionation during reductive dechlorination of tce in batch experiments with iron samples from reactive barriers., Journal of contaminant hydrology 66 (2003) 25–37.

[817] M. Bill, C. Schüth, J. A. C. Barth, R. M. Kalin, Carbon isotope fractionation during abiotic reductive dehalogenation of trichloroethene (tce)., Chemosphere 44 (2001) 1281–1286.

[818] A. Tiehm, K. R. Schmidt, B. Pfeifer, M. Heidinger, S. Ertl, Growth kinetics and stable carbon isotope fractionation during aerobic degradation of cis-1,2-dichloroethene and vinyl chloride., Water research 42 (2008) 2431–2438.

[819] Y. Dong, Y. Dong, E. C. Butler, R. P. Philp, L. R. Krumholz, Impacts of microbial community composition on isotope fractionation during reductive dechlorination of tetrachloroethylene, Biodegradation 22 (2011) 431–444.

[820] S. R. Clingenpeel, J. L. Moan, D. M. McGrath, B. A. Hungate, M. E. Watwood, Stable carbon isotope fractionation in chlorinated ethene degradation by bacteria expressing three toluene oxygenases, Frontiers in Microbiology 3 (2012).

[821] Y. Han, C. Liu, J. Horita, W. Yan, Trichloroethene (tce) hydrodechlorination by nife nanoparticles: Influence of aqueous anions on catalytic pathways., Chemosphere 205 (2018) 404–413.

[822] A. Horst, G. Lacrampe-Couloume, B. S. Lollar, Vapor pressure isotope effects in halogenated organic compounds and alcohols dissolved in water., Analytical chemistry 88 (2016) 12066–12071.

[823] H. Li, S. Wei, N. Liu, Y. nan Du, G.-S. Ding, Interspecies transfer of biosynthetic cobalamin for complete dechlorination of trichloroethene by dehalococcoides mccartyi., Water science and technology : a journal of the International Association on Water Pollution Research 85 (2022) 1335–1350.

[824] M. Julien, A. Gilbert, K. Yamada, R. J. Robins, P. Höhener, N. Yoshida, G. S. Remaud, Expanded uncertainty associated with determination of isotope enrichment factors: Comparison of two point calculation and rayleigh-plot., Talanta 176 (2018) 367–373.

[825] G. Imfeld, C. E. Aragonés, I. Fetzer, E. C. Meszaros, S. Zeiger, I. Nijenhuis, M. Nikolausz, S. Delerce, H. H. Richnow, Characterization of microbial communities in the aqueous phase of a constructed model wetland treating 1,2-dichloroethene-contaminated groundwater., FEMS microbiology ecology 72 (2010) 74–88.

[826] K. R. Schmidt, T. Augenstein, M. Heidinger, S. Ertl, A. Tiehm, Aerobic biodegradation of cis-1,2-dichloroethene as sole carbon source: Stable carbon isotope fractionation and growth characteristics., Chemosphere 78 (2010) 527–532.

[827] Y. Abe, R. Aravena, J. Zopfi, O. Shouakar-Stash, E. E. Cox, J. D. Roberts, D. Hunkeler, Carbon and chlorine isotope fractionation during aerobic oxidation and reductive dechlorination of vinyl chloride and cis-1,2-dichloroethene., Environmental science & technology 43 (2009) 101–107.

[828] T. Gilevska, N. Ivdra, M. Bonifacie, H. H. Richnow, Improvement of analytical method for chlorine dual-inlet isotope ratio mass spectrometry of organochlorines., Rapid communications in mass spectrometry : RCM 29 (2015) 1343–1350.

[829] B. D. Holt, L. J. Heraty, N. C. Sturchio, Extraction of chlorinated aliphatic hydrocarbons from groundwater at micromolar concentrations for isotopic analysis of chlorine., Environmental pollution 113 (2001) 263–269.

[830] K. L. Brungard, J. Munakata-Marr, C. A. Johnson, K. W. Mandernack, Stable carbon isotope fractionation of trans-1,2-dichloroethylene during co-metabolic degradation by methanotrophic bacteria, Chemical Geology 195 (2003) 59–67.

[831] L. J. Heraty, M. E. Fuller, L. Huang, T. A. Abrajano, N. C. Sturchio, Isotopic fractionation of carbon and chlorine by microbial degradation of dichloromethane, Organic Geochemistry 30 (1999) 793–799.

[832] M. Lincker, V. Lagneau, S. Guillon, P. Wanner, Identification of chlorohydrocarbon degradation pathways in aquitards using dual element compound-specific isotope measurements in aquifers., Chemosphere (2022).

[833] D. Buchner, P. R. Martin, J. Scheckenbach, S. Kümmel, F. Gelman, S. B. Haderlein, Expanding the calibration range of compound-specific chlorine isotope analysis by the preparation of a 37 cl-enriched tetrachloroethylene., Rapid communications in mass spectrometry (2022).

[834] H. Wienkenjohann, B. Jin, M. Rolle, Diffusive-dispersive isotope fractionation of chlorinated ethenes in groundwater: The key role of incomplete mixing and its multi-scale effects, Water Resources Research 59 (2023).

[835] A. Willmann, A.-L. Trautmann, A. Kushmaro, A. Tiehm, Intrinsic and bioaugmented aerobic trichloroethene degradation at seven sites, Heliyon 9 (2023).

[836] E. Phillips, O. Bulka, K. J. Picott, S. Kümmel, E. Edwards, I. Nijenhuis, M. Gehre, S. Dworatzek, J. S. Webb, B. S. Lollar, Investigation of active site amino acid influence on carbon and chlorine isotope fractionation during reductive dechlorination., FEMS microbiology ecology (2022).

[837] B. A. Asfaw, K. Sakaguchi-Söder, T. Schiedek, N. Michelsen, A. Bernstein, H. Siebner, C. Schüth, Isotopic evidence (δ13c, δ37cl, δ2h) for distinct transformation mechanisms of chloroform: Catalyzed h2-water system vs. zero-valent iron (zvi), Journal of Environmental Chemical Engineering (2023).

[838] Q. Cai, C. Shi, S. Yuan, M. Tong, Integrated anaerobic–aerobic biodegradation of mixed chlorinated solvents by electrolysis coupled with groundwater circulation in a simulated aquifer, Environmental Science and Pollution Research 30 (2022) 31188–31201.

[839] S. D. Emsbo-Mattingly, K. L. Flanders, E. R. Litman, Integrated differentiation of multiple trichloroethylene and tetrachloroethylene groundwater impacts using spatial concentration, biodegradation indices, chemical fingerprinting and carbon/chlorine isotope patterns, Environmental Forensics 24 (2022) 329 – 350.

[840] Z. Yuan, W. Dong, W. zhong Jiang, X. Shen, Isotope method to identify and quantify organic pollutant biodegradation during natural attenuation monitoring, Journal of Chemical Technology & Biotechnology (2022).

[841] E. Kühnel, D. D. P. Laffan, G. C. Lloyd-Jones, T. M. del Campo, I. R. Shepperson, J. L. Slaughter, Mechanism of methyl esterification of carboxylic acids by trimethylsilyldiazomethane., Angewandte Chemie 46 (2007) 7075–7078.

[842] A. Shrivastava, S. Jain, P. lal Sahu, S. Shukla, K. Sahu, Improved method for differentiation of synthetic and natural endogenous anabolic steroids using gas chromatography isotope ratio mass spectrometry (gc/c/irms) followed by two-fold high performance liquid chromatography (hplc) cleanup method: A perspective, Indian Journal of Pharmaceutical Education and Research 53 (2019) 460–465.

[843] A. Murata, U. H. Engelhardt, P. Fleischmann, K. Yamada, N. Yoshida, D. Juchelka, A. Hilkert, T. Ohnishi, N. Watanabe, P. Winterhalter, Purification and gas chromatography-combustion-isotope ratio mass spectrometry of aroma compounds from green tea products and comparison to bulk analysis., Journal of agricultural and food chemistry 61 (2013) 11321–11325.

[844] X. Zhu, Y. Zhong, H. Wang, D. Li, Y. Deng, S. Gao, P. Peng, Compound-specific carbon isotope analysis for mechanistic characterization of debromination of decabrominated diphenyl ether., Rapid communications in mass spectrometry 34 (2020).

[845] L. Iannella, F. Botré, C. Colamonici, D. Curcio, C. Ciccarelli, M. Mazzarino, X. de la Torre, Carbon isotopic characterization of prednisolone and prednisone pharmaceutical formulations: implications in antidoping analysis., Drug testing and analysis 12 (2020) 1587–1598.

[846] M. Saccon, R. Busca, C. Facca, L. Huang, S. Irei, A. Kornilova, D. A. Lane, J. Rudolph, Method for the determination of concentration and stable carbon isotope ratios of atmospheric phenols, Atmospheric Measurement Techniques 6 (2013) 2965–2974.

[847] T. A. B. Broek, M. D. McCarthy, A new approach to δ15n compound-specific amino acid trophic position measurements: preparative high pressure liquid chromatography technique for purifying underivatized amino acids for stable isotope analysis, Limnology and Oceanography: Methods 12 (2014).